ROLES OF MEMBRANE CURVATURE AND EXOSOME SECRETION DURING FAST-MEDIATED CELL-CELL FUSION

by

Jolene A. Read

Submitted in partial fulfilment of the requirements
for the degree of Doctor of Philosophy

at

Dalhousie University
Halifax, Nova Scotia
May 2014

TABLE OF CONTENTS

LIST OF TABLES

LIST OF FIGURES

ABSTRACT

The fusogenic reoviruses are a unique group of viruses that encode Fusion-Associated Small Transmembrane (FAST) proteins, a family of non-structural membrane proteins that induce cell-cell membrane fusion in infected cells. The compact FAST proteins range in size from 98 to 148 amino acids, making them an ideal model for studying the process of cell-cell fusion. In this work, we have examined the mechanisms by which the FAST proteins modulate membrane curvature during membrane fusion through the examination of (1) a novel cytosolic fusion-inducing lipid packing sensor (FLiPS) element, and (2) the induction of exosome secretion by the FAST proteins during syncytiogenesis.

Unlike the archetypal enveloped virus fusion proteins, the FAST proteins position the majority of the protein within the cytoplasm. We now show a unique 20 amino acid motif in the endodomain of baboon reovirus p15 functions as a novel FLiPS element. We show p15FLiPS is essential for pore formation during cell-cell fusion and reliant on a hydrophobic helix-loop-helix architecture. Furthermore, we show that p15FLiPS preferentially partitions into membranes fraught with lipid packing defects, and this partitioning is impeded when packing defects are blocked. Finally, p15FLiPS can be functionally replaced with other heterologous lipid packing sensor motifs. Therefore, we propose p15FLiPS binds to the highly curved rim of the nascent fusion pore, thereby lowering the energy to pore formation.

Exosomes are secreted membrane vesicles that function in intercellular communication. The role of exosome secretion in cell-cell fusion has not yet been determined. Here, we show that FAST proteins are secreted in exosomes during cell-cell fusion, and their incorperation does not significantly alter the exosome proteome. We show that export of p14 to exosomes is dependent on TSG101 and the cytosolic endodomain of p14. Finally, we demonstrate that exogenous p14-exosomes are sufficient to induce cell-cell fusion. Taken together, we suggest that the FAST proteins hijack the exosome secretion pathway to enhance cell-cell fusion, thereby augmenting the overall spread of virus.

Taken together, these results suggest that FAST proteins modulate membrane curvature during cell-cell fusion through use of specific lipid packing sensors and interactions with host proteins such as the ESCRT complex.

LIST OF ABBREVIATIONS USED

AFF-1	anchor cell fusion failure-1
ANOVA	analysis of variance
ANX1	annexin A1
AH	amphipathic helix
ALPS	amphipathic lipid-packing sensor
AqRV	Aquareovirus
ARF	ADP-ribosylation factor
ARV	avian reovirus
AU	arbitrary units
Auth	authentic
BAR	Bin/amphiphysin/Rvs
BroRV	Broome reovirus
BRV	baboon reovirus
Bis-ANS	4,4′-dianilino-1,1′-binaphthyl-5,5′-disulfonic acid dipotassium salt
BSA	bovine serum albumin
CD	circular dichroism
cDNA	complementary deoxyribonucleic acid
cRAP	Common Repository of Adventitious Proteins
Chol	cholesterol
DDA	data dependent acquisition
DMA	5-(N,N-dimethyl) amiloride hydrochloride
DMEM	Dulbecco's Modified Eagle Medium
DMSO	dimethyl sulfoxide
DNA	deoxyribonucleic acid
DOPC	1,2-dioleoyl-*sn*-glycero-3-phosphocholine
DOPE	1,2-dioleoyl-*sn*-glycero-3-phosphoethanolamine
DPC	dodecylphosphocholine
EAP	endosome-associated proteins
Ecto	ectodomain
ECV	extracellular vesicle
EDTA	ethylenediaminetetraacetic acid
EFF-1	epithelial fusion failure-1
Endo	endodomain
ENTH	epsin N-terminal homology
ER	endoplasmic reticulum
ESCRT	endosomal sorting complex required for transport
FAST	fusion-associated small transmembrane
FBS	fetal bovine serum
FC	founder cell
FCM	fusion-competent myoblast
FDR	false discovery rate
FP	fusion peptide
FRET	fluorescence resonance energy transfer

GCRV	grass carp reovirus
GFP	green fluorescent protein
GLUE	GRAM-like ubiquitin-binding in Eap45
GP	glycoprotein
HA	hemagglutinin
HBS	HEPES-buffered saline
HBSS	Hank's balanced salt solution
HERV-W	human endogenous retrovirus type W
HIV	human immunodeficiency virus
HP	hydrophobic patch
HPLC	high-performance liquid chromatography
hpi	hours post-infection
hpt	hours post-transfection
Hrs	hepatocyte growth factor–regulated tyrosine kinase substrate
ILV	intralumenal vesicle
LBPA	lysobisphosphatidic acid
LC-MS/MS	liquid chromatography tandem mass spectrometery
LPPG	1-palmitoyl-2-hydroxy-*sn*-glycero-3-[phospho-*rac*-(1-glycerol)]
M-CFS	macrophage colony-stimulating factor 1
MOI	multiplicity of infection
mRNA	messenger ribonucleic acid
miRNA	micro ribonucleic acid
MVB	multivesicular body
Myr	myristic acid
NBD	N-(7-nitro-2-1,3-benzoxadiazol-4-yl)
NBV	Nelson Bay reovirus
NMR	nuclear magnetic resonance
NOESY	Nuclear Overhausser Effects spectroscopy
PB	polybasic
PBS	phosphate-buffered saline
PCR	polymerase chain reaction
PDI	protein disulphide isomerase
PEI	polyethylenimine
PI3P	phosphatidylinositol-3-phosphate
PSM	Peptide to spectrum match
PVDF	polyvinylidene difluoride
RNA	ribonucleic acid
RRV	reptilian reovirus
Scr	scrambled
SD	standard deviation
SDS	sodium dodecyl sulphate
SM	sphingomyelin
SNARE	Soluble N-ethylmaleimide-sensitive factor activating protein receptor
TBS-T	Tris-buffered saline with Tween-20
TEM	transmission electron microscopy
TEX	tumor-associated exosomes

TF	transfected
TFA	trifluoroacetic acid
TM	transmembrane
TOCSY	total correlation spectroscopy
TSG101	tumor-supressor gene 101
TfR	transferrin receptor
UEV	ubiquitin E2 variant
UIM	ubiquitin-interacting motif
UV	ultraviolet
WCL	whole cell lysate
w/v	weight / volume

ACKNOWLEDGEMENTS

I would like to start by thanking my supervisor, Dr. Roy Duncan. Thank you for giving me the freedom to explore my research interests. You provided the perfect mix of insightful comments and independence. Thank you for all of your encouragement and always believing in me.

I would also like to thank my committee members, Dr. Jan Rainey, Dr. Jim Fawcett, Dr. Roger McLeod, and Dr. Craig McCormick. You always came to my committee meetings with keen interest in my project and provided many useful suggestions which have shaped my research into what it is today. Jim, thank you especially for allowing me access to the mass spectrometry facility.

To the Duncan lab members over the years: thanks for being so awesome to work with. A special thank you to Jing, Nichole, and Roberto – you truly keep the lab together. Nichole, you always go the extra mile to help. Roberto, thanks for teaching me how to fix any imaginable piece of lab equipment, including old HPLC machines. You've always been there to help and I appreciate it.

None of the work in this thesis would be possible without support from my funding sources: Canadian Institute of Health Research (CIHR), Nova Scotia Health Research Foundation (NSHRF), Eliza Ritchie Doctoral Scholarship Fund, and Killam Trusts. The funding you provided helped me focus on my research and achieve my goals without having to worry about money.

To Dr. Robert Ireland, Dr. Amanda Cockshutt, and especially Dr. Doug Campbell. Thank you for seeing my potential and encouraging me to go to graduate school. I honestly wouldn't have had the confidence to start this journey without you.

A huge thank you goes out to my parents. You have provided unwaiving support through the long, hard years of post-secondary education. Even though I am pretty sure you don't understand the details of my research, I always knew that it was as important to you as it was for me. You've always supported me in every way possible and I couldn't have done it without you. Love you both.

Finally, thank you to my better half, Eric. Eric, you've seen me at my best and worst, you've scheduled dinner (and your life) around my lab schedule, and you've embraced my choice to be a scientist. You've always been patient, loving, and supportive. I am looking forward to starting the next chapter of our lives together. I love you.

CHAPTER 1
INTRODUCTION

1.1 Overview

Cell fusion is a tightly regulated and complicated process that is essential in development and homeostasis of eukaryotic organisms. For sexually reproducing organisms, it begins with sperm-ovum merger to unite gamete genomes. In multicellular creatures, cell fusion is used as a strategy to sculpt, repair and maintain organs and tissues. Furthermore, cell fusion has been implicated in pathological events such as infection and cancer. The formation of a multinucleated syncytium by a virus has traditionally been thought to be limited to infections by enveloped viruses, which encode specialized proteinaceous membrane fusion machinery essential for virus entry. It is unusual, therefore, that the non-enveloped fusogenic reoviruses, belonging to the *Orthoreovirus* and *Aquareovirus* genera, very effectively induce syncytiogenesis. Close investigation of these viruses has attributed this unusual phenotype exclusively to the Fusion-Associated Small Transmembrane (FAST) proteins. The FAST proteins are expressed only in the membranes of host cells upon infection. After trafficking to the plasma membrane, these proteins induce cell-cell fusion, an event thought to be involved in the localized spread of the virus. Since the only known function of the FAST proteins is syncytiogenesis, they serve as an optimal model to study the process of cell-cell fusion and biological membrane fusion in general. The cumulative data presented in this body of work suggests that the FAST protein family can capably sense areas of high membrane curvature and effectively localize to areas of high membrane curvature, namely small extracellular vesicles. Collectively, the work presented in this thesis advances our understanding on the important role of membrane curvature in the membrane fusion pathway and provides insights into the role of both membrane fusogens and cellular proteins in modulating and stabilizing membrane curvature during cell-cell fusion.

This introductory chapter will introduce our current understanding of how cell fusion occurs at a molecular level, and will highlight the importance of membrane fusion from a range of models. A variety of membrane fusion proteins will be described,

including the FAST family of proteins, the model system for the studies conducted herein.

1.2 Cell-Cell Fusion

Cell fusion is the process by which two or more mononuclear cells merge to form a bi- or multinucleated cell, known as a syncytium. A number of different cell-cell fusion events have been studied in varying detail, including the mammalian examples of sperm-egg fusion, trophoblast fusion in the placenta, myoblast fusion, and macrophage fusion. Non-human examples of developmental cell fusion have also been described in *Caenorhabditis elegans*, during formation of tubular networks in *Neurospora crassa*, and during muscle cell development in *Drosophila melanogaster*. This section will outline the general process of cell fusion, using each of these examples. Cell fusion proteins (*e.g.* proteins that are necessary and sufficient to fuse cell membranes) will be presented where they are known; however, these key players remain elusive in many cases.

1.2.1 Sperm-Egg Fusion

Sexual reproduction requires that two gametes fuse to allow union of their genomes. For membrane fusion to occur between the egg and sperm, the sperm must overcome a number of pre-fusion obstacles. The first barrier the sperm must navigate is a thick hyaluronic acid matrix secreted by approximately 3,000 cumulus cells that surround the egg, and it does so through the secretion of specific hydrolases (Lin et al., 1994). Once through this obstruction, the sperm must penetrate the egg's outer coating, the zona pellucida. Interaction of the sperm with the zona pellucida stimulates secretion of enzymes by a specialized lysosome-like compartment in the sperm head called the acrosome (Jin et al., 2011). Exocytosis of the acrosome results in significant remodelling of the sperm cell surface, including a new membrane surface (the inner acrosomal membrane) and a change of morphology (Stein et al., 2004), thereby confering fusion competence. Once through the zona pellucida, the sperm reaches the perivitelline space, and only then can sperm and egg membrane fusion occur. Gene disruption studies have revealed two transmembrane proteins required for sperm-egg fusion in mice: CD9 and Izumo1.

CD9 is a tetraspanin protein expressed on the egg surface. CD9-deficient eggs are fully capable of binding the sperm membrane, but are defective in membrane fusion (Kaji et al., 2000). The exact mechanism of how CD9 may participate in membrane fusion is unclear, however it is hypothesized that this protein could organize a multi-protein fusion complex at the site of sperm-egg binding (Jegou et al., 2011). Knock out of the CD9 gene in mice results in marked loss of fertility, and eggs produced from these animals have altered microvillus architecture on the egg surface (Runge et al., 2007). Immunoelectron microscopy analysis has also revealed that CD9 is incorporated into specialized extracellular vesicles (called exosomes) secreted into the perivitelline space (Miyado et al., 2008). Exosomes bearing CD9 molecules are secreted by the mouse egg just prior to fertilization, suggesting a role in sperm-egg fusion. Furthermore, CD9-deficient mouse eggs do not produce exosomes, implying CD9 plays an important role in exosome production (Miyado et al., 2008). Interestingly, exogenous addition of CD9 egg exosomes rendered sperm capable of fusing with CD9-defieicent eggs (Miyado et al., 2008). It seems therefore, that extracellular CD9 is essential for sperm-egg fusion.

Izumo1, an immunoglobulin type I membrane protein, appears on the sperm cell surface after the acrosome reaction at the anterior head of the sperm where fusion will take place. This protein was elusive for many years but was eventually identified through the use of an inhibiting monoclonal antibody and mice deficient in this gene (Inoue et al., 2005). Izumo1-deficient sperm from are able to penetrate the egg cell surface normally, but are incapable of fusing, causing an accumulation of sperm within the perivitelline space. However, Izumo1 alone cannot promote membrane fusion, suggesting it is not the membrane fusion protein, but is nonetheless an essential factor required for sperm-egg fusion (Inoue et al. 2013). Even though CD9 and Izumo1 are both essential in sperm-egg fusion, there is no evidence of a direct interaction between the two proteins. It is also unknown if other proteins are involved in the CD9/Izumo1 fusion process.

Another protein implicated in gamete fusion is HAP2-GCS1. This fusion factor is broadly conserved in all major eukaryotic taxa except fungi, and is required for fertilization in plants and protists (Wong et al., 2010; Wong and Johnson, 2010). Whether HAP2-GCS1 directly fuses membranes is unclear, although it does function downstream of membrane attachment during gamete fusion in Chlamydomonas and Plasmodium (Liu

et al., 2008). It has been proposed that HAP2-GCS1 represents a key early innovation in in the fusion of gamete plasma membranes in the evolution of sexual reproduction (Wong and Johnson, 2010).

1.2.2 Trophoblast Fusion

The placenta is a transitory organ used for nutrient uptake, gas exchange, and waste elimination between the fetus and the mother. In the placenta of some (but not all) mammals, cytotrophoblasts fuse to form the syncytiotrophoblast. The syncytiotrophoblast is a highly polarized multinucleated cell, juxtaposed between fetal and maternal blood supplies. This multinucleated tissue is critical for the aforementioned functions, as well as antiviral defenses and hormone secretion (Delorme-Axford et al., 2013a; Fuchs and Ellinger, 2004; Pierce and Midgley, 1963). Syncytiotrophoblasts are generated by intercellular fusion of cytotrophoblasts, and throughout pregnancy this highly dynamic syncytium is maintained by the continuous fusion with these mononucleated progenitor cells. Little is known about the proteins or pathways that govern trophoblast fusion, except syncytin (Gong et al., 2007; Mi et al., 2000). Syncytin is a single-pass transmembrane protein that can induce cell-cell fusion when expressed ectopically in cell culture, and is derived from the envelope protein of the endogenous retrovirus HERV-W (Kammerer et al., 2011). Fusion of trophoblasts into synctiotrophoblasts therefore appears to be dependent on capture of a viral protein to facilitate cell fusion. Syncytin has been identified in primates, rodents, rabbits, and canines, suggesting syncytin may be a widely used mediator of cell fusion in the placenta (Esnault et al., 2013; Gong et al., 2007; Heidmann et al., 2009; Cornelis et al., 2012).

1.2.3 Myoblast Fusion

During skeletal muscle development, thousands of myoblast cells fuse together to form the myofiber. Often these cells migrate long distances prior to fusion, and fusion involves two cell types, necessitating proper cell recognition and adhesion to assure accurate and efficient fusion. In addition to the early fusion events that occur during embryogenesis, vertebrate muscle tissue is able to regenerate in response to damage and disease via fusion with satellite cells. Using the *Drosophila*, zebrafish, and mouse

models, multiple essential genes for myoblast fusion have been identified. A unifying feature of these genes is that they play a role in Arp2/3-mediated actin polymerization (Richardson et al., 2007).

In *Drosophila*, muscle fibres form via the fusion of founder cells (FC) and fusion-competent myoblasts (FCM). The fusion interface between the two cells is demarcated by an actin-rich structure, with a thin sheath of actin in the FC, and a thick actin focus in the FCM (Sens et al., 2010). A single podosome with multiple finger-like structures protrudes from this site, rich in immunoglobulin domain-containing adhesive proteins including Kirre and Roughest in FC and Sns and Hibris in FCM, many of which are essential for fusion and are thought to play a role in recognition and adhesion between the two cell types (Galletta et al., 2004). Elegant light and electron microscopy studies revealed these podosomes protrude from FCMs into FCs, with numerous finger-like protrusions extending from the podosome tip to generate what has been called a fusogenic synapse (Chen, 2011; Sens et al., 2010). A number of intracellular signalling proteins are also essential to myoblast fusion including small GTPases and their guanine nucleotide exchange factors, and p21-activated kinases (PAKs) (Duan et al. 2012), all of which are involved in cytoskeletal rearrangements (Brugnera et al., 2002; Chen et al., 2003; Erickson et al., 1997; Hakeda-Suzuki et al., 2002). A role for actin polymerization is consistent with the dynamic nature of the podosome-like structures when observed by live cell imaging (Sens et al., 2010), and with the demonstrated role of PAKs and actin filament assembly during formation of these structures (Duan et al., 2012; Shilagardi et al., 2013). Despite detailed knowledge of the physical architecture of the fusion site, the exact link between actin rearrangements, podosome formation and lipid bilayer destabilization that leads to membrane fusion is still unclear. Membrane curvature and actin-driven close membrane apposition at the tips of the podosome-like structures may contribute to the fusion process (Chen, 2011). The nature of the protein fusogen is also unclear, since none of the currently identified factors directly mediate membrane fusion.

1.2.4 Macrophage Fusion

Homotypic fusion of macrophages occurs in two sites: in bone, where multinucleated osteoclasts mediate bone resorption, and in sites of inflammation, where

multinucleated giant cells form in sites such as tuberculoid lesions. Though macrophage fusion is not required for the expression of osteoclast-like properties, mononucleated osteoclasts have been shown to resorb bone poorly when compared with multinucleated osteoclasts (Yagi et al., 2005). In contrast to the well-defined requirement of multinucleation for osteoclast function, little is known about the functional consequences of giant cell formation. At least for the foreign body giant cells which are formed in host response to foreign material in the body, such as implants, it can be assumed that cell-cell fusion leads to increased cell size and therefore an enhanced capacity to degrade large particles (Zhao et al., 1991). The molecular mechanism of macrophage fusion is still poorly understood but recent data support the hypothesis that the molecular machinery used for osteoclast and multinucleated giant cell formation may at least in part be shared (Helming and Gordon, 2007; Vignery, 2005).

To fuse, macrophages must acquire a fusion-competent status. This fusion program involves enhanced transcription of essential fusion factors and is governed by exogenous stimuli such as M-CSF and RANKL for osteoclasts (Khan et al., 2014; Xing et al., 2012), and IL-4 for giant cells (Lemaire et al., 1996; McNally and Anderson, 1995). In both cases, exposure to the triggering cytokine is believed to upregulate expression of fusion mediators like E-cadherin and CD47, which confer the fusion-competent state (Moreno et al., 2007). Chemotaxis of macrophages towards each other is mediated by the chemokine CCL2 (Kyriakides et al., 2004) and DC-STAMP may also play a role during this process (Yagi et al., 2005). Next, cellular adhesion occurs through engagement of E-cadherin (Moreno et al., 2007) and exposure of the phosphatidylserine to localized areas in the outer leaflet of the plasma membrane (Helming et al., 2009) preceding membrane fusion. Interestingly, MFR and CD47 required for macrophage adhesion and fusion both contain immunoglobulin domains and act as a receptor-ligand pair on opposing membranes, similar to the immunoglobulin-domain proteins which engage during myoblast fusion (Vignery, 2000). Additional surface adhesion may also occur through through β1- and β2-integrins and/or other unknown adhesion factors (Puissegur et al., 2007). Cytoskeletal rearrangements, important not only during fusion but also for formation of the final, functional multinucleated cell, are mediated by the small GTPase RAC1 and guanine nucleotide exchange factor DOCK180 (Jay et al., 2007;

Pajcini et al., 2008). As with myoblast fusion, the identity of the protein, or proteins, which mediate membrane fusion have not been determined.

1.2.5 Cell Fusion in *C. elegans*

Approximately 30% of all somatic cells in *C. elegans* fuse to form a total of 44 syncytia in the pharynx, skin, vulva, hymen, uterus, excretory system, and glands. Genetic screens have identified two proteins that fuse and sculpt cells in this organism – epithelial fusion failure-1 (EFF-1) and anchor cell fusion failure (AFF-1) (Shemer et al., 2004; Sapir et al., 2007). Both EFF-1 and AFF-1 are necessary and sufficient to fuse cells, demonstrated by ectopic expression in insect and mammalian cells and by pseudotyping of enveloped viruses (Podbilewicz et al., 2006; Avinoam et al., 2011). EFF-1 has also been shown to localize at the site of fusion (del Campo et al., 2005). Furthermore, mutations to EFF-1 block membrane fusion completely, at a stage upstream of pore formation (Mohler et al., 2002). Taken together, these data suggests that EFF-1 and AFF-1 proteins are *bona fide* cell-cell fusion proteins.

EFF-1 and AFF-1 are both type I transmembrane glycoproteins that belong to an ancestral family of homotypic cell fusogens (F family) essential for somatic fusion. EFF-1 contains a transmembrane domain and an extracellular hydrophobic peptide, an arrangement reminiscent of the well-characterized enveloped virus fusion proteins and syncytin. Diverse signalling pathways, transcription factors, and vacuolar ATPase proteins precisely control the expression and activities of EFF-1 and AFF-1, ensuring appropriate timing of fusion (Pellegrino et al., 2011; Friedlander-Shani and Podbilewicz, 2011; Kontani et al., 2005). Epidermal cell fusion in *C. elegans* typically initiates between two cells with the formation of one or more fusion pores (Mohler et al., 1998). As the pores expand, small vesicles are shed and are hypothesized to remove membrane material from the fusion site (Mohler et al., 1998; Nguyen et al., 1999).

A newly released crystal structure of EFF-1 reveals that this protein is structurally equivalent to class II enveloped virus fusion proteins (Section 1.3.3 Class II Enveloped Virus Fusion Proteins) (Perez-Vargas et al., 2014). A striking difference is the lack of a hydrophobic fusion loop in the ectodomain of EFF-1. This suggests that despite the high degree of three-dimensional similarity between EFF-1 and class II enveloped virus fusion

proteins, EFF-1 probably has a different mechanism of action that does not involve engagement of the target membrane. Instead, EFF-1 is required in both membranes for fusion and may function via trans-trimerization, analogous to SNARE-mediated fusion. Despite the differences in mechanism of action, this new structure highlights the possible evolutionary link between enveloped viruses and eukaryotic cell-cell fusion, as has been previously demonstrated with the discovery of syncytin.

1.2.6 Cell fusion in *Neurospora crassa* and Yeast

N. crassa colonies comprise a complex network of syncytial hyphae. At least four different cell fusion events occur during the life history of this organism (Fleissner et al., 2008). During colony initiation, germinating spores attract and grow toward each other, fusing to form a cellular network that develops into a mycelial colony. Like cell fusion in other organisms, the process of hyphal fusion requires cell recognition, adhesion, and membrane merger. Genetic analyses have revealed multiple mutants that are unable to fuse. However, with the exception of *Δprm1*, these mutants are defective in stages prior to actual membrane fusion such as competence, cell-cell signalling, or growth (Fleissner et al., 2009; Fu et al., 2011).

Interestingly, *prm1* encoded by *Saccharomyces cerevisiae* is also essential for membrane fusion during yeast mating membrane fusion (Olmo and Grote, 2010). Prm1 has four transmembrane domains and functions as disulphide-linked dimer (Olmo and Grote, 2010). *Δprm1* mating pairs experience one of three fates: arrest as unfused mating pairs with no intervening cell walls, lysis once their plasma membranes come into contact, or fusion. Electron microscopy studies have revealed that the two plasma membranes in an unfused *Δprm1* prezygote were seperated by only ~8 nm but failed to fuse. Additional studies have shown that approximately one third of *Δprm1* mating pairs lyse after membrane contact (Jin et al., 2004). However, almost half of *Δprm1* mating pairs fuse on standard yeast extract-peptone-dextrose (YPD) medium, implying that Prm1 is important, but not required, for fusion (Heiman and Walter, 2000). Furthermore, a surprisingly small amount of Prm1 actually localizes to cell fusion sites, but is nonetheless thought to be functional at these sites (Olmo and Grote, 2010). This protein

may also serve to control membrane organization during cell fusion of mating yeast (Curto et al., 2014).

1.2.7 Summary of Cell-Cell Fusion

Vastly different model systems have contributed to our current understanding of the mechanisms of cell-cell fusion. A unifying theme in all examples presented herein is a procession of cell recognition, intercellular approach, adhesion and finally, membrane merger. Although much is known about the steps preceding the actual membrane merger process, much less is known about the actual membrane fusion step itself or about the proteins required for this step. The discovery of several classes of *bona fide* cell fusogens, including the syncytins and the EFF-1/AFF-1 proteins has drawn comparisons between these endogenous cell fusogens and the well-characterized glycoprotein fusogens made by enveloped viruses (White JM et al., 2008). However, the apparent lack of cell fusogens that resemble enveloped virus fusion proteins in the remaining models of intercellular fusion hints that different strategies may be used to complete the job of membrane merger. Because enveloped viruses contain only a small number of membrane proteins, identification of viral fusion proteins has been relatively easy. As such, they provide the basis for much of our understanding of protein-mediated membrane fusion.

1.3 Enveloped Virus to Cell Fusion

As obligatory intracellular pathogens, viruses must transfer their genome across cellular membranes to initiate an infection that ultimately leads to production of progeny viruses. For enveloped viruses, this necessitates the merger of the virus membrane with target cell membranes and the formation of a fusion pore through which the genome is released. Membrane integrity and compartmentalization is essential for cellular life, therefore, spontaneous membrane fusion does not occur. This problem is circumvented by enveloped viruses through the use of specialized membrane protein complexes that are designed to fuse the virus and target membranes. Much study has been devoted to these proteins, and biochemical, structural, and computational analyses have provided a great deal of insight into this type of membrane fusion. It would seem that all enveloped virus fusion proteins proceed via a common set of structural rearrangements used to drive the

membrane fusion pathway (Harrison, 2008; Plemper, 2011; White JM et al., 2008). First, upon attachment of the virus to a host membrane, massive conformational changes occur within the ectodomain of the enveloped virus fusion protein, which protrudes on the outside of the virion. These changes are triggered either by receptor binding and/or by acidification within the endosome compartment. The enveloped virus fusion protein changes from a native, pre-fusion conformation to an extended intermediate that contains a hydrophobic or amphipathic fusion peptide (FP) at the tip where it can interact with the target cell membrane (Tamm, 2003). Thus, the extended intermediate engages both the target and the virus membranes. The extended intermediate then refolds onto itself to generate a post-fusion, trimeric hairpin structure that positions the FP and transmembrane domain in close proximity at the same end of the hairpin (Armstrong et al., 2000; Reuven et al., 2012). These drastic conformational changes are thought to provide the mechanical energy and membrane curvature changes required to overcome the large energy barrier to pore formation (Chernomordik and Kozlov, 2008; Cohen and Melikyan, 2004). This series of generalized events is illustrated in Figure 1.1.

1.3.1 Classes of Enveloped Virus Fusion Proteins

The different structures of enveloped virus fusion proteins provides the basis for subcategorizing these proteins into at least three, and possibly four, classes (Li and Modis, 2014), enveloped virus fusion proteins share some common features. All contain a single-pass transmembrane domain and relatively small endodomain residing inside the virus particle, with a large, highly structured, multimeric ectodomain projecting outside the virus membrane that contains a moderately hydrophobic FP with membrane-destabilizing attributes. On a structural level, all enveloped virus fusion proteins also form hairpin trimers in their post-fusion states (Figure 1.2). The following sections will discuss what is known about the fusion mechanisms of class I, II, and III enveloped virus fusion proteins. Much of what is known about membrane fusion as a whole has been derived from intensive structural and biophysical studies on these proteins. It is important to note that while there is high-resolution structural data for the pre- and post-fusion structures and some extended intermediate structures, the structural transitions are

inferred from biochemical findings, and how these structural transitions actually promote membrane merger is still speculative.

1.3.2 Class I Fusion Proteins

Representatives of the class I enveloped virus fusion proteins were the first to be crystallized in both the pre- and post-fusion fusion conformations (Wilson et al., 1981; Bullough et al., 1994). Their post-fusion structures feature a prominent alpha-helical coiled coil, a characteristic that is unique to class I fusion proteins (Figure 1.2 A). The fusion proteins from several notable viruses are included in this class: influenza HA, paramyxovirus F, HIV Env, and Ebola GP proteins. All class I proteins are homotrimers that are synthesized as a fusion-incompetent precursor requiring proteolytic cleavage to liberate the N-terminal FP (Chandran et al., 2005; Follis et al., 2006). Often, cleavage is mediated by ubiquitous cellular proteases such as furin endoproteases (Stieneke-Grober et al., 1992) or secreted TMPRSS2 proteins (Hatesuer et al., 2013). Triggering of the mature class I fusion protein can be achieved by an acidic pH (e.g. influenza HA) or through engagement of a receptor (e.g. paramyxoviruses) (Skehel and Wiley, 2000; Smith et al., 2009).

Influenza HA is the founding member of the class I proteins, and to date remains the best characterized. HA is produced as a precursor protein (HA0), which is cleaved into receptor binding (HA1) and fusion (HA2) subunits, which remain linked via disulphide bonds. HA1 binds sialic acid on the cell surface, allowing the virus to be internalized through the endosomal pathway. The acidic pH in the endosomal compartment triggers conformational changes which drive membrane fusion (Skehel et al., 1982). The pre-fusion form of HA sits on the virion surface as a trimer, with its N-terminal FP protected in the trimer interface and the C-terminus extending toward the transmembrane domain (Wilson et al., 1981). There are three longer central helices and three shorter outer helices, which all pack together. Acidification results in protonation of key residues in HA1 and HA2, thereby unclamping the coiled coils. Two major structural changes occur to promote membrane fusion: FP extension and C-terminal inversion, thereby poising the FP for interaction with the target membrane (Bullough et al., 1994). The C-terminal region is then thought to undergo a fold-back event, forming the final

hairpin structure with a six-helix bundle characteristic of the class I fusogens. The final post-fusion structure is superficially reminiscent of the pre-fusion state, although with several notable differences in the arrangement and length of the alpha-helices and connecting loops (White et al., 2008).

1.3.3 Class II Fusion Proteins

Class II enveloped virus fusion proteins are structurally and evolutionarily distinct from the prototypical class I proteins. They are found in *Flaviviridae* viruses such as dengue and yellow fever, and alphaviruses such as Semliki Forest virus. High-resolution crystal structures have also been elucidated for class II proteins in the pre- and post-fusion states (Gibbons et al., 2003; Lescar et al., 2001; Wengler et al., 1999). These structures show that although there are differences in the protein folds and stoichiometry between class I and II proteins, both classes use the same general topology and physical strategy to drive membrane fusion. Several major differences for class II fusion proteins include: a dimeric stoichiometry in the pre-fusion state, an internal 'fusion loop' instead of a terminal FP, and unlike influenza HA, which undergoes major extensive refolding, class II fusion proteins retain most of their folded structure during fusion, instead flexing at linker regions. Finally, class II proteins are rich in beta-sheets, unlike the predominantly alpha-helical class I proteins (Figure 1.2). Upon triggering through acidification of the endosome, the dimeric class II fusion complex transiently dissociates and domains adjacent to the transmembrane domains and fusion loops are rotated into a position perpendicular to the viral and target membrane. The proteins are then reorganized into a trimeric complex, whereby the pre-hairpin intermediate refolds onto itself, bringing the transmembrane domains and fusion loops in close proximity (Gibbons et al., 2003).

1.3.4 Class III Fusion Proteins

Class III fusion proteins include glycoprotein B of herpesviruses, the G protein of vesicular stomatitis virus, and gp64 of baculovirus. Examination of native G trimers has revealed a tripod-like structure, consisting of four domains with a mix of alpha-helices and beta-sheets (Roche et al., 2007). The fusion loops are bipartite, comprising two

hydrophobic loops positioned at the tip of an elongated three-stranded □eta-sheet present in each monomer, pointing toward the virus envelope. Only domain III undergoes major conformational changes during fusion, which is pH triggered. The tripod legs swing upward, driving the fusion loops toward the target membrane (Roche et al., 2006). Repositioning of the domains ultimately results in a classic hairpin post-fusion conformation. In striking contrast to class I and II fusion proteins, G protein refolding is reversible. There is also evidence that the trimers dissociate into monomeric intermediates during the structural transitions that accompany the fusion reaction (Albertini et al., 2011).

1.3.5 Class IV Fusion Proteins

In 2013, the structures of the E2 membrane fusion proteins from pestivirus and hepatitis C virus, both flaviviruses, were unexpectly found to have distinctive, novel folds compared to all other classes of enveloped virus fusion proteins, even other flavivirus members, which have class II membrane fusion proteins (Li et al., 2013; El Omari et al., 2013; and Kong et al., 2013). It has been proposed, therefore, that these proteins belong to a new class of membrane fusion proteins (Li and Modis, 2014). The structures of the E2 proteins from these viruses reveal a novel architecture consisting of two immunoglobulin-like domains followed by a unique elongated domain and a membrane anchor, with the overall fold and topology differing significantly from all previously determined protein structures of enveloped virus membrane fusion proteins. Since these new E2 structures lack structural characteristics of other classes – a hydrophobic FP (all classes), a helical core (class I and III), and a flexible, multidomain architecture (class II and III) – they have tentatively been classified as class IV fusion proteins (Li and Modis, 2014). These new structures provide a striking example of how structurally divergent viral membrane fusion proteins can be, even within a single virus family.

Several outstanding questions remain regarding this new class of membrane fusion proteins. First, do the E1 proteins (which associate as a dimer with E2 proteins) from pestiviruses and hepatitis C viruses contain the same pattern of folding as the E2 proteins or do they resemble class II membrane fusion proteins? Second, what is the molecular mechanism of membrane fusion in pestiviruses and hepatitis C viruses? Does it

involve a similar extension, target membrane engagement, and foldback as the other classes of membrane fusion proteins? Third, what are the dynamics between the E1 and E2 proteins, and how do these associations relate to fusion? Uncovering the answers to these questions will be essential going forward to fully understand which structural features are essential for induction of virus to cell fusion.

1.3.6 Summary of Enveloped Virus Fusion Proteins

There are four basic principles that appear to be common in all studied examples of enveloped virus membrane fusion: (1) The pre-fusion conformer of the enveloped virus fusion protein is located in a single membrane (i.e. the virus membrane); (2) fusion must be triggered by receptor binding, exposure to an acidic pH, or a combination of both; (3) fusion-competent complexes undergo extensive conformational changes which serve to expose the FP for insertion into the target membrane; and (4) fold-back leads to a remarkably similar trimeric hairpin structure for all classes, which brings the FP and the transmembrane domain into the same lipid environment. A model summarizing points (3) and (4) is diagrammed in Figure 1.1. While refolding of the protein into a hairpin structure is theorized to provide a mechanical pulling force that bends the membranes and thus primes them for fusion, the actual mechanism may not be this simple. For example, formation of the hairpin structure may not be sufficient for membrane merger (Borrego-Diaz et al., 2003; Park et al., 2003). Furthermore, the pulling forces that the fusion proteins can exert is limited by the strength of membrane tethering by the FP. If binding is weak, as might be the case for these short and moderately hydrophobic motifs, the force of hairpin-formation would detach the FP anchors from the target membrane. From this perspective, a concerted action from many fusion units may be required for the short FPs found in VSV G protein (Roche et al., 2006). In addition, some studies suggest pore formation precedes formation of the final, post-fusion trimeric hairpin conformation (Markosyan et al., 2003), while others indicate the final trimeric hairpin structure can itself promote membrane fusion (Kim et al., 2011), raising questions regarding the actual role of fusion protein conformational changes in the fusion process.

In summary, while the textbook model of enveloped virus-mediated membrane fusion has been widely accepted, this model should be viewed as a working model that needs to be revised as more structural and molecular details are discovered.

1.4 Lipid Dynamics During Membrane Fusion

While X-ray crystallography has provided atomic-level details on the structures of pre- and post-fusion conformations of enveloped virus fusion proteins, much less is known about the molecular details of lipid merger. Theoretical and experimental studies of membrane fusion intermediates from diverse membrane fusion models, including those from virus-to-cell fusion (Section 1.3) and cell-to-cell fusion (Section 1.2), have converged on a common pathway of lipid remodelling during membrane fusion. A universal five-step pathway has been described: (1) membrane approach; (2) close membrane apposition (by dimpling or other membrane deformations); (3) mixing of only proximal leaflets of the membrane (hemifusion) with no aqueous content mixing; (4) merger of the distal leaflets resulting in micropore formation and aqueous content mixing; and (5) pore enlargement (Chernomordik and Kozlov, 2003). This model is diagrammed in Figure 1.3. Implicit in this model is the idea that protein fusogens impart stresses in the membrane that must be resolved through membrane fusion.

1.4.1 Membrane Approach and Close Apposition

Biological membrane fusion begins with two bilayers initially separated by a sizable gap. Opposing membranes tethered at adherens junctions are separated by an estimated 10-25 nm (Oda and Takeichi, 2011), however in order for fusion to occur, the membranes must be brought within less than 3 nm (Chernomordik and Kozlov, 2003). In computational models when bilayers are brought within 1 nm, fusion becomes energetically favourable due to relaxation of short-range water-mediated repulsion (Kozlovsky et al., 2004). In order to bring biological membranes into extreme close proximity, a localized area must be depleted of protein, potentially through a process of molecular sieving (Chernomordik et al., 2006; Martens and McMahon, 2008). These protein-free patches must then be brought together to form an intimate area of contact between the bilayers to be fused.

Several strategies have been suggested to facilitate this area of close contact in protein-mediated fusion. It has been proposed that the critical step in the initiation of lipid rearrangements by fusion proteins consists in local bending of the bilayer into small protrusions often referred to as 'dimples' or 'nipples' (Chernomordik et al., 2006; Kuzmin et al., 2001). These localized areas of extreme membrane curvature are protein-depleted. Furthermore, the tips of these protrusions are highly stressed and demarcated with lipid packing defects, and therefore primed for spontaneous fusion to relieve the energy penalty of such extreme curvature (McMahon et al., 2010). It is becoming increasingly more accepted that FPs may serve as a wedge, partially penetrating the outer leaflet of the membrane bilayer to the depth of the lipid glycerol backbone. Since this is the most rigid part of the membrane, it acts as a fulcrum through which the FP insertion can force apart lipid headgroups to generate positive membrane curvature (i.e. the outer leaflet bulges outward) and dimple formation (Martens and McMahon, 2008). Since FPs are only partially hydrophobic, their insertion must be shallow, consistent with the wedge mechanism used by curvature-generating proteins such as the C2 domains of synaptotagmin, which use hydrophobic loops in an analogous manner (Fuhrmans and Marrink, 2012; McMahon et al., 2010). However, other studies suggest fusion peptides may insert deeper into the bilayer, forcing apart acyl changes to generate negative curvature required for promotion of hemifusion (Lai and Freed, 2014; Qiang et al., 2009). Regardless of the actual mechanism, the concept that membrane fusion involves curvature changes that lead to membrane protrusion is supported by the observation of small protrusions on liposomes or cells studded with HA proteins (Frolov et al., 2000; Kanaseki et al., 1997). These dimples are thought to be bi-functional, bringing the membranes closer together but also loading the membrane with sufficient energy (due to unfavourable bending) to drive hemifusion and fusion pore formation.

1.4.2 Hemifusion Intermediate

Hemifusion structures represent connections between proximal leaflets of fusing membranes, with distal leaflets remaining distinct and no aqueous connection (Chernomordik and Kozlov, 2008). Functionally, this has been measured as lipid mixing in the absence of content mixing. Most, if not all, protein-mediated membrane fusion is

thought to use a hemifusion intermediate, including exocytic membrane fusion (Xu et al., 2005), viral membrane fusion (Chernomorkdik and Kozlov, 2005), and cell-cell fusion (Podbilewicz et al., 2006; Sapir et al., 2008). Although the definition of a hemifusion intermediate is straightforward, the experimental verification and characterization has not proved as simple, due to the small size and transient nature of this intermediate. While initial theoretical studies suggested formation of a hemifusion stalk would require considerable energy to form, newer estimates using a point-like protrusion for membrane contact suggest considerably less energy may be required to form this interemediate due to the limited area of membrane contact (Kuzmin et al., 2001; Cohen and Melikian, 2004).

1.4.3 Fusion Pore Formation and Expansion

Hemifusion and pore formation are thought to be two significant kinetic barriers that must be overcome in order to fuse two membranes. Experimental evidence and theory converge on the idea that these two hurdles are progressively more energy-demanding, with initial stages having a relatively low energy barrier, and later stages, namely pore formation and pore expansion, accruing the highest energy cost (Cohen and Melikyan, 2004). The molecular mechanism of transition from a hemifused state to a stable pore is largely unknown.

A fusion pore results from the merger of both the proximal and distal leaflets of the fusing membranes, resulting in an aqueous connection between the two cytosols that were initially separated by the apposed membranes. Experiments show that pore formation does not readily occur either in a single bilayer or within the hemifusion diaphragm (Chernomordik et al., 1987; Markosyan et al., 2000). Appreciable external forces are required to rupture the hemifusion intermediate (Melikyan et al., 1997). It has been suggested that the extensive conformational changes in the ectodomains of SNARE and enveloped virus fusion proteins result in a tilting of the transmembrane domain, which in turn imparts stress on the fusing membrane, leading to a rupture of the hemifusion intermediate and pore formation (Knecht and Grubmuller, 2003; Kozlov and Chernomordik, 1998). Alternatively, the lipid rearrangements required for pore formation may also arise via specific FP and transmembrane domain interactions, which facilitate a

deepening of the insertion of the FP that forces the rupture of the hemifusion intermediate (Chang et al., 2008; Tamm, 2003). Once formed, the stability of the fusion pore is still not assured, because the extreme curvature of the membrane is highly unfavorable (Zhang and Jackson, 2010), and studies on the nature of the fusion pore have revealed that fusion pores are subject to opening and closing (Chanturiya et al., 1997). For the most part, the role of proteins in stabilizing this highly stressed lipidic intermediate is largely unknown.

Once the initial micropore has formed, it must expand to allow the passage of cytosol, organelles, and a nucleus in the case of cell-cell fusion. Mechanisms of pore expansion are largely uncharacterized. Pore expansion in cells seems to require cellular metabolism and is restricted by the actin cytoskeleton (Chen et al., 2008; Richard et al., 2009). It appears that pore expansion at the late stages of cell-cell fusion is promoted, either directly or indirectly, by intracellular curvature-generating proteins such as dynamin, epsin N-terminal homology (ENTH)-domain proteins or Bin/amphiphysin/Rvs (BAR)-domain proteins (Richard et al., 2011).

1.5 Fusogenic Reoviruses

Historically, the name reovirus was termed ‘respiratory, enteric orphan’ virus, since the first isolates were derived from gastrointestinal and respiratory tracts and were not associated with disease. The family *Reoviridae* is a diverse family of non-enveloped, 60-90 nm diameter icosahedral viruses with segmented, dsRNA genomes. Isolates from two genera within the *Reoviridae* family, *Orthoreovirus* and *Aquareovirus*, encode non-structural fusion-associated small transmembrane (FAST) proteins. These proteins, whose only known function is to induce syncytiogenesis, are thought to increase intercellular spread of the virus by fostering syncytium formation and release of virions via cytopathic effects associated with syncytium formation. Since FAST proteins are non-structural, they play no role in entry of the virus, giving them a completely different job description than enveloped virus fusion proteins, whose primary function is to induce virus-cell fusion to promote virus entry. Accumulating evidence suggests that the fusogenic reoviruses may have adopted the FAST proteins as a unique virulence factor aiding in pathogenesis and viral dissemination.

A number of diverse reoviruses have been found to encode functional FAST proteins. These FAST proteins, named as per their molecular weight, include: the homologous p10 proteins from avian (ARV) and bat reoviruses, such as Nelson Bay reovirus (NBV) (Shmulevitz and Duncan, 2000), p15 from baboon reovirus (BRV) (Dawe and Duncan, 2002), p14 from reptilian reovirus (RRV) (Duncan et al., 2004), p13 from Broome reovirus (BroRV), another bat reovirus isolate (Thalmann et al., 2010), and the p16 and p22 FAST proteins from aquareoviruses (AqRV) (Racine et al., 2009). These proteins are the smallest known autonomous fusogens and are both necessary and sufficient to induce membrane fusion in cell-to-cell and *in vitro* liposome models (Top et al., 2005). All members of the FAST family assume a type I topology in the host plasma membrane, with a single transmembrane domain separating a small N-terminal ectodomain of 20-41 residues and a proportionally larger C-terminal endodomain of 36-141 residues (Figure 1.4). The small size of the FAST ectodomains and their unusual asymmetric membrane topology, with the majority of their mass contained with the transmembrane domain and endodomain, poignantly contrasts with enveloped virus fusion proteins, suggesting a different mechanism of action. Unlike enveloped virus fusogens, the cytosolic FAST protein endodomains are well positioned to take advantage of cellular pathways to help drive the fusion reaction.

The accepted model of large conformational changes providing mechanical energy to draw membranes together and force fusion may not be correct for FAST proteins. First, unlike enveloped virus fusion proteins, FAST proteins show no receptor-binding capacity and are non-triggered. Second, in contrast to enveloped virus fusion proteins, whose first job is to draw the two membranes to be fused close together, the FAST proteins use surrogate cadherin proteins to accomplish this task (Salsman et al., 2008). Third, a hemifusion intermediate cannot be detected in FAST protein-mediated fusion using standard assays used to detect fusion intermediates induced by enveloped virus fusion proteins (Clancy et al., 2010). These results suggest the possibility that the nature of the fusion intermediates or the mechanisms used to transit through the various stages of the fusion reaction may differ between these distinct classes of viral fusogens and may therefore provide novel insights on the procession of cell-cell fusion.

1.5.1 Reptilian Reovirus p14

Originally isolated from pathogenic python reovirus isolates (Duncan et al., 2004), RRV p14 is a small 14 kDa cell surface-localized membrane protein, which utilizes an internal reverse signal-anchor sequence to direct an N_{exo}/C_{cyto} membrane topology. This topology results in the co-translational translocation of a small, myristoylated ectodomain across the bilayer (Corcoran and Duncan, 2004). Mutational analyses and *in vitro* lipid mixing assays using a synthetic peptide of the p14 ectodomain have revealed the N-terminal myristic acid is essential for membrane destabilization and cell-cell fusion (Corcoran et al., 2004). Aside from the transmembrane domain, the only region of p14 that possesses any hydrophobic character is a short region in the 38-residue ectodomain, which has been characterized as a FP, critical for *in vitro* lipid mixing and syncytiogenesis (Corcoran et al., 2004). Structural data indicate a non-myristoylated version of the p14 ectodomain consists of an N-terminal extended loop, flanked by two proline hinges, while the remaining two thirds of the ectodomain is disordered (Corcoran et al., 2004). In addition to its membrane destabilization properties, the p14 ectodomain also serves as a homo-multimerization motif for p14 (Corcoran et al., 2011).

The 19-residue transmembrane domain of p14 is also directly involved in membrane fusion, essential for both pore formation and syncytiogenesis (Clancy and Duncan, 2009). Interestingly, p14 maintains functionality when its own transmembrane domain is replaced with that of p10 or p15 FAST proteins, suggesting that this portion of the p14 FAST protein functions in a sequence-independent, modular fashion (Clancy and Duncan, 2009). Recent structural analyses indicate the p14 transmembrane domain also assumes a unique arced architecture (Muzaddid Sarkar, unpublished data).

The endodomains of all FAST proteins contain a membrane-proximal cluster of basic residues, although the primary sequence of this region varies between isolates. Recent studies indicate these residues are essential in p14 for trafficking through the ER-Golgi secretory route and that an autonomous, tribasic Golgi signal directs the trafficking of p14 from the Golgi to the plasma membrane (Parmar et al., 2014). Truncation studies have also revealed that the membrane-distal portion of the p14 endodomain is a positive effector of pore formation, pore expansion, and syncytiogenesis (Barry and Duncan, 2009), an unusual attribute for membrane fusion proteins since the cytoplasmic tails of

most enveloped virus fusion proteins either play no role or are inhibitory in membrane fusion.

Intriguingly, a small percentage of the p14 endodomain is also cleaved, likely via intramembrane proteolysis (Top et al., 2009). This soluble fragment has been shown to function in *trans* to enhance fusion pore expansion in diverse cell-cell fusion models including FAST-mediated cell-cell fusion, hemagglutinin-mediated syncytiogenesis, and fusion of C2C12 cells (Top et al., 2009), suggesting the p14 endodomain activates signaling pathways which are common to diverse cell-cell fusion events. The endodomain is also expected to interact with numerous cellular proteins, as over 80 genetic interaction partners have been revealed with yeast-two hybrid technology (Julie Boutlier, unpublished data). Indeed one such partner, annexin A1, was shown to intereact with p14 in a direct, calcium-dependent manner and annexin A1 was recently confirmed as an essential positive-effector of pore expansion in FAST- and measles-mediated fusion (Ciechonska et al., 2014).

Finally, p14 proteins function from a subset of heterogeneous, detergent-insoluble membrane microdomains (Corcoran et al., 2006), which may be required for forming areas of close membrane-membrane contact and provide a lipid composition that is suitable for membrane fusion. Taken together, p14 has strict sequence requirements in the ecto-, endo-, and transmembrane domains, and membrane fusion is contingent on the cooperation of all of these domains.

1.5.2 Baboon Reovirus p15

BRV was originally isolated from baboons housed at Southwest National Primate Research Center who suffered from meningoencephalomyelitis (Duncan et al., 1995), and more recent studies suggest that most cases of meningoencephalomyelitis among baboons housed at this facility are related to BRV infection (Kumar et al., 2013). BRV is a fusogenic reovirus, and thus encodes a FAST protein, found in the S4 genome segment (Dawe and Duncan, 2002). The BRV p15 FAST protein features an N-terminal myristoylation site, an N-proximal proline-rich motif, a single-pass transmembrane domain, a membrane-proximal polybasic motif, and a cytosolic hydrophobic patch in the endodomain (Dawe and Duncan, 2002). Like p14, the N-terminal myristic acid is

required for lipid-mixing and cell-cell fusion (Top et al., 2012). The ectodomain of p15, however, is unlike all other FAST proteins: it is extraordinarily small (a mere 19 residues) and has a short, essential polyproline tract. Structural and biochemical analyses indicate that the p15 ectodomain forms a polyproline type II helix and functions as an atypical FP, which displays an unusual delay in membrane fusion, correlating with massive liposome aggregation (Top et al., 2012). Therefore, the interaction of the p15 ectodomain with liposome membranes induces a biphasic membrane fusion reaction, whereby peptide-induced liposome aggregation is a rate-limiting event that precedes membrane merger.

The transmembrane domain of p15, unlike p14, is not interchangeable with heterologous transmembrane domains from other FAST proteins (Clancy and Duncan, 2011). A series of point mutations have also revealed the essential nature of helix-breaking, β-branched amino acids (such as isoleucine, leucine, and valine), as well as glycine and serine residues directly in membrane fusion (Clancy and Duncan, 2011).

Analysis of the p15 endodomain has been limited. Elegant topographical studies have confirmed the hydrophobic patch in the p15 endodomain, which was originally predicted to function as a second transmembrane domain, is not a membrane-spanning domain (Dawe et al., 2005). The role of the hydrophobic patch, or other regions of the p15 endodomain in cell-cell membrane fusion is unclear at this time.

1.6 Objectives

Generation of bilayer curvature is thought to be an intrinsic part of membrane fusion. However, the details of how fusion proteins induce and/or stabilize membrane curvature are currently unclear. The objective of this work was to investigate the role of membrane curvature in cell-cell fusion using the minimalist FAST proteins as a model.

In Chapter 3, my goal was to investigate the role of an unusual cytoplasmic hydrophobic patch (HP) in the endodomain of BRV p15. Using mutagenic and biophysical approaches, I was able to demonstrate that the p15HP functions as a novel membrane curvature-sensing motif, a role not yet ascribed to any membrane fusion protein. I also determined that under the correct lipid to peptide ratios, the p15HP was also capable of destabilizing lipid bilayers. Since this motif is able to both sense

membrane curvature and destabilize membranes under the correct conditions, I coined the term fusion-inducing lipid-packing sensor (FLiPS) to describe this new fusion motif. Although my studies were limited to the FAST proteins, it is possible that other membrane fusion proteins employ similar mechanisms that have yet to be discovered.

In Chapter 4, my goal was to determine if FAST proteins were trafficked to extracellular vesicles. Several lines of evidence suggested this might be the case, and using the p14 FAST proteins I was able to demonstrate p14 upregulates formation of extracellular vesicles and is incorporated in these vesicles. Several approaches, including quantitative mass spectrometry, confirmed these vesicles share many of the attributes of exosomes, and additional approaches indicated a role for Tsg101 in recruiting p14 to exosomes. Furthermore, I determined that p14 exosomes are fusogenic, and interfering with exosome production inhibited p14-induced cell-cell fusion, implying p14 exosomes are functionally relevant to syncytium formation.

Taken together, this work provides important new insights into the interaction of the FAST proteins with highly curved membrane geometries, whether that be the FLiPS motif interacting with a nascent fusion pore or the trafficking of FAST proteins to small, highly curved extracellular vesicles.

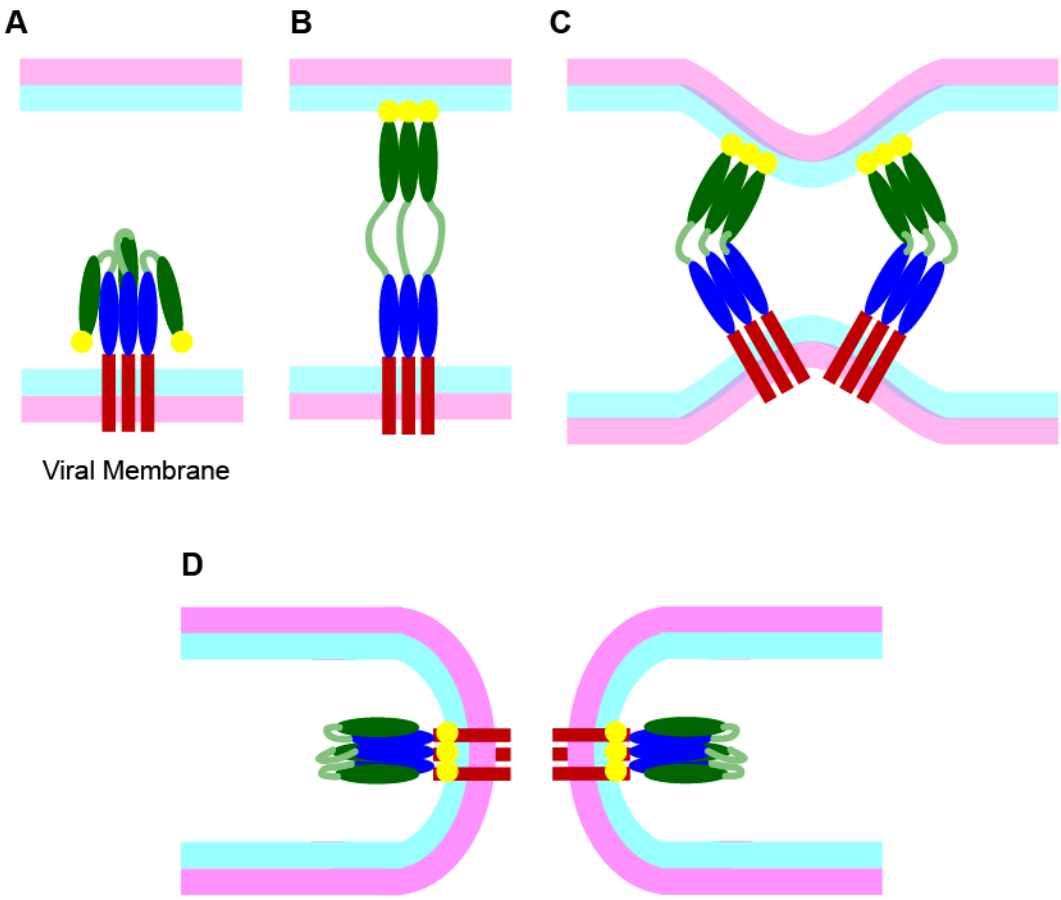

Figure 1.1 Conformational changes of enveloped virus fusion proteins that drive membrane fusion. (A) A fusion-competent enveloped virus fusion protein sits in a metastable conformation in the virus membrane. **(B)** After triggering (receptor binding or endosomal acidification), the fusogen undergoes extensive conformational changes into an extended conformation. The fusion peptide (yellow circle) engages the target membrane. **(C)** Collapse of the extended intermediate pulls the virus and target membranes together. **(D)** Formation of a fusion pore coincides with hairpin formation. Both the fusion peptide and the transmembrane domain (pink rod) sit in the same membrane.

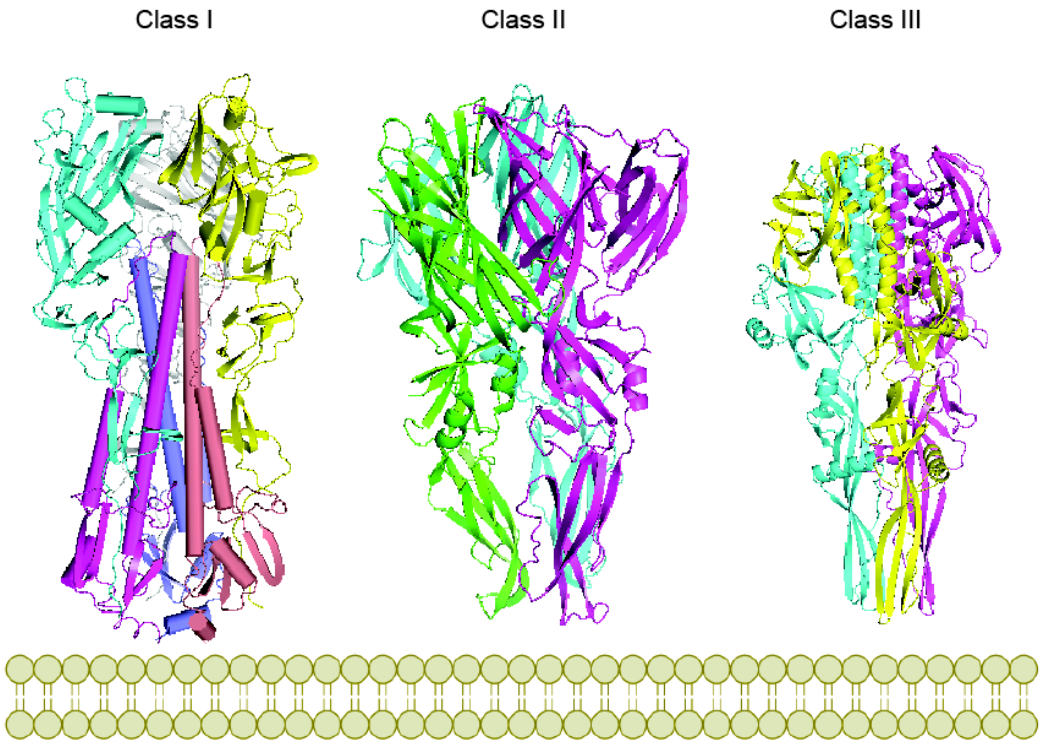

Figure 1.2 Post-fusion conformations of enveloped virus membrane fusion proteins. Ribbon diagrams of representative class I, II, and III enveloped virus fusion proteins, positioned with respect to the lipid bilayer. Images were rendered from PDB structure files using MacPyMOL v1.3. Class I - Influenza hemagglutinin (PDB ID: 3QQO), Class II - Tick-borne encephalitis virus envelope glycoprotein E (PDB ID: 1URZ), and Class III - Vesicular stomatitis virus glycoprotein G (PDB ID 2CMZ).

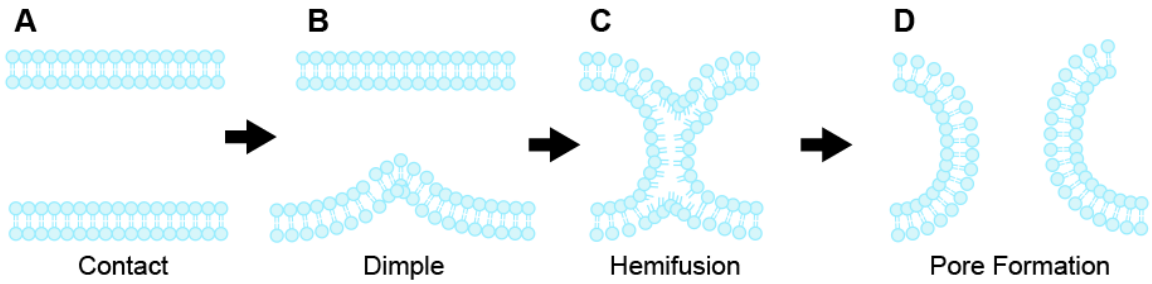

Figure 1.3 Intermediates of lipid bilayer fusion. (A) Pre-fusion contact between apposing lipid bilayers. **(B)** Formation of a point-like protrusion in a single lipid bilayer minimizes the energy of hydration repulsion between the apposing bilayers and brings the bilayers into close contact. **(C)** Formation of a hemifusion stalk results in mixing of proximal leaflets of the bilayer. **(D)** Formation of a fusion pore results in mixing of both leaflets of the membrane and aqueous contents.

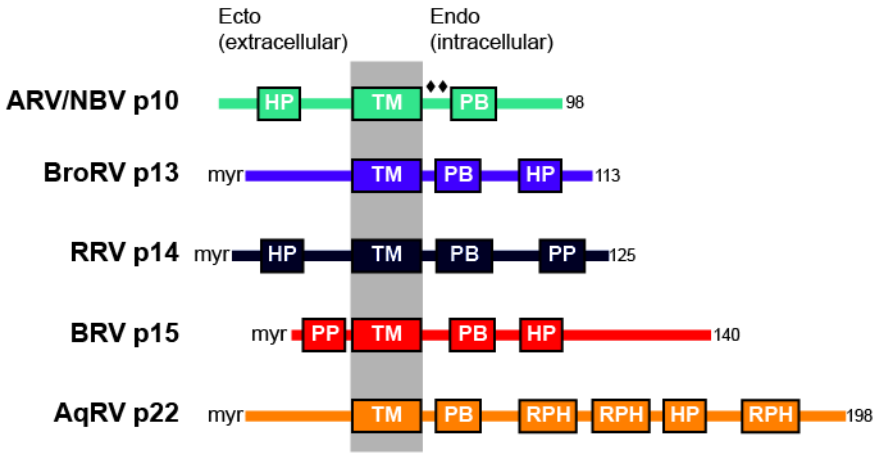

Figure 1.4 The FAST family of cell fusion proteins. Schematic representation of avian reovirus (ARV), Nelson Bay reovirus (NBV), Broome reovirus (BroRV), reptilian reovirus (RRV), baboon reovirus (BRV), and aquareovirus (AqRV) FAST proteins depicting the endo-, transmembrane (TM), and ectodomains and their distribution across the plasma membrane (grey box). Numbers indicate the number of the C-terminal amino acid. Hydrophobic patch (HP), dipalmitic acid (♦♦), polybasic cluster (PB), N-terminal myristic acid (myr), polyproline sequence (PP), and arginine/proline/histidine-rich sequence (RPH).

CHAPTER 2
MATERIALS AND METHODS

2.1 Cells

All cells were maintained at 37°C in a 5 % CO_2 atmosphere. Cells were grown in 175 cm^2 or 225 cm^2 vented flasks and were propagated to a maximum confluency of 90%. Cells were subcultured every 2 to 3 days with trypsin-EDTA dissociation reagent (Gibco). The continuous quail fibroblast line (QM5) was maintained in medium 199 with Earle's salts (Gibco) supplemented with 10% heat-inactivated fetal bovine serum (FBS). Vero cells were grown in medium 199 with Earle's salts supplemented with 5% heat-inactivated FBS. Human fibrosarcoma (HT1080) and human embryonic kidney (HEK) 293T cells were maintained in Dulbecco's Modified Eagle Medium (DMEM) supplemented with 10% heat-inactivated FBS. Cell culture medium for HEK393T cells was also buffered with supplemental HEPES (final concentration of 25 mM).

2.2 Antibodies

Rabbit polyclonal antisera raised against p14 (anti-p14) was described previously (Corcoran and Duncan, 2004). Rabbit antiserum against the p14 ectodomain (residues 5 to 31) was prepared by New England Peptide (anti-p14ecto). Polyclonal rabbit antisera against the p15 endodomain, residues 90 to 140 (anti-p15C) was described previously (Dawe et al., 2005). All other antibodies are available commercially: GFP (Sigma, N-terminal), actin (Sigma), CD81 (Santa Cruz Biotechnology, Inc., 5A6), annexin A1 (Santa Cruz Biotechnology, Inc., EH17a), TSG101 (Santa Cruz Biotechnology, Inc., sc-136111), protein disulphide isomerase (Abcam, ab31811), FLAG (Sigma, M2), Rab 11 (Invitrogen, 3H18L5), transferrin receptor (Zymed Laboratories Inc.), and caveolin-1 (Santa Cruz Biotechnology, Inc., N-20). Goat anti-rabbit and goat anti-mouse horseradish peroxidase-conjugated antibodies (Jackson ImmunoResearch) were used for immunoblotting at 1:10,000 dilution. Goat anti-rabbit secondary conjugated to 10 nm gold particles (Abcam) was used for immunogold staining.

2.3 Cloning and Plasmids

2.3.1 Vectors

All FAST proteins were cloned into pcDNA3 mammalian expression vectors (Invitrogen) as previously described (Corcoran and Duncan, 2004; Dawe et al., 2005; Shmulevitz and Duncan, 2000), with an optimized translational start site using the Kozak consensus sequence (GCACGATGG). Human TSG101 was kindly provided by Dr. Julie Boutilier (Dalhousie University). The human transferrin receptor construct, generously provided by C. Parish (Cornell University), was subcloned into pcDNA3. All constructs were sequenced in the forward and reverse direction, using T7 promoter and SP6 sequencing primers, respectively, to confirm nucleotide sequence before use in experiments (MCLAB). For constructs greater than 800 base pairs, additional custom internal sequencing primers were used.

2.3.2 Site-Directed Mutagenesis

The QuikChange site-directed mutagenesis kit (Agilent Technologies) was used according to manufacturer's recommendations to generate all point-mutants of p15, using pcDNA3-p15 as a template and custom oligonucleotide primers (IDT Technologies).

2.3.3 p15 Chimeras

A previously described gene splicing technique was used to generate p15 chimeric proteins (Heckman and Pease, 2007). Briefly, two PCR products representing the nucleotide sequences upstream and downstream of the p15HP were amplified with complementary overhang regions representing the chimeric amphipathic helix to be inserted. PCR-mediated overlap extension was then used to generate the full-length chimeric p15 protein. The p15HP (residues 68-87; LGLLSYGAGVASLPLLNVIA) was replaced with the amphipathic helix motif from human ArfGAP1 (residues 199-223; FLNSAMSSLYSGWSSFTTGASKFAS), yeast Kes1p (residues 7-29; SSSWTSFLKSIASFNGDLSSLSA), yeast Vps41 (residues 359-376, TTNIGSLLSSAASSFRGT), human BRAP/BIN2 (residues 16-34, QVQKKFSRAQEKVLQKLGK), honeybee melittin (residues 1-25,

GIGAVLKVLTTGLPALSWIKRKRQQ), or *Bacillus subtilis* DivIVA (residues 21-41, EVNEFLAQVRKDYEIVLR).

2.4 DNA Transfections and Syncytial Indexing

Subconfluent monolayers seeded in multi-well plates or experimental dishes were transiently transfected with polyethylenimine (PEI; Polysciences Inc.). Plasmids encoding the gene of interest (0.5 μg per well of a 12-well plate) were added to 100 μL OptiMEM (Gibco) containing 3 μg PEI. The transfection mixture was added directly to 400 μL of serum-free growth medium. Transfection volumes were scaled according to surface area for larger or smaller vessels. At 4 to 6 hours post-transfection (hpt), the transfection medium was aspirated and replaced with complete growth medium. Cells were fixed at indicated times with methanol and Wright-Giemsa stained (Siemens Healthcare Diagnostics). Images were captured on a Nikon Diaphot TMD inverted microscope using the 20x objective. Fusogenicity of various constructs was determined by averaging the number of syncytial nuclei from five random fields of view from three separate experiments. Results are reported as the number of syncytial nuclei per field of view ± SEM.

2.5 Immunoblotting

Protein samples in 1x Laemmli sample buffer were heated to 90°C for 5 minutes then loaded on Tris-glycine 10, 12.5, or 15% polyacrylamide gels (Laemmli, 1970). Gels were electrophoresed at 170V for one hour using Mini-Protean III cells (BioRad) and transferred to polyvinylidene difluoride (PVDF) membranes using a wet transfer apparatus (BioRad) at 100V for one hour. Membranes were blocked in 5% (w/v) non-fat skim milk powder in Tris-buffered saline with Tween-20 (TBS-T; 150mM NaCl, 20mM Tris, pH 7.6, 0.1% Tween-20). Blots were probed with the indicated primary antibodies diluted in 3% non-fat skim milk in TBS-T for either one hour at room temperature or overnight at 4°C. Membranes were washed extensively with TBS-T, and probed with horseradish peroxidase-conjugated secondary antibodies. Blots were developed with ECLplus detection reagent (GE Healthcare) after extensive washing with TBS-T. Images were captured on a Kodak 4000 mm Pro CCD imager.

2.6 Synthetic Peptides

All peptides were synthesized by Dalton Chemical Laboratories, Inc. (Toronto, ON) and purified to >95% purity. Sequences are as follows: p15HP (authentic): acetyl-LGLLSYGAGVASLPLLNVIA-amide and p15HP (scrambled): acetyl-VLAPGLNALSLGVLASLIYG-amide. Peptides were stored at -80ºC as a lyophilized powder until use. Stock solutions were prepared in sterile dimethyl sulfoxide (DMSO; Sigma) and were used within one week.

2.7 Liposome Assays

2.7.1 Preparation of Liposomes

Liposomes were prepared as previously described (Read and Duncan, 2011). Briefly, lipids dissolved in chloroform were mixed in a 1:1:1 molar ratio of 1,2-dioleoyl-*sn*-glycero-3-phosphocholine (DOPC), 1,2-dioleoyl-*sn*-glycero-3-phosphoethanolamine (DOPE), and cholesterol or a 1:1:1:2 molar ratio of DOPC, DOPE, sphingomyelin, and cholesterol (Avanti Polar Lipids). The mixture was dried into a uniform lipid film using a rotavacuuum apparatus, and desiccated for one hour under full vacuum. The lipid film was flushed with nitrogen and thoroughly resuspended in HEPES-buffered saline (HBS; 150 mM NaCl, 10 mM HEPES, pH 7.4) by shaking for one hour at 37°C. The emulsion was extruded through a polycarbonate filter (50, 100, or 400 nm pore size) eleven times using a LiposoFast extruder apparatus (Avestin).

2.7.2 Liposome Aggregation Assay

Optical densities of 1 mM liposome suspensions mixed with p15HP peptide at various lipid:peptide ratios were monitored at 600 nm using a Varian Cary UV-visible spectrophotometer. For kinetic analyses, data was collected every 0.1 seconds for one minute; for static measurements, a single reading was taken after a 10 minute incubation period to allow for maximum liposome aggregation. Experiments were done at 37°C with stirring to prevent aggregated liposomes from dropping out of the light path.

2.7.3 NBD-Rhodamine FRET Lipid Mixing Assay

Fluorescent liposomes were labeled with 2% rhodamine-DOPE and 2% N-(7-nitro-2-1,3-benzoxadiazol-4-yl) (NBD)-DOPE, a quenching concentration of the FRET pair (Read and Duncan, 2011). Fluorescent and non-fluorescent liposomes were mixed at a 1:9 ratio in HBS, with a final lipid concentration of 100 μM. Peptide-induced lipid mixing assays were carried out at 37°C in a Cary Varian spectrofluorimeter with excitation and emission wavelengths of 465 nm and 530 nm respectively and a 10 nm slit width. Peptides were mixed with liposomes at a final concentration of 10, 25, or 50 μM in a total volume of 2 mL HBS. In control experiments, DMSO was added to liposomes in place of peptide. Fluorescence readings were obtained over a period of 600 seconds every 0.1 seconds. Maximum fluorescence was determined via the addition of 0.1% (v/v) Triton X-100 to solubilize liposomes. Percent lipid mixing was calculated as follows:

$$[(F_{exp} - F_0) / (F_{max} - F_0)] \times 100$$

where F_{exp} = experimental fluorescence, F_0 = baseline fluorescence, and F_{max} = fluorescence of Triton X-100 solubilized liposomes.

2.7.4 Liposome Flotation Assay

p15HP peptides and liposomes were mixed at 1:750 ratio and incubated in HEPES-buffered saline (HBS; 10mM HEPES, 150mM NaCl, pH 7.4) for 30 minutes at 37°C in a total volume of 150 μL. The suspension was adjusted to 30% (w/v) sucrose by adding 100 μL of a 75% (w/v) sucrose solution in HBS. The resulting high-sucrose suspension was overlaid with 100 μL of 25% (w/v) sucrose in HBS and 200 μL of sucrose-free HBS. The sample was centrifuged at 240,000 *x g* for 1 h in a Beckman TLS-55 swing bucket rotor. The bottom (200 μL), middle (100 μL) and top (200 μL) fractions were gently removed from the top downwards with a Hamilton syringe and analyzed by reverse phase-HPLC to determine the fraction of free and bound peptide.

2.7.5 Bis-ANS Competition Assay

Binding of 4,4′-dianilino-1,1′-binaphthyl-5,5′-disulfonic acid dipotassium salt (bis-ANS; Invitrogen) to liposomes was accomplished by adding a 10 mM stock solution in methanol to 100 μM liposomes in HBS. The liposome concentration was kept constant and bis-ANS was added at varying final concentrations (0.1 to 15 μM). Bis-ANS fluorescence was monitored on a Varian Cary Eclipse spectrofluorimeter with excitation and emission wavelengths of 395 nm and 500 nm, respectively and a slit width of 5 nm. Liposomes were pre-blocked with 10 μM bis-ANS by incubating for 10 minutes at room temperature. Blocked liposomes were pelleted in a Beckman TLS-55 swing bucket rotor at 100,000 *x g* and washed thoroughly several times with HBS to remove traces of excess fluorophore. Pre-blocked liposomes were then incubated with p15HP peptide under conditions identical to the liposome flotation assay.

2.8 Reverse-Phase HPLC

Fractions obtained from the liposome flotation assay were analyzed by reverse phase HPLC using a Waters 2680 Separations Module. A water, 0.1% trifluoroacetic acid (TFA; solvent A) and acetonitrile, 0.085% TFA (solvent B) mobile phase linear gradient was used (Table 2.1) with a flow rate of 1 mL/min and a Vydac 214MS C4 reverse phase column (5 μm particle, 250 mm × 4.6 mm; Grace Davison Discovery Sciences). Peptide elution was monitored at 215 nm with a Waters 2487 dual wavelength detection unit.

Table 2.1 RP-HPLC solvent system.

Time (minutes)	Solvent A (%)	Solvent B (%)
0	80	20
20	40	60
25	20	80

Solvent A (water + 0.1% trifluoroacetic acid)
Solvent B (acetonitrile + 0.085% trifluoroacetic acid)

2.9 Tyrosine Fluorescence Measurements

Intrinsic tyrosine fluorescence spectra were obtained on a PTI QuantaMaster 40 spectrofluorimeter. Excitation and emission wavelengths of 276 nm and 305 nm, respectively, were used. Binding data for p15 HP to liposomes was obtained as follows: aliquots of 50 nm liposomes were titrated into a peptide solution to achieve the desired lipid:peptide ratio. Three experimental spectra were obtained. Fluorescence spectra of each liposome concentration was acquired in the absence of peptide and were subtracted from the original spectra to minimize the effect of light scattering from liposomes.

2.10 Circular Dichroism Spectroscopy

Far-ultraviolet CD spectra were obtained using a Jasco J-810 spectropolarimeter with a 0.1 or 1 cm optical path. p15HP peptides (authentic or scrambled; 5 or 100 μM) were dissolved in 2 mM phosphate buffer with no lipid or 18 mM sodium dodecyl sulfate or 16 mM 1-palmitoyl-2-hydroxy-*sn*-glycero-3-[phospho-*rac*-(1-glycerol)] (LPPG). Spectra were acquired from 260 to 190 nm in 1 nm steps at a temperature of 37°C. All measurements were collected in triplicate. Machine data were converted to the mean residue ellipticity, [θ], averaged over all trials, blank subtracted, and subjected to sliding-window averaging over 3 nm stretches so that [θ] reported at a given wavelength (λ) is: $[\theta] = ¼[\theta]_{\lambda-1} + ½[\theta]_{\lambda} + ¼[\theta]_{\lambda+1}$.

Quantitative amino acid analysis was performed to ensure equal concentrations of each peptide were dissolved (Hospital for Sick Children, Toronto, ON).

2.11 Exosome Collection

2.11.1 Preparation of Exosome-Collection Medium

Cell culture medium (DMEM or medium 199) supplemented with 20% heat-inactivated FBS was centrifuged at 100,000 x g in a Beckman SW-32 swinging bucket rotor for 16 to 18 hours to pellet bovine exosomes. The resulting supernatant was carefully removed without disturbing the pellet, filtered with a 0.2 μm filter, diluted to 10% FBS with serum-free medium and stored at 4°C.

2.11.2 Exosome Isolation

Cells were plated in 150 mm^2 cell culture dishes, seeding 6.5 x 10^6 trypsinized cells per dish for HT1080 cells or 1.7 x 10^7 trypsinized cells for QM5 cells. A minimum of two dishes were pooled for each sample. Cells were transfected with pcDNA3-p14 or a mutated construct of p14 in exosome-collection medium containing 2.5% to 5% FBS. Exosomes were collected in the conditioned medium for 16 to 36 hpt. Conditioned medium was subjected to pre-clearing by successive centrifugations at 500 *x g* for 10 minutes, 2,000 *x g* for 10 minutes, and 10,000 *x g* for 30 minutes at 4°C. Pre-cleared conditioned medium was then subjected to ultracentrifugation at 110,000 *x g* in an SW32 swinging bucket rotor (Beckman) for 70 minutes. The exosome-enriched pellet was resuspended in 1 mL filter-sterilized phosphate-buffered saline (PBS) and re-pelleted at 110,000 *x g* for 1 hour in a TLA-100.1 fixed angle rotor (Beckman). The final pellet was resuspended in 50 μL PBS. This procedure is summarized in Figure 2.1. Samples that were assayed for protein were resuspended in PBS and solubilized with 0.1% Triton X-100 and 0.1% sodium dodecyl sulphate and tested with the CBQCA protein quantitation kit (Molecular Probes). Samples that were subjected to western blotting were precipitated with 4 volumes acetone per volume exosome suspension. The protein pellet was dried and resuspended in 20 μL 2x Laemmli protein loading buffer.

2.11.3 Sucrose Gradient Purification of Exosomes

Exosomes harvested by the standard protocol described in the previous section (Section 2.9.2 "Exosome Isolation"), were loaded in the bottom layer of an ice-cold step sucrose gradient (2.75 M, 2.5 M, 2.0 M, 1.75 M, 1.5 M, 1.2 M, 1.0 M, 0.75 M, 0.5 M, 0 M) in an ultraclear SW60 ultracentrifuge tube (Beckman). All sucrose solutions were prepared in 20 mM HEPES buffer, pH 7.4. Gradients were centrifuged for 18 hours at 250,000 *x g* at 4°C using slow acceleration and deceleration. Fractions were harvested from the top using a blunt needle and syringe. Twenty micro-liters of each fraction was saved for refractometric determination of sucrose concentration. The remainder of the fraction was diluted with 3 mL HBS and centrifuged at 100,000 x g for one hour in a TLA-100.3 fixed angle rotor (Beckman) to re-pellet exosomes. Samples were resuspended in 100 μL PBS with 0.1% Triton X-100 and 0.1% sodium dodecyl sulphate

and acetone precipitated. Protein pellets were resuspended in 20 μL 1x Laemmli protein loading buffer and subjected to western blotting.

2.12 Virus

The python isolate of reptilian reovirus (RRV) was obtained from W. Ahne (University of Munich). RRV was plaque purified and passaged in Vero cells by Nichole McMullen as previously described (Duncan et al., 2004). Briefly, Vero cells were grown in 175 cm^2 vented flasks to approximately 80% confluency. Medium was removed and cells were inoculated with virus at an MOI of 0.1 in a total volume of 4 mL. Virus was allowed to attach to cells at room temperature for one hour. Inoculum was aspirated and fresh growth medium was added. Cells were incubated for 3 to 4 days at 28°C (or until cells were lifted), then transferred to -80°C overnight. Flasks were thawed at room temperature and medium containing virus and lysed cells were transferred to 50 mL conical tubes. Cellular debris was separated by centrifugation at 1,500 *x g* for 10 minutes. Stock virus was stored at -80°C until time of use. Titer was determined using a standard plaque assay (Duncan et al., 1996). Virus from passages 3 and 4 were used for experimental infections. All experimental infections were at an MOI of 1.

2.13 Pharmacological Agents

A 6 mg/mL stock solution of 5-(N,N-dimethyl) amiloride hydrochloride (DMA; Sigma) was prepared in sterile water and passed through a 0.2 μm filter prior to use. HT1080 cells were pre-treated with 300 nM DMA 12 hours before transfection and treated with an increased dose (50 μM to 150 μM) at 6 hours post-transfection.

2.14 Transmission Electron Microscopy

Technical assistance for processing of specimens was kindly provided by Mary Ann Trevors (Electron Microscopy Core Facility, Faculty of Medicine, Dalhousie University). Whole-mounted exosomes and sectioned cells were visualized on a JEOL JEM 1230 transmission electron microscope and images were captured using a Hamamatsu ORCA-HR digital camera.

2.14.1 Whole-Mount Exosomes

Exosome pellets were resuspended in 50 μL 2% paraformaldehyde in PBS. Samples were spotted on Formvar/carbon-coated grids, allowing sample to adsorb for 20 minutes. Grids were washed with PBS and transferred to 1% gluteraldehyde in PBS for 5 minutes. Grids were then washed 8 x 2 minutes in distilled water and stained with 2% uranyl acetate for 1 minute. Samples were visualized with transmission electron microscopy at 80kV. Sizes of exosomes were measured using ImageJ64 software (National Institutes of Health). A minimum of 125 vesicles was measured in each of three separate experiments.

2.14.2 Immunogold Staining of Whole-Mount Exosomes

Samples were prepared as for whole-mounted samples described in Section 2.13.1 "Whole-Mount Exosomes", except samples were blocked with 50 mM glycine in PBS and 5% bovine serum albumin (BSA) in PBS and probed with anti-p14ecto primary antibody and goat anti rabbit secondary antibody conjugated to 10 nm gold particles.

2.14.3 Flat Embedding and Oriented Sectioning of Cells

Six thousand Vero cells were seeded on sterile Thermanox coverslips (Thermo Scientific) that had been trimmed to ~3 mm^2 squares. Cells were infected with RRV at an MOI of 1. Cells were fixed at 20 hours post-infection for a minimum of 12 hours at 4°C, using a final concentration of 2.5% gluteraldehyde, added directly to the medium to preserve delicate plasma membrane structures and extracellular vesicles. Samples were washed three times with 0.1 M sodium cacodylate buffer and post-fixed with 1% osmium tetraoxide for 2 hours. Samples were stained with 0.25% uranyl acetate at 4°C overnight, then dehydrated with a graduated series of acetone (50% to 100% over 80 minutes). Samples were infiltrated and embedded with epon-araldite resin and allowed to cure in a 60°C oven for 48 hours. Ultrathin sections (100 nm) were cut using an LKB Huxley ultramicrotome with a diamond knife and placed on 300 mesh copper grids and stained with 2% uranyl acetate and lead citrate. All embedding steps were done in a flat

embedding capsule. Coverslips were removed after curing. Sectioning was done parallel to the plane of the cell.

2.14.4 Immunogold Staining of Cells

Cells at ~50% confluency in 6-well cluster plates were transfected with p14. At ~24 hours post-transfection, cells were blocked with 1% BSA and 5% normal goat serum in HBSS, then probed with anti-p14ecto (1:100) at 4°C for one hour, followed by extensive washing with blocking buffer. Cells were probed with goat anti-rabbit secondary antibody (1:100) conjugated to 10 nm gold particles for 2 hours at 4°C followed by extensive washing with PBS. PBS supplemented with 50 mM EDTA was used to gently lift cells, which were then pelleted at 750 *x g* for 5 min in a microfuge tube. The cell pellet was fixed in 2.5% gluteraldehyde in PBS. Fixed cell pellets were embedded and sectioned as described in Section 2.13.3 "Flat Embedding and Sectioning of Cells", except flat embedding capsules were not used.

2.15 Proteomic Analysis of Exosomes

A total of 25 μg of exosomal protein per sample was subjected to mass spectrometry. Three technical replicates were performed on each of two biological replicates. Mass spectrometry samples were kindly processed by Dr. Alejandro Cohen (Proteomics Core Facility, Faculty of Medicine, Dalhousie University).

2.15.1 In-solution digestions

Exosome samples were resuspended in 60 μL of 8 M urea and sonicated for 10 minutes at 37°C in an ultrasonic bath (Branson Ultrasonic Corporation). Samples were diluted to a final volume of 200 μL in 8 M urea and 400 mM ammonium bicarbonate solution. Each sample was reduced and alkylated using 10 μl of 0.5 M dithiothreitol and 20 μl of 0.7 M iodoacetamide. Each sample then received 10 μL of 100 mM $CaCl_2$ and were diluted 1:5 with distilled water to reduce the urea concentration before digestion. Samples were digested with 150 μL of 0.02 μg/μL trypsin solution and incubated at 37°C for 16 hours. Digestion was stopped by adding sufficient TFA to reduce the pH to less

than 3. Samples were desalted and buffer-exchanged to a 50% acetotnitrile-0.1% TFA solution by solid phase extraction using Oasis HLB 3cc Extraction Columns (Waters) and then dried using a vacuum concentrator (Speed Vac Concentrator, Thermo Electron Corporation). Finally, samples were resuspended in 15 μL of 3% acetonitrile, 0.5% formic acid in LC-MS grade water.

2.15.2 LC-MS/MS and Data Analysis

Electrospray ionization (ESI) LC-MS/MS was performed using a nano flow HPLC system (Ultimate3000, Dionex) interfaced to a hybrid ion trap-orbitrap high resolution tandem mass spectrometer (VelosPro, ThermoScientific) operated in data dependent acquisition (DDA) mode. One micro-liter of each sample was injected onto a capillary column (C18 Onyx Monolithic, 0.10 x 150 mm Phenomenex) at a flow rate of 300 nL/min. Samples were sprayed at 1.6kV using fused silica non-coated emitters (20-um ID with 10-um ID tip PicoTip Emitter, New Objective). Chromatographic separation was carried out using a linear gradient from 3% B to 35% B over 30 minutes, then increasing to 95%B over 5 minutes (A: 0.1% formic acid in water, B: 0.1% formic acid in acetonitrile). The raw files were acquired (Xcalibur, ThermoFisher) and exported to Proteome Discoverer v1.4 (ThermoFisher) software for peptide and protein identification using Sequest database search algorithm. Peptide to spectrum match (PSM) validation was done using Percolator, with a False Discovery Rate set to 0.01. Protein quantification was performed using Sieve 2.1. Frames were generated using a minimum and maximum *m/z* of 300 and 1,500, respectively, a minimum frame time of 2.50 minutes, a minimum *m/z* width of 10.00 ppm, and start and stop retention times of 3.00 and 59.00 minutes, respectively. Frames were generated based on MS/MS scan retention times and precursuor *m/z* values. Identified frames were imported into Proteome Discoverer for peptide re-identification, as described above.

2.16 Exosome Transfer Experiments

Exosomes were isolated from donor p14-transfected QM5 cells using the procedure described in Section 2.9 “Exosome Collection”. QM5 recipient cells were seeded in 24-well cluster plates at a density of 2.1 x 10^5 cells/well. Each well was treated

with 12.5 μg exosomal protein, unless otherwise stated. Some exosome preparations were blocked with anti-p14ecto (1:50) or anti-CD81 (1.:25), treated with 0.5 μL DNase I (Invitrogen), sonicated for 10 minutes in an ultrasonic bath (Branson Ultrasonic Corporation), or treated with trypsin (Invitrogen) for one hour at 37°C. Recipient cells were fixed at 20 hours post exosome-treatment unless otherwise stated, and Wright-Giemsa stained. Each well was inspected to entirety and images of all syncytial foci were captured and quantified both for the number of syncytial foci and number of nuclei per syncytium. All experiments were done three times with fresh preparations of donor exosomes.

2.17 Co-Immunoprecipitations

Two 10 cm^2 dishes, each seeded with 2.2 x 10^6 HT1080 cells, were transfected with vector or pcDNA3-p14. At 18 hours post-transfection, cells were washed three times with ice-cold PBS and each dish was lysed in 1 mL non-denaturing lysis buffer (20 mM TrisHCl, 137 mM NaCl, 10% glycerol, 1% Igepal CA-630, 2 mM EDTA, pH 8.0) and Halt protease inhibitor cocktail (Pierce Biotechnology, Inc.). Lysates were collected in a centrifuge tube and incubated on ice for 30 minutes prior to passing through a 27 gauge syringe 10 times. Lysates were cleared of insoluble cellular debris by centrifugation at 10,000 *x g* for 10 minutes. Pre-cleared lysates were added to 10 μL of Protein G Dynabeads (Invitrogen) pre-adsorbed with anti-TSG101 (1 μg) or anti-FLAG (0.5 μg) and incubated at 4°C for one hour with shaking, followed by extensive washing with non-denaturing lysis buffer. Co-immunoprecipitated proteins were eluted by boiling with 40 μL 2x Laemmli protein loading buffer. Samples were subjected to western blotting and membranes were probed with anti-p14.

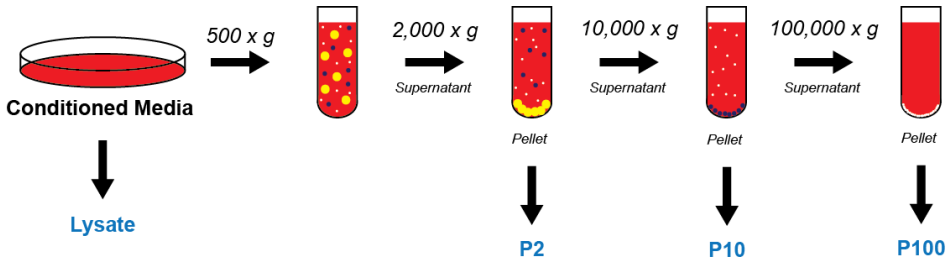

Figure 2.1 Exosome enrichment workflow. Conditioned medium is harvested from cells and is centrifuged at 500 *x g* to remove any cellular debris. The medium is then subjected to a series of centrifugations at 2,000 *x g*; 10,000 *x g*; and 100,000 *x g*. At each step, the cell lysate or extracellular vesicle pellet (P2, P10, and P100) are saved and subjected to further analysis such as western blotting.

CHAPTER 3

THE p15 HYDROPOBIC PATCH FUNCTIONS AS A NOVEL HELIX-LOOP-HELIX FUSION-INDUCING LIPID PACKING SENSOR (FLiPS) IN CELL-CELL FUSION

3.1 Introduction

A remarkable feature of biological membranes is their dynamic ability to assume different shapes. This is beautifully exemplified by the elaborate architecture of cellular organelles such as the endoplasmic reticulum, whose geometry ranges from highly curved tubules to flatter cisternal structures (Hu et al., 2008). Lipid bilayers, however, intrinsically resist stretching and bending (Graham and Kozlov, 2010; Janmey and Kinnunen, 2006a; Stachowiak et al., 2013). Consequently, a number of strategies are used by the cell to bend membranes, including: (i) recruitment or synthesis of phospholipids whose headgroups or acyl chains promote membrane curvature (Kooijman et al., 2005); (ii) incorporation and clustering of integral membrane proteins whose transmembrane domains are funnel shaped (Fertuck and Salpeter, 1974); (iii) alterations of membrane tension by remodeling of the cytoskeleton (Lieber et al., 2013); (iv) scaffolding of the bilayer by peripheral membrane proteins that physically constrain the membrane into the desired shape (Ren et al., 2006); and (v) the shallow insertion of a small hydrophobic moiety (such as the face of an amphipathic helix) into the membrane (McMahon and Gallop, 2005). Ultimately, these mechanisms are not mutually exclusive and the desired membrane shape is achieved through the interplay of both lipids and proteins. Since membrane curvature is unfavorable, specialized proteins are also used to stabilize areas of curvature.

3.1.1 Membrane Curvature Sensing by Amphipathic Helices

Most membrane curvature sensor proteins detect bent membranes through inherent lipid packing defects in the bilayer, rather than by the physical, geometrical flexure of the membrane (Bigay and Antonny, 2012; Davies et al., 2001; Vamparys et al., 2013). Lipid packing defects are low-density areas in the surface of the bilayer that arise from the mismatch between the curvature of the membrane and the shape of the lipids

(Figure 3.1). This mismatch results in phospholipids with splayed acyl chains and gapped headgroups, ultimately resulting in intermittent patches of hydrophobic exposure. The compact arrangement of phospholipids and concomitant induction of lipid packing defects within a given bilayer can be altered in several ways, including introduction of curvature stresses and incorporation of phospholipids whose intrinsic conical shape (i.e. phosphatidylethanolamine) makes them less prone to align with the bilayer than conical phospholipids (i.e. phosphatidylcholine) (Vamparys et al. 2013). Since lipid molecules are not stiff, a lipid packing defect should not be considered as an empty cavity with a defined size, but rather as a region of the bilayer with a time-averaged lower atomic density (Janmey and Kinnunen, 2006). Moreover, two adjacent phospholipids will tilt only by about 2° with respect to each other as the curvature radius decreases up to 30 nm (Antonny, 2011). Locally, the impact of membrane curvature on lipid packing geometry seems quite modest, however, accumulation of these defects in the overall area of a curved membrane is highly unfavorable. Therefore, membrane curvature sensor proteins use specialized amphipathic or hydrophobic moieties to detect the increased frequency of lipid packing defects in curved membranes (Drin et al., 2007).

Defining the features of an amphipathic helix (AH) well-suited to curvature sensing is a topic that has received much recent attention (Bhatia et al., 2010; Cui et al., 2011; Drin and Antonny, 2010). It is generally accepted that the center of the helix is positioned roughly at the level of the lipid phosphate headgroup and the glycerol backbone (Hristova et al., 1999). As a consequence, the amino acid side chains are exposed to the complex, anisotropic layer that separates the aqueous phase from the hydrocarbon core. Therefore, the overall composition of the AH is thought to influence bilayer partitioning characteristics, since most, if not all, sidechains will be intercalated within the lipid bilayer. A proposed balance between two physiochemical parameters - electrostatic attraction and hydrophobic effect – is thought to govern the adsorption of an AH to a lipid membrane (Antonny, 2011). Canonical curvature sensing AHs, such as the amphipathic lipid packing sensors (ALPS), have a hydrophobic face that is rich in bulky aromatic sidechains, while the polar face is enriched in serine and threonine residues. With no net charge, ALPS motifs lack electrostatics as a driving force for bilayer partitioning, therefore insertion of hydrophobic sidechains is the predominant factor

(Vanni et al., 2013). Since curved membranes have a higher frequency of lipid packing defects, ALPS motifs will preferentially bind at these sites (Hatzakis et al., 2009). The chemistry of each turn of the ALPS motif is roughly similar, and the strong imbalance between the polar and nonpolar faces exacerbates the attraction to loose lipid packing. As such, ALPS motifs behave as a type of molecular velcro where a strong global interaction is the consequence of many weak and identical interactions (Antonny, 2011). This model may also be generalized to other hydrophobic moieties such as acylation and hydrophobic loops (Gerlach et al., 2010; Plomann et al., 2010; Martens et al., 2007), although these motifs display a less acute sensitivity to lipid packing.

3.1.2 Membrane Curvature Generation by Amphipathic Helices

Although some AHs may be curvature-sensitive, numerous proteins harboring these motifs can also induce curvature (Campelo et al., 2008). For example, curvature sensors may exhibit concentration-dependent curvature induction (Ambroggio et al., 2013; Stachowiak et al., 2013), and by employing a combination of AHs, hydrophobic loops and curved scaffolding domains, BAR domain proteins can sense, induce and stabilize membrane curvature (Frost et al., 2009; Gallop et al., 2006). Generally, AHs with a positively charged polar face, when presented with an anionic membrane, will be curvature inducing by wedging between phospholipid headgroups in flat membranes. Therefore, it is now clear that some proteins may sense membrane curvature, others may induce it, and some fulfill both functions. The explanation behind this varied interfacial chemistry continues to be an area of vigorous research.

3.1.3 Fusion Peptides, Membrane Curvature, and Bilayer Fusion

The processes of generating a hemifusion intermediate and/or forming a pore during membrane fusion are both dependent on the induction and/or stabilization of membrane curvature. Traditionally, FPs from enveloped virus fusion proteins have been linked to promotion of negative curvature, required for the formation of the hemifusion stalk (Tamm and Han, 2000; Tenchov et al., 2013; Yao and Hong, 2014). Other roles assigned to the FP include formation of positive curvature to generate membrane dimples (Lee, 2010), dehydration (Hughson, 1995), and disordering of acyl chains (Larsson and

Kasson, 2013). Biophysical assays have shown that FPs partition exclusively in the outer leaflet of the membrane (Luneberg et al., 1995), a mechanism reminiscent of the wedging mechanism used by curvature-sensing and curvature-inducing AHs. However, more recent computational models show FPs can exert a wide variety of effects on membrane curvature, dependent on the local environment of the lipid/water system used in the model, with the possibility of induction of positive or negative curvature by the same peptide under different conditions (Nishizawa and Nishizawa, 2010; Yao and Hong, 2013). A recent study also suggests, at least in the case of the influenza HA FP, FPs may cause positive curvature stress, which the authors propose helps in fusion pore formation (Fuhrmans and Marrink, 2012). Aside from this computational evidence, the involvement of curvature inducers or sensors endogenous to the fusion protein in the formation of fusion pores during cell-cell or intracellular vesicle membrane fusion remains unclear.

The ectodomains of the avian reovirus p10, reptilian reovirus p14 and baboon reovirus p15 FAST proteins contain a cystine loop, proline-hinged loop, or polyproline type II helix, respectively (Barry et al., 2010; Corcoran et al., 2004; Top et al., 2012). All three of these motifs are structurally distinct from, but functionally equivalent to, enveloped virus FPs, by using hydrophobic residues to promote lipid mixing. While the FPs of enveloped viruses and FAST proteins are clearly involved in membrane destabilization required for bilayer fusion, how these proteins promote or stabilize curvature changes required for pore formation has not been determined.

3.1.4 Rationale and Objectives

The FAST proteins differ from enveloped virus fusogens and SNARE proteins in their small size and asymmetric membrane topology, positioning the majority of their mass on the distal side of contacting membrane bilayers (Boutilier and Duncan, 2011). FAST protein endodomains are required for cell-cell fusion (Barry and Duncan, 2009), but their mechanism of action remains unclear. The baboon reovirus p15 FAST protein exhibits the most exaggerated asymmetric membrane topology, with a meager 19-residue ectodomain positioned outside the cell, and a comparatively large 97-residue cytoplasmic endodomain (Dawe et al., 2005). As with all FAST proteins, p15 contains a membrane-proximal polybasic motif in its endodomain, thought to be involved in cell surface

trafficking (Parmar et al., 2014). The only other distinctive feature in the endodomain is a 20-residue stretch of predominantly apolar residues just downstream from the polybasic motif, termed the hydrophobic patch (HP). The role of p15HP in cell-cell fusion has not been examined.

The objective of this chapter was to characterize the role of the membrane-proximal, cytosolic HP of p15. Thinking about the membrane curvature encountered during membrane fusion, we hypothesized that the p15HP might function to stabilize the high positive membrane curvature present in the rim of a fusion pore, thereby lowering the energy barrier to pore formation. I determined this was the case by demonstrating the p15HP functions as a fusion-inducing lipid packing sensor (FLiPS) to promote pore formation during cell-cell fusion.

3.2 Results

3.2.1 The p15HP is Essential for Syncytium Formation

To determine whether the p15HP plays a role in p15-mediated syncytium formation, the sequence of the p15HP was scrambled in the context of a p15 backbone (Figure 3.2 A). Syncytium formation in transiently transfected QM5 cells was assessed by examination of fixed, Giemsa stained cells at 10 hours post-transfection (hpt) (Figure 3.2 B). As expected, authentic p15 (p15HP-Auth) exhibited robust syncytium formation, as indicated by a clustering of nuclei and presence of a single, continuous cytoplasm (indicated by arrows). In contrast, p15 with a scrambled HP (p15HP-Scr) showed no evidence of syncytium formation. To rule out the possibility of delayed fusion kinetics, syncytiogenesis of p15HP-Scr was also assessed at 24 hpt, however no evidence of fusion was observed. A western blot of equal protein loads of whole cell-lysates from each of these cells confirmed equal expression of both constructs (Figure 3.2 C). The p15HP therefore functions in a sequence-specific manner to promote syncytium formation.

3.2.2 Glycine and Proline Residues in p15HP are Essential for Fusion Activity

To discern which amino acids were required for syncytium formation, p15HP residues were mutated to alanine in consecutive groups of three. Where alanine was a

naturally encoded amino acid, no substitution was made. Syncytium formation was quantified in transfected QM5 cells using a standard syncytiogenesis assay based on the average number of syncytial nuclei per microscopic field of view at a given timepoint (Corcoran and Duncan, 2004). Mutations of two regions, p15GAG (residues 74 to 76) and p15LPL (residues 80 to 82), completely abolished syncytium formation (Figure 3.3 A), but had no effect on protein expression levels as determined by western blotting (Figure 3.3 B). To more precisely identify which residue(s) in these mutation-sensitive regions were essential for cell fusion activity, each residue was individually substituted with alanine. Substitutions of Leu80 or Leu82 had no significant effect on syncytium formation, while G74A, G76A, and P81A mutants were virtually non-fusogenic (Figure 3.3 C and D).

Syncytium formation is the endpoint of plasma membrane fusion, therefore to more closely define the stage of membrane fusion in which mutants were defective, a fluorescent cellular pore-formation assay was used (Barry and Duncan, 2009). This assay measures the passage of a low molecular weight aqueous dye during the early stages of pore formation. Briefly, donor QM5 cells were co-transfected with a p15 construct and GFP, at a low seeding density to prevent the occurrence of cell-cell fusion. Meanwhile, target Vero cells were loaded with the cell-permanent aqueous dye, calcein red. Calcein-loaded target cells were resuspended and co-seeded with donor cells. The extent of pore formation was measured using flow cytometry with a dual-gating strategy to quantify the transfer of calcein red to green cells. All measurements are recorded in the absence of visible syncytia. Results of the pore-forming assay were kindly provided by Dr. Eileen Clancy. Results indicated that p15GAG and p15LPL mutants were both defective at pore formation (Figure 3.3 E). Taken together, the p15HP is therefore essential for cell-cell fusion and pore formation, which is dependent on glycine and proline residues near the center of the HP.

3.2.3 Structural Properties of p15HP

Given the helix-breaking propensity of glycine and proline residues (Pace and Scholtz, 1998), we suspected these essential residues might influence the secondary structure of the p15HP. Secondary structure predictions based on the sequence of the p15

endodomain (residues 44-140) (Kelley and Sternberg, 2009) suggested a helix-loop-helix conformation for authentic p15HP, while the fusion-dead mutants p15GAG, p15LPL and p15HP-Scr were predicted to be completely alpha-helical (Figure 3.4 A). We experimentally confirmed these predictions using far-UV circular dichroism spectroscopy on synthetic peptides corresponding to the authentic and scrambled versions of p15HP. Both peptides were unstructured in phosphate buffer, as indicated by a strong negative band at 195 nm (Figure 3.4 B, left panel). However, in the presence of 1-palmitoyl-2-hydroxy-sn-glycero-3-[phospho-rac-(1-glycerol)] (LPPG) or sodium dodecyl sulphate (SDS) micelles, both peptides folded into alpha-helical conformations, as evidenced by minima at 222 and 208 nm and a maximum at 190 nm (Figure 3.4 B, middle and right panels). Reduced signals at these key minima and maxima was observed for p15HP-Auth compared to p15HP-Scr, suggesting reduced alpha-helical content for this peptide, consistent with secondary structure predictions.

The functional implications of a predicted helix-loop-helix architecture prompted atomic-level determination of the structure of p15HP using solution-state nuclear magnetic resonance (NMR) spectroscopy. Using 2D ^{1}H-^{1}H total correlation spectroscopy (TOCSY), 2D ^{1}H-^{1}H Nuclear Overhausser Effects spectroscopy (NOESY), and natural abundance 2D ^{1}H-^{15}N heteronuclear single quantum coherence spectroscopy (HSQC) and 2D ^{1}H-^{13}C HSQC, a high-resolution structure was calculated. Structures were kindly provided by Dr. Muzaddid Sarkar. A 50-member structural ensemble indicted that most p15HP conformers contain two alpha-helical segments at the N- and C-termini, connected by an unstructured loop (Figure 3.5 A and B). Due to the relatively unstructured central loop, the orientation of the two flanking helices relative to each other is generally random. The C-terminal helix consistently extends from Leu82 to Ile86 in all 50 conformers and there is a distinctive partitioning of Leu82, Leu83, Val85, and Ile86 into a hydrophobic face. The N-terminal helix shows a higher degree of structural variability, but spans residues Leu70 to Tyr73 in the majority of conformers. Interestingly, essential residues Gly74, Gly76, and Pro81 are never found as part of a helical structure, but rather are always found in the unstructured loop region. Therefore, we conclude p15HP assumes a helix-loop-helix architecture when in a membranous environment.

To determine the importance of residues forming a hydrophobic face on the terminal helices, further mutational analysis was performed. Key residues in the N- and C-terminal helices were sequentially replaced with the uncharged, polar residue asparagine. Asparagine replacement of the N-terminal Leu71 helical residue reduced syncytium formation by ~20% (Figure 3.6 A). When combined with a similar replacement of Tyr73, syncytium formation was reduced by ~50% relative to authentic p15. Additional replacements of Val77 and Leu80 in the loop region had no further inhibitory effect ($p>0.05$ when compared by one-way ANOVA), but when combined with substitution of Ile86 in the C-terminal helix reduced syncytium formation to less than 20% of authentic p15. Furthermore, when strategic polar residues (Ser73 and Ser79) were substituted with lysine residues, syncytium formation was significantly inhibited (Figure 3.6 B), even though these residues were tolerant of alanine substitutions, suggesting the unstructured loop region is incompatible with a positive charge. Our structural and functional studies, therefore, indicate a helix-loop-helix conformation is a functional requirement of the p15HP.

3.2.4 Membrane-Interactive and Membrane-Perturbing Characteristics of p15HP

We noted strong membrane-induced conformational changes in p15HP (Figure 3.4 B), therefore we performed a series of experiments to define the membrane-peptide interactions of p15HP. First, we took advantage of a single tyrosine residue in p15HP peptide since tyrosine residues naturally exhibit intrinisic fluorescence due to their aromatic sidechain. This intrinsic fluorescence can be used as a probe for peptide membrane interactions since insertion of the sidechain into a hydrophobic results in an increase in the magnitude of fluorescence (Douliez et al., 2000). The steady-state fluorescence emission spectrum of p15HP at an excitation wavelength of 274 nm showed a characteristic emission band at 305 nm (Figure 3.7 A). When increasing concentrations of 50 nm liposomes were added, the relative tyrosine fluorescence intensity of p15 HP at 305 nm increased in a dose-dependent manner (Figure 3.7 B), suggesting an intercalation of Tyr73 into a hydrophobic membrane environment. Since only a short, 20 amino acid peptide was used for these studies, re-folding of the protein onto itself is unlikely to have

caused the increase in emission intensity. Therefore, we suggest p15HP inserts directly into lipid membranes.

The functional importance of the predicted p15HP helix-loop-helix architecture as a membrane-interaction motif was also confirmed using more biologically relevant conditions, by expressing the p15 endodomain (residues 44-140) in QM5 cells. Endodomain constructs contained either the authentic p15HP sequence or one of two different alanine substitutions (p15GAG and p15P81A) that disrupt the predicted helix-loop-helix conformation (Figure 3.4 A) and abrogate p15-induced membrane fusion (Figure 3.3 A and D). Membrane fractions of vesiculated lysates were separated from soluble cellular material by ultracentrifugation. Membrane pellets were further treated with alkaline sodium carbonate to strip peripheral membrane proteins, thereby separating lysates into soluble, peripheral, and integral membrane fractions. Western blotting indicated the authentic p15 endodomain exclusively associated with the peripheral membrane fraction, while endodomains containing the alanine substitutions were primarily or exclusively associated with the soluble fraction (Figure 3.7 B), further suggesting p15HP helix-loop-helix architecture is required for interaction with membrane bilayers.

Next, we wanted to determine if p15HP was capable of perturbing membranes. First, we assessed lipid mixing with a fluorescent fluorescence-based liposome assay (Read and Duncan, 2011). Briefly, unlabeled liposomes were mixed with a population of liposomes labeled with a quenching concentration of NBD and rhodamine fluorophores. Upon mixing of lipid bilayers, dilution of the fluorophores occurs resulting in fluorophore dequenching. Our observed differences in membrane-induced helicity were mirrored by differential effects of the authentic and scrambled p15HP peptides on liposomes (1:1:1 molar ratio of DOPE:DOPC:Chol). While both peptides induced dose-dependent lipid mixing, the fluorescence signal from the scrambled peptide deteriorated after 200 seconds at a high 4:1 lipid:peptide ratio (Figure 3.8 A). To determine if loss of p15HP-Scr signal was due to lipososome aggregation, we measured the turbidity of liposome suspensions at various lipid:peptide ratios. p15HP-Scr peptide induced dose-dependent aggregation of 100 nm liposomes (Figure 3.8 B, hatched bars). Notably at the high 4:1 lipid:peptide ratio of p15HP-Scr (which correlated with a loss of signal in the

lipid mixing assay) a massive increase in turbidity was observed. Strikingly, no such increase in turbidity was induced by the authentic p15HP peptide at any ratio tested (Figure 3.8 B, white bars). Thus, the avidity and membrane-perturbing effects of p15HP on lipid bilayers is influenced by the amino acid sequence and by a predicted helix-loop-helix conformation in the p15HP.

3.2.5 Preferential partitioning of p15HP into highly curved lipid bilayers containing hydrophobic defects

To further define the physical basis of p15HP membrane interactions, we developed an assay to measure the effect of membrane curvature on p15HP membrane partitioning, based on the use of sucrose gradients and buoyant density to separate liposome-associated peptides from free peptides (Figure 3.9 A, left panel). Buoyant density was considered the preferred method of lipid recovery, as small liposomes do not sediment efficiently (Bigay et al., 2005). To validate our assay, a control flotation experiment was performed in the absence of peptide to verify equal recovery of all liposome sizes. Regardless of size, NBD-labelled liposomes floated to the buffer-sucrose interface equally (Figure 3.9 A, right panels). Using fluorescence readings from the top fraction (buffer-sucrose interface) and bottom fraction (dense sucrose cushion), ~95% of fluorescent liposomes of each liposome size were recovered. A linear detection range for p15HP-Auth and p15HP-Scr peptides was established using reverse-phase HPLC on a C4 column (Figure 3.9 C), and unlabelled liposomes were not detected by HPLC nor did they interfere with peptide detection (Figure 3.9 D, E and 3.10 C).

To assess differential effects of membrane curvature on p15HP membrane partitioning, peptide was incubated with liposomes of varying diameters (50, 100 or 400 nm) at a constant peptide:lipid molar ratio (1:750). Results indicated a progressive, size-dependent increase in association of p15HP-Auth with liposomes as liposome size decreased. Association of p15HP with liposomes increased from background levels (~3% of total peptide) to ~40% of total peptide with 50 nm liposomes (Figure 3.10 A and B). Approximately 30% of p15HP-Auth associated with 100 nm liposomes, while only background levels (~5%) fractionated with 400 nm liposomes (Figure 3.10 A and B). In marked contrast, the scrambled version of p15HP displayed avid (>90%), size-

indiscriminate association with 50, 100, and 400 nm liposomes (Figure 3.10 D). Thus, the membrane curvature sensitivity displayed by p15HP is influenced by amino acid sequence.

Next, we used the hydrophobic probe 4,4'-dianilino-1,1'-binaphthyl-5,5'-disulfonic acid (bis-ANS) as a hydrophobic partitioning competitor. Since bis-ANS only fluoresces in apolar environments, binding of the probe to exposed hydrophobic clefts in liposomes was monitored by measuring fluorescence emission at 500 nm (Figure 3.11). Binding curves were generated and fit using the non-linear curve-fitting tool for saturation binding (GraphPad Prism). Calculations indicated K_D values (concentration of bis-ANS required to reach half-maximal binding) were similar for all liposome sizes, but B_{max} inversely correlated with liposome size (Table 3.1). These results confirmed the presence of more numerous hydrophobic defects in 50 and 100 nm liposomes and verified an equal affinity of bis-ANS for all sized liposomes. After pre-treatment of liposome suspensions with 10 μM bis-ANS, a saturating concentration for all liposome sizes (Figure 3.11), p15HP-Auth partitioned into liposomes at levels only slightly above background (5-11% of total peptide), and bis-ANS eliminated the size-dependent partitioning of p15HP into liposomes (Figure 3.12 A and B). The p15HP therefore senses membrane curvature via lipid packing defects in highly curved lipid bilayers.

Table 3.1 Calculated K_D and B_{max} constants for bis-ANS liposome binding curves.

Liposome Diameter (nm)	K_D (μM)	B_{max} (A.U.)
50	1.903 ± 0.152	349.8 ± 7.685
100	2.143 ± 0.186	325.3 ± 8.011
400	1.579 ± 0.142	214.0 ± 5.051

Results are reported as mean ± standard error for three experiments.

3.2.6 Heterologous Lipid-Packing Sensors can Functionally Replace p15HP

The p15HP is the first example of lipid packing sensor involved in membrane fusion, and although p15HP does not assume a continuous amphipathic helical structure, it does sense membrane curvature in a manner analogous to ALPS motifs (Antonny, 2011). To determine whether ALPS motifs can functionally replace p15HP during cell-cell membrane fusion, a series of chimeric p15 constructs containing various ALPS motifs in place of the p15HP were created and assessed for their syncytiogenic activity. These ALPS motifs were from the membrane curvature sensing modules of Golgi-localized ArfGAP1 [FLNSAMSSLYSGWSSFTTGASKFAS], the sterol transporter protein Kes1p [SSSWTSFLKSIASFNGDLSSLSA], and the vacuole fusion protein sorting effector subunit Vps41 [TTNIGSLLSSAASSFRGT] (Figure 3.13 A). Despite a clear preference of all heterologous motifs for non-plasma membrane localization (Cabrera et al., 2010; Fairn et al., 2007; Levi et al., 2008), all three chimeras successfully induced syncytium formation (Figure 3.13 B). In fact, replacement of p15HP with the Kes1p ALPS motif actually augmented p15 fusion activity, independent of relative protein expression levels (Figure 3.13 C). Mutation of residues in the hydrophobic face of ALPS motifs (i.e. L69A, W80A, and F90A in the ArfGAP1 motif [ArfGAP1-HF in Figure 3D], and W10A, F13A, and F20A in the Kes1p motif [Kes1p-HF in Figure 3D]) that renders them insensitive to membrane curvature (Bigay et al., 2005; Gonzalez-Rubio et al., 2011; Levi et al., 2008), reduced syncytium formation by >95% (Figure 3.13 D). Thus, fusion activity of chimeric p15-ALPS constructs is dependent on the hydrophobic face of the ALPS motifs.

To ascertain if ALPS AHs are unique in their ability to functionally replace the p15HP, three functionally distinct membrane-interactive AHs were also used (Figure 3.14 A). The H0-NBAR AH motif [QVQKKFSRAQEKVLQKLGK] from BRAP/BIN2 has a strong positively-charged polar face and generates lipid bilayer curvature (Fernandes et al., 2008), melittin [GIGAVLKVLTTGLPALSWI KRKRQQ] is a pore-forming lytic peptide (Lee et al., 2013), and DivIVA [EVNEFLAQVRKDYEIVLR] is an AH from the *Bacillus subtilis* bacterium that localizes exclusively to areas of negative curvature (Ramamurthi et al., 2009). All three of these chimeric proteins were incapable of forming

syncytia (Figure 3.13 B), despite equal protein expression levels (Figure 3.13 C). We concluded, therefore, that only AHs that sense positive membrane curvature can functionally replace p15HP.

3.2.7 RRV p14 Contains a Previously Unidentified AH

Finally, we were interested in determining whether other FAST proteins were similarly reliant on an internal lipid packing sensor. The HP of the p14 FAST protein resides in the extracellular ectodomain, where it functions as a fusion peptide to promote early stages of membrane fusion (Corcoran et al., 2004). However, we noted the presence of a previously unrecognized AH located in a membrane-proximal region in the p14 endodomain (Figure 3.15 A). A p14 construct containing an ArfGAP1 ALPS motif substitution of this AH retained ~65% cell-cell fusion activity (Figure 3.15 B), while p15 containing the p14AH in place of its own HP retained ~45% fusion activity (Figure 3.15 C). These results suggest the FAST proteins may be generally dependent on a cytosolic, membrane-proximal curvature sensor for membrane fusion.

3.3 Discussion

A lipidic fusion pore is an obligatory intermediate in membrane fusion, and its formation requires energy to bend membranes into highly curved shapes. Pore formation is likely a rate-limiting hurdle in membrane fusion, and stabilization and/or expansion of the nascent fusion pore is thought to require the input of external forces. How membrane fusion proteins overcome this barrier remains unresolved. In the study presented in this chapter, we investigated the role of p15HP in cellular fusion. We now show that a membrane-proximal hydrophobic patch present in the cytoplasmic tail of the p15 FAST protein preferentially partitions into membranes with high positive curvature. This partitioning is based on the presence of hydrophobic defects present in highly curved membranes, and requires a helix-loop-helix conformation in the p15HP. Furthermore, the p15HP can be functionally replaced by ALPS motifs from heterologous proteins, but not by other membrane-interactive AHs. We propose the FAST proteins use a novel cytoplasmic, fusion-inducing lipid packing sensor (FLiPS) to stabilize hydrophobic defects present in the rim of nascent fusion pores or other areas involving induction of

positive curvature such as membrane protrusions. An accumulation of FLiPS motifs at the highly curved rim of the pore during FAST-mediated intercellular membrane fusion might provide the required energy by relaxing membrane bending energy. Herein, we provide the first direct evidence of how protein fusogens may mediate pore formation by extending the known roles of generic membrane curvature-sensing moieties to a novel role in the membrane fusion pathway.

3.3.1 p15 FLiPS - A Novel Lipid Packing Sensor

The conclusion that p15HP functions as a FLiPS is supported by several lines of evidence: (1) p15HP directly adsorbs to lipid bilayers (Figure 3.7 B, C and Figure 3.10 B); (2) p15HP undergoes membrane-induced folding to a partially helical structure (Figure 3.4 B and Figure 3.5); (3) membrane-partitioning of the p15HP is curvature-dependent and occurs via exposed hydrophobic defects in the membrane (Figure 3.10 B and Figure 3.12 B); (4) p15HP-Scr avidly and indiscriminately interacts with liposomes of all curvatures, but is non-functional in the p15 backbone (Figure3.2 B and Figure3.10 D); and (5) the HP can functionally be replaced with heterologous ALPS motifs but not by other AHs (Figure 3.13 B and Figure 3.14 B). The p15FLiPS differs functionally from traditional lipid packing sensors in that it is the first example of such a motif being required for cell-cell fusion, functioning at or upstream of pore formation to promote syncytiogenesis (Figure 3.2 B and Figure 3.3 A and E). The p15 FLiPS can also destabilize membranes, as indicated by the peptide-induced membrane perturbation observed in liposome aggregation and liposome fusion studies (Figure 3.8). Curvature sensing versus membrane destabilization presumably reflects the different peptide:lipid ratios employed in these assays (1:750 versus 1:2, respectively) . We propose p15 FLiPS operates in a manner similar to, but structurally distinct from, ALPS motifs.

The first described ALPS motif from ArfGAP1 was characterized as an AH having a strong hydrophobic moment, including a hydrophobic face rich in aromatic sidechains and a polar face rich in Ser and Thr residues and devoid of charge (Bigay et al., 2005). A bioinformatic search based on these physiochemical parameters revealed these characteristics are well-conserved in a multitude of curvature-sensitive proteins present in both human and yeast proteomes, suggesting the ALPS motif could be a

generalized mechanism of curvature-sensing by proteins (Drin et al., 2007; Gautier et al., 2008). In contrast, p15FLiPS is composed of predominantly non-aromatic apolar residues, exhibits limited amphipathic character, and has two small helices split in the middle by an essential loop region (Figure 3.5 D). While p15FLiPS appears quite distinct from ALPS motifs, it can nonetheless be functionally replaced with such motifs (Figure 3.13 B). Furthermore, p15 chimeric proteins which have the HP replaced with ALPS motifs from ArfGAP1 and Kes1p, also require bulky hydrophobic residues for function (Figure 3.13 D), suggesting these chimeric proteins are also reliant on a hydrophobic insertion mechanism.

Membrane curvature sensing can be achieved by diverse, unrelated structural motifs such as alpha-helices, alkyl chains, and proteins modified with hydrocarbon groups (Hatzakis et al., 2009). Likewise, other groups have documented hydrophobic loops or wedges that confer curvature-sensitivity to their respective protein (Hui et al., 2009; Plomann et al., 2010). The fact that so many diverse, unrelated structural motifs can all sense membrane curvature suggests that membrane-curvature sensing is a generic property of curved membranes rather than a property of the anchoring molecule itself. Based on this reasoning, one could anticipate that membrane curvature would promote the redistribution of proteins that are anchored in membranes through other types of hydrophobic moieties, such as p15FLiPS.

We propose physiochemical heterogeneity of curvature-sensing modules may also be reflected in the family of FAST cell fusion proteins. A p14 protein containing the previously unrecognized membrane-proximal AH in RRV p14 replaced by the ArfGAP1 ALPS motif, or a p15 protein containing the p15FLiPS by the p14 AH, maintained fusogenicity, albeit at a reduced level (Figure 3.15 C and D). Although we have not experimentally defined the peptide-membrane interactions of the p14 membrane-proximal AH, we propose that this motif is functionally equivalent to the p15FLiPS motif. Closer examination of other FAST proteins also reveals other putative FLiPS motifs. For example, BroRV p13 and AqRV p22 both contain distinctive, membrane-proximal HPs in their endodomain (Thalmann et al., 2010; Racine et al., 2009). Like p15FLiPS, these motifs are generally more hydrophobic than amphiphilic in nature. Although the precise localization and sequence differs from p15FLiPS, these motifs

could also function in an analogous manner. The homologous p10 FAST proteins from ARV and NBV do not contain an obvious cytosolic AH or HP, but instead feature a palmitoylated membrane-proximal dicysteine motif, which is absolutely required for fusion (Shmulevitz et al., 2003). Although physically much different than the p15FLiPS motif or p14AH we have described in this work, this may be another example of the tolerated diversity amongst curvature-sensing motifs. Therefore, we propose a universal, membrane-proximal FLiPS element in all FAST proteins that drives pore formation and syncytiogenesis (Figure 3.16). Moreover, membrane-proximal AHs or hydrophobic regions have also been noted in the cytoplasmic tails of some enveloped viral fusogens, including HIV gp41 (Yang et al., 2010), influenza virus HA (Kozerski et al., 2000), and murine leukemia virus (Melikyan et al., 2000), as well as in proteins involved in intracellular fusion such as atlastin (Moss et al., 2011) and complexin 1(Seiler et al., 2009), perhaps suggesting a more widespread phenomenon of lipid-packing sensing during diverse membrane fusion events.

3.3.2 p15FLiPS is a Curvature Sensor, Not Inducer

The phenomena of curvature-sensing and curvature-induction are not mutually exclusive, and may be concentration-dependent (Stachowiak et al., 2013). The evidence we present in this work supports the role of p15FLiPS as a curvature sensor, not a curvature inducer. First, the almost complete absence of p15HP association with large unilamellar vesicles (i.e. 400 nm diameter; Figure 3.10 A and B) suggests the p15HP does not bind to flat membranes, a pre-requisite for curvature induction. Second, curvature induction in a liposomal model often presents as tubulation. No apparent turbidity increase of liposomes is observed in the presence of p15HP, suggesting a lack of tubulation (Figure 3.8 A), although we cannot formally exclude this possibility without electron microscopy studies. Therefore we conclude p15FLiPS functions exclusively as a lipid packing sensor.

A hallmark of curvature-inducing AHs is a net charge on the polar face of the helix. This charge is thought to provide an electrostatic attraction between the AH and the oppositely charged membrane. The majority of our studies utilized a synthetic peptide of p15HP in isolation. However, in the context of the complete p15 protein, the HP is

anchored close to the membrane by the transmembrane domain and is also adjacent to a charged polybasic cluster. A recently published study revealed charges in the regions flanking curvature-sensitive AHs may modulate curvature-sensitivity (Chong et al., 2014), therefore, it is possible that the polybasic cluster modulates membrane binding by p15 HP during membrane fusion by adding an electrostatic component. This could serve to increase bilayer avidity or induce curvature in flat membranes. Furthermore, at high lipid:peptide ratios (2:1 or 4:1), the p15HP can induce lipid mixing between liposomes (Figure 3.8 B). It may be that at these high peptide doses, the p15HP can induce positive curvature and promote membrane fusion, either by creating fusogenic dimples or inducing liposome tubulation, as occurs with the N-BAR domain of endophilin (Gallop et al, 2006), the hydrophobic loops in the C2 domains of synaptotagmin-1 and Doc2 proteins (Groffen et al, 2010; Martens et al, 2007), or by FPs in enveloped virus fusogens. Thus, we cannot formally exclude that high localized concentrations of membrane-anchored p15HP at cell-cell fusion sites might also induce positive curvature to promote formation of nascent fusion pores.

3.3.3 Comparison of p15FLiPS with Enveloped Virus FPs

Results also indicate the unique helix-loop-helix conformation of the p15HP is essential for its function as a FLiPS. Circular dichroism studies indicate the p15HP is only partially helical in a membrane environment (Figure 3.4 B), and a helix-loop-helix conformation in DPC micelles was determined by NMR (Figure 3.5). Mutational analyses reveal that point substitutions likely to generate a straight helix (Figure 3.4 A) disrupt pore formation and cell fusion activity (Figure 3.3 A and D). Furthermore, a hydrophobic face in the N- and C-terminal helices and a central loop intolerant of the introduction of positive charge are further requirements (Figure 3.6). This architecture is somewhat reminiscent of the helical hairpin structure of the influenza virus HA fusion peptide (Lorieau et al., 2011).

A comparison of the attributes of p15HP with those of the FPs of enveloped virus fusogens reveals a number of similarities. It has been noted that FPs from all classes of enveloped virus fusion proteins are enriched in Gly and Ala residues (Epand, 2003); a clear compositional bias toward glycine and alanine residues is also observed in p15HP,

and two central Gly residues are absolutely required for pore formation (Figure 3.2 E). Furthermore, class II internal FPs (i.e. FPs not residing at the N-terminal position) often contain a central Pro residue. In the case of Ebola and avian sarcoma/leukosis virus, this central Pro is essential for membrane interaction (Gomara et al., 2004; Delos et al., 2000). The Pro residue of p15HP in the loop region is also essential for intercellular membrane fusion (Figure 3.13 D). Despite these compositional and structural similarities, it is difficult to rationalize that a FP, which sits outside of the virus membrane and therefore has access to the proximal leaflets of fusing membrane, and the p15HP, which sits inside the cytosol and therefore has access to the distal leaflet of only one of the fusing membranes, might function via a common mechanism. Additionally, previous work from our lab has conclusively demonstrated that the myristoylated, polyproline rich ectodomain of p15 functions as an extracellular fusion peptide (Top et al., 2012). Therefore, it seems unlikely that a protein as small as p15 would evolve two functionally redundant FPs.

3.3.4 The Role of Cellular Membrane Curvature Sensing Proteins in Cell-Cell Fusion

Membrane curvature sensing by specific protein motifs has been previously shown to play an important role in such diverse processes as eukaryotic vesicular trafficking (Antonny, 2011), organization of the nuclear pore complex (Doucet & Hetzer, 2010), invasion of host cells by parasites (Reese & Boothroyd, 2009) and localization of proteins within dividing bacteria (Ramamurthi & Losick, 2009). Presently, no specific role of membrane curvature sensing has been ascribed to membrane fusion proteins involved in cell-cell or virus-cell fusion. Instead, cellular curvature-generating proteins such as dynamin, ENTH domain proteins, and BAR domain proteins have recently been shown to promote the fusion pore expansion stage of cell-cell fusion and vesicle exocytosis (Leikina et al., 2013; Richard et al., 2011; Trouillon and Ewing, 2013). In the case of influenza HA and baculovirus gp64-mediated cell-cell fusion, dynamin is required at a stage downstream of pore formation, because pharmacological inhibition of this protein does not affect lipid mixing or pore formation, only pore expansion (Richard et al., 2011). The basis for these effects is unknown, but it is hypothesized that these

proteins accumulate at the edge of the nascent pore, thereby lowering the energy of this energy-expensive step. Dynamin, however, may play a role in depolymerisation of actin rather than generation or stabilization of positive membrane curvature, at least in the case of exocytic vesicle fusion (Gonzalez-Jamett et al, 2013), and it is unclear if dynamin or other curvature-generating proteins localize at the fusion site.

3.3.5 Summary and Future Directions

Membrane fusion events culminating in formation of a fusion pore in p15-mediated cell-cell fusion are thought to be initiated by the N-terminally myristoylated polyproline FP, involved in lipid mixing and membrane aggregation (Top et al., 2012). This action is combined with the membrane-destabilizing effects of the transmembrane domain (Clancy and Duncan, 2011). Prior to the work presented in this chapter, it was unclear how this nascent fusion pore is stabilized, both in p15-mediated membrane fusion and more generally. Based upon the data presented in this chapter, we present a model in which the nascent fusion pore in p15-mediated membrane fusion is stabilized by the cytosolic FLiPS element via insertion of hydrophobic residues into lipid packing defects at the rim of the fusion pore. We propose this first example of a lipid packing sensor in a viral membrane fusion protein masks hydrophobic defects in the rim of nascent fusion pores (or other areas with membrane curvature strain that are formed during the membrane fusion pathway), thereby lowering the energy barrier to stable pore formation. The fusion pore, therefore, may not proceed through highly curved lipid domains devoid of proteins, but rather as a proteolipid complex formed when lipid packing defects are bound by FLiPS elements in the FAST proteins, and possibly in other protein fusogens.

Although this model is intellectually satisfying, there are still a number of unresolved questions. For instance, *to what depth does the p15FLiPS penetrate in the membrane? What is the concentration of p15 at the site of fusion? What is the lipid composition at the site of fusion and how does that impact the lipid packing density? Is the fusion pore really lipidic or is it a mixture of proteins and lipids? Is there a role for cellular proteins in stabilizing the fusion pore through either direct interaction with the membrane or through a protein-protein interaction with the p15 endodomain?* Resolving these issues will be extremely important going forward in unraveling the roles of lipids

and proteins in not only FAST-mediated cell-cell fusion, but for membrane fusion phenomena in general.

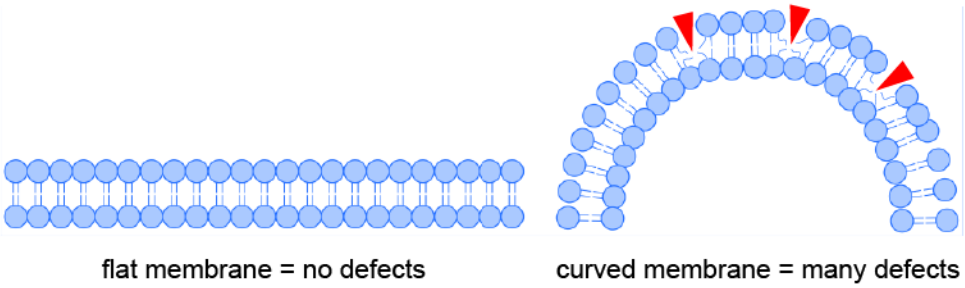

Figure 3.1 Defects in lipid packing in highly curved bilayers. Schematic of a planar bilayer (left) and a highly curved bilayer (right). Lipids pack poorly in highly curved bilayers, leading to exposure of the hydrophobic core of the membrane in these areas (red arrows).

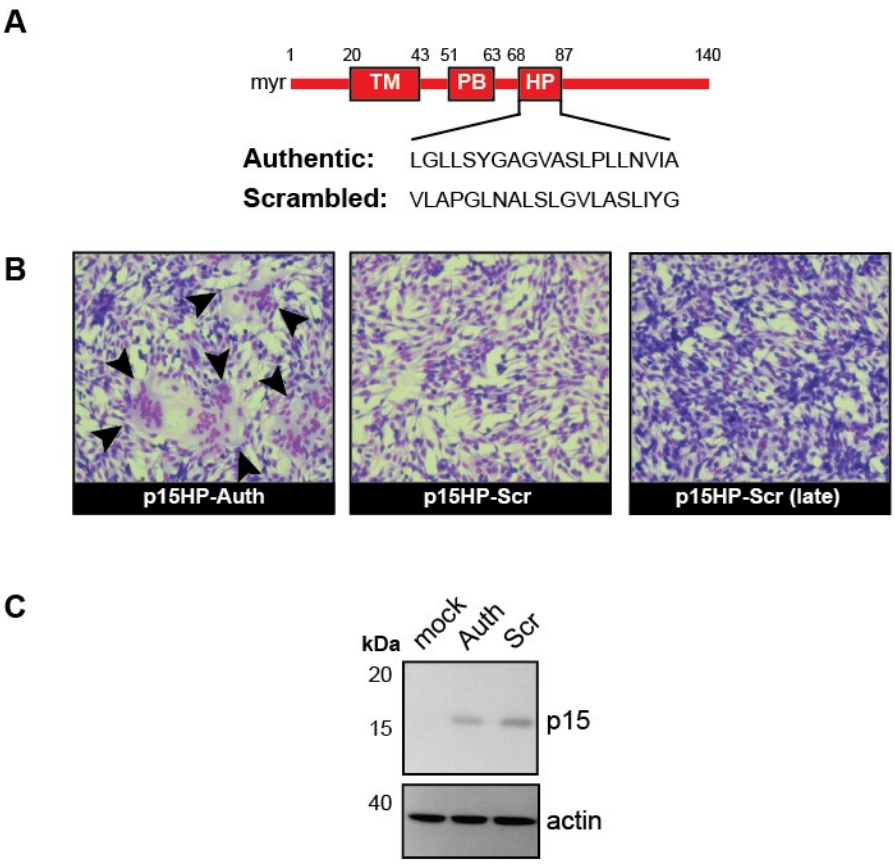

Figure 3.2 The p15 hydrophobic patch is required for p15-mediated cell-cell fusion. **(A)** Schematic of the p15 protein indicating locations of the N-terminal myristic acid (myr), transmembrane domain (TM), polybasic cluster (PB) and hydrophobic patch (HP). Numbers indicate amino acid positions in p15. The sequences of authentic and scrambled versions of p15HP are depicted below. **(B)** QM5 cells were transfected with wild-type p15 (p15HP-Auth) or p15 with a scrambled HP (p15HP-Scr), then fixed and Giemsa stained 10 hpt or 24 hpt (p15HP-Scr (late)) to detect syncytiogenesis. Arrows indicate the borders of syncytia. **(C)** Western blot of equal protein loads of whole cell lysates from QM5 cells transfected with empty pcDNA3 (mock), wild-type p15 (Auth), or p15 with a scrambled HP (Scr) probed with anti-p15C or anti-actin.

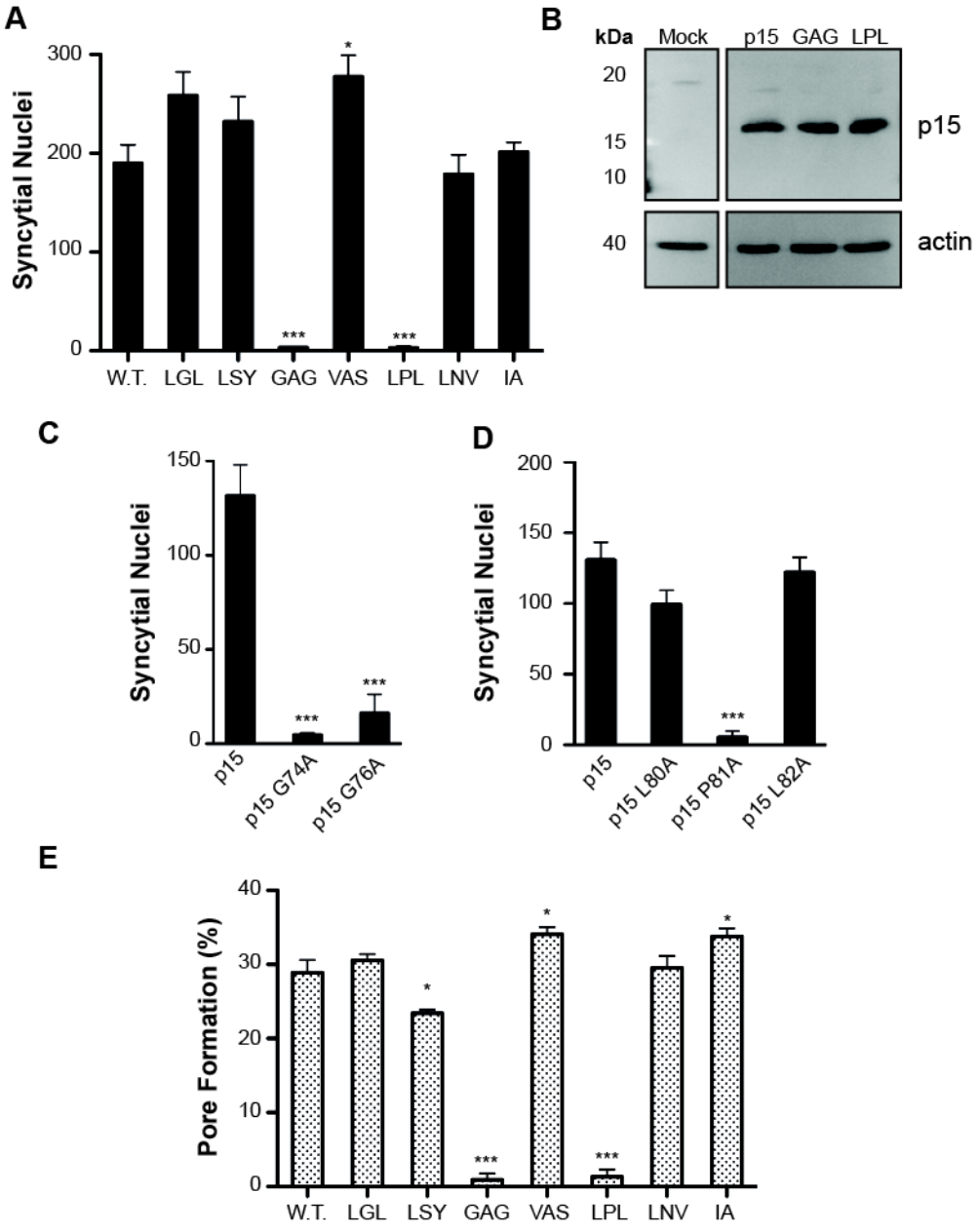
A
Syncytial Nuclei
300
200
100
0
*
***
***
W.T.
LGL
LSY
GAG
VAS
LPL
LNV
IA
B
kDa
Mock
p15
GAG
LPL
20
15
10
40
p15
actin
C
Syncytial Nuclei
150
100
50
0
***
***
p15
p15 G74A
p15 G76A
D
Syncytial Nuclei
200
150
100
50
0
***
p15
p15 L80A
p15 P81A
p15 L82A
E
Pore Formation (%)
40
30
20
10
0
*
***
*
***
*
W.T.
LGL
LSY
GAG
VAS
LPL
LNV
IA

Figure 3.3 Central glycine and proline residues of the p15 hydrophobic patch are essential for pore formation and syncytiogenesis. QM5 cells were transiently transfected with wild-type p15 (W.T.) or p15HP alanine scan mutants. **(A)** Cells were fixed and Giemsa-stained at 8 hours post-transfection to determine the extent of cell-cell fusion induced by each construct. Bars represent the mean number of syncytial nuclei per field ± SEM from three separate experiments. p15HP alanine scan mutants were named according to the three consecutive residues replaced by alanine. **(B)** Equal protein loads were subjected to western blotting and probed with anti-p15c or anti-actin. **(C and D)** Fusogencity of single amino acid mutants. The extent of cell-cell fusion was determined as in panel A. **(E)** The extent of pore formation was determined by co-transfection of GFP with wild-type p15 (W.T.) or p15HP alanine scan constructs. Transfected QM5 cells were overlaid with calcein red-labeled Vero cells 4 hpt. Cells were fixed 9 hpt and measured for dual staining cells by FACS with gating for GFP positive cells. 10,000 gated cells were counted and the percentage of GFP positive cells staining red is indicated. Results are shown as the means ± the SEM of Overton subtractions obtained from two pooled experiments done in duplicate. Data for pore formation was kindly provided by Dr. Eileen Clancy. Statistical significance was determined using a one-way ANOVA with Dunnett's post-test. *** ($p \leq 0.001$); ** ($p \leq 0.01$); * ($p \leq 0.05$).

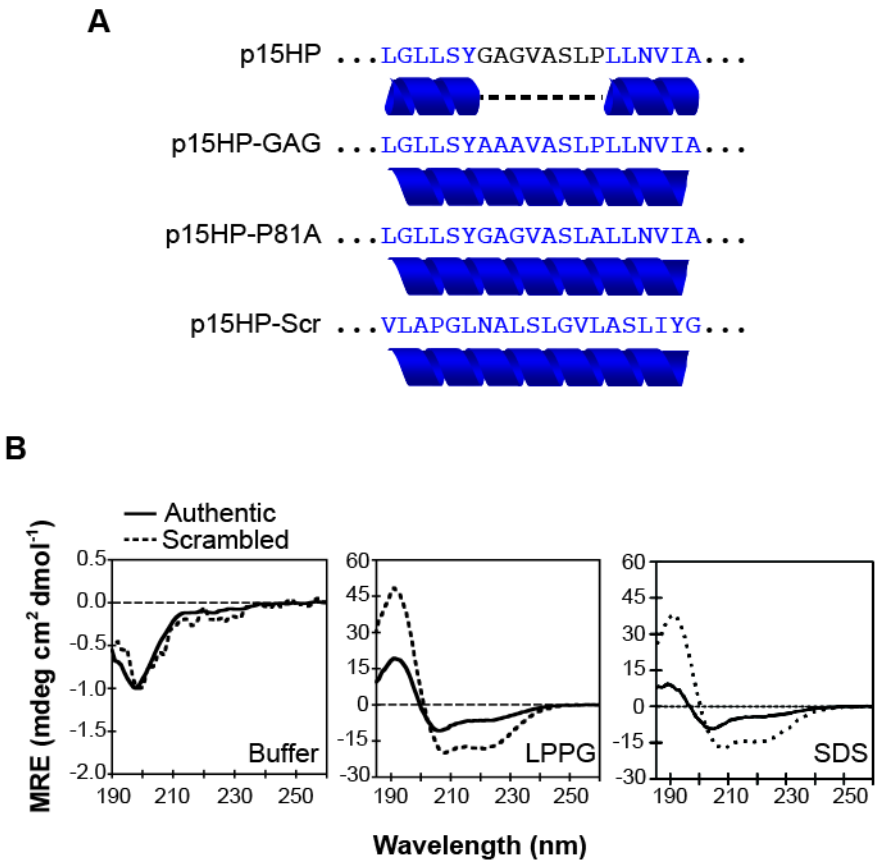

Figure 3.4 Secondary structure characteristics of the p15 hydrophobic patch. (A) Secondary structure predictions (PHYRE^2; (Kelley and Sternberg, 2009)) of authentic p15HP, mutants p15GAG and p15P81A, and scrambled p15HP. Residues predicted to be α-helical are highlighted in purple and underscored with a helix. Residues predicted to be random coil are black and underscored with a dashed line. Although only p15HP are illustrated, the complete endodomain sequence was used for analysis. **(B)** CD spectra of authentic p15 HP (black trace) or scrambled p15HP (dashed trace) peptides in phosphate buffer (left), 1-palmitoyl-2-hydroxy-sn-glycero-3-[phospho-rac-(1-glycerol)] (LPPG) micelles (middle), or sodium dodecyl sulphate (SDS) micelles (right).

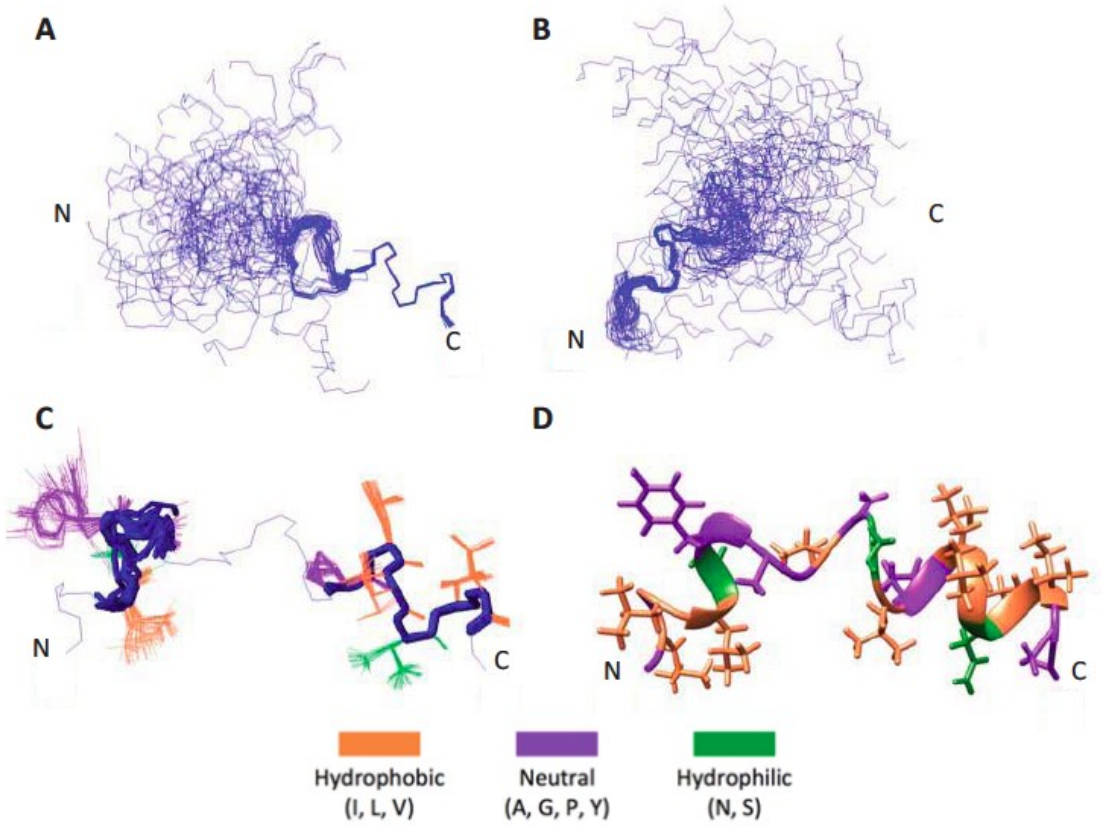

Figure 3.5 NMR structural determination of the p15 hydrophobic patch helix-loop-helix. (**A**) Ensemble of the 50 lowest energy structures (out of 100 calculated) with the C-terminal P81-I86 helix superposed. (**B**) Ensemble of the 50 lowest energy structures with the N-terminal L71-G74 helix superposed. (**C**) Backbone superposition of the two terminal helices (L71-G74 and P81-I86) of all 50 ensemble members onto the lowest-energy conformer. (**D**) Lowest energy conformer of p15HP. In this conformer, the α-helical segments span residues L71-G74 and P81-I86 at the termini, connected by an unstructured turn/loop. This figure was kindly generated by Dr. Muzaddid Sarkar.

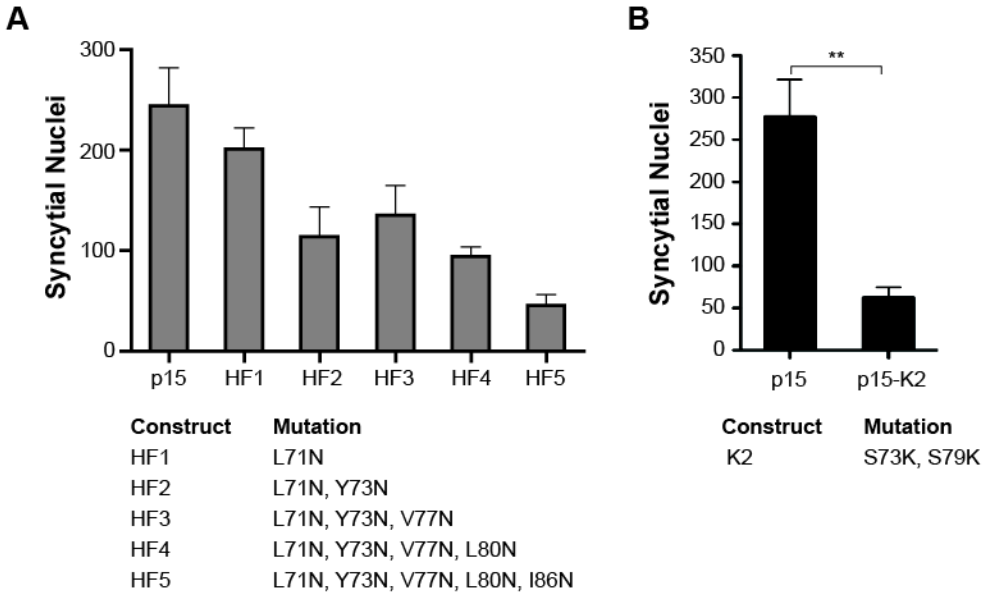

Figure 3.6 p15-mediated cell-cell fusion requires a hydrophobic face in the hydrophobic patch. **(A, B)** QM5 cells transfected with the indicated p15 constructs were fixed at 10 hpt, Giemsa-stained, and the average number of syncytial nuclei quantified and converted to percent fusion relative to wild-type p15. Results are mean ± SEM from three separate experiments. In panel (B), statistical significance was assessed using a two-tailed, unpaired t-test. ** ($p \leq 0.01$).

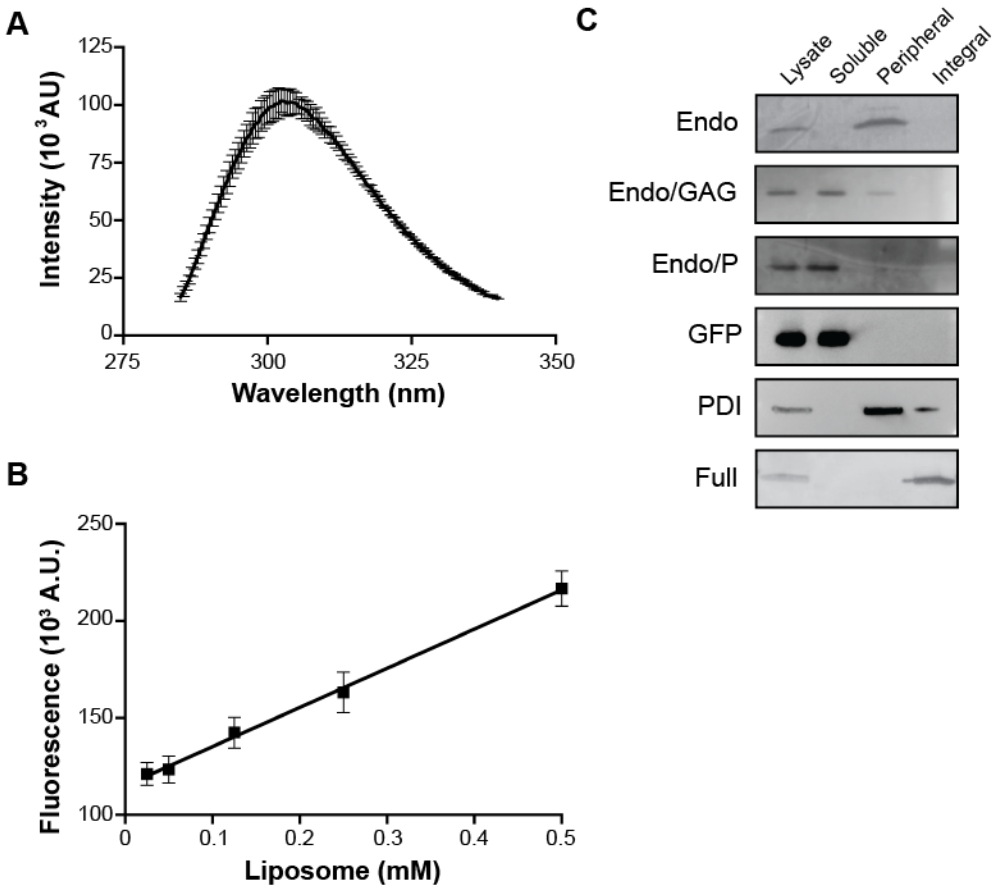

Figure 3.7 Membrane interactions of the p15 hydrophobic patch. (A) Tyrosine fluorescence emission spectrum of p15HP peptide in HBS. An excitation wavelength of 274 nm was used. Error bars represent SD from three experiments. (**B**) Fluorescence emission intensity of p15HP peptide at 305 nm in the presence of 50 nm liposomes (1:1:1 DOPE:DOPE:Chol). Fluorescence = ($F_{peptide+liposome}$) − ($F_{liposome}$) for each given concentration of liposomes. **(C)** Membrane fractions of lysates from QM5 cells expressing authentic p15 endodomain (Endo), or glycine or proline endodomain mutants (Endo/GAG, Endo/P) were resuspended in alkaline sodium carbonate. Peripheral and integral membrane proteins were isolated by centrifugation, and samples were immunoprecipitated with α-p15C and analyzed by western blotting. Full-length p15, protein disulphide isomerase (PDI) and GFP served as positive controls for the integral, peripheral and soluble fractions, respectively.

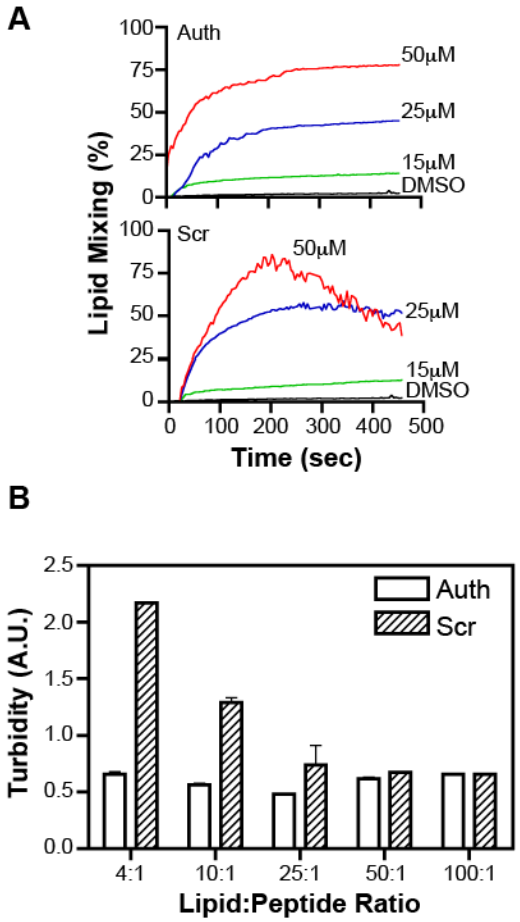

Figure 3.8 Membrane-perturbing effects of the p15 hydrophobic patch. (A) Timecourse of lipid mixing of 100 nm liposomes (1:1:1 DOPC:DOPE:Chol) induced by different concentrations of the authentic (top) or scrambled (bottom) versions of the p15HP peptide. DMSO served as a solvent control. **(B)** Dose-dependent effects of authentic (Auth) and scrambled (Scr) p15HP peptides at varying lipid:peptide ratios on aggregation of DOPC:DOPC:cholesterol (1:1:1 molar ratio) liposomes were determined by measuring turbidity at 600 nm.

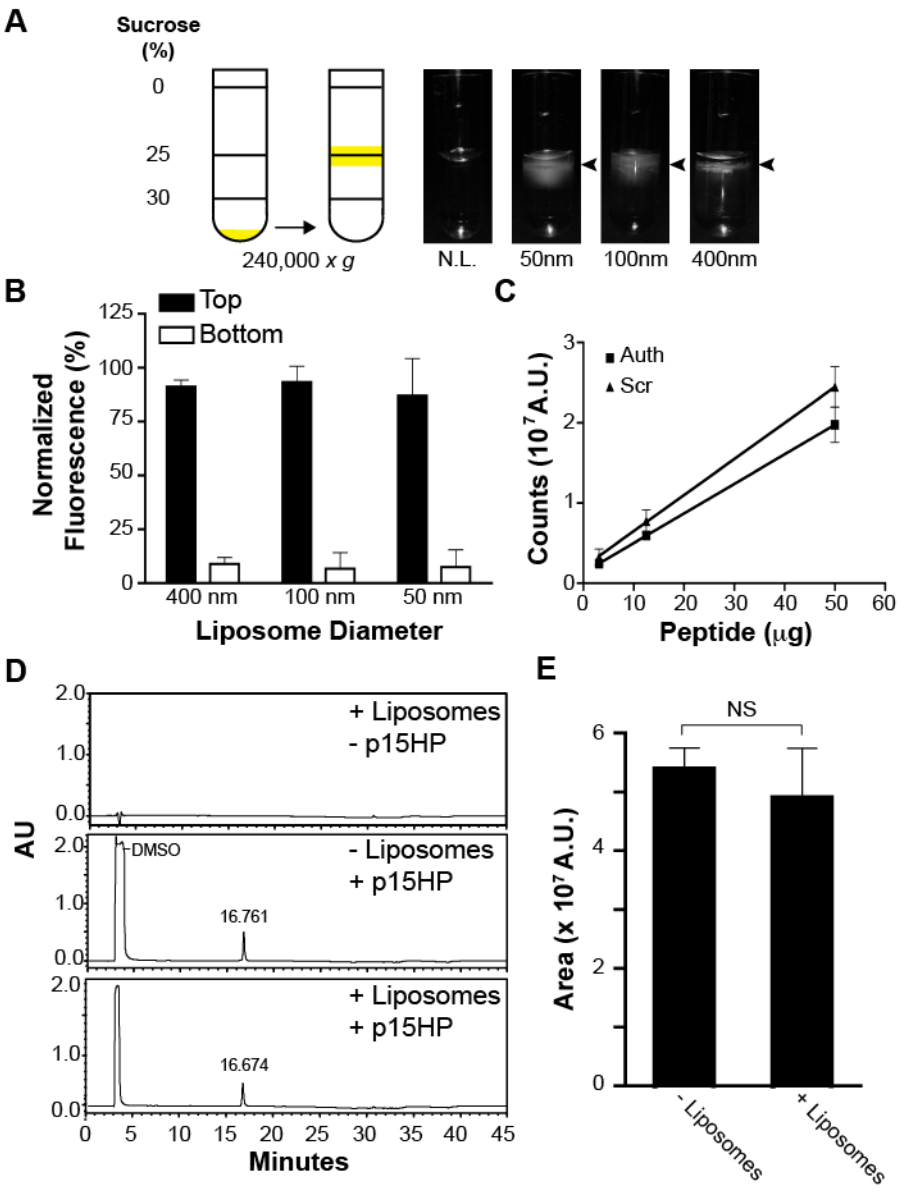
A
Sucrose (%)
0
25
30
240,000 x g
N.L.
50nm
100nm
400nm
B
Top
Bottom
Normalized Fluorescence (%)
125
100
75
50
25
0
400 nm
100 nm
50 nm
Liposome Diameter
C
Auth
Scr
Counts (10^7 A.U.)
3
2
1
0
0
10
20
30
40
50
60
Peptide (μg)
D
+ Liposomes
- p15HP
- Liposomes
+ p15HP
DMSO
16.761
+ Liposomes
+ p15HP
16.674
AU
2.0
1.0
0.0
0
5
10
15
20
25
30
35
40
45
Minutes
E
NS
Area (x 10^7 A.U.)
6
4
2
0
- Liposomes
+ Liposomes

Figure 3.9 Development of a membrane curvature-sensing assay. (A) Liposomes (1:1:1 DOPC:DOPE:chol) labeled with 1% NBD extruded to various diameters (50 nm, 100 nm, and 400 nm) were adjusted to 30% (w/v) sucrose and overlaid with 25% (w/v) sucrose and 0% (w/v) sucrose. Tubes were centrifuged at 240,000 *x g* for 1h and floated liposomes (indicated by an arrow) were photographed. N.L., sample with no liposomes. **(B)** NBD-liposomes of various diameters (400 nm, 100 nm, or 50 nm) were floated as in panel (A). The layers of the gradient were harvested and solubilized with 1.5% SDS and NBD fluorescence was determined. All fluorescent readings fell within a linear detection range determined for each liposome diameter. Fluorescence % = (F_{Exp} / F_{Input}). F_{Input}. **(C)** Linear detection range of authentic (Auth) and scrambled (Scr) p15HP peptide by reverse phase HPLC. Elution peaks were detected at 215 nm and the area under the curve was quantified using Waters software. **(D)** HPLC chromatograms of 100 nm liposomes alone (top), 30 μg p15 HP synthetic peptide alone (middle), or 100 nm liposome mixed with 30 μg p15HP peptide (bottom). Retention times are indicated on the chromatogram. **(E)** Integration of peaks of authentic p15 HP in the absence and presence of liposomes. Bars represent the mean of three experiments ± SD.

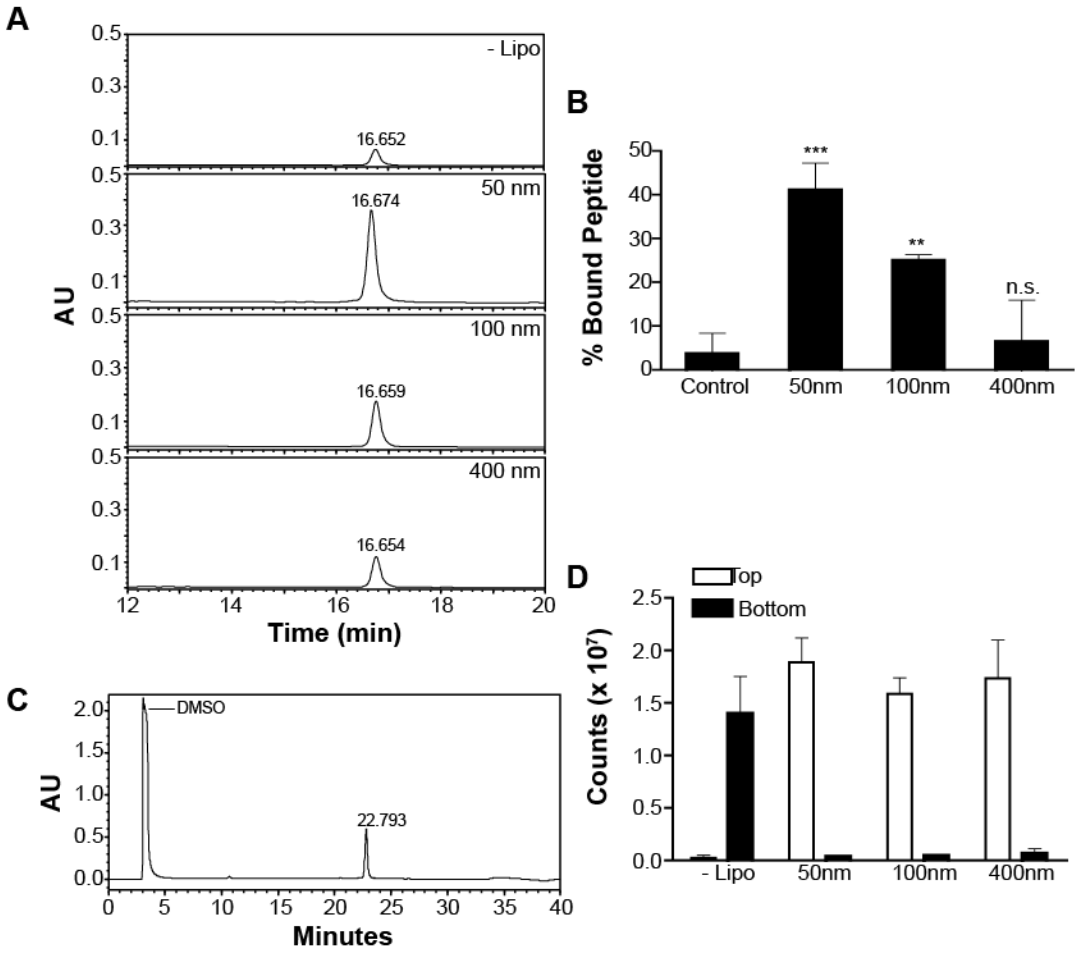

Figure 3.10 The p15 hydrophobic patch preferentially partitions to highly curved liposomes. (A) The p15 HP peptide was mixed with liposomes (1:1:1 DOPC:DOPE:cholesterol) of the indicated diameters at a 1:750 peptide:lipid molar ratio. Liposomes were separated from free peptide by flotation on sucrose gradients, and peptide present in the top liposome fraction detected by HPLC. Retention times are indicated on the graph. **(B)** The liposome (top) and free peptide (bottom) sucrose fractions were analyzed by HPLC as in panel A using liposomes of the indicated diameters, and relative peptide concentration quantified by integrating the area under the peak. % Bound Peptide = $Area_{Top}$ / Total $Area_{Top+Bottom}$. Bars represent the mean ± SD of three experiments. Statistical significance was assessed using a on-way ANOVA ($p = 0.0002$) with Dunnett's post-hoc test. *** ($p \leq 0.001$); ** ($p \leq 0.01$); n.s. ($p > 0.05$). **(C)** HPLC chromatogram of 12.5 μg of scrambled p15 HP synthetic peptide. **(D)** As in panel B, to assess partitioning of scrambled p15 HP to liposomes of varying diameters (50 nm, 100 nm, or 400 nm). Bars represent the mean of three experiments ± SD.

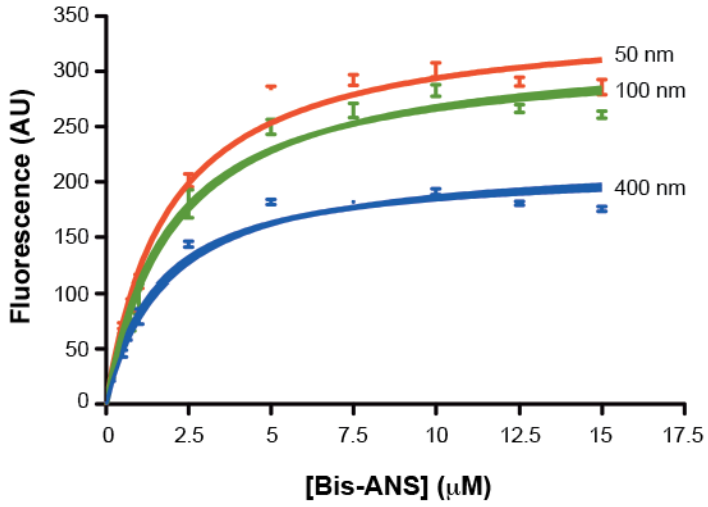

Figure 3.11 Binding curves of bis-ANS to 50, 100, and 400 nm liposomes. Bis-ANS fluorescence was detected on a Cary Varian fluorimeter with an excitation of 395 nm and an emission of 500 nm, and the fluorescence data were fit to one-site binding hyperbola nonlinear regression (GraphPad Prism). Data points represent the mean ± SD of three experiments.

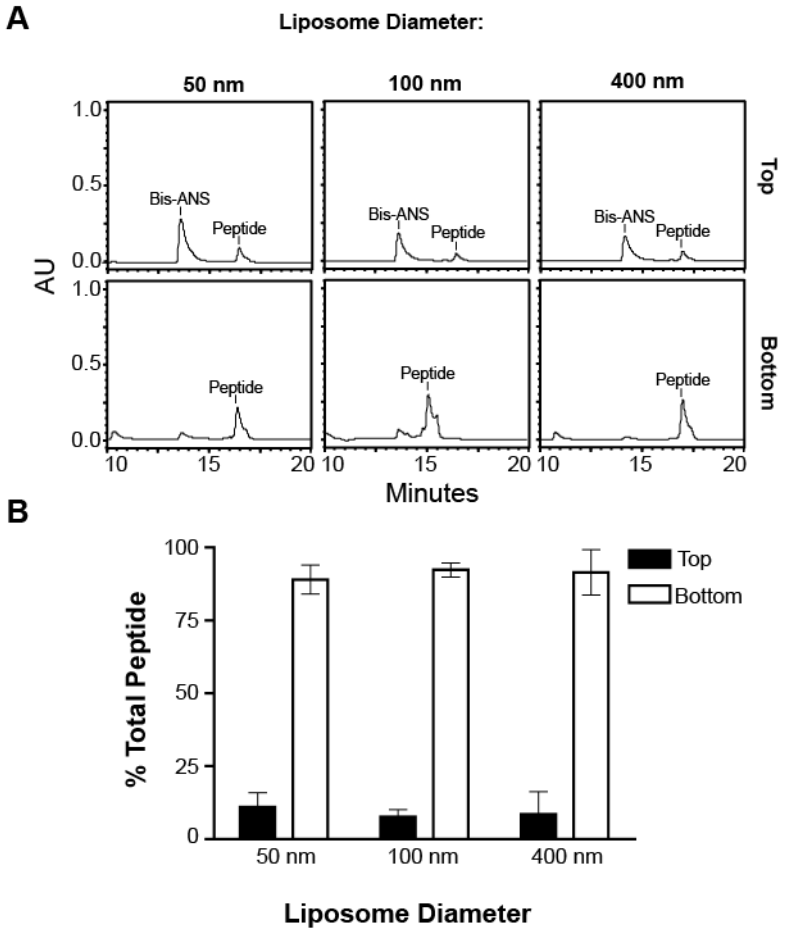

Figure 3.12 The p15 hydrophobic patch is insensitive to membrane curvature when lipid packing defects are blocked with bis-ANS. (A) HPLC chromatograms of the top (liposomes) and bottom (free peptide) fractions from liposome flotation assays, using liposomes of the indicated diameter that were pre-treated with 10 μM bis-ANS before mixing with p15HP peptide. **(B)** The amount of p15HP associated with top (black bars) and bottom (white bars) fractions of the sucrose gradient was determined by integrating the area under the chromatogram peaks. Results are mean ± SD from three experiments.

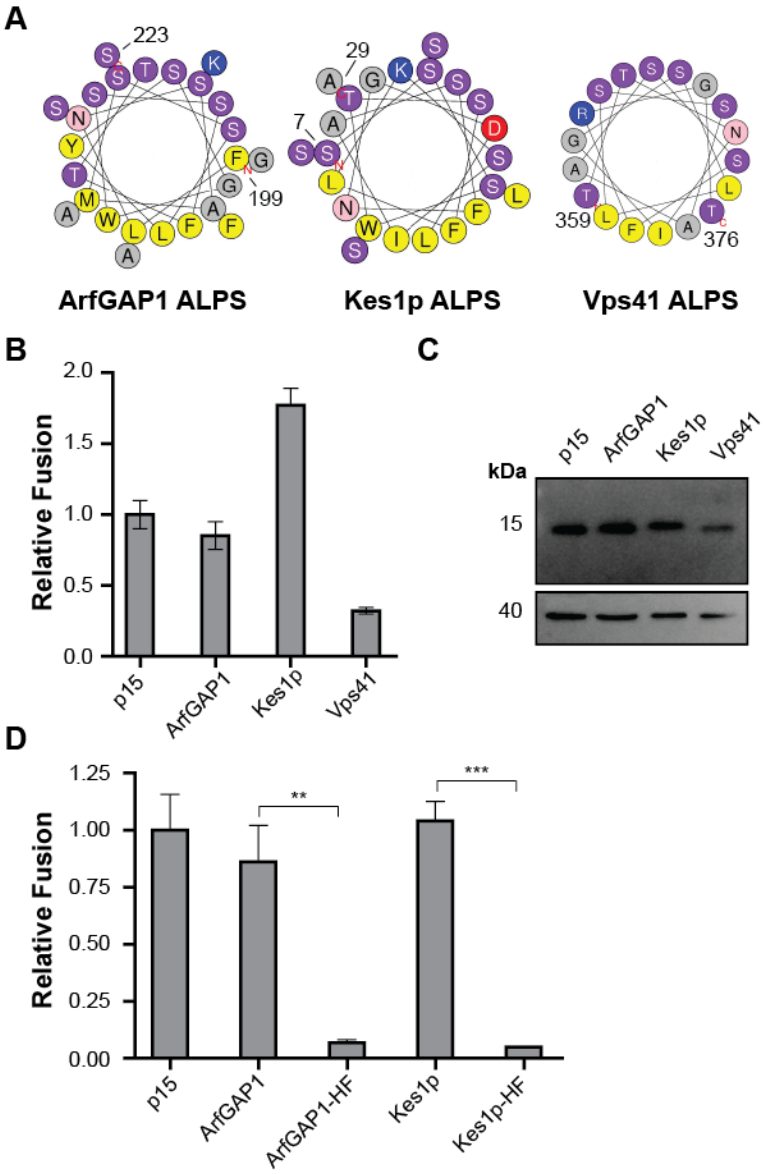
A
223
199
29
7
359
376
ArfGAP1 ALPS
Kes1p ALPS
Vps41 ALPS
B
Relative Fusion
2.0
1.5
1.0
0.5
0.0
p15
ArfGAP1
Kes1p
Vps41
C
kDa
15
40
p15
ArfGAP1
Kes1p
Vps41
D
Relative Fusion
1.25
1.00
0.75
0.50
0.25
0.00
**
***
p15
ArfGAP1
ArfGAP1-HF
Kes1p
Kes1p-HF

Figure 3.13 Heterologous ALPS motifs can functionally replace the p15 hydrophobic patch in a p15 backbone. (A) Helical wheel representations of ALPS motifs from the indicated proteins. Numbers indicate the location of these motifs in their respective proteins. Color code: yellow, hydrophobic; purple, serine and threonine residues; grey, glycine and alanine residues; blue, basic residues. Images were generated with HeliQuest (Gautier et al., 2008). **(B)** Relative fusogenicity of constructs from panel (A). Results are mean number of syncytial nuclei/microscopic field ± SD in transfected QM5 cells for triplicate samples, expressed as percent relative to parental p15, from a representative experiment (n=2). **(C)** Western blot of equivalent protein loads of lysates from QM5 cells transfected the indicated p15 constructs probed with anti-p15c or anti-actin. **(D)** The average number of syncytial nuclei in QM5 cells transfected with chimeric p15 constructs containing the indicated authentic ALPS motifs (ArfGAP1 and Kes1p) or the same motifs containing substitutions of residues in the hydrophobic face (HF) and was quantified and converted to percent fusion relative to wild-type p15. Results are mean ± SEM from three experiments. Statistical significance was assessed using two-tailed, unpaired t-tests. ** ($p \leq 0.01$); *** ($p \leq 0.001$).

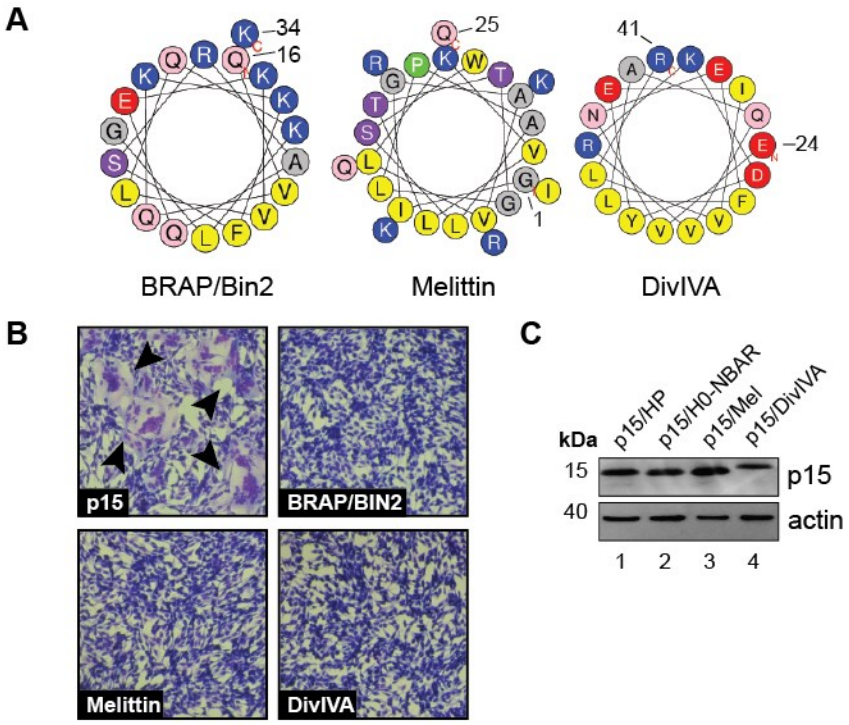

Figure 3.14 The p15 hydrophobic patch cannot be replaced with heterologous membrane-interactive amphipathic helices. (A) Helical wheel projections of heterologous amphipathic helices from the indicated proteins. Numbers indicate the location of these motifs in their respective proteins. Color code: yellow, hydrophobic; purple, serine and threonine residues; grey, glycine and alanine residues; blue, basic residues. Images were generated with HeliQuest (Gautier et al., 2008). **(B)** Syncytium formation in Giemsa-stained, transfected QM5 cell monolayers expressing p15 or chimeric p15 constructs where p15HP was replaced by the indicated amphipathic helices. All chimeric constructs failed to induce syncytium formation. **(C)** Western blot of equivalent protein loads of lysates from cells expressing the indicated p15 constructs probed with anti-p15c or anti-actin.

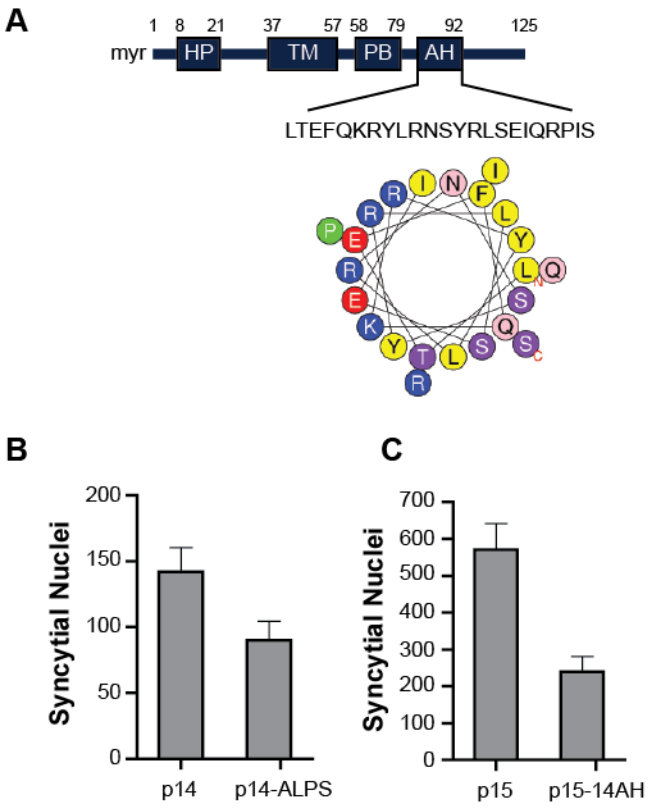

Figure 3.15 The ArfGAP1 ALPS motif can functionally replace an amphipathic helix in the p14 FAST protein. (A) Schematic of the p14 FAST protein indicating the location of the ectodomain hydrophobic patch (HP), transmembrane domain (TM), polybasic cluster (PB), and amphipathic helix (AH). Sequence of the amphipathic helix is depicted below with helical wheel representation. Color code: yellow, hydrophobic; purple, serine and threonine residues; grey, glycine and alanine residues; blue, basic residues. Images were generated with HeliQuest (Gautier et al., 2008). **(B, C)** Fusogenicity of p14 and p14 containing the ArfGAP1 ALPS motif in place of the p14 AH **(C)**, and p15 and p15 containing the p14 AH in place of the p15HP **(D)**. Results are mean number of syncytial nuclei/microscopic field ± SD for triplicate samples from a representative experiment (n=2).

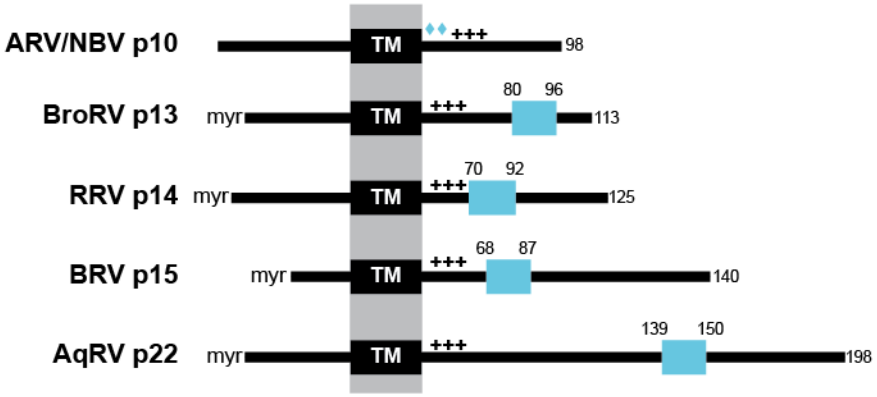

Protein	Putative FLiPS Sequence
ARV/NBV p10	dipalmitic acid
BroRV p13	LDPSVICSLGGSAPNL
RRV p14	LTEFQKRYLRNSYRLSEIQRPIS
BRV p15	LGLLSYGAGVASLPLLNVIA
AqRV p22	VQ QTSFIPLVPL

Figure 3.16 Putative FLiPS elements in the FAST family of proteins. Schematic representation of indicated FAST proteins with putative FLiPS element highlighted in cyan and membrane denoted in grey. Numbers indicate amino acid sequence within each respective protein. myr, myristic acid; TM, transmembrane; +++, polybasic cluster.

CHAPTER 4
INVESTIGATING THE ROLE OF EXOSOME-PACKAGED FAST PROTEINS IN CELL-CELL FUSION

4.1 Introduction

Exosomes represent a specific subtype of secreted membrane vesicles produced by a wide variety of cells *in vitro* and *in vivo*. Exosomes can be distinguished from other types of extracellular vesicles (ECVs), such as shedding microvesicles and membrane blebs, by their subcellular origin in multivesicular bodies (MVB). Although once thought to be 'garbage cans' of the cell, accumulating evidence suggests that exosomes carry functional payloads of protein, lipid, and nucleic acid that alter the physiology of target cells. Hence, exosomes are now believed to play an important role in intercellular communication (Thery et al., 2009). It has become clear that exosomes are involved in a multitude of physiological processes, including virus lifecycles (Wurdinger et al., 2012). The connection between the enveloped virus lifecycle (particularly retroviruses) and exosome biogenesis has been an area of intensive study over the past ten years, however, only a handful of publications have looked at the role of exosomes in non-enveloped virus lifecycles.

The objective of this chapter was to explore the role of the exosome biogenesis in FAST protein-mediated cellular fusion. I hypothesized that fusogenic reoviruses utilize the host exosome pathway to secrete FAST proteins in membrane-bound packages to the extracellular environment. Exosomal release of FAST proteins, and subsequent uptake by neighbouring uninfected cells, would facilitate increased rates of cell fusion, and therefore enhanced spread of fusogenic reoviruses to uninfected cells.

4.1.1 Secreted Extracellular Vesicles

A wide variety of vesicles are actively released from living cells into the extracellular space with their contents reflecting the cellular composition and physiologic state of the cell of origin. Specially selected cargoes include: RNA (mRNA, miRNA, and noncoding sequences), cDNA and genomic sequences, and a large component of proteins and lipids (Vlassov et al., 2012). Upon release, ECVs circulate in the extracellular space

adjacent to the site of discharge where they can be broken down or taken up by neighboring cells (Cocucci et al., 2009). They can also enter adjoining bodily fluids and systemic circulation to travel to distant sites in the body (Caby et al., 2005).

There are three broad classes of secreted extracellular vesicles: exosomes, microvesicles (also referred to as shedding microvesicles, microparticles, or ectosomes), and apoptotic bodies (and/or membrane blebs). The following sections will outline key features of each of these classes (summarized in Table 4.1). The distinguishing features of each ECV subtype and correct nomenclature is currently an area of intensive study.

Table 4.1 Attributes of secreted extracellular vesicles.

	Exosome	**Microvesicle**	**Apoptotic Body**
Diameter	30 nm to 120 nm	50 nm to 2 μm	500 nm to 5 μm
Flotation Density	1.14 – 1.19 g mL^{-1}	N.D.	1.24 – 1.28 g mL^{-1}
Morphology	cup-shaped	heterogeneous	heterogeneous
Notable Lipid Species	LBPA[a] cholesterol ceramide sphingomyelin	cholesterol	phosphatidylserine
SM Exposure	Low	High	High
Lipid Rafts	Yes	Yes	No
Protein Markers	Alix TSG101 Hsp70 CD63 CD81 CD9	selectins integrins CD40 metalloproteinases	histones annexin A5 C3b
Membrane of Origin	MVB	plasma membrane	plasma membrane
Mechanism of Discharge	exocytosis of MVB	budding from plasma membrane	cell shrinkage and death

[a] Present only in intralumenal vesicles, not secreted exosomes
LBPA, lysobisphosphatidic acid; MVB, multivesicular body; N.D., not determined.

4.1.1.1 Exosomes

Exosomes range in size from 30 to 100 nm and are generated by budding of inward invaginations of the limiting membrane of endosomally-derived vesicular compartments (Figure 4.1). As intralumenal vesicles (ILVs) accumulate within these compartments, they are referred to collectively as a MVB. MVBs can be targeted for cargo degradation via the lysosomal pathway, or they can fuse with the plasma membrane to release their ILV freight to the extracellular space, where they are now referred to as exosomes.

Work in yeast and mammalian cell models have revealed the predominant mode of transmembrane cargoes sorting into ILVs is a two-step process. First, endosomal membranes, which have specialized tetraspanin-enriched microdomains, are thought to cluster proteins required for ILV formation through a dense network of protein-protein interactions, sometimes referred to as the tetraspanin web (Perez-Hernandez et al., 2013). Secondly, fine-tuning of cargo selection is provided by the endosomal sorting complex required for transport (ESCRT) proteins, composed of four distinct complexes, ESCRT-0 to ESCRT-III (Colombo et al., 2013). The combined presence of phosphatidylinositol-3-phosphate in the endosomal membrane (Raiborg et al., 2001; Slagsvold et al., 2005), mono-ubiquitinated cargoes (Shields et al., 2009), and curved membrane topology (Fyfe et al., 2011) sequentially recruits members of the ESCRT complex, which drive membrane budding and fission (Wollert and Hurley, 2010). It should also be noted there have been reports of ESCRT-independent sorting mechanisms by tetraspanin proteins, such as CD63 (van Niel et al., 2011), therefore ILV cargo-sorting by tetraspanin and ESCRT proteins may be mutually dependent in some cases or mutually exclusive in others.

Large-scale proteomic studies have revealed that exosomes do not contain a random array of cellular proteins, rather a specific subset of proteins originating from the plasma membrane, endocytic pathway, and cytosol (Olver and Vidal, 2007). Available data suggest that no single protein is indicative of an exosomal identity. Rather a combination of proteins such as TSG101 (ESCRT-I), Alix (ESCRT accessory protein), and CD9, CD63, and CD81 (tetraspanins) are considered to be suitable exosome markers. The use of exosomal markers in research should be cautious, however, because there has

not been a careful assessment of sensitivity or specificity of these markers and other ESCRT-independent pathways of exosome biogenesis have also been described, so these exosomes would presumably be devoid of Alix and TSG101.

4.1.1.2 Microvesicles

Microvesicles are released by outward budding directly from the plasma membrane. These vesicles tend to be larger (>100nm in diameter) and more heterogeneous in size than exosomes. Like exosomes, however, microvesicles are enriched in a specific subset of proteins, including integrins and selectins (Muralidharan-Chari et al., 2010). The release of microvesicles from the plasma membrane is likely controlled by localized cytoskeleton dynamics and changes in bilayer phospholipid composition, resulting in the detachment of small membrane protrusions that are released into the extracellular space. This process is thought to be initiated by the translocation of phosphatidylserine to the outer leaflet of the plasma membrane, triggering an ARF6-driven signaling cascade resulting in the activation of phospholipase D and phosphorylation of myosin light chain by ERK, which is required for microvesicle release (Muralidharan-Chari et al., 2009). Other pathways leading to microvesicle release have also been reported, including a calcium-dependent pathway in blood cells, in which calcium-sensitive proteases such as calpain fragment the cortical cytoskeleton in response to elevated intracellular calcium, resulting in membrane protrusion and microvesicle release (Fox et al., 1991).

Interestingly, recent observations indicate that virus-independent budding from the plasma membrane can be mediated by the endosome to plasma membrane relocation of TSG101 (Choudhuri et al., 2014; Nabhan et al., 2012) and in membrane shedding during plasma membrane repair (Jimenez et al., 2014). This type of budding is topologically identical to microvesicle exvagination from the plasma membrane, however cargo selection and the mechanism of vesicle scission are more closely related to that of an exosome. Thus, it seems that the original distinction between exosomes and microvesicles based on composition, function and membrane of origin are fading.

4.1.1.3 Membrane Blebs and Apoptotic Bodies

In contrast to exosomes and microvesicles, which are released as part of normal cellular processes, membrane blebs and apoptotic bodies are released exclusively during programmed cell death. Apoptotic bodies are much larger than exosomes and microvesicles, ranging from 500 nm to 5 μm, and are characterized by fragmented chromosomal material (including DNA and histone proteins) and sometimes inclusion of intact cellular organelles. Smaller membrane blebs are also released during apoptosis, ranging from 50 nm to 500 nm. Available data suggests these blebs are the result of contraction of cortical actin during early stages of apoptosis, resulting from caspase-mediated cleavage and consequent activation of ROCK1 to drive actomyosin contraction (Coleman et al., 2001; Cotter et al., 1992). Blebs are formed when the plasma membrane delaminates from the cortical cytoskeletal network to form protuberances that are expanded by increased hydrostatic pressure (Tinevez et al., 2009). As apoptosis progresses, larger blebs break away from the cell body to form membrane-clad apoptotic bodies. During the process of apoptosis, phosphatidylserine translocates to the outer leaflet of the plasma membrane, and is subsequently bound by annexin V in the extracellular space. The complement component C3b also binds the membrane surface, all of which serve as signals for phagocytosis by macrophages (Hochreiter-Hufford and Ravichandran, 2013). Therefore, unlike microvesicles and exosomes, which can stably circulate in bodily fluids upon their release, apoptotic bodies are generally rapidly phagocytosed.

4.1.2 Exosome Biogenesis and Cargo Selection

Several different mechanisms of exosome cargo selection have been identified. The following sections will discuss ESCRT-dependent and ESCRT-independent mechanisms of cargo selection. An attractive hypothesis is that these independent pathways have evolved to generate distinctive pools of ILVs which are destined to different fates within the cell, such as lysosomal degradation, receptor recycling, or exosomal secretion.

4.1.2.1 ESCRT-Dependent Generation of ILVs

ESCRT-dependent trafficking of ILV cargo proteins is the best characterized mechanism of cargo selection. ESCRT protein machinery is conserved from yeast to humans and genetic screens have shown the ESCRT complex is absolutely required for the formation of ILVs and the sorting of cargo proteins, at least in yeast (Hurley, 2008). Assembly of a complete ESCRT complex is mediated by a complex interplay of membrane-binding domains and protein-protein interaction motifs within the subunits of the complex, thereby allowing assembly, budding, and fission to occur only in the presence of the correct membrane composition and loaded with the correct cargo proteins. This series of events is summarized in Figure 4.2.

Hepatocyte growth factor–regulated tyrosine kinase substrate (Hrs), an ESCRT-0 protein, binds specifically to proteins tagged with a single ubiquitin moiety via its ubiquitin-interacting motif (UIM) (Raiborg et al., 2002). This modular adaptor protein also binds to phosphatidylinositol-3-phosphate (PI3P) by a FYVE domain and to clathrin lattices by a clathrin-binding domain, ensuring specific targeting and localization to only cargo-loaded endosomal membranes (Komada et al., 1997; Raiborg et al., 2002). Furthermore, this multi-domain adaptor protein contains a P(S/T)XP motif that recruits the soluble, monomeric units of the ESCRT-I complex via the ubiquitin E2 variant (UEV) domain of TSG101 (Teo et al., 2004). ESCRT-I, composed of TSG101, Vps37, MVB12 and Vps28 proteins, recruits the ESCRT-II members EAP20, EAP30 and EAP45 (Russell et al., 2006). The Vps28 subunit of ESCRT-I binds to the N-terminus of the EAP45 subunit of ESCRT-II, which contains a GRAM-like ubiquitin-binding (GLUE) domain, capable of binding both PI3P and ubiquitin (Teo et al., 2006). Finally, ESCRT-III, composed of CHMP2, CHMP3, CHMP4, CHMP6 and the accessory protein Alix, are recruited to the endosomal membrane (Peck et al., 2004). ESCRT-III comprises the membrane-scission machine that detaches the neck of the budding ILV (Hanson et al., 2008; Wollert and Hurley, 2010). Finally, the ATPase Vps4 drives the disassembly of the ESCRT-III complex, which is excluded from the nascent vesicle (Davies et al., 2010). Altogether, recruitment of each ESCRT complex is sequential and relies on specific protein-protein interactions, both with cargo molecules and other ESCRT members.

A common theme between ESCRT-0, ESCRT-I and ESCRT-II proteins is the omnipresence of ubiquitin-binding domains, suggesting these proteins specifically select ubiquitylated cargo. Newly published work by Mageswaran et al., however, challenges this assumption (Mageswaran et al., 2014). This group demonstrated the existence of a ubiquitin-independent, ESCRT-dependent mechanism of ILV cargo selection. They propose the key event that determines the fate of a MVB-associated protein seems to be the competition between the interaction of the protein with the membrane and ESCRT machinery: if the membrane interaction is stronger, the protein becomes a cargo; if the interaction with ESCRT proteins is stronger, the protein is disassembled and recycled with the ESCRT proteins. Because transmembrane proteins have a permanent membrane-tether, membrane interaction always wins and thus even proteins that interact strongly with ESCRT members are efficiently sorted into ILVs. This suggests the principles governing ESCRT assembly and cargo selection may be surprisingly flexible and simpler than previously thought.

4.1.2.2 ESCRT-Independent Generation of ILVs

Although formation of MVBs in yeast is fully dependent on the ESCRT complex, mammalian cells are capable of generating ILVs in the absence of key ESCRT proteins, suggesting ESCRT-independent pathways of ILV formation in higher eukaryotes.

One such unconventional pathway is a lipid-based pathway. Lysobisphosphatidic acid (LBPA) and ceramide are understood to be organized into special microdomains in the endosomal membrane, and are thought to serve as platforms for spontaneous membrane budding. *In vitro* studies have shown this to be true in LBPA-enriched liposomes, but only when the lumenal pH resembles that of late endosomal compartments (Matsuo et al., 2004). Likewise, the sphingolipid ceramide is also capable of causing inward budding of giant unilamellar liposomes (Trajkovic et al., 2008). *In cellulo* inhibition of neutral sphingomyelinase enzymes responsible for the generation of ceramide in endosomal membranes has also been shown to block exosome secretion in some cases (Gills et al., 2012; Trajkovic et al., 2008). Taken together, these data suggest that LBPA and ceramide form microdomains for selection of raft-associated cargo.

Another form of ESCRT-independent MVB sorting is higher order homo-multimerization. For example, antibody-induced clustering of transmembrane proteins may re-direct their trafficking into a MVB (Vidal et al., 1997). Furthermore, prion proteins and the amyloid precursor proteins are also sorted to exosomes due to their propensity to form higher-order oligomers in lipid rafts (Taylor and Hooper, 2007). Finally, proteins can be directed into this exosomal protein sorting pathway by exposing cell surface proteins to exogenous cross-linking agents, by attaching membrane anchors to highly oligomeric cytoplasmic proteins, or by adding multiple homo-oligomerization domains to intracellular acylated proteins, even in the absence of Vps4 (Fang et al., 2007).

A final form of ESCRT-independent exosome sorting is the presence of generic membrane-anchoring motifs, such as acylation or PIP-binding motifs, which when added to heterologous proteins are sufficient for exosome targeting (Shen et al., 2011). Taken together, a wide-variety of *cis*-acting signals may direct proteins to ILVs and exosomes in an ESCRT-independent manner.

4.1.3 Determinants of ILV Fate

There are three possible fates for ILVs once formed in an MVB: (i) fusion of the MVB with the lysosome, ultimately resulting in degradation of luminal contents; (ii) back-fusion of an ILV membrane with the MVB limiting membrane, leading to receptor recycling; or (iii) fusion of the MVB limiting membrane with the plasma membrane, resulting in extracellular release cargo in the form of exosomes. The machineries involved in mobilization of secretory MVBs to the cell periphery, and their docking and fusion with the cell surface are still at an early stage of comprehension. In cells derived from hematopoietic origin, a spike in intracellular calcium is required for exosome-release in a Rab11-dependent manner (Savina et al., 2003). Other non-hematopoetic cells do not require calcium stimulation and more or less constitutively secrete exosomes. In these cells, it seems Rab27a, Rab27b (Ostrowski et al., 2010) and Rab35 (Hsu et al., 2010a) play an active role in the docking and fusion of MVBs with the plasma membrane. It is known that Rab7 is required for MVB to lysosome fusion post-cargo selection (Vanlandingham and Ceresa, 2009), however, the criteria determining why

some MVBs fuse to lysosomes while others fuse to the plasma membrane is unknown. In dendritic cells, two distinct MVB pathways have been proposed for the sorting of MHC molecules, whereby ILVs containing mono-ubiquitinated MHC molecules are directed for lysosomal degradation and ILVs containing non-ubiquitnated MHC (also rich in detergent-resistant lipids and tetraspanins) are destined for secretory MVBs (Buschow et al., 2009). Collectively, these observations suggest the existence of two distinct types of MVBs: one for degradation and one for exosome generation, with ILV composition determining the fate of the organelle.

4.1.4 Interactions of Exosomes with Target Cells

The functionality of exosomes depends on their ability to selectively deliver cargo to target cells. The cellular and molecular basis of exosome targeting is still being delineated, but specificity is thought to be determined by cellular adhesion molecules, such as integrins (Clayton et al., 2004) or tetraspanin molecules (Rana and Zoller, 2011) present in the membrane of the exosome. After binding to target cells, exosomes may hypothetically remain stably associated with the plasma membrane, directly fuse with the plasma membrane, or be internalized through endocytic or phagocytic pathways. Detection of fusion of small EVs with the plasma membrane by fluorescence microscopy in live cells is limited by the resolution of the microscope (~200 nm) and the fast dynamics of fusion events. Nevertheless, direct evidence for fusion of exosomes with target cell membranes has been obtained by labeling exosomes with a lipophilic dye, in which self-quenching is relieved upon fusion via dilution in the target membrane, resulting in a rapid localized increase in fluorescence of target cells (Montecalvo et al., 2012). The basis for this fusion event and the protein fusogens involved have not been determined. Several other studies have provided evidence for the accumulation of captured exosomes in endocytic or phagocytic compartments, with uptake depending on the actin cytoskeleton, phosphatidylinositol 3-kinase activity, and dynamin-2 (Feng et al., 2010; Nanbo et al., 2013; Tian et al., 2010).

4.1.5 Pleiotropic Functions of Exosomes and Microvesicles

Because the composition of an exosome will depend largely on the cell from which it derives, it follows that exosome function will also vary depending on the cell of origin. The first characterized function of exosomes was as an alternative secretion pathway, used to remove obsolete receptors (Johnstone et al., 1989). In the last 10 years, it has become appreciated that exosomes play a role in many diverse processes, including viral lifecycles and syncytiogenesis.

4.1.5.1 Exosomes, Microvesicles, and Viruses

The exosome biogenesis pathway plays a clear role in the lifecycle of many enveloped viruses. In 2003, Gould and colleagues proposed the 'Trojan Exosome Hypothesis', which proposed that enveloped viruses, particularly retroviruses, usurp the endogenous cellular exosome machinery in order to assemble viral components, acquire an envelope, and as a means to exit the cell (Gould et al., 2003). Extensive work has attempted to test this hypothesis, yet the actual budding location of the virus (i.e. plasma membrane versus the lumen of multivesicular bodies) remains controversial. In spite of this incongruity in the literature, it is clear that rhabdoviruses, filoviruses, arenaviruses, herpesviruses, and hepatitis B and C viruses use ESCRT proteins as part of their exit modality (McDonald and Martin-Serrano, 2009).

Non-enveloped viruses, however, do not bud as part of viral egress. Consequently, little effort has been afforded to investigating the role of the exosome pathway in the lifecycle of any non-enveloped viruses, as it was thought to be largely irrelevant. A recent opinion paper hypothesized that the non-enveloped virus, cocksakievirus B, exploits the microvesicle-release pathway via virus-induced, calcium-dependent, calpain-dependent actin depolymerization (Inal and Jorfi, 2013). Furthermore, release of hepatitis E virions from a hepatoma cell line has been shown to be completely dependent on TSG101 (Nagashima et al., 2011), although it is unknown why. Interestingly, the so-called 'non-enveloped' picornavirus, hepatitis A virus, was recently shown to acquire an 'exosome envelope', which allowed virions to escape the effects of neutralizing antibodies (Feng et al., 2013). These examples suggest other non-enveloped

viruses, such as the fusogenic reoviruses that we are interested in, may utilize host exosome biogenesis.

4.1.5.2 Exosomes, Microvesicles and Cell-Cell Fusion

Recently, it has become clear that many syncytial precursor cells, and the syncytium itself, secrete extracellular membrane vesicles. For example, a recent in-depth study of the secretome of primary muscle satellite cells and human neonatal myoblasts undergoing differentiation revealed these cells secrete exosomes (of endosomal origin) and microvesicles (of plasma membrane origin) (Le Bihan et al., 2012). This data has also been confirmed in mouse myoblast C2C12 cells (Geminard et al., 2004). There is also strong evidence that syncytiotrophoblast tissue releases both exosomes and microvesicles, which are used in the adaptation of the maternal immune system to pregnancy. In fact, the constitutive biogenesis of exosomes by the syncytiotrophoblast is a normal feature of pregnancy, whereas the release of so-called 'placental debris', or syncytiotrophoblast microvesicles (composed of apoptotic blebs and necrotic tissue particles) is associated with pre-eclampsia and placental oxidative stress (Redman and Sargent, 2008). It has also been recently determined that syncytiotrophoblast-derived exosomes carry a specific placental miRNA cluster that is implicated in conferring antiviral effects to target cells (Delorme-Axford et al., 2013). Finally, the egg releases CD9-bearing exosomes prior to sperm-egg fusion (Miyado et al., 2008). These exosomes are thought to interact with the sperm membrane, preparing it for fusion.

These studies confirm that cells that have undergone membrane fusion as a part of their normal natural history are capable of secreting functional extracellular membrane vesicles, however, the specific role of exosomes (and of other extracellular membrane vesicles) in generation and maintenance of the syncytium is largely unknown. There is some evidence that exosomes derived from human placental explants, primary trophoblast cells, and BeWo cell cultures contain the putative syncytiotrophoblast fusogen, syncytin-1 (Tolosa et al., 2012). The functional effect of syncytin-positive exosomes on membrane fusion or maintenance of the syncytium has yet to be examined, although it has been questioned in the literature whether syncytin-exosomes are a key ingredient in promoting further rounds of cell-cell fusion (Record, 2014).

Whether or not exosomes produced by other cells that undergo cell-cell fusion, such as myotubes or osteoclasts, also contain cell fusion proteins and fusion-associated factors is unknown, due to that fact that most endogenous cell fusion proteins have yet to be discovered.

4.1.6 Summary

Given the void in the literature regarding the role of exosomes in cell-cell fusion and non-enveloped virus lifecycles, we sought to examine this pathway in FAST protein-mediated cell-cell fusion. We now show that the FAST proteins are trafficked to exosomes in an ESCRT-dependent manner, and this event is reliant on a discrete stretch of amino acids in the endodomain of RRV p14. Finally, we show that purified exosomes are sufficient to induce cell-cell fusion, suggesting a central role for exosome biogenesis in the FAST model of cellular fusion.

4.2 Results

4.2.1 FAST Proteins are Secreted in Extracellular Membrane Vesicles

In previous functional studies of the FAST proteins, numerous attempts were made to construct recombinant pseudotyped viruses ((Brown et al., 2009) and unpublished data). Interestingly, in multiple, independent preparations of virus, RRV p14 consistently co-purified in small extracellular membranous vesicles (Edward Methange and Dimitri Lavillette, personal communications). This held true, even when different parental viruses were used, including vesicular stomatitis virus, human immunodeficiency virus, simian immunodeficiency virus, and murine leukemia virus. Based on these observations, we hypothesized that the FAST proteins were secreted in extracellular vesicles and these vesicles might have bioactive properties essential for FAST-mediated cell-cell fusion.

Previous work on HIV has shown that viruses purified from cell culture supernatants are often contaminated with a large amount of extracellular membrane vesicles, whose budding is induced by the virus (Bess et al., 1997; Gluschankof et al., 1997). Since all previous observations regarding FAST proteins and extracellular vesicles had been made in the context of virus packaging cell lines, we wanted to eliminate the

presence of other viral proteins that might influence the release of extracellular vesicles. Therefore, we transiently transfected quail fibroblast (QM5) cells with an expression plasmid encoding the model FAST protein, p14 (Figure 4.3 A). As expected, p14 induced cell-cell fusion as early as 4 hpt, and syncytia became larger and more numerous with time (Figure 4.3 B). To evaluate secretion of p14 into the extracellular space, we harvested extracellular membrane fractions from the conditioned medium using differential centrifugation. Successive centrifugations were applied to conditioned medium to crudely separate different-sized particles (Figure 2.1), including large cellular debris and apoptotic bodies in the 2,000 *x g* pellet (P2), microvesicles and membrane blebs in the 10,000 *x g* pellet (P10), and exosomes and microvesicles in the 100,000 *x g* fraction (P100). The pellets were subjected to western blotting and probed for the presence of p14 (Figure 4.3 C). At as early as 6 hpt, p14 was observed the P100 fraction, and the amount of p14 in this fraction increased over time. p14 was less abundant in P2 and P10 fractions, and only appeared at later time points. Culture supernatant cleared of all ECVs (Sup) was devoid of p14, suggesting p14 is exclusively secreted in membrane vesicles. The amount of total protein in each pellet also correlated with the p14 levels, with approximately 6-fold more protein in the P100 fraction than in P2 and P10 fractions (Figure 4.3 D). Finally, to eliminate the possibility that ECV secretion was an artifact of transfection-mediated overexpression, we transfected cells with GFP or a mutated transferrin receptor incapable of trafficking to extracellular vesicles. The mutated transferrin receptor has a key tyrosine-based motif which serves as an Alix-binding site. When mutated, Alix is incapable of binding transferring receptor, and is therefore not sorted to exosomes (Geminard et al., 2004). As expected, little to none of the soluble or transmembrane protein controls were detected in ECV fractions (Figure 4.3 E), suggesting secretion of p14 is unrelated to transfection overexpression.

To further confirm the presence of p14 in the membranes of ECVs, vesicle pellets were treated with alkaline sodium carbonate solution to release lumenal proteins or a concentrated sodium chloride solution to strip proteins peripherally associated with the membrane. Using both treatments, p14 was retained in the pellet fraction, suggesting p14 is an integral membrane protein (Figure 4.4 A). As a control to demonstrate complete membrane disruption, endogenous annexin A1 (ANX1), a peripheral membrane protein

known to reside in the lumen of ECVs (Gerke et al., 2005), was successfully stripped with the alkaline treatment (Figure 4.4 A). The salt treatment was unable to dissociate ANX1 from the membrane pellet, as has been previously demonstrated with Annexin A2 (Harder et al., 1997).

To verify the orientation of p14, we used a C-terminally FLAG-tagged construct in an epitope availability assay. Briefly, p14-FLAG was immunoprecipitated in the presence or absence of solubilizing detergents (0.1% sodium deoxycholate, 0.1% sodium dodecyl sulphate, and 1% Triton X-100) with various antibodies directed against N- or C-terminal epitopes, or the full-length protein. While antiserum recognizing the p14 N-terminal ectodomain or full-length protein immunoprecipitated p14 vesicles in the absence of detergent, the C-terminal FLAG tag was only accessible when ECVs were treated with detergent (Figure 4.4 B), suggesting p14 assumes the correct N_{out}/C_{in} topology. Taken together, these results suggest that p14 is secreted in ECVs as an integral membrane protein with the same topology as plasma membrane-localized p14.

To better understand if ECV-secretion is a general characteristic shared by all FAST proteins, we examined extracellular vesicle pellets from QM5 cells transfected with ARV p10 or BRV p15, harvested at 24 hpt or 10 hpt, respectively when syncytia were small (Figure 4.5 A). p10 and p15 FAST proteins were both present in all ECV fractions, however, the ECV secretion profile of p10 more closely matched that of p14, with an enrichment in the P100 fraction. p15, although most enriched in the P2 fraction, was also present in the P100 fraction (Figure 4.5 B). Therefore, we conclude that extracellular secretion is a shared characteristic of FAST proteins.

4.2.2 RRV p14 Stimulates ECV Secretion

To determine if expression of p14 induces secretion of small ECVs, the P100 fraction from human fibroscarcoma (HT1080) cells was harvested and assayed for total protein or total cholesterol. Although mock transfection significantly increased the total protein and cholesterol in the P100 fraction by approximately two-fold, expression of p14 significantly increased total secreted protein and cholesterol by approximately five-fold over non-transfected cells and by greater than two-fold over mock transfected cells (Figure 4.6 A). We found no significant difference between calculated cholesterol:protein

ratios (Figure 4.6 B), suggesting increases in protein levels observed for p14 cannot be accounted for by a skewing of protein to lipid ratios in vesicles. We conclude, therefore, that p14 increases the number of ECVs secreted.

4.2.3 p14 is Present in the Membrane of Exosomes

Given the characteristics of the p14 FAST protein – propensity to oligomerize (Corcoran et al., 2011), localization in lipid rafts (Corcoran et al., 2006), and N-terminal acylation (Corcoran et al., 2004) - we suspected that p14 was secreted in exosomes. To test this hypothesis, we first purified putative exosomes using our standard differential unltracentrifugation protocol, and characterized the P100 pellet by ultrastructural analysis. In transmission electron micrographs of whole mounted P100 samples isolated from HT1080 cells transfected with p14, we found a homogeneous mixture of exosome-typical cup-shaped structures, with a visible absence of contaminating disrupted (non-vesicular) membrane structures (Figure 4.7 A). These exosome-like vesicular structures ranged in size from approximately 30 to 210 nm, with a mean vesicle size of 90.7 ± 36.4 nm (Figure 4.7 B). These vesicles were also immunopositive for p14 (Figure 4.7 C). Immunoblot analysis of whole cell lysates (WCL; Figure 4.8, lanes 1 and 2) and the P100 fraction (Figure 4.8, lanes 3 and 4) from mock-transfected or p14-transfected cells were positive for the exosomal marker proteins CD81, ANX1, Rab11, TSG101, and Hsp70, as well as the plasma membrane marker caveolin-1. Contaminating cellular proteins from the secretory pathway, such as ER-localized protein disulphide isomerase and actin, were absent (Figure 4.8).

To extend these observations with a more stringent analysis, we loaded the P100 fraction from HT1080 cells transfected with p14 on a discontinuous sucrose gradient. Exosomes typically band in fractions with a characteristic density of 1.14-1.19 g mL^{-1}, whereas contaminating cellular membranes or apoptotic blebs band at 1.24-1.29 g mL^{-1}, and lipoproteins or aggregated proteins band at <1.03 g mL^{-1} and >3.0 g mL^{-1}, respectively. Immunoblotting of sucrose gradient-separated vesicles demonstrated the presence of p14 in 1.13 g ml^{-1} to 1.16 g ml^{-1} fractions, overlapping with the tetraspanin exosome marker CD81 (Figure 4.9, lanes 6, 7, and 8). Taken together, these data support our hypothesis that p14 is secreted in exosomes.

4.2.4 In-Depth Analysis of the Exosome Proteome

The cellular interactome of the soluble endodomain fragment of p14 was recently determined using a yeast-two-hybrid methodology (Julie Boutlier, unpublished data). Since over 80 proteins were identified as interaction partners with the p14 endodomain, we reasoned that p14 might recruit cellular proteins into exosomes. To test this hypothesis, purified exosome pellets were subjected to LC-MS/MS in data-dependent acquisition mode to maximize detection of low abundance proteins. Proteins were identified using Proteome Discoverer and Sequest software (Figure 4.10). Two biological replicates, with three technical replicates each, were analyzed for each sample. Only those proteins identified in both biological replicates were used for further analysis. A total of 188 proteins were identified in control exosomes, while 172 proteins were identified in p14-exosomes (Appendix 1). Classically secreted proteins identified using the 'Human Compendium of Secreted Proteins' (Eichelbaum et al., 2012) and common contaminant proteins were disregarded from the protein lists (Figure 4.10), reducing the total number of proteins to 168 for control exosomes and 159 for p14-exosomes (Figure 4.11). Approximately three quarters of all proteins identified for control and p14 samples were classified as non-secreted proteins (Figure 4.11 A) and subjected to further analysis. A total of 153 proteins were common between control and p14 samples, leaving 15 proteins uniquely assigned to control samples and 6 proteins uniquely assigned to p14-exosomes (Figure 4.11 B, Tables 4.2 and 4.3), suggesting a surprisingly similar molecular composition between control and p14 exosomes.

Table 4.2 Proteins uniquely identified in control exosomes isolated from mock-transfected HT1080 cells.

UniProt Accession	Gene Symbol	Protein Name	Unique Peptides	Sequence Coverage
P68431	HIST1H3A	Histone H3.1	1	52.94%
Q13509	TUBB3	Tubulin beta-3 chain	1	36.22%
G3V1B3	RPL21	60S ribosomal protein L21	2	29.89%
M0R3D6	RPL18A	60S ribosomal protein L18a	3	21.99%
Q562R1	ACTBL2	Beta-actin-like protein 2	1	19.68%
D6RBI2	MATR3	Matrin-3	1	19.27%
E9PMW7	EEF1D	Elongation factor 1-delta	1	18.46%
I3L3P7	RPS15A	40S ribosomal protein S15a	1	14.00%
B4DU28	ADAM10	Disintegrin and metalloproteinase domain-containing protein 10	3	12.53%
E7ENQ1	MAP4K4	Mitogen-activated protein kinase kinase kinase kinase 4	10	10.83%
P52907	CAPZA1	F-actin-capping protein subunit alpha-1	2	9.79%
A6NLG9	BGN	Biglycan	3	9.77%
F8W0G4	PCBP2	Poly(rC)-binding protein 2	1	8.23%
B4DVY1	EIF3D	Eukaryotic translation initiation factor 3 subunit D	2	7.83%
F5H7A2	PODXL	Podocalyxin	1	2.47%

To more closely define the cellular origin of identified proteins, we used Gene Ontology mapping using cellular component GO Slim annotations (http://go.princeton.edu/cgi-bin/GOTermMapper). A vast majority of the control and p14 exosome proteins are designated as intracellular proteins, although there is a strong enrichment of extracellular proteins compared to genomic background frequencies as well (Figure 4.11 C). Our samples were also enriched in plasma membrane proteins, cytoskeletal proteins, cytoplasmic membrane vesicle proteins, ribosomal proteins, and lysosomal proteins compared to background. These findings are consistent with the

endosomal origin of exosomes. Interestingly, 20/23 of the most frequently identified exosome proteins in ExoCarta, a database of exosome proteomic data
(Simpson et al., 2012), were consistently identified in both replicates of p14 and control exosomes (Appendix 1, Table A.3). Furthermore, using KEGG Brite Hierarchical analysis (Kanehisa and Goto, 2000), we identified 38/48 proteins in the exosome protein family cluster (Appendix 1, Table A.4). Together, these results strongly confirm an exosomal identity for control and p14 exosomes.

Table 4.3 Proteins uniquely identified in p14-exosomes isolated from HT1080 cells transiently-transfected with p14.

UniProt Accession	Gene Symbol	Protein Name	Unique Peptides	Sequence Coverage
Q9BQE3	TUBA1C	Tubulin alpha-1C chain	1	51.45%
P62979	RPS27A	Ubiquitin-40S ribosomal protein S27a	6	42.31%
Q80FJ1		Membrane fusion protein p14	1	17.60%
F5H3P5	ACTR3	Actin-related protein 3	2	11.52%
D6PXK4	ACTN4	Alpha-actinin-4	2	2.89%
F5GXQ1	ITIH4	35 kDa inter-alpha-trypsin inhibitor heavy chain H4	1	1.79%

4.2.5 Label-Free Spectral Count Based Quantitative Analysis

To more precisely evaluate the exosome proteome changes induced by p14, raw MS data was analyzed using label-free spectral counting and Sieve software to identify changes in protein abundances (Figure 4.12). Chromatograms of control and p14 MS spectra were aligned to account for slight chromatographic variances between samples. Once aligned, chromatographic peaks were automatically framed, using an iterative recursive base peak framing algorithm. A total of 19579 frames, each representative of a single or group of chromatographic peaks, were identified. The intensity of the peaks within each frame (area in the *m/z* plane) was quantified to determine where statistically significant differential expression has occurred. Proteins were re-identified based on

MS/MS raw data embedded in these files and ranked based on the calculated p-value (Fisher's exact t-test). Only those proteins with a p-value ≤ 0.05 combined with a ratio ≥ 2.0 or ≤ 0.5 were considered to be differentially expressed. Figure 4.13 shows a volcano plot relating the fold change and p value calculated for each peptide in a representative biological replicate. Although 43 peptides were significantly over- or under-expressed, this collapsed to only 5 proteins, once peptides from the same protein were grouped. Surprisingly, only 4 proteins other than p14 were consistently differentially expressed between control and p14 exosomes. The identities and summary statistics for all of the proteins quantified and identified in this label-free LC-MS study are shown in Table 4.4. As expected, p14 was statistically increased in both biological replicates and scored as the most enriched protein. Other enriched proteins included the ribosomal proteins RPL27A and RPL7 and the cell adhesion protein FN1. Interestingly, ANXA5 was under-represented in p14 samples compared to control exosomes, suggesting a possible depletion of phosphatidylserine in p14-exosomes. Taken together, there is a large overlap in proteins secreted in control exosomes and p14-exosomes, suggesting p14 exploits, but does not alter, exosome biogenesis pathways.

Table 4.4 Proteins with statistically significant altered protein abundance ratios in p14 exosomes compared to control exosomes.

Gene Symbol	Protein Name	Replicate #1		Replicate #2	
		Ratio[a]	p-value[b]	Ratio[a]	p-value[b]
	Membrane fusion protein p14	40.28	0.0177	5.51	0.0129
RPL27A	60S ribosomal protein L27a	7.20	0.00383	2.00	0.0125
RPL7	60S ribosomal protein L7	3.03	0.0021	2.93	0.0055
FN1	Fibronectin	2.39	0.0131	2.71	0.0297
ANXA5	Annexin A5	0.47	0.0159	0.48	0.0494

[a] ratio of p14 vs. control
[b] p-value calculated with Fisher's exact t-test

4.2.6 The Cytosolic Endodomain of p14 Interacts with TSG101

Our proteomic studies failed to identify ESCRT proteins present in p14 or control exosomes with the exception of Alix, likely due to the fact that ESCRT proteins are excluded from incorporation into the nascent ILV (Mageswaran et al., 2014). To more closely examine the relationship between p14 and the ESCRT proteins, we performed a co-immunoprecipitation experiment. Using an antibody directed against TSG101 or an IgG control, we immunoprecipitated solubilized cellular lysates of HT1080 cells transfected with empty vector or p14. Immunocomplexes were isolated on magnetic beads, eluted in protein sample buffer and subjected to immunoblotting. Western blotting revealed an interaction between TSG101 and p14 (Figure 4.14), suggesting p14 may be recruited to exosomes via interaction with the ESCRT complex.

Next, we created a series of p14-mutants to identify p14-specific *cis*-elements of exosome trafficking (Figure 4.15 A). N-terminal myristoylation and homo-multimerization were determined as non-essential factors for export of p14 in exosomes, as a non-myristoylated version of p14 (p14G2A) and an N-terminally truncated version of p14 devoid of the homo-multimerization domain (p14Δ30) were present in exosomes at approximately equal levels as parental p14 (Figure 4.15 B, top panels). Notably, both of these constructs are incapable of inducing cell-cell fusion (data not shown), suggesting the process of syncytiogenesis does not contribute secretion of p14-exosomes. Next, a series of C-terminal truncation mutants with progressive deletions in the cytoplasmic endodomain were examined for their ability to traffic into exosomes. The p14c78 construct, although expressed at equal levels as p14 in cell lysates, was completely absent from exosomes (Figure 4.15B). Extension of the p14c78 by 10 or 27 amino acids (constructs p14c88 and p15c105, respectively) restored trafficking to exosomes, albeit not to the full extent of authentic p14 (Figure 4.15 B, bottom panel). Transmission electron micrographs of HT1080 cells surface-stained for p14 showed normal trafficking of p14G2A to the plasma membrane and clustering in membrane microdomains, as well as surface-associated ~100 nm extracellular vesicles (Figure 4.15 C, top panel). p14c78, however, was found at the plasma membrane but there was no evidence of membrane-associated extracellular vesicles (Figure 4.15 C, bottom panel). Furthermore, there was a marked decrease in recruitment of TSG101, but not CD81, to exosomes isolated from

cells expressing p14c78, compared to wild-type p14 or p14Δ30. Recruitment of p14 and TSG101 to exosomes are therefore coincident, but the p14-induced increase in exosome release is not dependent on incorporation of either p14 or TSG1010 into exosomes. Taken together, these data suggest that the the p14 endodomain is required for recruitment to exosomes in a TSG101-dependent manner.

4.2.7 p14-Exosomes Enhance the Rate of Cell-Cell Fusion

To determine if extracellular exosomes contribute to the overall rate of syncytiogenesis, we tested p14-exosomes for their ability to fuse cells. Addition of purified p14-exosomes to naive QM5 cells induced cell-cell fusion as early as 3 hours after addition and continued to increase up to 20 hours (Figure 4.16 A). At approximately 22 hours, an obvious decrease in the number of syncytial foci was noted. This event correlated with the appearance of cell-free voids in the monolayer (data not shown), suggesting syncytial cell death or detachment from the substratum. Therefore, 20 hours was determined to be the optimal time point for all subsequent experiments. The number of syncytial foci formed was directly related to the amount of total exosomal protein in a dose-dependent manner (Figure 4.16 B). Furthermore, the number of nuclei per syncytial focus (i.e. the relative size of the syncytium) was not dependent on exosome-dose. In fact, there was no significant difference in the number of nuclei per syncytium for any of the doses (Figure 4.16 C). Therefore, it is the number of syncytia, not the size of the syncytium that increases with increased exosome dose.

To determine which component of p14-exosomes was responsible for conferring a syncytiogenic phenotype to recipient cells, we applied a variety of treatments to purified p14-exosomes prior to treating QM5 cells (Figure 4.16 D). Treatment of cells with DNaseI to eliminate the possibility of plasmid DNA contamination from conditioned medium, had no significant effect on induction of cell fusion. However, disruption of exosome structure via sonication, trypsinization of surface proteins, or treatment of exosomes with antibodies against the p14 ectodomain or CD81 all significantly reduced syncytium formation. Therefore, an intact exosome displaying p14 and CD81 molecules is required to initiate cell-cell fusion. Furthermore, treatment of HT1080 cells with 5-(N,N-dimethyl) amiloride hydrochloride (DMA), an inhibitor of H^+/Na^+ and Na^+/Ca^{2+}

exchangers required for exosome secretion, significantly decreased p14-mediated syncytiogenesis in a dose-dependent manner (Figure 4.17) Therefore, although syncytiogenesis is not required to recruit p14 to exosomes, exosomes carrying p14 do contribute to the rate of cell-cell fusion.

4.2.8 RRV-Infected Cells Produce p14-Exosomes

To determine if exosomes play a role in RRV infection, we pelleted cell culture supernatants from Vero cells infected with RRV at 20 hours post-infection (after the onset of cell-fusion but prior to cell lysis). A massive accumulation of p14 was observed in cell lysates of RRV-infected cells, and an enrichment of p14 in the P100 fraction was also observed (Figure 4.18 A). Avian reovirus-infected cells were previously shown to undergo syncytium-induced cytopathic effects, including apoptosis (Salsman et al., 2005), so to exclude the possibility of isolation of apoptotic bodies, we determined the relative densities of RRV-exosomes. At early time points (when syncytia were fully attached to the substratum and no visible cell lysis had occurred; 20 hpi), p14 banded exclusively in fractions consistent with exosome densities (Figure 4.18 B, top panel, lanes 5 and 6). At a later time point that corresponded with maximum virus release (44 hpi), two populations of p14-ECVs were present. The density of the first population was consistent with that of exosomes (Figure 4.18 B, bottom panel, lane 5) and a more abundant, denser population was also present (Figure 4.18 B, bottom panel, lanes 7 to 10), from 1.19 g mL^{-1} to 1.26 g mL^{-1}, a density profile characteristic of apoptotic bodies. A cup-shaped morphology typical of exosomes was observed from the 1.13 g ml^{-1} exosome fraction (Figure 4.18C). Finally, RRV-infected cells were sectioned parallel to the plane of growth and imaged with electron microscopy. RRV-infected cells showed evidence of a discontinuous plasma membrane and many ECVs, while mock-infected cells displayed a uniform, continuous plasma membrane and a notable lack of ECVs. Altogether, we conclude that p14-exosomes are also produced during the RRV lifecycle.

4.3 Discussion

In the present study, we demonstrate with biochemical and proteomic approaches that a portion of the cellular pool of FAST proteins is secreted in exosomes, both in a

transfection and infection model. Our results demonstrate that the p14 FAST protein interacts with ESCRT-I complex member TSG101, either directly or indirectly through the formation of a complex, and traffics to exosomes with a molecular composition that is remarkably similar to that of endogenous cellular exosomes. Furthermore, recruitment of p14 to exosomes is dependent on the cytosolic p14 endodomain. Finally, we have demonstrated that secretion of p14-exosomes contributes to the rate of cell-cell fusion. Overall, we suggest the FAST proteins hijack the exosome biogenesis pathway to enhance cell-cell fusion, ultimately leading to increased viral dissemination. Our work is the first characterization of a non-enveloped virus protein to be trafficked to exosomes.

4.3.1 Exosome or Microvesicle?

Our results demonstrate that the p14 FAST protein is secreted in exosomes. Several lines of evidence support this conclusion. First, p14 co-segregated with a plethora of exosomal markers by fractionation of conditioned medium. This was determined by two independent approaches: western blotting (Figure 4.8) and LC-MS/MS (Appendix 1, Table A1 and A2). Second, p14 interacts with the ESCRT-I protein TSG101 (Figure 4.14), a key player in exosome cargo selection and biogenesis. Third, the physical characteristics of p14-vesicles are consistent with those described in the literature for exosomes, including a homogenous cup-shaped vesicle of ~90 nm diameter (Figure 4.7) with a characteristic density (Figure 4.9 and 4.18). Fourth, pharmacological inhibition of exosome secretion with DMA inhibited p14-mediated syncytiogenesis in a dose-dependent fashion (Figure 4.16). Therefore, we conclude that p14 is secreted via an exosomal route.

We did note the presence of several microvesicle markers in our exosome preparations, including: caveolin-1 (Figure 4.8), β1-integrin, MMP-14, and basagin (Appendix 1, Tables A1 and A2). ECV isolated from biofluids (such as culture supernatants) unavoidably contain a mixed origin population, therefore a simple explanation for the presence of these microvesicle marker proteins is contamination of our exosome preparations with microvesicles, which are known to co-sediment with exosomes (Raposo and Stoorvogel, 2013). The development of more sophisticated strategies for isolation of specific populations of exosomes and/or microvesicles is

helping to overcome this common problem in the exosome field. Methodologies including immunocapture on magnetic beads (Clayton et al., 2003), field flow fractionation (Kang et al., 2008), sorting and quantification by flow cytometry (Clayton et al., 2003), antibody-coated microfluidic devices (Chen et al., 2010), and fluorescent single particle sorting by nanoparticle-tracking analysis (Dragovic et al., 2011) are all emerging approaches aimed at providing pure populations of ECVs. Since our understanding of the pathways and factors involved in formation of exosomes and microvesicles remains incomplete, it is also conceivable that that these two pathways may not be mutually exclusive. Thus, while the present results are largely consistent with p14 being secreted in exosomes, and hence through the MVB route, we do not exclude the possibility that p14 might also be released by plasma membrane budding of microvesicles.

4.3.2 p14 Interacts with TSG101

We observed interaction of p14 with TSG101 by two independent methodologies: a yeast-two hybrid screen using the soluble p14 endodomain as bait (Julie Boutlier, unpublished results) and by co-immunoprecipiation of p14-transfected cell lysates (Figure 4.14). TSG101 is an essential ESCRT component and that is typically associated with the inward budding of MVB in the endosomal pathway (Babst et al., 2000). TSG101 interacts with the early endosomal protein Hrs (Lu et al., 2003) and the accessory protein Alix to facilitate trafficking of cargo from early to late endosomes (Bissig and Gruenberg, 2014), where additional ESCRT proteins and the ATPase VPS4 drive the formation and delivery of endosomal cargo to MVBs (Teis et al., 2008).

However, TSG101 is also implicated in outward budding of the plasma membrane, a process most commonly associated with egress of enveloped viruses (McDonald and Martin-Serrano, 2009). The best-characterized example of viral budding involving the ESCRT machinery is HIV. HIV budding is driven by the viral Gag protein, which localizes to the plasma membrane of host cells. In the late domain of HIV Gag is a critical PTAP motif that interacts with the UEV domain of TSG101(Pornillos et al., 2003), enabling Gag to recruit TSG101 and other ESCRT proteins, which normally reside on endosomal membranes, to the cell surface. By such recruitment, plasma membrane

budding occurs. Many other viruses, such as HIV-1 and Ebola viruses, also exploit TSG101 or other ESCRT components to aid their budding at the cell surface (Martin-Serrano and Neil, 2011).

More recent evidence suggests the existence of a virus-independent cellular process resulting in the generation of microvesicles distinct from exosomes and, like budding viruses, produced by direct plasma membrane budding. This process is also dependent on TSG101 and Alix proteins (Jimenez et al., 2014; Nabhan et al., 2012; Romancino et al., 2013). The shedding of ESCRT-dependent microvesicles clearly complicates the classification of secreted vesicles and blurs the (arbitrary) distinctions between microvesicles and exosomes. Currently a consensus on classification of these vesicles does not yet exist (Witwer et al., 2013). Thus, although interaction between TSG101 and p14 suggests ESCRT-dependent membrane budding, this alone is insufficient evidence to determine whether p14 exosomes are endosome or plasma membrane-derived. Furthermore, proteomic analyses indicated an enrichment in plasma membrane and endosomal proteins (Figure 4.11 C), and electron microscopy failed to identify direct evidence of plasma membrane budding or fusion of a MVB with the plasma membrane. Vesicles containing p14 might therefore arise from the endosomal and/or plasma membrane routes.

All documented protein-protein interactions between TSG101 and other proteins are reliant on a specific amino acid motif and/or a mono-ubiquitin tag. For example, P(T/S)AP motifs located in the late-domain of retroviruses interact with a conserved set of aromatic residues present in the UEV domain of TSG101 (Pornillos et al., 2002). A number of cellular proteins are also reliant on LYPX(n)L motifs for interaction with TSG101, although usually in combination with a mono-ubiquitin tag (Baietti et al., 2012; Geminard et al., 2004; Hurley et al., 2006). Furthermore, even interactions between TSG101 and other ESCRT members such as Hrs (ESCRT-0), Vps27 (ESCRT-I) and Alix are ubiquitin- and P(S/T)XP-dependent. The p14 endodomain lacks a P(S/T)XP or LYPX(n)L motif, and we have no evidence of steady-state ubiquitylation of p14, suggesting a novel *cis*-element involved in exosome trafficking. It is possible that residues 78 to 88 ($_{79}$RNSYRLSEI$_{88}$) play a role in recruitment of TSG101 to the p14 endodomain, as truncated p14c78 is not sequestered in exosomes whereas p14c88 is

(Figure 4.15 B). Furthermore, p14c78 recruits distinctly less TSG101 to exosome pellets than exosome-associated p14 and p14Δ30 (Figure 4.15 D). Therefore, we conclude that p14 either interacts with TSG101 via a novel protein-protein interaction motif or uses an intermediary scaffolding protein with a canonical TSG101 binding motif to bridge this interaction. Going forward, it will be essential to perform additional co-immunoprecipitation experiments to determine if p14c78 and p14c88 interact with TSG101 to help define the region of the p14 endodomain that mediates this interaction.

Interestingly, although p14c78 itself was not recruited to exosomes, which also resulted in decreased recruitment of TSG101 to exosomes, p14c78-transfected cells still exhibited the increased exosome release associated with p14-transfected cells. This conclusion is based on the equivalent levels of CD81 present in the exosome fraction from p14- and p14c78-transfected cells (Figure 4.15D) and increased protein in the P100 pellet (data not shown). It therefore appears that features of p14 that are independent of those involved in incorporation into exosomes mediate increased exosome production.

4.3.3 Proteomic Analysis of p14-Exosomes

An in-depth proteomic analysis identified a total of 505 proteins in control exosomes and 534 proteins in p14-exosomes. This initial number was reduced considerably since we only considered proteins identified in both biological replicates (Appendix 1, Table A1 and A2). Exclusion of classically secreted proteins and common contaminant proteins further reduced the number of proteins by ~25% (Figure 4.11 A and B). We hypothesized that p14 might recruit cellular protein partners involved in cell-cell fusion to exosomes. Using a non-quantitative comparative approach, 153 proteins were found in common between control and p14-exosomes. Surprisingly, merely 15 and 6 proteins were determined to be unique to control or p14-exosomes, respectively. Therefore we conclude that p14 does not abundantly recruit cellular protein partners to p14-exosomes, and that p14 probably exploits common cellular pathways for exosome production.

In our comparative analyses, we used p14 as in internal positive control. As expected, p14 was only identified in p14-exosomes (Table 4.2). Other proteins uniquely identified in p14-exosomes included three cytoskeletal proteins, a ribosomal protein, and

a serum protein (35 kDa inter-alpha-trypsin inhibitor heavy chain H4). These proteins suggest a possible role of cytoskeletal dynamics or modulation of translation by p14 exosomes. Proteins excluded from p14 exosomes were more diverse and included cytoskeletal proteins, proteins involved in protein translation, and signaling proteins. Caution should be exercised when interpreting these results, as many of these proteins were identified based on a single unique peptide, therefore validation of these results will be required in the future.

Changes in proteins involved in protein translation were also observed in our quantitative spectral counting analyses. Two 60S ribosomal proteins were statistically enriched in p14-exosomes (Table 4.4). Interestingly, 17 ribosomal proteins were also identified in the pool of proteins common between control and p14-exosomes, although there was no statistical difference in the abundance of these proteins between samples. Several groups have also reported the presence of ribosomal proteins in mast cell exosomes (Valadi et al., 2007) and cancer cell exosomes (Graner et al., 2009), although identification of ribosomal proteins in exosomes is somewhat rare. Intriguingly, Valadi et al. have also documented the presence of exosomal mRNAs, which can be translated in target cells (Valadi et al., 2007). This group speculated that the presence of ribosomal proteins in exosomes could directly contribute to translation of mRNA in target cells, although this hypothesis has yet to be tested. It is an intriguing possibility that the fusogenic p14 exosomes could modulate translation of protein in the target cell.

Spectral counting is a common strategy used in proteomics for determining relative protein abundances of unlabeled protein samples using LC-MS/MS. Previous studies have shown that spectral counts correlate linearly with protein abundance in complex samples over a large dynamic range (Old et al., 2005). Like our non-quantitative comparative analysis, we found very few differences between control and p14-exosomes using spectral counting. Using p14 as an internal control, we consistently found a strong enrichment of p14 only in p14-exosomes (Table 4.4). Other than p14, we were only able to confidently identify four proteins at statistically different abundances between the samples, further suggesting limited recruitment of cellular partners to p14-exosomes.

A caveat to this experiment is that we were limited in the amount of exosomal protein we were able to isolate for each replicate. This limitation occurred for two

reasons: (1) in general, only 1-3% yield of protein (compared to total cellular protein) is expected when harvesting exosomes (Record, 2014), necessitating large-scale experiments to harvest adequate protein for analysis, and (2) p14 fuses cells relatively quickly, necessitating harvesting of exosome samples at timepoints much earlier than used by other groups (Witwer et al., 2013), thereby significantly decreasing our overall protein yield. Spectral counting is only considered to be highly reliable for measuring large changes in relatively abundant proteins with many associated peptides (and spectra), but is limited in the quantification of low-abundance proteins (Usaite et al., 2008). Therefore, the relatively low input of exosome protein to LC-MS/MS analyses likely contributed to our inability to detect large differences between control and p14 exosomes. This is evident in our inability to detect TSG101 in our proteomic analysis, yet western blots clearly revealed the presence of TSG101 in the exosome fraction. The use of multiple technical replicates, as we employed in our workflow, is one strategy to improve the reliability of spectral counting. However, despite these measures, spectral counting is still limited in accurate quantification of low spectral counts associated with low-abundance proteins that are most often of the greatest biological relevance. Consequently, ratios of low abundance proteins are often under-estimated (Old et al., 2005).

4.3.4 p14-Exosomes Mediate Particle-Directed Cell-Cell Fusion

In an effort to determine the influence of p14-exosomes on the overall cell-cell fusion phenotype, we added exogenous p14-exosomes to target cells. We now conclude that p14-exosomes function as nano-sized cell fusion packages, dependent on membrane-incorporated p14 for their mechanism of action. Several observations support this conclusion. First, we observed the formation of syncytia as early as 3 hours after exosome addition of exogenous p14-exosomes to target cells (Figure 4.17 A). Second, exosomes blocked with p14ecto antibodies, stripped with trypsin, or disrupted by sonicatation were virtually non-fusogenic (Figure 4.17 D). Previous studies have shown liposomes decorated with p14 proteins (Top et al., 2005) and proteo-lipid complexes of p14 and cationic transfection reagents (Noyce et al., 2011) are sufficient to induce cell fusion. The absence of syncytia in cells treated with control exosomes indicates cell-cell

fusion is due to the presence of p14 in exosomes. However, cellular exosomal proteins may also play a role in this process, since antibody-blocking CD81 proteins also reduced cell-cell fusion (Figure 4.17 D). Other studies have suggested tetraspanin molecules are important for recognition and binding to the target cell (Rana et al., 2012), therefore it is possible that CD81 does not play a role in membrane fusion per se, but in target cell recognition.

Interestingly, we found that the amount of exosomal protein added to target cells did not influence the size of syncytial foci, only the overall number of foci that were formed (Figure 4.17 C). Two explanations could account for this observation: (1) p14 fusion proteins are not reusable – once all p14 molecules delivered to the target cell have undergone one round of fusion, they are no longer functional so the syncytium cannot further expand, or (2) a threshold concentration of p14 is required to induce fusion - once multiple cells have fused, the density of p14 in the membrane drops below the required threshold. This obstacle would be overcome in p14-transfected or RRV-infected cells since active translation of new p14, would provide a continual new supply of p14 to the plasma membrane. In exosome-induced cell fusion, translation of new p14 would not occur. Therefore, exosome-induced cell-cell fusion could be a valuable tool in the future for determining the number of p14 molecules required for membrane fusion and whether a certain localized density is required to act as a fusion platform, as is required for the p10 proteins (Key and Duncan, 2014).

Induction of cell fusion by p14-exosomes is reminiscent of the "fusion-from-without" phenomenon observed with enveloped virus particles. Fusion-from-without is the rapid induction of cell fusion (usually within 1 to 2 hours) at high multiplicities of infection, in the absence of viral protein synthesis (Clavel and Charneau, 1994). How this fusion occurs is not entirely clear, but is thought to involve bridging of two cells by the virus particle. Endocytosis (Nanbo et al., 2013), phagocytosis (Feng et al., 2010), and direct fusion (Montecalvo et al., 2012) have all been postulated as mechanisms of delivery of exosomal cargo to target cells, therefore it will be interesting to see which strategy is used by the fusogenic p14-exosomes. Inhibiting endocytic and phagocytic processes in target cells or by microscopic tracking of uptake of fluorescently labeled exosomes could help address this issue.

4.3.5 Role of Fusogenic p14-Exosomes in Cell-Cell Fusion

Based on the data presented in this chapter, we conclude that the secretion of p14 in exosomes plays an active role in driving cell-cell fusion because: (1) we observe an induction of exosome secretion by p14 (Figure 4.6 A), (2) blockage of exosome secretion resulted in decreased cell-cell fusion (Figure 4.16), and (3) cell fusion was induced by exogenous p14-exosomes (Figure 4.17). Based on these results and conclusions presented in the previous sections, we present a model in which the FAST proteins traffic through the canonical MVB pathway (Figure 4.19). Sequestering of p14 into ILVs in the MVB is dependent on an interaction between TSG101 and the endodomain of p14, and likely occurs in a tetraspanin-enriched microdomain. MVBs, replete with p14-exosomes, then fuse with the plasma membrane, thereby releasing fusogenic exosomes into the extracellular space. Once liberated in the extracellular milieu, p14-exosomes interact with target cells, either directly on the plasma membrane via interactions of exosome CD81 with the cell surface or through internalization and recycling of p14 to the plasma membrane. Altogether, the release of exosomes loaded with p14 increases the rate of syncytium formation by fusing non-transfected or non-infected cells. It is possible this is a common strategy employed by other membrane fusion proteins because the endogenous fusogen syncytin and enveloped virus fusion proteins have also been documented to traffic to exosomes (Gould et al., 2003; Tolosa et al., 2012). Exosome secretion is also observed during myoblast differentiation and fusion (Forterre et al., 2014; Le Bihan et al., 2012), although the exact role of these exosomes has yet to be determined. Finally, eggs release CD9-positive exosomes into the perivitelline space prior to sperm-egg fusion, a process required for membrane fusion to occur between the egg and the sperm (Miyado et al., 2008).

4.3.6 Role of Exosome Release in RRV Infection

Release of p14-exosomes also occurs very efficiently during RRV infection (Figure 4.18). Furthermore, a shift in the density of p14 ECVs later in virus lifecycle is observed (Figure 4.18 B). These denser fractions that are positive for p14 are also positive for RRV genomic RNA (data not shown), raising the intriguing possibility that

fusogenic reoviruses may coat themselves in p14-exosomes. A recent publication demonstrated a 'non-enveloped' picornavirus hijacks the exosome pathway to acquire an envelope devoid of virus proteins (Feng et al., 2013). Therefore, it is not unreasonable to consider the possibility that RRV, a virus traditionally classified as non-enveloped, could acquire an exosome envelope. Furthermore, acquisition of an envelope by reovirus is not unprecedented as reoviruses infecting the wasp parasitoid, *Hyposoter exiguae*, have been found to transiently acquire an envelope (Stoltz and Makkay, 2000). These envelopes were, however, rapidly shed, making their detection difficult. Therefore, it is possible that the centrifugation techniques used in our study were too harsh for isolation of any intact enveloped RRV.

Previous work has shown that syncytium formation mediated by fusogenic reoviruses enhances the rate of virus progeny release through syncytium-induced apoptosis and membrane destabilization (Duncan et al., 1996b; Salsman et al., 2005). It was concluded, therefore, that the role of the FAST protein during virus was two-fold: (1) the induction of prolific cell-cell fusion, thereby increasing the pool of cellular resources for virus replication without releasing extracellular virus which could be detected by the immune system, and (2) the formation of large syncytia late in the virus infection cycle, which cause membrane destabilization and eventually apoptosis, leading to enhanced progeny release. Our work raises the possibility that FAST-exosomes may also serve to cloak virus particles, or at the very least serve to enhance the initial cell-cell transmission step via enhancement of the rate of syncytiogenesis.

Although we did not examine the nucleic acid content of p14-exosomes, the abundance of ribosomal proteins suggests that mRNAs may be recruited to p14-exosomes. During virus infection, host-translation is severely impeded by the virus. Massive amounts of viral mRNAs are produced to produce protein components of new virus particles and proteins required for the virus lifecycle. Since the majority of the mRNA during infection would be derived from the virus, it is likely that any mRNA incorporated into exosomes would be virus-derived. Therefore, exosomes could serve as a unique mechanism to 'transduce' bystander cells prior to infection. This could serve to prime target cells for production of viral proteins once the bystander cell became infected. Alternatively, miRNAs, of cellular- or virus-origin, could be packaged in

exosomes, functioning in a similar manner to promote virus replication. A possible group of miRNA targets could include innate immunity effector proteins. Transfer of miRNAs against innate immunity would therefore decrease the innate immune response in the target cell to ready this cell for subsequent infection. Sequencing of exosomal mRNA and miRNA will be necessary in the future to determine the role of exosomal nucleic acids in fusogenic reovirus infection.

It is also possible that the exosomes, rather than the syncytia, serve as the main virulence factor of the fusogenic reoviruses. We have shown that exosomes are replete with p14 proteins, which could elicit a strong innate or adaptive immune response. Previous work has shown that p14-mediated perturbation of the membrane induces a robust innate immune response (Noyce et al., 2011), therefore transfer of p14 via exosomes would likely also induce an innate immunity response. Thus, vesicular sequestration and exosomal export of viral RNA or protein may serve both as a viral strategy to evade pathogen sensing within infected cells and as a host strategy to induce an unopposed innate response in bystander cells, as has been previously demonstrated in hepatitis C infection (Dreux et al., 2012).

4.3.7 Summary and Future Directions

To summarize, we present a model whereby FAST proteins are packaged into exosomes, where they serve as enhancers of cell-cell fusion. Packaging is dependent on the cytosolic endodomain, which directly interacts with the ESCRT-I member TSG101. Once secreted, FAST-exosomes independently induce cell-cell fusion, thereby increasing the overall rate of syncytiogenesis.

Although this work has provided original insights into the roles of exosomes in FAST-mediated cell-cell fusion, a number of outstanding questions remain. *From what membrane do FAST-exosomes originate?* This is an important question that could have consequences on our overall model of how FAST proteins fuse membranes. If budding occurs at the plasma membrane, one could envision these buds acting as fusion-primed microdomains which bridge the gap between adjacent membranes, like an extended dimple. Furthermore, membrane budding is known to be localized at specialized membrane microdomains enriched in fusogenic lipids. Perhaps extracellular vesiculation

is simply a failed fusion attempt and the real purpose is to form fusogenic membrane exvaginations.

Do FAST-exosomes carry other bioactive molecules that are important for cell-cell fusion? Although we undertook an extensive proteomic study of p14-exosomes, we have not yet examined the mRNA, miRNA, or lipid content, both of which could contribute to overall functionally of the exosomes.

Is exosome secretion a generalized mechanism used by all syncytial tissue? There is strong evidence that syncytiotrophoblasts constitutively secrete exosomes, which are involved in modulation of the maternal immune system (Mincheva-Nilsson and Baranov, 2010; Tolosa et al., 2012) and protection against virus infection (Delorme-Axford et al., 2013a). There is also evidence that other syncytial tissues such as enveloped-virus infected cells and myotubes secrete exosomes. Do exosomes generally play a role in cell-cell fusion or in the maintenance of syncytial tissue?

Is exosome secretion a cellular mechanism whereby the host cell is trying to remove undesired viral transmembrane proteins from host membranes? Or do fusogenic reoviruses actively usurp the pathway for their own advantage? There is some evidence that exosome secretion can help protect against proteotoxicity by re-routing misfolded proteins that leak through ER-associated degradation (ERAD), Golgi quality control (GQC), and peripheral quality control at the plasma membrane to exosomes(Wang et al., 2011). This raises the possibility that p14-exosome secretion is a form of cellular protein quality control, and perhaps induction of cell-cell fusion by p14-exosomes is fortuitous consequence.

The continued investigation of the role of FAST-exosomes in cell-cell fusion will undoubtedly contribute to our overall understanding of the cell-cell fusion in diverse systems. Use of the FAST proteins as model exosome protein will surely provide insight into the molecular mechanisms of cargo selection and exosome secretion in general.

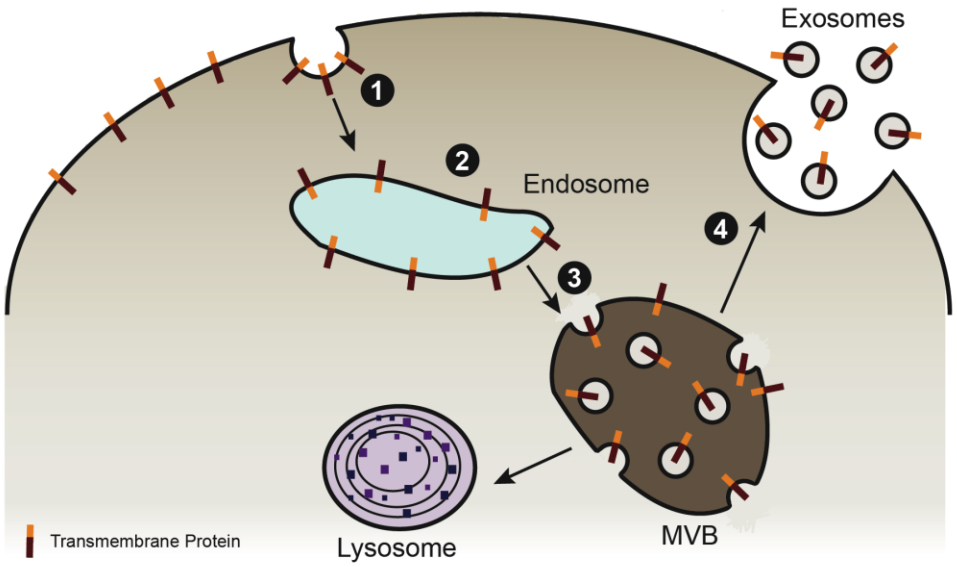

Figure 4.1 Classical exosome biogenesis pathway. (1) Endocytic vesicles deliver transmembrane (TM) cargo and membrane to the endosomal compartment in the peripheral cytoplasm. **(2)** TM cargo passes through early and late endosomal compartments. **(3)** As late endosomes move toward the perinuclear space, they acidify, acquire hydrolytic enzymes, and mature into multivesicular bodies (MVBs). Selected TM cargo is sorted into intralumenal vesicles (ILVs), formed through inward invagination of the MVB limiting membrane. **(4)** The limiting membrane of the MVB fuses with the plasma membrane, releasing ILVs, now referred to as exosomes, to the extracellular space. Alternatively, the MVB may fuse with the lysosome, whereby all intralumenal cargo will be degraded.

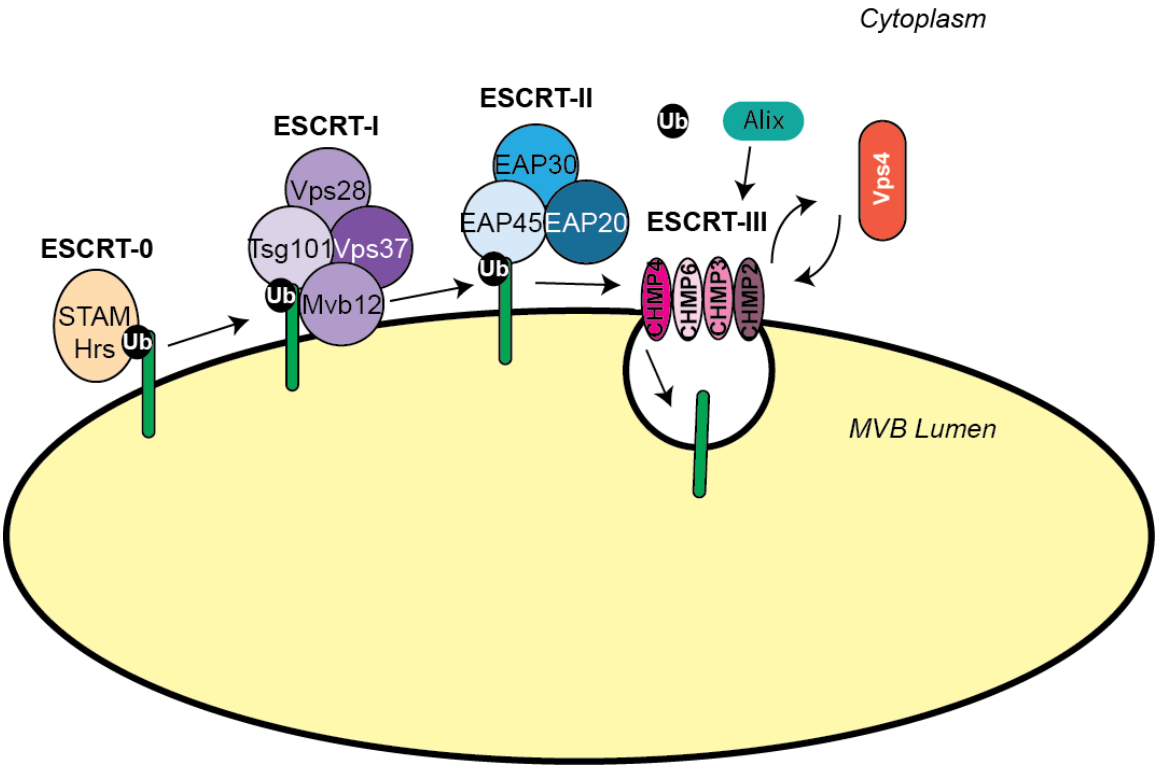

Figure 4.2 The sequential recruitment of the endosomal sorting complexes required for transport (ESCRT) complex in the sorting of internalized plasma membrane proteins to intralumenal vesicles. At early endosomes, the internalized ubiquitinated cargo is captured by ESCRT-0, through the ubiquitin-interacting motifs (UIM) of Vps27 and Hrs. Following ESCRT-0-mediated concentration of ubiquitylated cargo, ESCRT-I and ESCRT-II are sequentially recruited to the endosomal membrane by the ubiquitin-conjugating enzyme E2 variant (UEV) domain in Tsg101, the ubiquitin-binding domain (UBD) of MVB12 and the GRAM-like ubiquitin-binding in EAP45 (GLUE) domain of EAP45, as well as by a direct interaction between the ESCRTs. Assembly of ESCRT-I and –II in turn initiates the oligomerization of ESCRT-III. ESCRT-III deubiquitinating enzymes ensure the dissociation of ubiquitin residues from molecules before sequestration into multivesicular bodies. ESCRT-III, composed of CHMPs, recruits supplementary factors like Alix and Vsp4. Vps4 will promote disassembly of ESCRT-III, resulting in dissociation from the membrane.

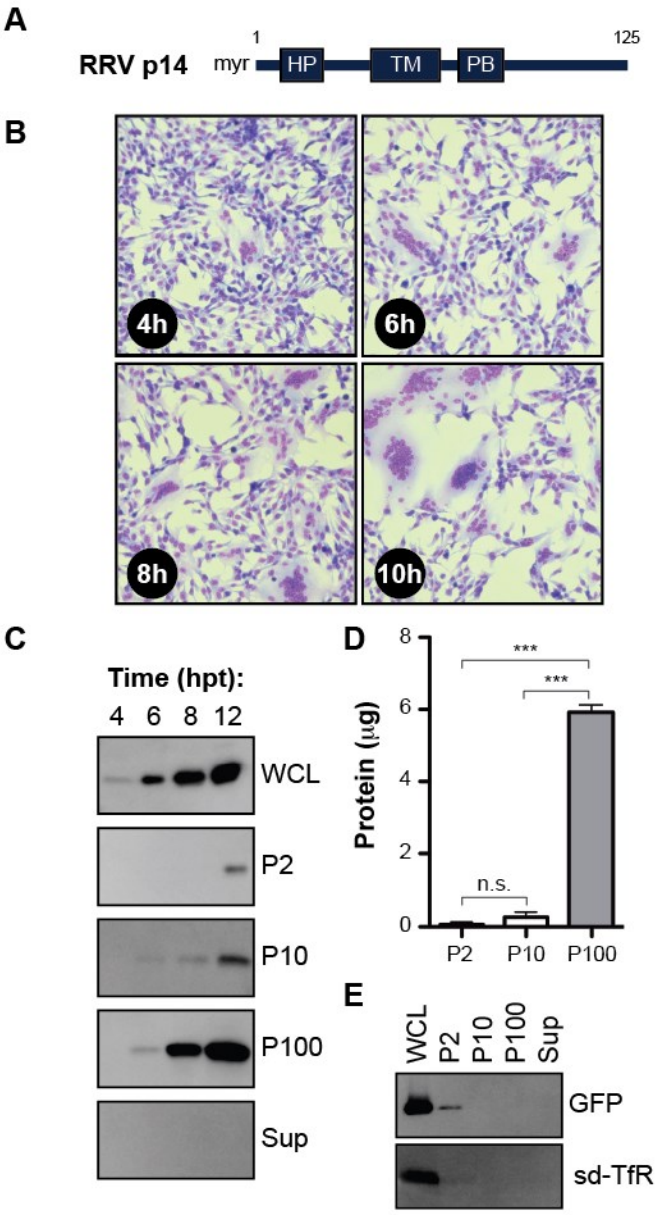
A
RRV p14
1
125
myr
HP
TM
PB
B
4h
6h
8h
10h
C
Time (hpt):
4 6 8 12
WCL
P2
P10
P100
Sup
D
Protein (μg)
8
6
4
2
0
***
***
n.s.
P2
P10
P100
E
WCL
P2
P10
P100
Sup
GFP
sd-TfR

Figure 4.3 Reptilian reovirus p14 is secreted in extracellular vesicles. (A) Schematic of reptilian reovirus (RRV) p14 FAST protein, depicting the N-terminal myristic acid (myr), ectodomain hydrophobic patch (HP), transmembrane domain (TM), and endodomain polybasic cluster (PB). Numbers indicate amino acid position in p14. **(B)** Timecourse of p14-mediated cell fusion. QM5 cells were transfected with p14, fixed and Giemsa-stained at various timepoints (4, 6, 8, or 10 hpt) and photographed under 200x magnification. **(C)** Western blots of whole cell lysates (WCL), purified extracellular vesicles (P2, P10, and P100), or conditioned medium cleared of all extracellular vesicles (Sup) from QM5 cells transfected with p14. Blots were probed with p14 antiserum (1:10,000). **(D)** Culture supernatants were subjected to differential centrifugation and the various fractions (P2, P10, or P100) were assayed for total protein using the CBQCA assay. Bars represent the mean of three independent experiments ± SD. Significance was assessed by one-way ANOVA ($p \leq 0.0001$) with Tukey post-hoc analysis. n.s., non-significant ($p > 0.05$); *** ($p \leq 0.0001$). **(E)** HEK393T cells were transfected with GFP or FLAG-tagged secretion-deficient transferrin receptor (sd-TfR) and blots were probed with anti-GFP (1:10,000) or anti-FLAG (1:10,000).

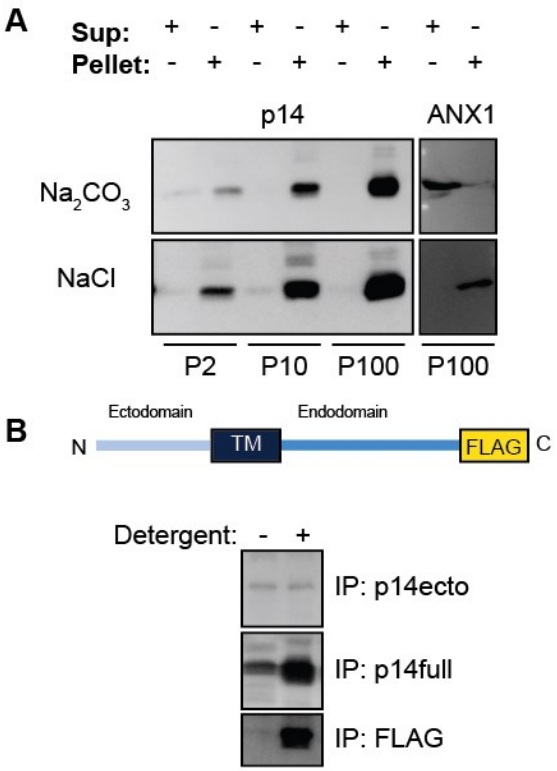

Figure 4.4 The p14 FAST protein has an N_{out}/C_{in} topology in extracellular vesicles. **(A)** Aliquots of pelleted extracellular vesicles isolated from the conditioned medium of QM5 cells transfected with p14 were incubated in the presence of 0.5 M NaCl (NaCl) or 0.1 M sodium carbonate (pH 11.6) (Na_2CO_3) and separated into soluble (S) and membrane (P) subfractions by ultracentrifugation. For comparison, annexin A1 (ANX1), an endogenous exosome luminal protein, was detected using an ANX1 antibody. **(B)** Top – schematic of C-terminally FLAG-tagged p14, showing the relative locations of the N-terminal ectodomain, transmembrane domain (TM), endodomain, and C-terminal FLAG tag. Bottom – Western blots of proteins immunoprecipitated from conditioned medium from cells transfected with C-terminally FLAG-tagged p14. Proteins were immunoprecipitated in the presence or absence of detergent (1% Triton X-100, 0.1% sodium dodecyl sulphate, 0.1% sodium deoxycholate) with anti-p14ecto, anti-p14full, or anti-FLAG antibodies.

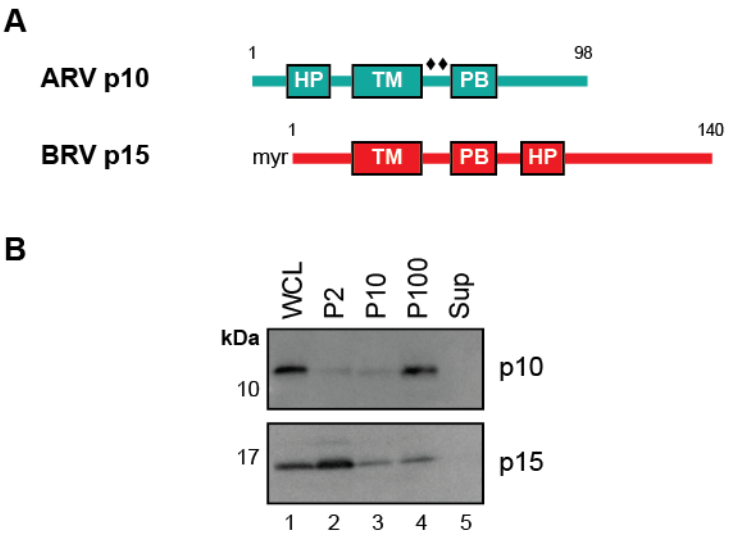

Figure 4.5 Avian reovirus and baboon reovirus FAST proteins are secreted in extracellular vesicles. (A) Schematic of avian reovirus (ARV) p10 (cyan) and baboon reovirus (BRV) p15 (red) FAST proteins, depicting N-terminal myristic acid (myr) or dipalmitoylation (♦♦), hydrophobic patch (HP), transmembrane domain (TM), and polybasic cluster (PB). Numbers indicate amino acid positions. **(B)** Western blots of whole cell lysates (WCL), purified extracellular vesicles (P2, P10, and P100), or conditioned medium cleared of all extracellular vesicles (Sup). HEK393T cells were transfected with C-terminally FLAG-tagged p10 or C-terminally FLAG-tagged p15 and harvested at 24 hpt or 10 hpt, respectively. Blots were probed with anti-FLAG (1:10,000).

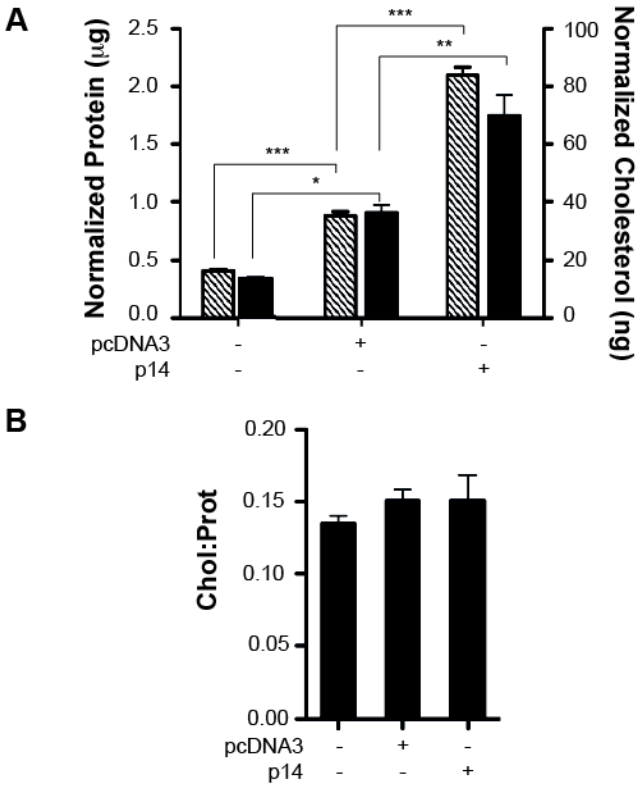

Figure 4.6 Induction of exosome secretion in HT1080 cells by p14. (A) Culture supernatants harvested at 18 hpt of non-transfected HT1080 cells or cells transfected with empty vector (pcDNA3) or p14 were subjected to differential centrifugation, and the p100 fractions were assayed for total protein content (hatched bars) using the CBQCA assay or for cholesterol content (black bars) using the Amplex Red cholesterol assay. Protein and cholesterol readings were normalized to mg total cellular protein. Statistical significance was determined by one-way ANOVA ($p \leq 0.0001$ for both protein values and cholesterol values), followed by Tukey's post-hoc test. * ($p \leq 0.05$); ** ($p \leq 0.01$); *** ($p \leq 0.001$). **(B)** Cholesterol:protein ratios were calculated on a per weight basis (µg cholesterol, µg protein), using data from panel A. Values were not statistically different ($p = 0.4306$), determined with a one-way ANOVA. The bars from all graphs represent the mean of three independent experiments ± SD.

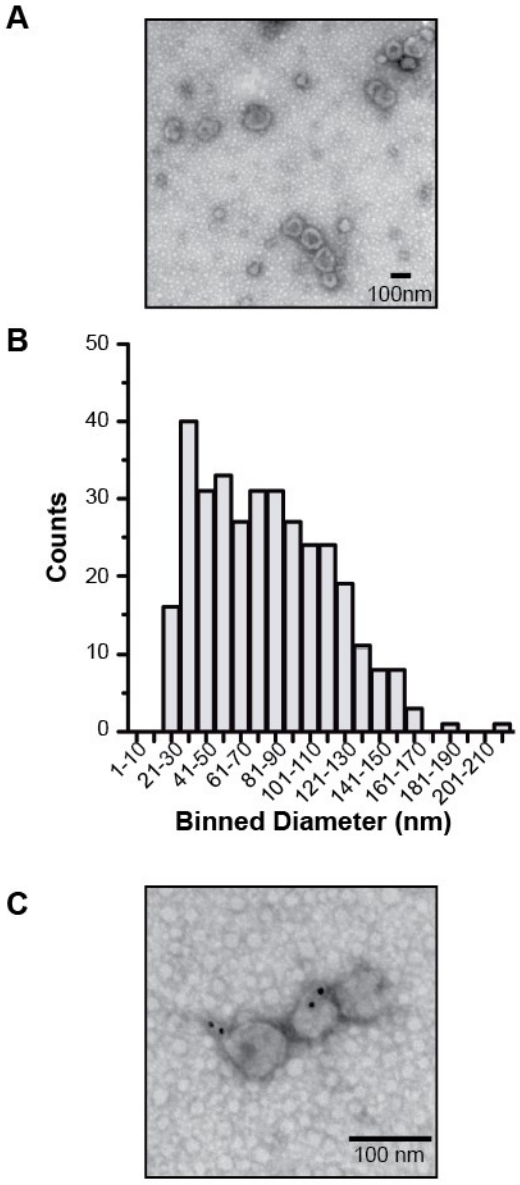

Figure 4.7 Ultrastructural analysis of p14 exosome-like vesicles. (A) Transmission electron micrograph of whole mount exosomes purified from HT1080 cells transfected with p14. Samples were negatively stained with uranyl acetate. **(B)** Binned diameters of exosomes purified from HT1080 cells transfected with p14. Sizes were determined using ImageJ software. A minimum of 125 vesicles were measured per experiment. Three separate experiments were performed; graph is representative of one experiment. **(C)** Whole mount exosomes from HT1080 cells transfected with p14 were stained with anti-p14ecto. Secondary antibodies were conjugated to 10 nm gold particles.

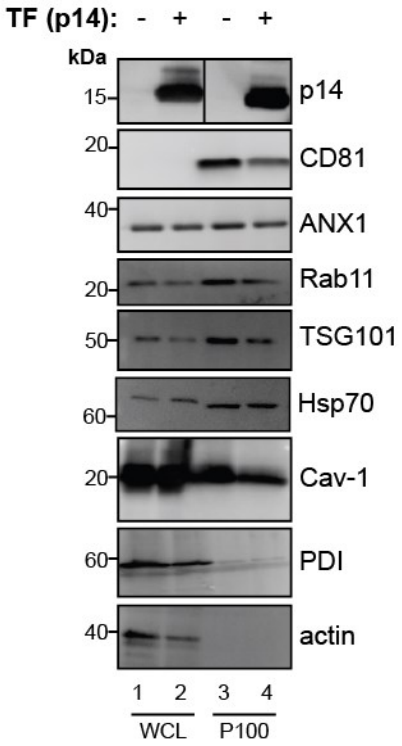

Figure 4.8 The P100 fraction from cells expressing p14 are positive for exosome marker proteins. HT1080 cells were mock transfected (-) or transiently transfected with p14. Western blots, illustrating the presence of p14, and exosome markers CD81, ANX1, Rab11, TSG101, and Hsp70, and plasma membrane marker caveolin-1 (Cav-1) in whole cell lysate (WCL) or exosomes (P100). Note that there is no detectable contamination of the exosomes by endoplasmic reticulum marker protein disulphide isomerase (PDI) or actin. Each lane represents an equal protein load.

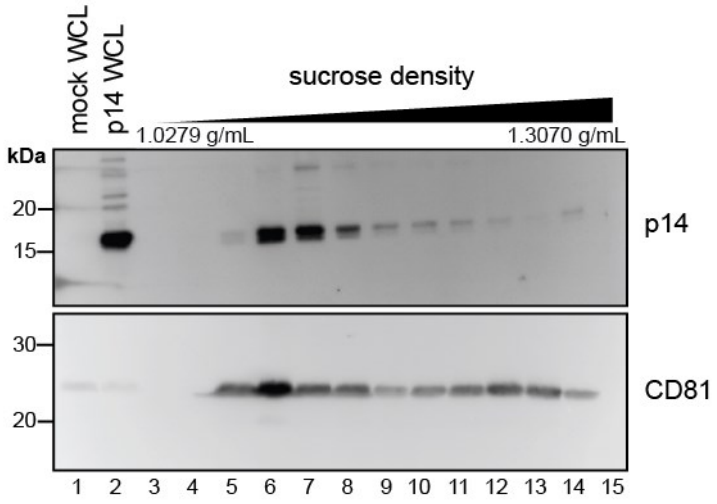

Figure 4.9 Density profiles of p14 exosome-like vesicles. Western blot analysis of fractions collected from purified exosomes on a step sucrose gradient from HT1080 cells transfected with p14. Blots were probed with anti-p14 (top) or anti-CD81 (bottom) antibodies. Lanes 1 and 2 represent whole cell lysates (WCL) from mock-transfected or p14-transfected cells.

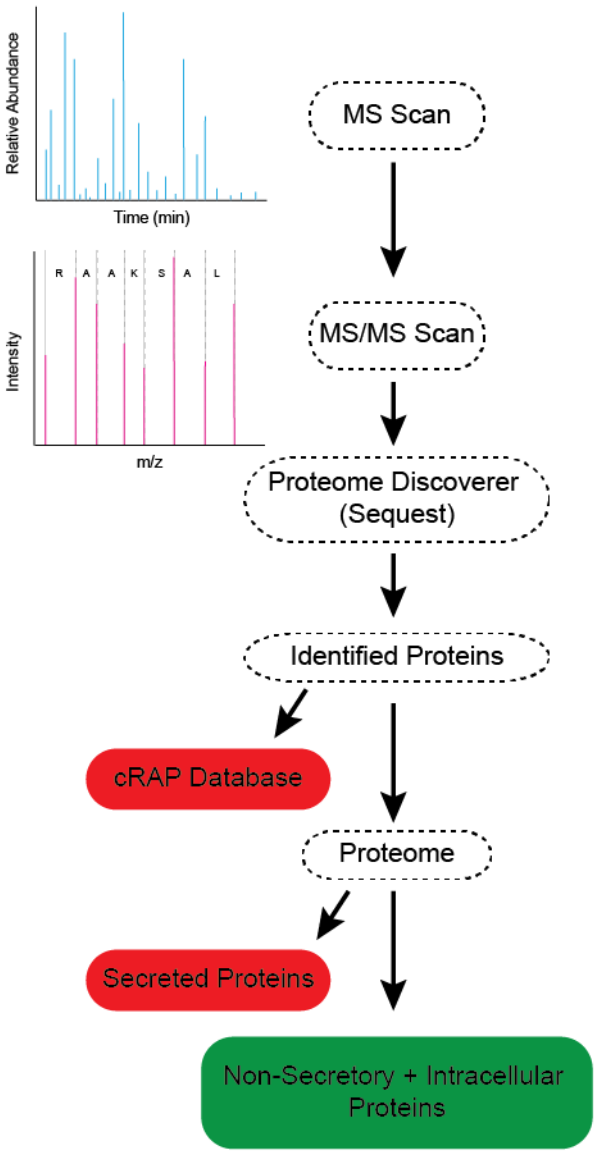

-Comparison of control vs p14
-manual verification

Figure 4.10 Workflow of proteomic analysis of control and p14-exosomes. Exosome pellets collected from control or p14-transfected cells were digested by tryptic in-solution digests. Peptides were separated by liquid chromatography followed by data-dependent tandem mass spectrometry. MS/MS data was analyzed with Proteome Discoverer software using the Sequest database using a false discovery rate of 0.01. Identified proteins were screened for contaminants using the common Repository of Adventitious Proteins (cRAP; http://www.thegpm.org/cRAP), which were excluded from further analysis. Remaining proteins were compared with the Compendium of Human Secreted Proteins (Eichelbaum et al., 2012). Non-secretome proteins were subjected to further analysis.

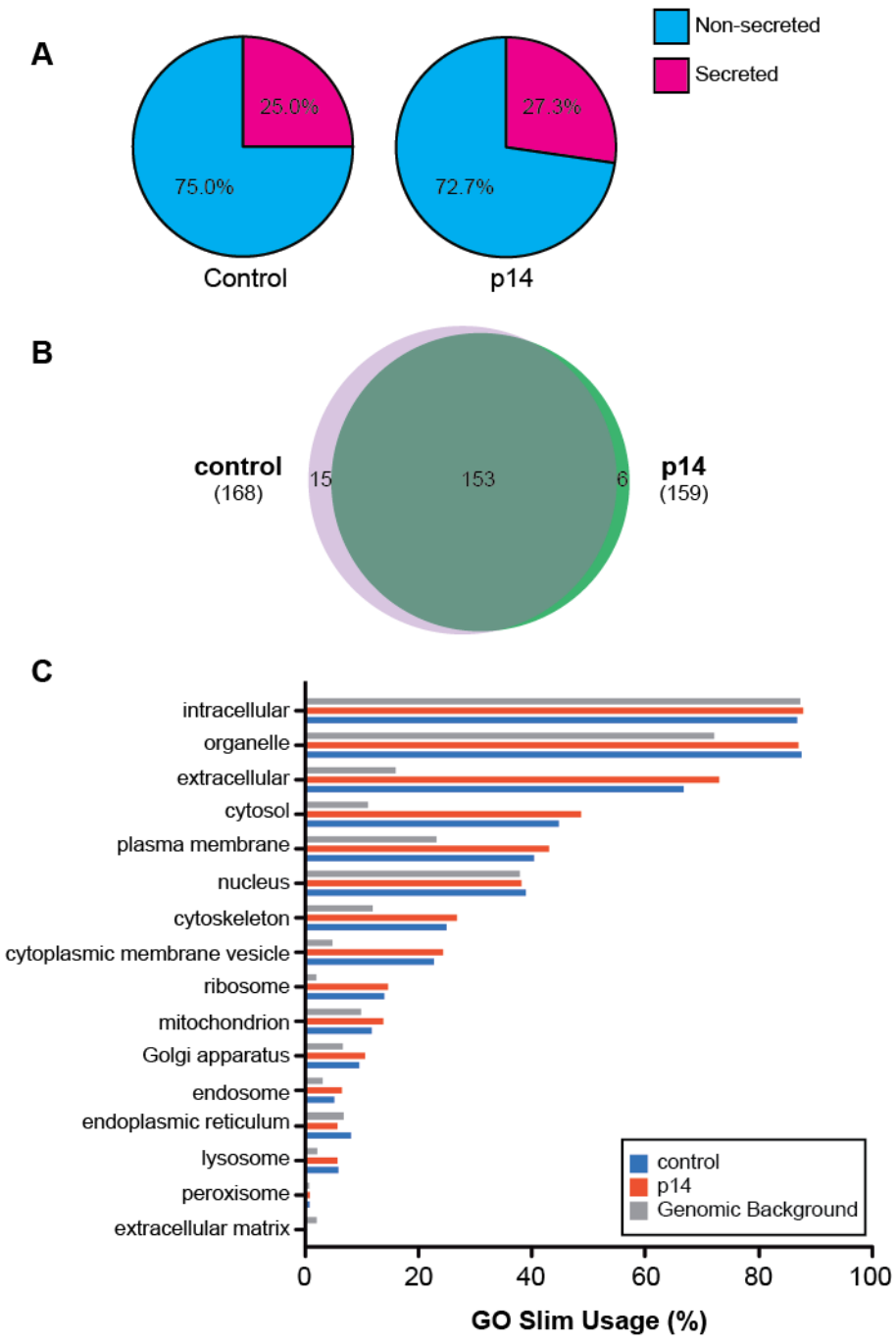
A
Non-secreted
Secreted
25.0%
75.0%
27.3%
72.7%
Control
p14
B
control
(168)
15
153
6
p14
(159)
C
intracellular
organelle
extracellular
cytosol
plasma membrane
nucleus
cytoskeleton
cytoplasmic membrane vesicle
ribosome
mitochondrion
Golgi apparatus
endosome
endoplasmic reticulum
lysosome
peroxisome
extracellular matrix
control
p14
Genomic Background
0
20
40
60
80
100
GO Slim Usage (%)

Figure 4.11 Proteomic characterization of the exosomes from p14-transfected cells. **(A)** Classification of proteins identified in both biological replicates of control and p14 exosome samples as either secreted or non-secreted proteins. Datasets were screened with the "Compendium of Human Secreted Proteins" database to determine classically secreted proteins (Eichelbaum et al., 2012). **(B)** Venn diagram of proteins identified in both biological replicates (6 total technical replicates) in control exosomes and p14 exosomes illustrating common and unique proteins between the samples. Common protein contaminants (Common Repository of Adventitious Proteins, cRAP; http://www.thegpm.org/) and soluble secreted proteins (panel A) were excluded. **(C)** Distributions of proteins from panel (B) across cellular compartments, compared to human genomic background, as determined by GO Slim annotation (http://go.princeton.edu/cgi-bin/GOTermMapper). Data is represented as a percentage of total proteins from each grouping (genomic background, control or p14) annotated within each subcellular compartment category. Control exosome proteome (blue bars), p14 exosome proteome (red bars), human genomic background (grey bars).

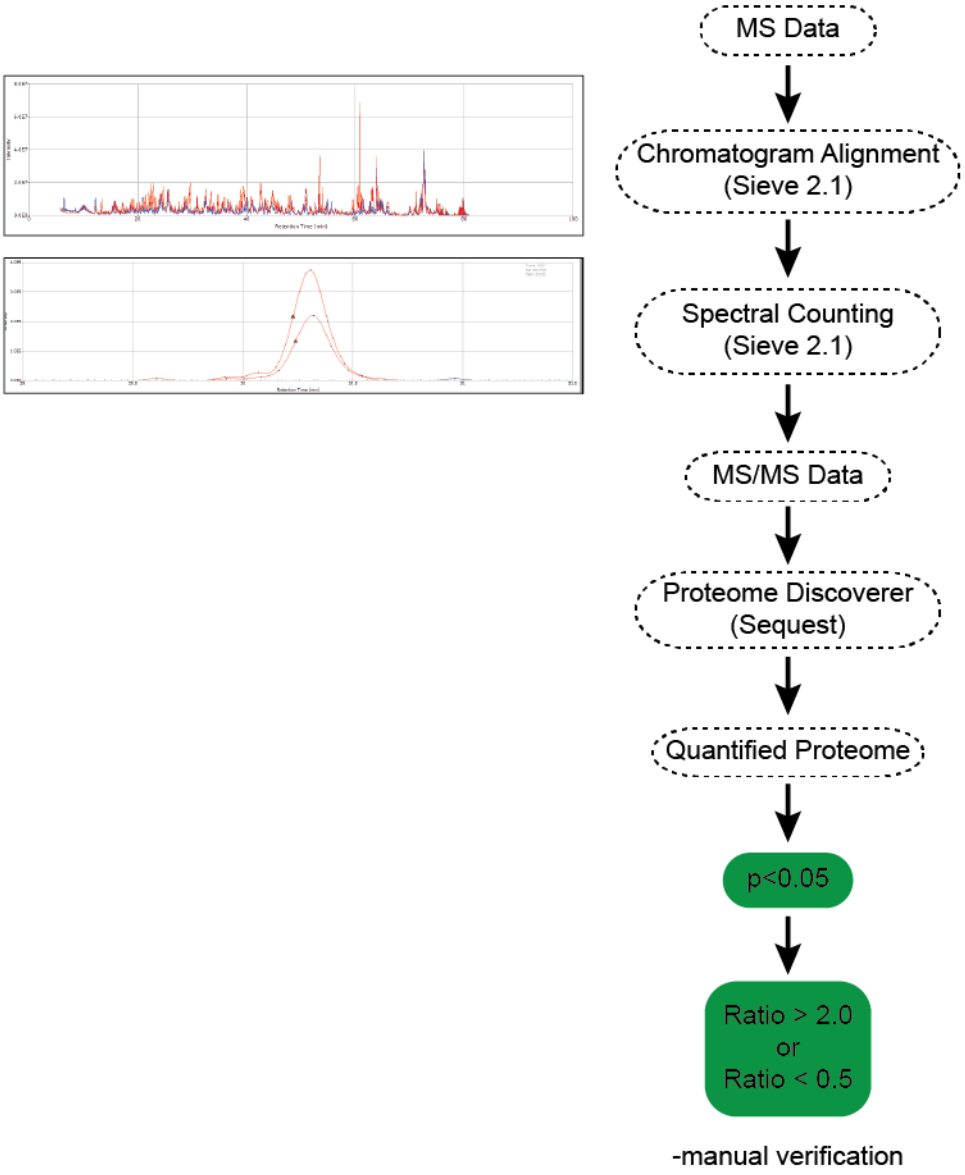

Figure 4.12 Workflow of quantitative spectral counting analysis. Raw MS files were analyzed by Sieve software for differential expression analysis. Raw MS chromatograms were automatically aligned to correct for inherent chromatographic variability between samples using full scan data. Chromatographic peaks were then framed and quantified by Sieve software, using a spectral counting approach. MS data was cross-referenced with MS/MS data to re-identify proteins using Proteome Discoverer with the Sequest database. Only peptides with a p-value less than 0.05 and a ratio greater than two or less than 0.5 were considered differentially expressed.

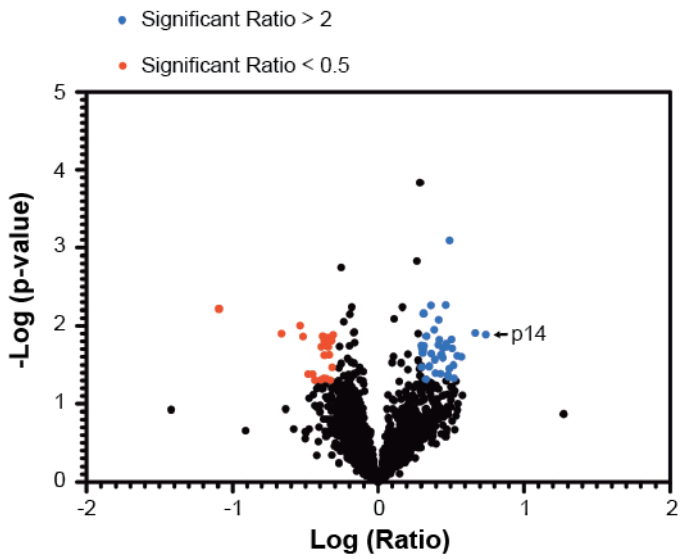

Figure 4.13 Quantitative analysis of p14 exosomes by MS-based spectral counting. Volcano plot showing *p* values (-log) versus protein ratio of p14/control exosomes (log) of 3,022 peptide frames that met protein identification criteria. (Red, 17 peptide frames with a significant ratio ≤ 0.5; blue, 35 peptide frames with a significant ratio ≥ 2). Significance was defined as a $p < 0.05$ (Fisher's exact t-test) for intensities of each framed peak comparing p14 to control exosome proteomes.

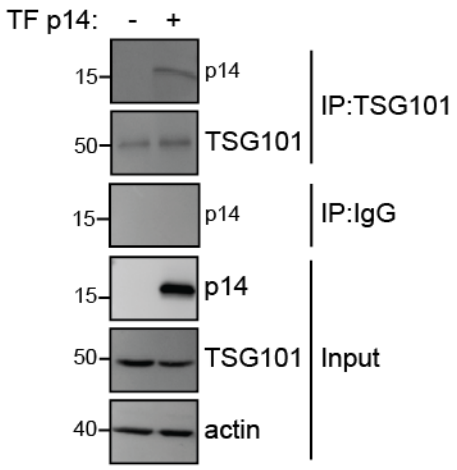

Figure 4.14 p14 co-immunoprecipitates with endogenous TSG101. HT1080 cells were transfected with empty vector (mock) or p14. Cell lysates were immunoprecipitated with anti-TSG101 or isotype control (IgG) and probed for p14 by western blotting. Input blots represent cell lysates not subjected to immunoprecipitation.

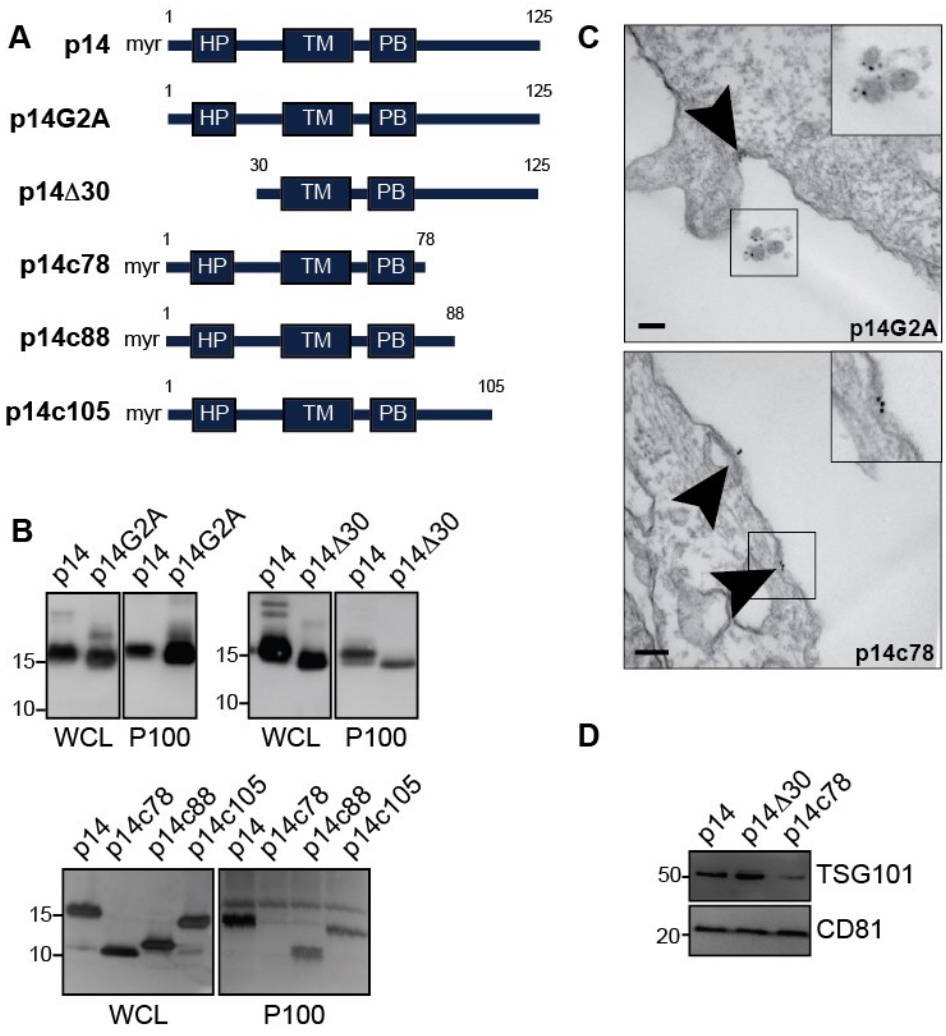
A
p14
myr
HP
TM
PB
1
125
p14G2A
p14Δ30
30
p14c78
78
p14c88
88
p14c105
105
B
p14
p14G2A
p14Δ30
15
10
WCL
P100
p14c78
p14c88
p14c105
C
p14G2A
p14c78
D
TSG101
CD81
50
20

Figure 4.15 The membrane-proximal portion of the p14 endodomain is required for secretion in exosomes. (A) Schematic representation of the indicated p14 constructs, depicting the N-terminal myristic acid, hydrophobic patch (HP), transmembrane domain (TM), and polybasic cluster (PB). Numbers indicate the N- and C-terminal amino acid positions. **(B)** Western blots of whole cell lysates (WCL) and exosomes (P100) harvested from HT1080 cells transiently transfected with the indicated p14 constructs. Blots in left and middle groupings were probed with anti-p14, rightmost grouping was probed with anti-p14ecto. **(C)** HT1080 cells transfected with p14G2A or p14c78 were live-stained with anti-p14ecto, fixed, processed, and thin-sectioned for transmission electron microscopy. p14G2A (top panel) is associated with extracellular vesicles (boxed region) and plasma membrane microdomains (arrow). p14c78 (bottom panel) is only associated with plasma membrane microdomains (arrows). Insets show a higher magnification of the boxed areas. Scale bars represent 100 nm. **(D)** Western blots demonstrating a decrease in recruitment of TSG101 to exosomes by p14c78. HT1080 cells were transfected with the indicated plasmids and exosomes were harvested by differential ultracentrifugation. Blots were probed with TSG101 and CD81 antibodies. Note equal levels of the exosome marker protein CD81 in all lanes.

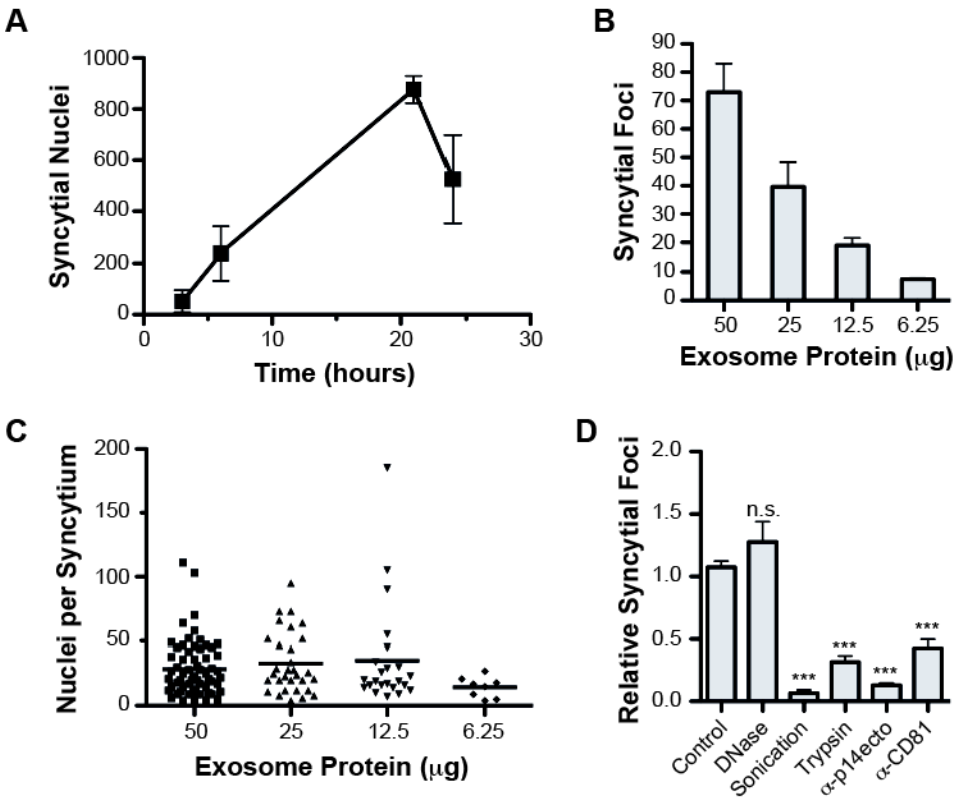

Figure 4.16 Purified p14 extracellular vesicles are sufficient to induce cell-cell fusion. Donor QM5 cells were transfected with p14 and exosomes were harvested from conditioned medium 16 hpt. Purified exosomes were added to naïve QM5 target cells in 24-well cluster plates. Cells were fixed and Giemsa-stained to determine the extent of cell-cell fusion. **(A)** Timecourse of cell-cell fusion induced by p14 extracellular vesicles. Data represents the total number of syncytial foci in a single well. **(B)** Titration of total exosomal protein. Protein concentration of purified exosome pellets was determined using the Bio-Rad DC protein assay, and cells were treated with different protein doses and fixed and stained at 20 hours post-treatment, as in panel A. **(C)** Number of nuclei per syncytial focus from cells in panel (A). No statistical significance was determined between samples ($p=0.2313$), determined with one-way ANOVA. **(D)** Exosomes preparations (12.5 μg total protein) were treated with PBS (control), DNaseI, sonication, trypsin digestion, or blocking with anti-p14ecto or anti-CD81 antibodies. Statistical significance was assessed using one-way ANOVA ($p\leq0.0001$) with Dunnett's post-hock test to compare each treatment to PBS control values. n.s. (non-significant, $p>0.05$); *** ($p\leq0.001$). Data from panels (A-D) is representative of the mean of three separate experiments (i.e. three separate purifications of extracellular vesicles) (± SD).

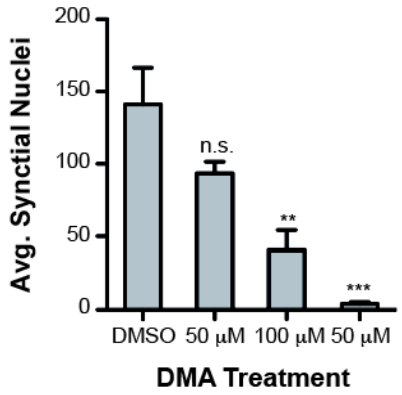

Figure 4.17 Pharmacological inhibition of exosome secretion impedes cell-cell fusion. HT1080 cells were pre-treated with 300 nM DMA 12 hours pre-transfection and treated with an additional dose (50, 100, or 150 μM or DMSO) at 6 hours post-transfection with p14. Cells were fixed at 12 hours post-transfection and Giemsa stained. Cell-cell fusion was quantified by counting the number of syncytial nuclei per field of view under 200x magnification. Bars represent the means of three independent experiments ± SEM. Statistical significance was tested by one-way ANOVA ($p<0.0001$), followed by Dunnett's post-test to compare each DMA treatment with DMSO control. n.s. (non-significant, $p>0.05$); ** ($p\leq0.01$); *** ($p\leq0.001$).

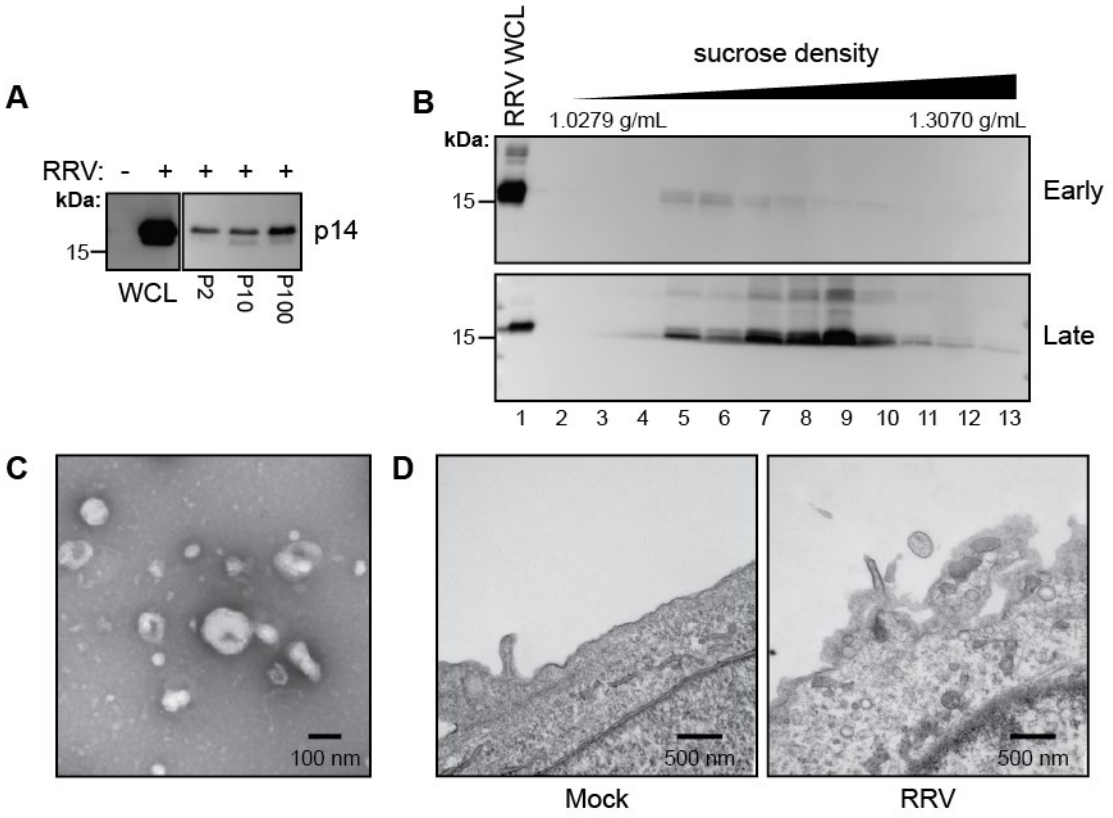

Figure 4.18 Cells infected with reptilian reovirus also secrete p14 exosomes. (A) Vero cells were infected with reptilian reovirus (RRV; MOI=1) and extracellular vesicles were pelleted by differential centrifugation (P2, P10, P100) at 16 hours. Whole cell lysates (WCL) and extracellular vesicle pellets were probed for p14 by western blotting. **(B)** Western blot analysis of fractions collected from the P100 fraction separated on a sucrose gradient. Cells were infected as in panel (A). P100 fractions were collected at 16 hours and 36 hours when cells were visibly undergoing lysis. **(C)** Extracellular vesicles from lane 5 (density = 1.127 g/mL) in panel (A). Vesicles were whole-mounted and negatively stained and examined by transmission electron microscopy. Scale bar represents 100 nm. **(D)** Differences in plasma membrane morphology between mock-infected and RRV-infected Vero cells. Cells were grown and fixed on a Thermanox coverslip, embedded and flat-sectioned. Scale bar represents 500 nm.

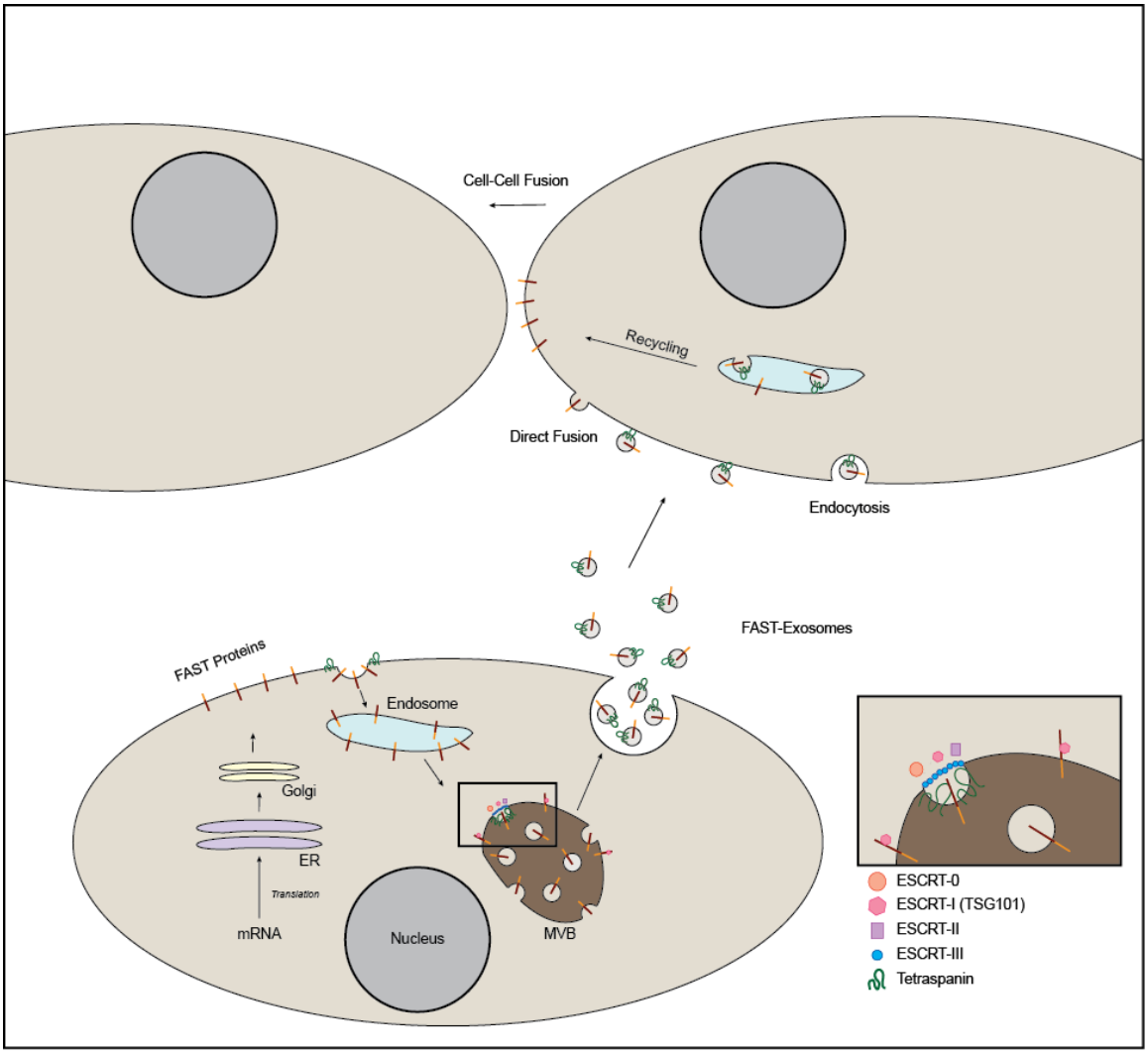

Figure 4.19 Model of exosome secretion in FAST-mediated cell-cell fusion. FAST proteins are trafficked to the plasma membrane of virus-infected cells. Here, they are internalized by endocytosis. They pass through the endosomal network to a multivesicular body (MVB), where they co-localize in a tetraspanin-enriched microdomain. The FAST endodomain recruits the ESCRT complex via interaction with TSG101. The ESCRT complex sorts the FAST proteins into intralumenal vesicles. Next, the limiting membrane of the MVB fuses with the plasma, thereby releasing FAST-exosomes, which are dispersed in the extracellular space. These exosomes deliver FAST proteins to uninfected target cells either via direct fusion with the plasma membrane or by endocytosis of exosomes, followed by receptor recycling. In both cases, FAST proteins are present in the plasma membrane of the target cell and can induce fusion with other neighbouring cells.

CHAPTER 5
CONCLUSIONS

The key objective of this thesis was to examine the role of membrane curvature in syncytiogenesis. Using the Fusion-Associated Small Transmembrane (FAST) proteins as a model for virus-induced cell-cell fusion, I examined the role of membrane curvature stabilization by the p15 FAST protein (Chapter 3), as well as membrane curvature changes resulting in secretion of extracellular membrane vesicles during p14-mediated cell-cell fusion (Chapter 4). The following sections will identify major themes from Chapters 3 and 4 and provide a context for the data within current conceptual paradigms.

5.1 Protein-Lined Fusion Pores

Lipid membranes that are destined for fusion must overcome large energy barriers in order to fuse. Two major barriers that must be overcome are hydration repulsion and disruption of planar bilayer structures. Consequently, energy must be spent not only on the removal of water from the gap between the fusing membranes, but also on physically re-shaping the membranes during each step of the fusion pathway including dimple formation, hemifusion, and pore formation. As fusion progresses, the lipid bilayers must bend and deform. These contortions are met with strong opposition for two reasons: (1) sharp curvature creates unfavorable void spaces within the surface of the bilayer, thereby exposing the acyl chains to water, adding an additional energetic cost, and (2) bilayers fundamentally resist bending in order to optimize the attractive dispersive forces between acyl chains (Chernomordik and Kozlov, 2008; Frolov and Zimmerberg, 2010). Surmounting these barriers under physiological conditions thus requires specialized membrane fusion proteins.

In a generalized model of membrane fusion, fusion proteins act as a mechanical scaffold – their main job is to pull the membranes close enough to fuse. Indeed, in protein-free model systems, bilayers can fuse spontaneously if brought in close enough proximity. For example, a course-grained liposome model demonstrated that as liposomes were brought within 1 to 1.5 nm of each other, small fluctuations in one of the monolayers triggered fusion via hemifusion (Marrink and Mark, 2003). Membrane fusion

proteins, therefore, must have a firm anchor in the membrane (in the form of a transmembrane segment), and they must interact in such a way to exert sufficient mechanical force to draw the membranes close enough to force spontaneous fusion. More recently, this model has been extended to include the formation of a dimple, which is essentially a fusion-primed pucker in the membrane (Efrat et al., 2007). Thus, in addition to acting as a mechanical scaffold, membrane fusion proteins must also be adept at generating membrane curvature. A variety of diverse membrane fusion proteins are thought to follow this model of membrane fusion, including enveloped virus fusion proteins, and the cell-cell fusion proteins EFF-1 and AFF-1 (Sapir et al., 2008). According to this model, fusion intermediates in protein-free and protein-induced fusion systems are purely lipidic, including the nascent fusion pore. Therefore, forces inherent to the bilayer (i.e. hydration repulsion, membrane tension, and curvature stress) are thought to be the driving forces for fusion progression.

Fusion pores are highly curved membrane structures, in which laterally mobile membrane constituents, such as lipids and proteins, can redistribute in such a way to minimize free energy. Depending on their molecular shape, lipids form structures of different curvatures. Hence, non-axisymmetrical lipids have been theorized to stabilize narrow, transient fusion pores via clustering and in-plane re-organization, with fusion intermediates acting as a molecular sieve in selection of the correctly shaped lipids to minimize the overall energy penalty (Jorgacevski et al., 2010). Based on this model, it was concluded that a fusion pore could be an energetically favorable intermediate in the presence of stabilizing anisotropic inclusions, such as lipids with the correct spontaneous curvature. Other molecular dynamics simulations have confirmed molecular sorting of lipids with intrinsic curvature into sites with strong mean curvature (Cooke and Deserno, 2006). Conversely, studies using small unilamellar vesicles with fluorescently labeled lipids have shown the curvature coupling coefficients of various bilayer phospholipids were relatively low (Kamal et al., 2009). Therefore, this (relatively) weak coupling between lipid shape and bilayer curvature implies that lipid redistribution is not likely to be a major force in fusion pore stabilization, as previously posited, as lipids do not seem to be discriminating sensors of membrane curvature.

If lipids are unable to fully stabilize the curved rim of a fusion pore, what other factors might contribute? As previously stated, proteins within the fusion site are also laterally mobile elements in the fusion site. Therefore, in a model analogous to inclusion of anisotropic lipids in the fusion pore, inclusion of protein in the pore could also provide stabilization. Studies of exocytic fusion pores have suggested this fusion pore is initially lined with protein (Han et al., 2004). It has been suggested that a circular arrangement of five to eight syntaxin transmembrane domains could form proteinaceous fusion pores that are interdigitated with bilayer lipids. Mutations at specific sites of the syntaxin protein either increase or decrease flux through the pore, suggesting these residues face the pore lumen. Such protein-lined fusion pores are theorized to be converted to an eventual stable lipidic fusion pore (Jackson and Chapman, 2008; Jackson, 2010). On the contrary, fusion pores in *in vitro* models can be formed in the absence of protein, arguing strongly against the existence of a proteinaceous fusion pore (Chanturiya et al., 1997). Lipid-anchored SNARE proteins lacking a transmembrane domain have also recently been shown to fully support membrane fusion, further arguing against the existence of a transmembrane-lined fusion pore in exocytosis (Xu et al., 2011; Zhou et al., 2013).

If lipids and transmembrane domains are insufficient to stabilize or expand a fusion pore, what other factors could contribute? In the case of a lipidic fusion pore, membrane fusion proteins are assumed to play a pivotal role in reducing the associated energy barriers. However, no specific role in stabilizing or driving pore formation has been directly attributed to any membrane fusion protein. Recent evidence suggests that cellular curvature-generating proteins may instead assume this role (Ciechonska et al., 2014; Leikina et al., 2013; Richard et al., 2011). In a study of influenza HA and baculovirus gp64 mediated cell-cell fusion, Richard et al. showed that increased intracellular concentrations of curvature generating proteins such as the epsin ENTH domain, GRAF1 BAR domain, or FCHo2 F-BAR domain promoted syncytium formation (Richard et al., 2011). Likewise, inhibition or depletion of intracellular dynamin inhibited syncytium formation, but not lipid mixing. Although no attempt was made to delineate the underlying mechanism of this phenomenon, the authors suggested that these proteins might accumulate at the rim of the nascent fusion pore, thereby lowering its energy. Ciechonska et al. and Leikina et al. argue that interaction of annexin A1 or dynamin,

respectively, with membrane platforms enriched in ceramide or phosphatidylinositol(4,5)bisphosphate is important for pore expansion. It was suggested that these proteins are unlikely to promote pore expansion via direct interaction with the fusion pore itself, but ather through modulation of the cortical actin network or other signaling pathways (Ciechonska et al., 2014; Leikina et al., 2013). Experimental evidence also supports a role for modulation of the actin cytoskeleton by dyanamin-2 in exocytic pore expansion in chromaffin cells (Gonzalez-Jamett et al., 2013). Therefore, although curvature-generating proteins are implicated in fusion pore formation and expansion, they may not directly associate with the pore itself.

In Chapter 3, we showed that a membrane-proximal hydrophobic patch in the endodomain of the p15 FAST protein functions as a novel fusion-inducing lipid packing sensor (FLiPS) element in cell-cell fusion. Using a series of biophysical, biochemical, and cellular assays, we conclusively demonstrated that p15FLiPS requires a unique helix-loop-helix architecture to preferentially partition into membranes containing lipid packing defects. Furthermore, we showed that proline and glycine residues, which contribute to the helix-loop-helix conformation, are essential for pore- and syncytium formation, implying that p15FLiPS functions at the fusion pore formation stage of cell-cell membrane fusion. Finally, we showed that p15FLiPS could be functionally replaced with heterologous lipid packing sensors from cellular proteins, but not with other amphipathic helices, and that lipid-packing sensor motifs in the context of p15 were still reliant on key hydrophobic residues thought to be essential for their membrane curvature sensitivity (Bigay et al., 2005; Gonzalez-Rubio et al., 2011; Levi et al., 2008). Taken together, we concluded that p15FLiPS is the first membrane curvature sensitive element identified in any membrane fusion protein to date, and we speculate that p15FLiPS works by masking hydrophobic defects caused by extreme curvature stresses during pore formation. Herein, we have provided the first direct evidence of how protein fusogens may mediate pore formation by extending the known roles of generic membrane curvature-sensing moieties to a novel role in the membrane fusion pathway.

Based on these results, we propose that during FAST protein-mediated membrane fusion, the fusion pore predominantly exists as a mixed protein-lipid structure. Unlike the transmembrane-lined pore model proposed in the exocytic fusion field, we

posit that the endodomain of p15 undergoes conformational changes during membrane fusion, driven by the insertion of p15FLiPS into the fusion pore. The attraction of p15FLiPS into a membrane rich in lipid packing defects, such as at the fusion pore, would drive the partial penetration and folding of p15FLiPS in the membrane, thereby swinging the endodomain from a cytosolic position to a juxtamembrane locale. In the future, experiments determining the depth of p15FLiPS membrane insertion as well as the nature of the FAST-mediated fusion pore will undoubtedly provide more insight into this hypothesis. The use of super-resolution microscopy approaches in the future will help elucidate the exact localization of the FLiPS motif during cell-cell membrane fusion, whether that be at the rim of the fusion pore or other areas of strong positive curvature such as at actin-driven membrane protrusions.

While all FAST proteins are predicted to contain compositionally diverse FLiPS elements (Figure 3.16), most enveloped virus fusion proteins have small cytoplasmic tails that either play no role or a negative regulatory role in membrane fusion. For example, the cytoplasmic tails of fusogens encoded by baculovirus (Long et al., 2006), severe acute respiratory virus coronavirus (Broer et al., 2006), vesicular stomatitis virus (Odell et al., 1997), and parainfluenza virus type 2 (Yao and Compans, 1995) have no influence on membrane fusion, while the cytoplasmic tails of fusogens from measles virus (Moll et al., 2002), some herpesviruses (Harman et al., 2002), and numerous retroviruses (Merten et al., 2006) play inhibitory roles in membrane fusion through control of fusion competence. Therefore, although membrane curvature sensing by a membrane-proximal stretch of amino acids in the cytoplasmic tails of FAST proteins is associated with pore formation, enveloped viruses may be reliant on an alternate strategy to achieve this objective. Since the initial size and dynamics of the fusion pore is a function of the protein mediating fusion (Plonsky et al., 2008), it is possible that mechanisms as diverse as the fusion proteins themselves are used to stabilize nascent fusion pores.

5.2 Exosomes in FAST-Mediated Cell-Cell Fusion: Extracellular Communication Devices or Fusion Platforms?

Two important syncytial tissues in the body, the syncytiotrophoblast and muscle tissue, are known to secrete large amounts of exosomes and microvesicles during

differentiation, fusion and post-fusion (Le Bihan et al., 2012; Mincheva-Nilsson and Baranov, 2010; Romancino et al., 2013). Proteomic and functional analyses have linked syncytiotrophoblast exosomes to viral immunity (Delorme-Axford et al., 2013b) and immune protection of the fetus (Southcombe et al., 2011; Stenqvist et al., 2013; Tolosa et al., 2012). Muscle cell exosomes are proposed to function as a novel class of 'myokine' effectors, exerting autocrine, paracrine and/or endocrine effects (Guescini et al., 2010), and regulating gene expression of specific target genes throughout myoblast differentiation (Forterre et al., 2014). Other than the discovery that syncytin is trafficked into syncytiotrophoblast exosomes (Tolosa et al., 2012), there are no studies directly linking exosomes to the actual process of cell-cell fusion for syncytiotrophoblasts, myoblasts, or in any other cell-cell fusion model. Moreover, we showed that FAST-exosomes were fusogenic, and therefore likely contribute to the overall progression of cell-cell fusion.

In Chapter 4, we presented the first study dedicated to examining the role of exosome secretion in cell-cell fusion. Using the FAST proteins to induce cell-cell fusion, we were able to conclusively show that FAST proteins are efficiently incorporated into exosomes, a process that correlates with p14 FAST protein interactions with a component of the host ESCRT machinery. The co-immunoprecipitation approach we used showed an interaction between p14 and TSG101, further studies will need to be completed to establish a direct causal relationship. For example, *does p14c78 fail to co-immunoprecipitate with TSG101? Does the extension mutant, p15c88, regain interaction with TSG101? Does the soluble p14 endodomain fragment, which is naturally produced as a cleavage product at low levels* (Top et al., 2009)*, act as a competitive inhibitor of exosome production? Is the interaction between direct between p14 and TSG101 or via a scaffolding complex? If so, what proteins make up the complex and how would they contribute to exosome biogenesis or membrane fusion? Does knockdown of TSG101 or other key ESCRT components such as Alix inhibit recruitment of p14 to exosomes and exosome biogenesis in general? Do knockdowns of these genes inhibit in release of infectious progeny of reptilian reovirus or other fusogenic reoviruses? How do exosomes get taken up by target cells?*

It is also apparent that the factors directing p14 incorporation into exosomes are not directly linked to increased exosome production. The p14c78 construct was not incorporated into exosomes but still induced the same level of exosome release as authentic p14, based on the levels of CD81 in the exosome fraction and quantification of total exosome protein. Interestingly, the truncation that converts p14c88 (which is incorporated into exosomes) to p14c78 removes the major portion of the p14 AH FLiPS motif (residues 70-92), suggesting the AH may be involved in sorting p14 into exosomes. It is unclear how this might occur, but it is conceivable that membrane curvature during exosome budding might recruit p14 based on affinity of the p14 FLiPS motif for these sites of curvature. Testing for the presence of p15FLiPS mutants in exosomes may also be informative in this regard. Since p14Δ30 (i.e., p14 lacking most of the ectodomain) induces robust exosome production and is itself incorporated into exosomes, p14 residues 31-78 may contain motifs involved in increased exosome biogenesis. This region of p14 encompasses the transmembrane domain and polybasic motif, either of which might promote exosome biogenesis. Screening our large panel of p14 transmembrane domain and polybasic mutants for exosome production should establish whether either of these motifs effect exosome production.

We also showed that the p15 FAST protein was present in the P100 exosome fraction, however, the majority of p15 was enriched in the P2 fraction (large membrane blebs). Previous studies have established that the short 19 amino acid ectodomain of p15 follows a biphasic fusion pathway, whereby massive aggregation of 100 nm liposomes precedes liposome fusion (Top et al., 2012). Therefore, the presence of p15 in the P2 fraction could be accounted for by exosome-exosome aggregration/fusion mediated by the p15 ectodomain. Examination of the isolated ECV fractions by electron microscopy could help establish whether exosome fusion is occurring.

Interestingly, our proteomic studies did not reveal large differences between constitutively secreted control exosomes and p14-exosomes, suggesting p14 exploits existing exosome biogenesis pathways. If FAST protein-exosomes function as paracrine signaling packages like those of myoblasts and trophoblasts, the proteomic analysis also suggests this activity may be independent of the protein content of the exosomes. The caveat here is that our proteomic analysis likely only identified major protein components

of exosomes, therefore minor undetected differences in protein composition might exert an effect. Additional proteomic studies on a larger scale, using increased quantities of exosomes to improve sensitivity or immunoaffinity purification of p14 exosomes to increase selectivity might help address this issue. An analysis of the RNA content of exosomes using RNA seq approaches is also warranted, since exosomes could serve as a "transduction" system to deliver mRNAs or miRNAs to neighbouring cells.

In Chapter 4, we presented two possible models for the role of FAST-exosomes in fusion. In the first model (Section 4.3.4), FAST proteins are trafficked through the endocytic route into secretory MVBs. Fusion of the MVB with the plasma membrane would result in extracellular release of FAST-exosomes, with the FAST proteins being transferred to recipient cells by either direct fusion with the plasma membrane or via recycling from an endocytic route. Once the recipient cell has a certain threshold of FAST protein in its plasma membrane, it could fuse with a neighbouring cell thereby increasing syncytiogenesis. In a second possible model (Section 4.3.6), we speculated that FAST protein-exosomes might originate from the plasma membrane. In this scenario, the act of budding is more important than the release of the exosome, since bud sites would act as fusion platforms by decreasing intermembrane distances while providing a curved surface replete with membrane-destabilizing FAST proteins. The combination of these factors would provide an ideal fusion platform. Since FAST proteins are known to be dependent on surrogate cadherins to mediate membrane approach (Salsman et al., 2008), it is easy to envision how a small plasma membrane protrusion, driven by ESCRT-mediated sorting of FAST proteins into a localized area, could bridge the ~20 nm gap between the membranes. It is interesting to imagine that formation of a protruding fusion platform could be a common feature in all cell-cell fusion models. The formation of these platforms could be generated using different combinations of lipids, membrane curvature-generating proteins, and cytoskeletal effector proteins, therefore, diverse proteins and diverse pathways could be used in different types of cell-cell fusion. Indeed, in *Drosophila* myoblast fusion, actin-rich invading podosomes have been described as an essential intermediate plasma membrane architecture for fusion of founder cells with fusion-competent myoblasts (Sens et al., 2010), although the size of these finger-like protrusions are much larger than we would

predict for a FAST protein bud site. In the future, determining the intracellular location of budding for FAST-exosomes and visualizing the purported fusion platforms will be essential to validate this hypothesis.

5.3 Comparison of FAST Proteins and Viroporins

Viroporins are virally-encoded proteins encoded by a wide range of animal viruses such as HIV-1 (Park and Opella, 2007), influenza A virus (Wang et al., 1993), coronaviruses (Ruch and Machamer, 2012), picornaviruses (Nieva et al., 2003), and togaviruses (Madan et al., 2005). Viroporins are involved in numerous stages of the virus lifecycle including virus entry, virus genome replication, viral assembly, and virus release, and account for much of the pathogenesis inflicted by these viruses(OuYang and Chou, 2014). Viroporins share a number of common features, including their small size (60 to 120 amino acids), the presence of one or two transmembrane domains, a stretch of basic residues involved in membrane destabilization, a membrane-proximal amphipathic helix involved in generation of membrane curvature, as well as their ability to permeabilize membranes or form ion channels upon oligomerization (Gonzalez and Carrasco, 2003; Nieva et al., 2012). Typically, the deletion of the viroporin-encoding gene from the viral genome drastically diminishes the formation of virus progeny and pathogenicity, underscoring the importance of these proteins in the viral life cycle.

Although viroporins participate in diverse steps in the virus life cycle, the main activity of viroporins is their involvement in virus assembly and release. In the case of non-enveloped viruses, a progressive increase in membrane permeability due to accumulation of viroporins in the membrane leads to cell lysis and subsequent release of assembled virus particles from infected cells (Raghava et al., 2011). For enveloped viruses, the last step of virus maturation is the budding of enveloped virus particles from the plasma membrane or internal membranes. The insertion of viroporins into the membrane leads to dissipation of the membrane potential, membrane curvature induction, and in the case of influenza M2, scission of the budding virus particle (Hsu et al., 2010b; Rossman and Lamb, 2011). In this manner, production of both viruses and vesicles – even those of non-viral origin – is promoted (Huang et al., 2011).

There are a number of striking parallels between the FAST proteins and viroporins. Both groups of proteins are small transmembrane anchored proteins with a cluster a basic amino acids and a membrane-proximal amphipathic helix (or FLiPS element) in their endodomain. Indeed, ARV p10 was initially classified as a viroporin, since ARV p10 rendered the plasma membrane of infected cells permeable to small molecules, such as hygromycin B, in the late stages of virus infection (Bodelon et al., 2002). Furthermore, this group demonstrated that expression of ARV p10 from a plasmid (i.e. independent of ARV infection) in various cell types also led to late-stage membrane leakiness, even when the ectodomain of p10 was deleted. The previous point is particularly salient because the ectodomain is required for cell-cell fusion activity, therefore the authors concluded that observed increases in membrane permeability were not a result of syncytiogenesis. Other (unrelated) studies of ARV-induced syncytium formation also conclusively showed that syncytiogenesis induced by p10 increases the rate of virus egress and virus-induced cytopathology, consistent with known roles of viroporins (Duncan et al., 1996b). This raises the question: are FAST proteins dedicated cell-cell fusion proteins that happen to cause increased membrane permeability, or are FAST proteins dedicated viroporins that happen to cause cell-cell fusion?

This question was addressed by Salsman et al., by examining the syncytium-inducing and membrane-lytic properties of FAST proteins (ARV p10, NBV p10, RRV p14, and BRVp15) in closer detail (Salsman et al., 2005). Unlike previous studies, they found membrane destabilization was completely dependent on syncytium formation and this effect occurred through a caspase-dependent apoptotic pathway when syncytia became large and unstable. Based on this result, they concluded that FAST proteins function as specific membrane fusion proteins, which serve a dual role in the virus infection cycle – mediating early cell-cell transmission of the virus via syncytial spread and late apoptosis-mediated lytic dissemination of virus. At the time, induction of apoptosis was taken as a sign that FAST proteins used different mechanisms to induce membrane permeabilization than viroporins, however, it is now established that viroporins, like FAST proteins, are able to induce caspase-mediated apoptosis, through alterations in calcium homeostasis (Aweya et al., 2013; Chami et al., 2003; Madan et al.,

2005; Marchal et al., 2012), further supporting the argument that FAST proteins could be viroporins.

Viroporins are known to play a critical role in the morphogenesis and release of enveloped virions. Although expressed at high levels within the host cell, they constitute only minor components of virus particles (Vieyres et al., 2013), suggesting the primary role of these proteins is membrane remodeling, not as essential virus structural proteins. It has been suggested that many viroporins are responsible for induction of curvature necessary for the budding process. For some viruses, such as HIV-1 (Baumgartel et al., 2011), hepatitis C virus (Corless et al., 2010), herpes simplex virus (Pawliczek and Crump, 2009), and Ebola and Marburg viruses (Silvestri et al., 2007), but not influenza A virus (Roberts et al., 2013; Rossman et al., 2010), closure and scission of the budded membrane depends on recruitment of the cellular ESCRT complex by late domains in the cytoplasmic portions of the viroporin proteins. Interestingly, not all ESCRT-dependent viruses require recruitment of all members of the ESCRT complex, suggesting some viroporin proteins may assume a redundant role to some of the ESCRT proteins.

Influenza M2 is a well-characterized viroporin encoded by influenza A. During virus entry, endosomal acidification activates the H^+-selective ion channel activity of M2, thereby acidifying the interior of the viral particle, allowing dissociation of the M1 protein from the viral genome. During viral egress, M2 localizes at the neck of budding virions, where it is responsible both for generating curvature necessary for budding (Schmidt et al., 2013), as well as ESCRT-independent scission of the neck of the bud (Rossman et al., 2010). The membrane-proximal AH in particular is required for membrane scission, and a peptide of this sequence alone is capable of inducing budding and scission of giant unilamellar vesicles (Rossman et al., 2010).

The M2 protein features a 29 amino acid N-terminal ectodomain, a single pass transmembrane domain that forms the pore of the ion channel, and a 54 amino acid cytoplasmic tail. Within the cytoplasmic tail, there is a 17 amino acid juxtamembrane AH and cholesterol binding motif (embedded in the AH). The layout and functional arrangement of M2 is strikingly similar to p14 (Figure 5.1 A). p14 has a 38 amino acid N-terminal ectodomain, a 19 residue single pass transmembrane domain, and a 68 residue endodomain, also containing a membrane-proximal AH. A comparison of AHs from M2

and p14 reveals that M2 has a stronger hydrophobic moment and greater net charge than p14 (Figure 5.1 B), suggesting the AH of M2 may slightly be better suited for curvature induction than that of p14. The cumulative work in Chapter 4 showed that p14 induces ECV secretion and as well as a direct interaction between p14 and TSG101. Therefore, like other viroporins, perhaps p14 is capable of producing membrane curvature required for budding, but is unable to mediate membrane scission, and therefore must recruit TSG101.

There is evidence that TSG101 interacts with viroporins from non-enveloped viruses, such as NS3 from Bluetongue virus (a reovirus), and African horse sickness virus (a closely related orbivirus). Interestingly, although both of these viruses are traditionally considered to be non-enveloped viruses, efficient virus egress is dependent on interaction of NS3 with TSG101 via a sub-optimal late domain in NS3 (Wirblich et al., 2006). This effect is speculated to be most pertinent in insect cells, where virus infection causes no cytopathic effect. It is conjectured, therefore, that NS3 interacts with TSG101 in order to establish a non-lytic egress route, although the precise mechanism is not yet clear. It has been suggested that a minor population of virus acquires an envelope from the plasma membrane through budding mediated by NS3 protein and TSG101 (Celma and Roy, 2009). Therefore, the majority of viroporins encoded by enveloped viruses (with the exception of influenza M2) and some viroporins from non-enveloped virus (NS3 from Bluetongue virus and African horse sickness virus) are dependent on interaction with host ESCRT proteins to facilitate membrane shedding.

Could the FAST proteins be vestigial viroporins that were once required for budding of an envelope that was lost in evolution? Consistent with the concept that reoviruses may have once been enveloped viruses, *Orbiviruses* and *Rotaviruses* (two other genera in the Reoviridae family), both transiently acquire an envelope during virus assembly and egress (Hyatt et al., 1993; Suzuki et al., 1993), and a reovirus infecting parasitoid wasps also transiently acquires an envelope from the plasma membrane (Stoltz and Makkay, 2000). Therefore, FAST proteins may once have served as small membrane proteins whose function was to organize budding sites for enveloped reovirus particles by inducing localized membrane remodeling and by providing a platform for virus assembly of virus particles. It is unclear if reoviruses were once enveloped why they would have

lost their envelope, however, it is possible that syncytium formation is a trade-off for loss of envelope, as lysis (and associated cytopathic effects) could be temporally deferred until syncytia become large and unstable.

Additionally, FAST proteins may play a role in calcium homeostasis during virus infection, as most viroporins are thought to do. Recent work has shown that p14 interacts with annexin A1 in a calcium-dependent manner (Ciechonska et al., 2014). Although there is no direct evidence that p14 or the other FAST proteins act as ion channels like all other known viroporins, it is a possibility. Therefore, determination if the FAST proteins are *bona fide* viroporins, that incidentally induce cell-cell fusion, will undoubtedly prove useful in determining fusogenic reovirus egress pathways and how cell-cell fusion progresses in this model.

5.4 Concluding Remarks

The cumulative data presented here and in other studies suggests that the FAST proteins function differently than all known membrane fusion proteins to mediate cell-cell membrane fusion. A fundamental difference between the FAST proteins and the prototypical enveloped virus proteins is their asymmetric topology in the host cell membrane. With cytosolic endodomains that are disproportionately large compared to other characterized fusion proteins, FAST proteins are perfectly positioned to interact with a variety of host cellular proteins to drive syncytiogenesis. Since many of the pre- and post- membrane fusion steps thought to be outsourced to cellular proteins such as cadherins, annexins, and ESCRT proteins, FAST proteins may represent the minimum package of membrane remodeling and destabilizing motifs required for membrane merger. As many of the proteins responsible for physiological cell-cell fusion events are not yet known, insight from how these nominal membrane fusion machines take advantage of host pathways to mediate each step of syncytiogenesis may provide useful information in elucidation of pathways and proteins used to drive developmental cell fusion.

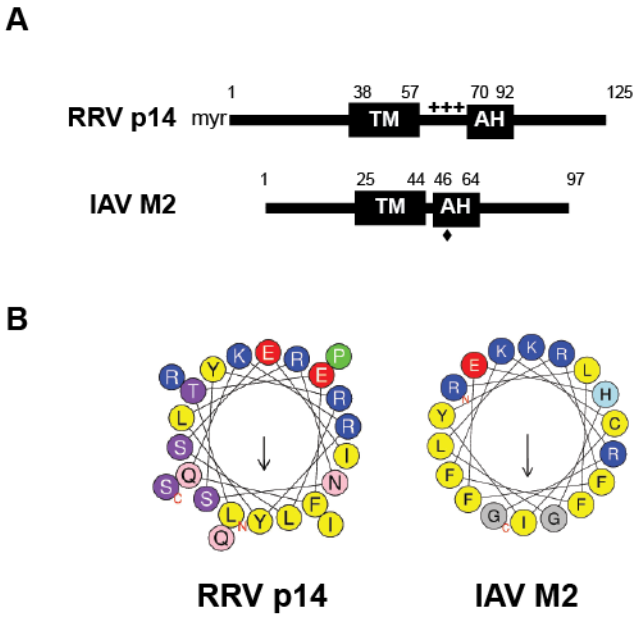

Figure 5.1 Comparison of structural and functional motifs between reptilian reovirus (RRV) p14 and influenza A virus (IAV) M2 proteins. (A) Schematic representation of p14 and M2 proteins. Numbers represent the amino acid position. myr, myristic acid; TM, transmembrane, +++, polybasic cluster, AH, amphipathic helix, ♦, palmitic acid. **(B)** Helical wheel projections of p14 and M2 proteins. Color code: yellow, hydrophobic residues; purple and pink, uncharged polar residues; green, proline; blue, positively charged residues; red, negatively charged residues; grey, glycine. Arrow represents the direction and magnitude of the hydrophobic moment.

REFERENCES

Albertini, A., Bressanelli, S., Lepault, J., and Gaudin, Y. (2011). Structure and working of viral fusion machinery. Curr. Top. Membr. *68*, 49-80.

Ambroggio, E.E., Sillibourne, J., Antonny, B., Manneville, J.B., and Goud, B. (2013). Arf1 and membrane curvature cooperate to recruit Arfaptin2 to liposomes. PLoS One. *8*, e62963.

Antonny, B. (2011). Mechanisms of membrane curvature sensing. Annu. Rev. Biochem. *80*, 101-123.

Armstrong, R.T., Kushnir, A.S., and White, J.M. (2000). The transmembrane domain of influenza hemagglutinin exhibits a stringent length requirement to support the hemifusion to fusion transition. J. Cell Biol. *151*, 425-437.

Avinoam, O., Fridman, K., Valansi, C., Abutbul, I., Zeev-Ben-Mordehai, T., Maurer, U.E., Sapir, A., Danino, D., Grunewald, K., White, J.M.*, et al.* (2011). Conserved eukaryotic fusogens can fuse viral envelopes to cells. Science. *332*, 589-592.

Aweya, J.J., Mak, T.M., Lim, S.G., and Tan, Y.J. (2013). The p7 protein of the hepatitis C virus induces cell death differently from the influenza A virus viroporin M2. Virus Res. *172*, 24-34.

Babst, M., Odorizzi, G., Estepa, E.J., and Emr, S.D. (2000). Mammalian tumor susceptibility gene 101 (TSG101) and the yeast homologue, Vps23p, both function in late endosomal trafficking. Traffic. *1*, 248-258.

Baietti, M.F., Zhang, Z., Mortier, E., Melchior, A., Degeest, G., Geeraerts, A., Ivarsson, Y., Depoortere, F., Coomans, C., Vermeiren, E.*, et al.* (2012). Syndecan-syntenin-ALIX regulates the biogenesis of exosomes. Nat. Cell Biol. *14*, 677-685.

Barry, C., and Duncan, R. (2009). Multifaceted sequence-dependent and -independent roles for reovirus FAST protein cytoplasmic tails in fusion pore formation and syncytiogenesis. J. Virol. *83*, 12185-12195.

Barry, C., Key, T., Haddad, R., and Duncan, R. (2010). Features of a spatially constrained cystine loop in the p10 FAST protein ectodomain define a new class of viral fusion peptides. J. Biol. Chem. *285*, 16424-16433.

Baumgartel, V., Ivanchenko, S., Dupont, A., Sergeev, M., Wiseman, P.W., Krausslich, H.G., Brauchle, C., Muller, B., and Lamb, D.C. (2011). Live-cell visualization of dynamics of HIV budding site interactions with an ESCRT component. Nat. Cell Biol. *13*, 469-474.

Bess, J.W.,Jr, Gorelick, R.J., Bosche, W.J., Henderson, L.E., and Arthur, L.O. (1997). Microvesicles are a source of contaminating cellular proteins found in purified HIV-1 preparations. Virology. *230*, 134-144.

Bhatia, V.K., Hatzakis, N.S., and Stamou, D. (2010). A unifying mechanism accounts for sensing of membrane curvature by BAR domains, amphipathic helices and membrane-anchored proteins. Semin. Cell Dev. Biol. *21*, 381-390.

Bigay, J., and Antonny, B. (2012). Curvature, lipid packing, and electrostatics of membrane organelles: Defining cellular territories in determining specificity. Dev. Cell. *23*, 886-895.

Bigay, J., Casella, J.F., Drin, G., Mesmin, B., and Antonny, B. (2005). ArfGAP1 responds to membrane curvature through the folding of a lipid packing sensor motif. EMBO J. *24*, 2244-2253.

Bissig, C., and Gruenberg, J. (2014). ALIX and the multivesicular endosome: ALIX in wonderland. Trends Cell Biol. *24*, 19-25.

Bodelon, G., Labrada, L., Martinez-Costas, J., and Benavente, J. (2002). Modification of late membrane permeability in avian reovirus-infected cells: Viroporin activity of the S1-encoded nonstructural p10 protein. J. Biol. Chem. *277*, 17789-17796.

Borrego-Diaz, E., Peeples, M.E., Markosyan, R.M., Melikyan, G.B., and Cohen, F.S. (2003). Completion of trimeric hairpin formation of influenza virus hemagglutinin promotes fusion pore opening and enlargement. Virology. *316*, 234-244.

Boutilier, J., and Duncan, R. (2011). The reovirus fusion-associated small transmembrane (FAST) proteins: Virus-encoded cellular fusogens. Curr. Top. Membr. *68*, 107-140.

Broer, R., Boson, B., Spaan, W., Cosset, F.L., and Corver, J. (2006). Important role for the transmembrane domain of severe acute respiratory syndrome coronavirus spike protein during entry. J. Virol. *80*, 1302-1310.

Brown, C.W., Stephenson, K.B., Hanson, S., Kucharczyk, M., Duncan, R., Bell, J.C., and Lichty, B.D. (2009). The p14 FAST protein of reptilian reovirus increases vesicular stomatitis virus neuropathogenesis. J. Virol. *83*, 552-561.

Brugnera, E., Haney, L., Grimsley, C., Lu, M., Walk, S.F., Tosello-Trampont, A.C., Macara, I.G., Madhani, H., Fink, G.R., and Ravichandran, K.S. (2002). Unconventional rac-GEF activity is mediated through the Dock180-ELMO complex. Nat. Cell Biol. *4*, 574-582.

Bullough, P.A., Hughson, F.M., Skehel, J.J., and Wiley, D.C. (1994). Structure of influenza haemagglutinin at the pH of membrane fusion. Nature. *371*, 37-43.

Buschow, S.I., Nolte-'t Hoen, E.N., van Niel, G., Pols, M.S., ten Broeke, T., Lauwen, M., Ossendorp, F., Melief, C.J., Raposo, G., Wubbolts, R.*, et al.* (2009). MHC II in dendritic cells is targeted to lysosomes or T cell-induced exosomes via distinct multivesicular body pathways. Traffic. *10*, 1528-1542.

Cabrera, M., Langemeyer, L., Mari, M., Rethmeier, R., Orban, I., Perz, A., Brocker, C., Griffith, J., Klose, D., Steinhoff, H.J., *et al.* (2010). Phosphorylation of a membrane curvature-sensing motif switches function of the HOPS subunit Vps41 in membrane tethering. J. Cell Biol. *191*, 845-859.

Caby, M.P., Lankar, D., Vincendeau-Scherrer, C., Raposo, G., and Bonnerot, C. (2005). Exosomal-like vesicles are present in human blood plasma. Int. Immunol. *17*, 879-887.

Campelo, F., McMahon, H.T., and Kozlov, M.M. (2008). The hydrophobic insertion mechanism of membrane curvature generation by proteins. Biophys. J. *95*, 2325-2339.

Celma, C.C., and Roy, P. (2009). A viral nonstructural protein regulates bluetongue virus trafficking and release. J. Virol. *83*, 6806-6816.

Chami, M., Ferrari, D., Nicotera, P., Paterlini-Brechot, P., and Rizzuto, R. (2003). Caspase-dependent alterations of Ca2+ signaling in the induction of apoptosis by hepatitis B virus X protein. J. Biol. Chem. *278*, 31745-31755.

Chandran, K., Sullivan, N.J., Felbor, U., Whelan, S.P., and Cunningham, J.M. (2005). Endosomal proteolysis of the ebola virus glycoprotein is necessary for infection. Science. *308*, 1643-1645.

Chang, D.K., Cheng, S.F., Kantchev, E.A., Lin, C.H., and Liu, Y.T. (2008). Membrane interaction and structure of the transmembrane domain of influenza hemagglutinin and its fusion peptide complex. BMC Biol. *6*, 2-7007-6-2.

Chanturiya, A., Chernomordik, L.V., and Zimmerberg, J. (1997). Flickering fusion pores comparable with initial exocytotic pores occur in protein-free phospholipid bilayers. Proc. Natl. Acad. Sci. U. S. A. *94*, 14423-14428.

Chen, A., Leikina, E., Melikov, K., Podbilewicz, B., Kozlov, M.M., and Chernomordik, L.V. (2008). Fusion-pore expansion during syncytium formation is restricted by an actin network. J. Cell. Sci. *121*, 3619-3628.

Chen, C., Skog, J., Hsu, C.H., Lessard, R.T., Balaj, L., Wurdinger, T., Carter, B.S., Breakefield, X.O., Toner, M., and Irimia, D. (2010). Microfluidic isolation and transcriptome analysis of serum microvesicles. Lab. Chip. *10*, 505-511.

Chen, E.H. (2011). Invasive podosomes and myoblast fusion. Curr. Top. Membr. *68*, 235-258.

Chen, E.H., Pryce, B.A., Tzeng, J.A., Gonzalez, G.A., and Olson, E.N. (2003). Control of myoblast fusion by a guanine nucleotide exchange factor, loner, and its effector ARF6. Cell. *114*, 751-762.

Chernomordik, L.V., and Kozlov, M.M. (2003). Protein-lipid interplay in fusion and fission of biological membranes. Annu. Rev. Biochem. *72*, 175-207.

Chernomordik, L., and Kozlov, M. (2005). Membrane hemifusion: crossing a chasm in two leaps. Cell. *123*, 375-382.

Chernomordik, L.V., Sukharev, S.I., Popov, S.V., Pastushenko, V.F., Sokirko, A.V., Abidor, I.G., and Chizmadzhev, Y.A. (1987). The electrical breakdown of cell and lipid membranes: The similarity of phenomenologies. Biochim. Biophys. Acta. *902*, 360-373.

Chernomordik, L.V., Zimmerberg, J., and Kozlov, M.M. (2006). Membranes of the world unite! J. Cell Biol. *175*, 201-207.

Chernomordik, L., and Kozlov, M. (2008). Mechanics of membrane fusion. Nature Struct Mol Biol. *15*, 675-683.

Chong, S.S., Taneva, S.G., Lee, J.M., and Cornell, R.B. (2014). The curvature sensitivity of a membrane-binding amphipathic helix can be modulated by the charge on a flanking region. Biochemistry. *53*, 450-461.

Choudhuri, K., Llodra, J., Roth, E.W., Tsai, J., Gordo, S., Wucherpfennig, K.W., Kam, L.C., Stokes, D.L., and Dustin, M.L. (2014). Polarized release of T-cell-receptor-enriched microvesicles at the immunological synapse. Nature. *507*, 118-123.

Ciechonska, M., Key, T., and Duncan, R. (2014). Efficient reovirus- and measles virus-mediated pore expansion during syncytium formation is dependent on annexin A1 and intracellular calcium. J. Virol.

Clancy, E.K., Barry, C., Ciechonska, M., and Duncan, R. (2010). Different activities of the reovirus FAST proteins and influenza hemagglutinin in cell-cell fusion assays and in response to membrane curvature agents. Virology. *397*, 119-129.

Clancy, E.K., and Duncan, R. (2009). Reovirus FAST protein transmembrane domains function in a modular, primary sequence-independent manner to mediate cell-cell membrane fusion. J. Virol. *83*, 2941-2950.

Clancy, E.K., and Duncan, R. (2011). Helix-destabilizing, beta-branched, and polar residues in the baboon reovirus p15 transmembrane domain influence the modularity of FAST proteins. J. Virol. *85*, 4707-4719.

Clavel, F., and Charneau, P. (1994). Fusion from without directed by human immunodeficiency virus particles. J. Virol. *68*, 1179-1185.

Clayton, A., Harris, C.L., Court, J., Mason, M.D., and Morgan, B.P. (2003). Antigen-presenting cell exosomes are protected from complement-mediated lysis by expression of CD55 and CD59. Eur. J. Immunol. *33*, 522-531.

Clayton, A., Turkes, A., Dewitt, S., Steadman, R., Mason, M.D., and Hallett, M.B. (2004). Adhesion and signaling by B cell-derived exosomes: The role of integrins. FASEB J. *18*, 977-979.

Cocucci, E., Racchetti, G., and Meldolesi, J. (2009). Shedding microvesicles: Artefacts no more. Trends Cell Biol. *19*, 43-51.

Cohen, F.S., and Melikyan, G.B. (2004). The energetics of membrane fusion from binding, through hemifusion, pore formation, and pore enlargement. J. Membr. Biol. *199*, 1-14.

Coleman, M.L., Sahai, E.A., Yeo, M., Bosch, M., Dewar, A., and Olson, M.F. (2001). Membrane blebbing during apoptosis results from caspase-mediated activation of ROCK I. Nat. Cell Biol. *3*, 339-345.

Colombo, M., Moita, C., van Niel, G., Kowal, J., Vigneron, J., Benaroch, P., Manel, N., Moita, L.F., Thery, C., and Raposo, G. (2013). Analysis of ESCRT functions in exosome biogenesis, composition and secretion highlights the heterogeneity of extracellular vesicles. J. Cell. Sci. *126*, 5553-5565.

Cooke, I.R., and Deserno, M. (2006). Coupling between lipid shape and membrane curvature. Biophys. J. *91*, 487-495.

Corcoran, J.A., Clancy, E.K., and Duncan, R. (2011). Homomultimerization of the reovirus p14 fusion-associated small transmembrane protein during transit through the ER-golgi complex secretory pathway. J. Gen. Virol. *92*, 162-166.

Corcoran, J.A., Salsman, J., de Antueno, R., Touhami, A., Jericho, M.H., Clancy, E.K., and Duncan, R. (2006). The p14 fusion-associated small transmembrane (FAST) protein effects membrane fusion from a subset of membrane microdomains. J. Biol. Chem. *281*, 31778-31789.

Corcoran, J.A., Syvitski, R., Top, D., Epand, R.M., Jakeman, D., and Duncan, R. (2004). Myristoylation, a protruding loop, and structural plasticity are essential features of a nonenveloped virus fusion peptide motif. J Biol Chem. *279*, 51386-94.

Corcoran, J., and Duncan, R. (2004). Reptilian reovirus utilizes a small type III protein with an external myristylated amino terminus to mediate cell-cell fusion. J Virol. *78*, 4342-4351.

Corless, L., Crump, C.M., Griffin, S.D., and Harris, M. (2010). Vps4 and the ESCRT-III complex are required for the release of infectious hepatitis C virus particles. J. Gen. Virol. *91*, 362-372.

Cornelis, G., Heidmann, O., Bernard-Stoecklin, S., Reynaud, K., Veron, G., Mulot, B., Dupressoir, A., and Heidmann, T. (2012). Ancestral capture of syncytin-Car1, a fusogenic endogenous retroviral envelope gene involved in placentation and conserved in carnivora. Proc. Natl. Acad. Sci. U. S. A. *109*, E432-41.

Cotter, T.G., Lennon, S.V., Glynn, J.M., and Green, D.R. (1992). Microfilament-disrupting agents prevent the formation of apoptotic bodies in tumor cells undergoing apoptosis. Cancer Res. *52*, 997-1005.

Cui, H., Lyman, E., and Voth, G.A. (2011). Mechanism of membrane curvature sensing by amphipathic helix containing proteins. Biophys. J. *100*, 1271-1279.

Curto, M.A., Sharifmoghadam, M.R., Calpena, E., De Leon, N., Hoya, M., Doncel, C., Leatherwood, J., and Valdevieso, M.H. (2014). Membrane organization and cell fusion during mating in fission yeast requires multipass membrane protein Prm1. Genetics. *196*, 1059-1076.

Davies, B.A., Azmi, I.F., Payne, J., Shestakova, A., Horazdovsky, B.F., Babst, M., and Katzmann, D.J. (2010). Coordination of substrate binding and ATP hydrolysis in Vps4-mediated ESCRT-III disassembly. Mol. Biol. Cell. *21*, 3396-3408.

Davies, S.M., Epand, R.M., Kraayenhof, R., and Cornell, R.B. (2001). Regulation of CTP: Phosphocholine cytidylyltransferase activity by the physical properties of lipid membranes: An important role for stored curvature strain energy. Biochemistry. *40*, 10522-10531.

Dawe, S., and Duncan, R. (2002). The S4 genome segment of baboon reovirus is bicistronic and encodes a novel fusion-associated small transmembrane protein. J. Virol. *76*, 2131-2140.

Dawe, S., Corcoran, J., Clancy, E., Salsman, S., and Duncan, R. (2005). An unusual topological arrangement of structural motifs in the baboon reovirus fusion-associated small transmembrane (FAST) protein. J Virol. *79*, 6216-6226.

del Campo, J.J., Opoku-Serebuoh, E., Isaacson, A.B., Scranton, V.L., Tucker, M., Han, M., and Mohler, W.A. (2005). Fusogenic activity of EFF-1 is regulated via dynamic localization in fusing somatic cells of C. elegans. Curr. Biol. *15*, 413-423.

Delorme-Axford, E., Donker, R.B., Mouillet, J.F., Chu, T., Bayer, A., Ouyang, Y., Wang, T., Stolz, D.B., Sarkar, S.N., Morelli, A.E.*, et al.* (2013a). Human placental trophoblasts confer viral resistance to recipient cells. Proc. Natl. Acad. Sci. U. S. A. *110*, 12048-12053.

Delorme-Axford, E., Donker, R.B., Mouillet, J.F., Chu, T., Bayer, A., Ouyang, Y., Wang, T., Stolz, D.B., Sarkar, S.N., Morelli, A.E.*, et al.* (2013b). Human placental trophoblasts confer viral resistance to recipient cells. Proc. Natl. Acad. Sci. U. S. A. *110*, 12048-12053.

Delos, S.E., Gilbert, J.M., and White, J.M. (2000). The central proline of an internal viral fusion peptide serves two important roles. J. Virol. *74*, 1686-1693.

Douliez, J.-P., Michon, T., and Marion, D. (2000). Steady state tyrosine fluorescence to study the lipid-binding properties of a wheat-specific lipid-transfer protein (nsLTP1). Biochim. Biophys. Acta - Biomembranes. *1467*, 65-72.

Dragovic, R.A., Gardiner, C., Brooks, A.S., Tannetta, D.S., Ferguson, D.J., Hole, P., Carr, B., Redman, C.W., Harris, A.L., Dobson, P.J.*, et al.* (2011). Sizing and phenotyping of cellular vesicles using nanoparticle tracking analysis. Nanomedicine. *7*, 780-788.

Dreux, M., Garaigorta, U., Boyd, B., Decembre, E., Chung, J., Whitten-Bauer, C., Wieland, S., and Chisari, F.V. (2012). Short-range exosomal transfer of viral RNA from infected cells to plasmacytoid dendritic cells triggers innate immunity. Cell. Host Microbe. *12*, 558-570.

Drin, G., and Antonny, B. (2010). Amphipathic helices and membrane curvature. FEBS Lett. *584*, 1840-1847.

Drin, G., Casella, J.F., Gautier, R., Boehmer, T., Schwartz, T.U., and Antonny, B. (2007). A general amphipathic alpha-helical motif for sensing membrane curvature. Nat. Struct. Mol. Biol. *14*, 138-146.

Duan, R., Jin, P., Luo, F., Zhang, G., Anderson, N., and Chen, E.H. (2012). Group I PAKs function downstream of rac to promote podosome invasion during myoblast fusion in vivo. J. Cell Biol. *199*, 169-185.

Duncan, R., Chen, Z., Walsh, S., and Wu, S. (1996). Avian reovirus-induced syncytium formation is independent of infectious progeny virus production and enhances the rate, but is not essential, for virus-induced cytopathology and virus egress. Virology. *224*, 453-464.

Duncan, R., Corcoran, J., Shou, J., and Stoltz, D. (2004). Reptilian reovirus: A new fusogenic orthoreovirus species. Virology. *319*, 131-140.

Duncan, R., Murphy, F.A., and Mirkovic, R.R. (1995). Characterization of a novel syncytium-inducing baboon reovirus. Virology. *212*, 752-756.

Efrat, A., Chernomordik, L.V., and Kozlov, M.M. (2007). Point-like protrusion as a prestalk intermediate in membrane fusion pathway. Biophys. J. *92*, L61-3.

Eichelbaum, K., Winter, M., Berriel Diaz, M., Herzig, S., and Krijgsveld, J. (2012). Selective enrichment of newly synthesized proteins for quantitative secretome analysis. Nat. Biotechnol. *30*, 984-990.

El Omari, K., Iourin, O., Harlos, K., Grimes, J., and Stuart, D. (2013). Structure of a pestivirus envelope glycoprotein clarifies its role in cell entry. Cell Rep. *3*, 30-35.

Epand, R.M. (2003). Fusion peptides and the mechanism of viral fusion. Biochim Biophys Acta. *1614*, 116-21.

Erickson, M.R., Galletta, B.J., and Abmayr, S.M. (1997). Drosophila myoblast city encodes a conserved protein that is essential for myoblast fusion, dorsal closure, and cytoskeletal organization. J. Cell Biol. *138*, 589-603.

Esnault, C., Cornelis, G., Heidmann, O., and Heidmann, T. (2013). Differential evolutionary fate of an ancestral primate endogenous retrovirus envelope gene, the EnvV syncytin, captured for a function in placentation. PLoS Genet. *9*, e1003400.

Fairn, G.D., Curwin, A.J., Stefan, C.J., and McMaster, C.R. (2007). The oxysterol binding protein Kes1p regulates golgi apparatus phosphatidylinositol-4-phosphate function. Proc. Natl. Acad. Sci. U. S. A. *104*, 15352-15357.

Fang, Y., Wu, N., Gan, X., Yan, W., Morrell, J.C., and Gould, S.J. (2007). Higher-order oligomerization targets plasma membrane proteins and HIV gag to exosomes. PLoS Biol. *5*, e158.

Feng, D., Zhao, W.L., Ye, Y.Y., Bai, X.C., Liu, R.Q., Chang, L.F., Zhou, Q., and Sui, S.F. (2010). Cellular internalization of exosomes occurs through phagocytosis. Traffic. *11*, 675-687.

Feng, Z., Hensley, L., McKnight, K.L., Hu, F., Madden, V., Ping, L., Jeong, S.H., Walker, C., Lanford, R.E., and Lemon, S.M. (2013). A pathogenic picornavirus acquires an envelope by hijacking cellular membranes. Nature. *496*, 367-371.

Fernandes, F., Loura, L.M., Chichon, F.J., Carrascosa, J.L., Fedorov, A., and Prieto, M. (2008). Role of helix 0 of the N-BAR domain in membrane curvature generation. Biophys. J. *94*, 3065-3073.

Fertuck, H.C., and Salpeter, M.M. (1974). Localization of acetylcholine receptor by 125I-labeled alpha-bungarotoxin binding at mouse motor endplates. Proc. Natl. Acad. Sci. U. S. A. *71*, 1376-1378.

Fleissner, A., Diamond, S., and Glass, N.L. (2009). The saccharomyces cerevisiae PRM1 homolog in neurospora crassa is involved in vegetative and sexual cell fusion events but also has postfertilization functions. Genetics. *181*, 497-510.

Fleissner, A., Simonin, A.R., and Glass, N.L. (2008). Cell fusion in the filamentous fungus, neurospora crassa. Methods Mol. Biol. *475*, 21-38.

Follis, K.E., York, J., and Nunberg, J.H. (2006). Furin cleavage of the SARS coronavirus spike glycoprotein enhances cell-cell fusion but does not affect virion entry. Virology. *350*, 358-369.

Forterre, A., Jalabert, A., Berger, E., Baudet, M., Chikh, K., Errazuriz, E., De Larichaudy, J., Chanon, S., Weiss-Gayet, M., Hesse, A.M., *et al.* (2014). Proteomic analysis of C2C12 myoblast and myotube exosome-like vesicles: A new paradigm for myoblast-myotube cross talk? PLoS One. *9*, e84153.

Fox, J.E., Austin, C.D., Reynolds, C.C., and Steffen, P.K. (1991). Evidence that agonist-induced activation of calpain causes the shedding of procoagulant-containing microvesicles from the membrane of aggregating platelets. J. Biol. Chem. *266*, 13289-13295.

Friedlander-Shani, L., and Podbilewicz, B. (2011). Heterochronic control of AFF-1-mediated cell-to-cell fusion in C. elegans. Adv. Exp. Med. Biol. *713*, 5-11.

Frolov, V.A., Cho, M.S., Bronk, P., Reese, T.S., and Zimmerberg, J. (2000). Multiple local contact sites are induced by GPI-linked influenza hemagglutinin during hemifusion and flickering pore formation. Traffic. *1*, 622-630.

Frolov, V.A., and Zimmerberg, J. (2010). Cooperative elastic stresses, the hydrophobic effect, and lipid tilt in membrane remodeling. FEBS Lett. *584*, 1824-1829.

Frost, A., Unger, V.M., and De Camilli, P. (2009). The BAR domain superfamily: Membrane-molding macromolecules. Cell. *137*, 191-196.

Fu, C., Iyer, P., Herkal, A., Abdullah, J., Stout, A., and Free, S.J. (2011). Identification and characterization of genes required for cell-to-cell fusion in neurospora crassa. Eukaryot. Cell. *10*, 1100-1109.

Fuchs, R., and Ellinger, I. (2004). Endocytic and transcytotic processes in villous syncytiotrophoblast: Role in nutrient transport to the human fetus. Traffic. *5*, 725-738.

Fuhrmans, M., and Marrink, S.J. (2012). Molecular view of the role of fusion peptides in promoting positive membrane curvature. J. Am. Chem. Soc. *134*, 1543-1552.

Fyfe, I., Schuh, A.L., Edwardson, J.M., and Audhya, A. (2011). Association of the endosomal sorting complex ESCRT-II with the Vps20 subunit of ESCRT-III generates a curvature-sensitive complex capable of nucleating ESCRT-III filaments. J. Biol. Chem. *286*, 34262-34270.

Galletta, B.J., Chakravarti, M., Banerjee, R., and Abmayr, S.M. (2004). SNS: Adhesive properties, localization requirements and ectodomain dependence in S2 cells and embryonic myoblasts. Mech. Dev. *121*, 1455-1468.

Gallop, J.L., Jao, C.C., Kent, H.M., Butler, P.J., Evans, P.R., Langen, R., and McMahon, H.T. (2006). Mechanism of endophilin N-BAR domain-mediated membrane curvature. EMBO J. *25*, 2898-2910.

Gautier, R., Douguet, D., Antonny, B., and Drin, G. (2008). HELIQUEST: A web server to screen sequences with specific alpha-helical properties. Bioinformatics. *24*, 2101-2102.

Geminard, C., De Gassart, A., Blanc, L., and Vidal, M. (2004). Degradation of AP2 during reticulocyte maturation enhances binding of hsc70 and alix to a common site on TFR for sorting into exosomes. Traffic. *5*, 181-193.

Gerke, V., Creutz, C.E., and Moss, S.E. (2005). Annexins: Linking Ca2+ signalling to membrane dynamics. Nat. Rev. Mol. Cell Biol. *6*, 449-461.

Gerlach, H., Laumann, V., Martens, S., Becker, C.F., Goody, R.S., and Geyer, M. (2010). HIV-1 nef membrane association depends on charge, curvature, composition and sequence. Nat. Chem. Biol. *6*, 46-53.

Gibbons, D.L., Erk, I., Reilly, B., Navaza, J., Kielian, M., Rey, F.A., and Lepault, J. (2003). Visualization of the target-membrane-inserted fusion protein of semliki forest virus by combined electron microscopy and crystallography. Cell. *114*, 573-583.

Gills, J.J., Zhang, C., Abu-Asab, M.S., Castillo, S.S., Marceau, C., LoPiccolo, J., Kozikowski, A.P., Tsokos, M., Goldkorn, T., and Dennis, P.A. (2012). Ceramide mediates nanovesicle shedding and cell death in response to phosphatidylinositol ether lipid analogs and perifosine. Cell. Death Dis. *3*, e340.

Gluschankof, P., Mondor, I., Gelderblom, H.R., and Sattentau, Q.J. (1997). Cell membrane vesicles are a major contaminant of gradient-enriched human immunodeficiency virus type-1 preparations. Virology. *230*, 125-133.

Gomara, M.J., Mora, P., Mingarro, I., and Nieva, J.L. (2004). Roles of a conserved proline in the internal fusion peptide of ebola glycoprotein. FEBS Lett. *569*, 261-266.

Gong, R., Huang, L., Shi, J., Luo, K., Qiu, G., Feng, H., Tien, P., and Xiao, G. (2007). Syncytin-A mediates the formation of syncytiotrophoblast involved in mouse placental development. Cell. Physiol. Biochem. *20*, 517-526.

Gonzalez, M.E., and Carrasco, L. (2003). Viroporins. FEBS Lett. *552*, 28-34.

Gonzalez-Jamett, A.M., Momboisse, F., Guerra, M.J., Ory, S., Baez-Matus, X., Barraza, N., Calco, V., Houy, S., Couve, E., Neely, A.*, et al.* (2013). Dynamin-2 regulates fusion pore expansion and quantal release through a mechanism that involves actin dynamics in neuroendocrine chromaffin cells. PLoS One. *8*, e70638.

Gonzalez-Rubio, P., Gautier, R., Etchebest, C., and Fuchs, P.F. (2011). Amphipathic-lipid-packing-sensor interactions with lipids assessed by atomistic molecular dynamics. Biochim. Biophys. Acta. *1808*, 2119-2127.

Gould, S.J., Booth, A.M., and Hildreth, J.E. (2003). The trojan exosome hypothesis. Proc. Natl. Acad. Sci. U. S. A. *100*, 10592-10597.

Graham, T.R., and Kozlov, M.M. (2010). Interplay of proteins and lipids in generating membrane curvature. Curr. Opin. Cell Biol. *22*, 430-436.

Graner, M.W., Alzate, O., Dechkovskaia, A.M., Keene, J.D., Sampson, J.H., Mitchell, D.A., and Bigner, D.D. (2009). Proteomic and immunologic analyses of brain tumor exosomes. FASEB J. *23*, 1541-1557.

Guescini, M., Guidolin, D., Vallorani, L., Casadei, L., Gioacchini, A.M., Tibollo, P., Battistelli, M., Falcieri, E., Battistin, L., Agnati, L.F*., et al.* (2010). C2C12 myoblasts release micro-vesicles containing mtDNA and proteins involved in signal transduction. Exp. Cell Res. *316*, 1977-1984.

Hakeda-Suzuki, S., Ng, J., Tzu, J., Dietzl, G., Sun, Y., Harms, M., Nardine, T., Luo, L., and Dickson, B.J. (2002). Rac function and regulation during drosophila development. Nature. *416*, 438-442.

Han, X., Wang, C.T., Bai, J., Chapman, E.R., and Jackson, M.B. (2004). Transmembrane segments of syntaxin line the fusion pore of Ca2+-triggered exocytosis. Science. *304*, 289-292.

Hanson, P.I., Roth, R., Lin, Y., and Heuser, J.E. (2008). Plasma membrane deformation by circular arrays of ESCRT-III protein filaments. J. Cell Biol. *180*, 389-402.

Harder, T., Kellner, R., Parton, R.G., and Gruenberg, J. (1997). Specific release of membrane-bound annexin II and cortical cytoskeletal elements by sequestration of membrane cholesterol. Mol. Biol. Cell. *8*, 533-545.

Harman, A., Browne, H., and Minson, T. (2002). The transmembrane domain and cytoplasmic tail of herpes simplex virus type 1 glycoprotein H play a role in membrane fusion. J. Virol. *76*, 10708-10716.

Harrison, S. (2008). Mechanism of viral membrane fusion. Nat Struct Biol. *15*, 690-8.

Hatesauer, B., Bertram, S., Mehnert, M., Bahgat, M., Nelson, P., Pohlman, S., and Schughart, K. (2013). Tmprss2 is essential for influenza H1N1 virus pathogenesis in mice. PLoS Pathogens. *9*, e1003774.

Hatzakis, N.S., Bhatia, V.K., Larsen, J., Madsen, K.L., Bolinger, P.Y., Kunding, A.H., Castillo, J., Gether, U., Hedegard, P., and Stamou, D. (2009). How curved membranes recruit amphipathic helices and protein anchoring motifs. Nat. Chem. Biol. *5*, 835-841.

Heckman, K.L., and Pease, L.R. (2007). Gene splicing and mutagenesis by PCR-driven overlap extension. Nat. Protoc. *2*, 924-932.

Heidmann, O., Vernochet, C., Dupressoir, A., and Heidmann, T. (2009). Identification of an endogenous retroviral envelope gene with fusogenic activity and placenta-specific expression in the rabbit: A new "syncytin" in a third order of mammals. Retrovirology. *6*, 107-4690-6-107.

Heiman, M.G., and Walter, P. (2000). Prm1p, a pheromone-regulated multispanning membrane protein, facilitates plasma membrane fusion during yeast mating. J. Cell Biol. *151*, 719-730.

Helming, L., and Gordon, S. (2007). The molecular basis of macrophage fusion. Immunobiology. *212*, 785-793.

Helming, L., Winter, J., and Gordon, S. (2009). The scavenger receptor CD36 plays a role in cytokine-induced macrophage fusion. J. Cell. Sci. *122*, 453-459.

Hochreiter-Hufford, A., and Ravichandran, K.S. (2013). Clearing the dead: Apoptotic cell sensing, recognition, engulfment, and digestion. Cold Spring Harb Perspect. Biol. *5*, a008748.

Hristova, K., Wimley, W.C., Mishra, V.K., Anantharamiah, G.M., Segrest, J.P., and White, S.H. (1999). An amphipathic alpha-helix at a membrane interface: A structural study using a novel X-ray diffraction method. J. Mol. Biol. *290*, 99-117.

Hsu, C., Morohashi, Y., Yoshimura, S., Manrique-Hoyos, N., Jung, S., Lauterbach, M.A., Bakhti, M., Gronborg, M., Mobius, W., Rhee, J.*, et al.* (2010a). Regulation of exosome secretion by Rab35 and its GTPase-activating proteins TBC1D10A-C. J. Cell Biol. *189*, 223-232.

Hsu, K., Han, J., Shinlapawittayatorn, K., Deschenes, I., and Marban, E. (2010b). Membrane potential depolarization as a triggering mechanism for vpu-mediated HIV-1 release. Biophys. J. *99*, 1718-1725.

Hu, J., Shibata, Y., Voss, C., Shemesh, T., Li, Z., Coughlin, M., Kozlov, M.M., Rapoport, T.A., and Prinz, W.A. (2008). Membrane proteins of the endoplasmic reticulum induce high-curvature tubules. Science. *319*, 1247-1250.

Huang, D.T., Chi, N., Chen, S.C., Lee, T.Y., and Hsu, K. (2011). Background K(2P) channels KCNK3/9/15 limit the budding of cell membrane-derived vesicles. Cell Biochem. Biophys. *61*, 585-594.

Hughson, F.M. (1995). Structural characterization of viral fusion proteins. Curr. Biol. *5*, 265-274.

Hui, E., Johnson, C.P., Yao, J., Dunning, F.M., and Chapman, E.R. (2009). Synaptotagmin-mediated bending of the target membrane is a critical step in ca(2+)-regulated fusion. Cell. *138*, 709-721.

Hurley, J.H., Lee, S., and Prag, G. (2006). Ubiquitin-binding domains. Biochem. J. *399*, 361-372.

Hurley, J.H. (2008). ESCRT complexes and the biogenesis of multivesicular bodies. Curr. Opin. Cell Biol. *20*, 4-11.

Hyatt, A.D., Zhao, Y., and Roy, P. (1993). Release of bluetongue virus-like particles from insect cells is mediated by BTV nonstructural protein NS3/NS3A. Virology. *193*, 592-603.

Inal, J.M., and Jorfi, S. (2013). Coxsackievirus B transmission and possible new roles for extracellular vesicles. Biochem. Soc. Trans. *41*, 299-302.

Inoue, N., Ikawa, M., Isotani, A., and Okabe, M. (2005). The immunoglobulin superfamily protein izumo is required for sperm to fuse with eggs. Nature. *434*, 234-238.

Inoue, N., Hamada, D., Kamikubo, H., Hirata, K., Kataoka, M., Yamamoto, M., Ikawa, M., Okabe, M. and Hagihara, Y. (2013). Molecular dissection of IZUMO1, a sperm protein essential for sperm-egg fusion. Development. *140,* 3221-3229.

Jackson, M.B. (2010). SNARE complex zipping as a driving force in the dilation of proteinaceous fusion pores. J. Membr. Biol. *235*, 89-100.

Jackson, M.B., and Chapman, E.R. (2008). The fusion pores of Ca2+ -triggered exocytosis. Nat. Struct. Mol. Biol. *15*, 684-689.

Janmey, P.A., and Kinnunen, P.K. (2006). Biophysical properties of lipids and dynamic membranes. Trends Cell Biol. *16*, 538-546.

Jay, S.M., Skokos, E., Laiwalla, F., Krady, M.M., and Kyriakides, T.R. (2007). Foreign body giant cell formation is preceded by lamellipodia formation and can be attenuated by inhibition of Rac1 activation. Am. J. Pathol. *171*, 632-640.

Jegou, A., Ziyyat, A., Barraud-Lange, V., Perez, E., Wolf, J.P., Pincet, F., and Gourier, C. (2011). CD9 tetraspanin generates fusion competent sites on the egg membrane for mammalian fertilization. Proc. Natl. Acad. Sci. U. S. A. *108*, 10946-10951.

Jimenez, A.J., Maiuri, P., Lafaurie-Janvore, J., Divoux, S., Piel, M., and Perez, F. (2014). ESCRT machinery is required for plasma membrane repair. Science. *343*, 1247136.

Jin, H., Carlile, C., Nolan, S., and Grote, E. (2004). Prm1 prevents contact-dependent lysis of yeast mating pairs. Eukaryot. Cell. *3*, 1664-1673.

Jin, M., Fujiwara, E., Kakiuchi, Y., Okabe, M., Satouh, Y., Baba, S.A., Chiba, K., and Hirohashi, N. (2011). Most fertilizing mouse spermatozoa begin their acrosome reaction before contact with the zona pellucida during in vitro fertilization. Proc. Natl. Acad. Sci. U. S. A. *108*, 4892-4896.

Johnstone, R.M., Bianchini, A., and Teng, K. (1989). Reticulocyte maturation and exosome release: Transferrin receptor containing exosomes shows multiple plasma membrane functions. Blood. *74*, 1844-1851.

Jorgacevski, J., Fosnaric, M., Vardjan, N., Stenovec, M., Potokar, M., Kreft, M., Kralj-Iglic, V., Iglic, A., and Zorec, R. (2010). Fusion pore stability of peptidergic vesicles. Mol. Membr. Biol. *27*, 65-80.

Kaji, K., Oda, S., Shikano, T., Ohnuki, T., Uematsu, Y., Sakagami, J., Tada, N., Miyazaki, S., and Kudo, A. (2000). The gamete fusion process is defective in eggs of Cd9-deficient mice. Nat. Genet. *24*, 279-282.

Kamal, M.M., Mills, D., Grzybek, M., and Howard, J. (2009). Measurement of the membrane curvature preference of phospholipids reveals only weak coupling between lipid shape and leaflet curvature. Proc. Natl. Acad. Sci. U. S. A. *106*, 22245-22250.

Kammerer, U., Germeyer, A., Stengel, S., Kapp, M., and Denner, J. (2011). Human endogenous retrovirus K (HERV-K) is expressed in villous and extravillous cytotrophoblast cells of the human placenta. J. Reprod. Immunol. *91*, 1-8.

Kanaseki, T., Kawasaki, K., Murata, M., Ikeuchi, Y., and Ohnishi, S. (1997). Structural features of membrane fusion between influenza virus and liposome as revealed by quick-freezing electron microscopy. J. Cell Biol. *137*, 1041-1056.

Kanehisa, M., and Goto, S. (2000). KEGG: Kyoto encyclopedia of genes and genomes. Nucleic Acids Res. *28*, 27-30.

Kang, D., Oh, S., Ahn, S.M., Lee, B.H., and Moon, M.H. (2008). Proteomic analysis of exosomes from human neural stem cells by flow field-flow fractionation and nanoflow liquid chromatography-tandem mass spectrometry. J. Proteome Res. *7*, 3475-3480.

Kelley, L.A., and Sternberg, M.J. (2009). Protein structure prediction on the web: A case study using the phyre server. Nat. Protoc. *4*, 363-371.

Kemble, G.W., Danieli, T., and White, J.M. (1994). Lipid-anchored influenza hemagglutinin promotes hemifusion, not complete fusion. Cell. *76*, 383-391.

Key, T., and Duncan, R. (2014). A compact, multifunctional fusion module directs cholesterol-dependent homomultimerization and syncytiogenic efficiency of reovirus p10 FAST proteins. PLoS Pathog. *10*, e1004023.

Khan, U.A., Hashimi, S.M., Khan, S., Quan, J., Bakr, M.M., Forwood, M.R., and Morrison, N.M. (2014). Differential expression of chemokines, chemokine receptors and proteinases by foreign body giant cells (FBGCs) and osteoclasts. J. Cell. Biochem.

Kim, C.S., Epand, R.F., Leikina, E., Epand, R.M., and Chernomordik, L.V. (2011). The final conformation of the complete ectodomain of the HA2 subunit of influenza hemagglutinin can by itself drive low pH-dependent fusion. J. Biol. Chem. *286*, 13226-13234.

Knecht, V., and Grubmuller, H. (2003). Mechanical coupling via the membrane fusion SNARE protein syntaxin 1A: A molecular dynamics study. Biophys. J. *84*, 1527-1547.

Komada, M., Masaki, R., Yamamoto, A., and Kitamura, N. (1997). Hrs, a tyrosine kinase substrate with a conserved double zinc finger domain, is localized to the cytoplasmic surface of early endosomes. J. Biol. Chem. *272*, 20538-20544.

Kong, L., Giang, E., Nieusma, T., Kadam, R.U., Cogburn, K.E., Hua, Y., Dai, X., Stanfield, R.L., Burton, D.R., Ward, A.B., Wilson, I.A., and Law, M. (2013). Science. *342*, 1090-1094.

Kontani, K., Moskowitz, I.P., and Rothman, J.H. (2005). Repression of cell-cell fusion by components of the C. elegans vacuolar ATPase complex. Dev. Cell. *8*, 787-794.

Kooijman, E.E., Chupin, V., Fuller, N.L., Kozlov, M.M., de Kruijff, B., Burger, K.N., and Rand, P.R. (2005). Spontaneous curvature of phosphatidic acid and lysophosphatidic acid. Biochemistry. *44*, 2097-2102.

Kozerski, C., Ponimaskin, E., Schroth-Diez, B., Schmidt, M.F., and Herrmann, A. (2000). Modification of the cytoplasmic domain of influenza virus hemagglutinin affects enlargement of the fusion pore. J. Virol. *74*, 7529-7537.

Kozlov, M.M., and Chernomordik, L.V. (1998). A mechanism of protein-mediated fusion: Coupling between refolding of the influenza hemagglutinin and lipid rearrangements. Biophys. J. *75*, 1384-1396.

Kozlovsky, Y., Efrat, A., Siegel, D.P., and Kozlov, M.M. (2004). Stalk phase formation: Effects of dehydration and saddle splay modulus. Biophys. J. *87*, 2508-2521.

Kumar, S., Dick, E.J.,Jr, Reddy, B.Y., Yang, A., Mubiru, J., Hubbard, G.B., and Owston, M.A. (2013). Reovirus-associated meningoencephalomyelitis in baboons. Vet. Pathol.

Kuzmin, P.I., Zimmerberg, J., Chizmadzhev, Y.A., and Cohen, F.S. (2001). A quantitative model for membrane fusion based on low-energy intermediates. Proc. Natl. Acad. Sci. U. S. A. *98*, 7235-7240.

Kyriakides, T.R., Foster, M.J., Keeney, G.E., Tsai, A., Giachelli, C.M., Clark-Lewis, I., Rollins, B.J., and Bornstein, P. (2004). The CC chemokine ligand, CCL2/MCP1, participates in macrophage fusion and foreign body giant cell formation. Am. J. Pathol. *165*, 2157-2166.

Laemmli, U.K. (1970). Cleavage of structural proteins during the assembly of the head of bacteriophage T4. Nature. *227*, 680-685.

Lai, A. and Freed, J. (2014). HIV-1 gp41 fusion peptide increases membrane ordering in a cholesterol-dependent fashion. Biophys. J. *106,* 172-181.

Larsson, P., and Kasson, P.M. (2013). Lipid tail protrusion in simulations predicts fusogenic activity of influenza fusion peptide mutants and conformational models. PLoS Comput. Biol. *9*, e1002950.

Le Bihan, M.C., Bigot, A., Jensen, S.S., Dennis, J.L., Rogowska-Wrzesinska, A., Laine, J., Gache, V., Furling, D., Jensen, O.N., Voit, T.*, et al.* (2012). In-depth analysis of the secretome identifies three major independent secretory pathways in differentiating human myoblasts. J. Proteomics. 77, 344-356.

Lee, K.K. (2010). Architecture of a nascent viral fusion pore. EMBO J. *29*, 1299-1311.

Lee, M.T., Sun, T.L., Hung, W.C., and Huang, H.W. (2013). Process of inducing pores in membranes by melittin. Proc. Natl. Acad. Sci. U. S. A. *110*, 14243-14248.

Leikina, E., Melikov, K., Sanyal, S., Verma, S.K., Eun, B., Gebert, C., Pfeifer, K., Lizunov, V.A., Kozlov, M.M., and Chernomordik, L.V. (2013). Extracellular annexins and dynamin are important for sequential steps in myoblast fusion. J. Cell Biol. *200*, 109-123.

Lemaire, I., Yang, H., Lauzon, W., and Gendron, N. (1996). M-CSF and GM-CSF promote alveolar macrophage differentiation into multinucleated giant cells with distinct phenotypes. J. Leukoc. Biol. *60*, 509-518.

Lescar, J., Roussel, A., Wien, M.W., Navaza, J., Fuller, S.D., Wengler, G., Wengler, G., and Rey, F.A. (2001). The fusion glycoprotein shell of semliki forest virus: An icosahedral assembly primed for fusogenic activation at endosomal pH. Cell. *105*, 137-148.

Levi, S., Rawet, M., Kliouchnikov, L., Parnis, A., and Cassel, D. (2008). Topology of amphipathic motifs mediating golgi localization in ArfGAP1 and its splice isoforms. J. Biol. Chem. *283*, 8564-8572.

Li, Y., Wang, J., Kanai, R., and Modis, Y. (2013). Crystal structure of glycoprotein E2 from bovine viral diarrhea virus. Proc. Nat. Acad. Sci. *110*, 6805-6810.

Li, Y., and Modis, Y. (2014). A novel membrane fusion protein family in flaviviridae? Trends Microbiol. *22*, 176-182.

Lieber, A.D., Yehudai-Resheff, S., Barnhart, E.L., Theriot, J.A., and Keren, K. (2013). Membrane tension in rapidly moving cells is determined by cytoskeletal forces. Curr. Biol. *23*, 1409-1417.

Lin, Y., Mahan, K., Lathrop, W.F., Myles, D.G., and Primakoff, P. (1994). A hyaluronidase activity of the sperm plasma membrane protein PH-20 enables sperm to penetrate the cumulus cell layer surrounding the egg. J. Cell Biol. *125*, 1157-1163.

Liu, Y., Tewari, R., Ning, J., Blagborough, A.M., Garbom, S., Pei, J., Grishin, N.V., Steele, R.E., Sinden, R.E., Snell, W.J.*, et al.* (2008). The conserved plant sterility gene HAP2 functions after attachment of fusogenic membranes in chlamydomonas and plasmodium gametes. Genes Dev. *22*, 1051-1068.

Long, G., Pan, X., Westenberg, M., and Vlak, J.M. (2006). Functional role of the cytoplasmic tail domain of the major envelope fusion protein of group II baculoviruses. J. Virol. *80*, 11226-11234.

Lorieau, J.L., Louis, J.M., and Bax, A. (2011). Helical hairpin structure of influenza hemagglutinin fusion peptide stabilized by charge-dipole interactions between the N-terminal amino group and the second helix. J. Am. Chem. Soc. *133*, 2824-2827.

Lu, Q., Hope, L.W., Brasch, M., Reinhard, C., and Cohen, S.N. (2003). TSG101 interaction with HRS mediates endosomal trafficking and receptor down-regulation. Proc. Natl. Acad. Sci. U. S. A. *100*, 7626-7631.

Luneberg, J., Martin, I., Nussler, F., Ruysschaert, J.M., and Herrmann, A. (1995). Structure and topology of the influenza virus fusion peptide in lipid bilayers. J. Biol. Chem. *270*, 27606-27614.

Madan, V., Garcia Mde, J., Sanz, M.A., and Carrasco, L. (2005). Viroporin activity of murine hepatitis virus E protein. FEBS Lett. *579*, 3607-3612.

Mageswaran, S.K., Dixon, M.G., Curtiss, M., Keener, J.P., and Babst, M. (2014). Binding to any ESCRT can mediate ubiquitin-independent cargo sorting. Traffic. *15*, 212-229.

Marchal, C., Vinatier, G., Sanial, M., Plessis, A., Pret, A.M., Limbourg-Bouchon, B., Theodore, L., and Netter, S. (2012). The HIV-1 vpu protein induces apoptosis in drosophila via activation of JNK signaling. PLoS One. *7*, e34310.

Markosyan, R.M., Cohen, F.S., and Melikyan, G.B. (2000). The lipid-anchored ectodomain of influenza virus hemagglutinin (GPI-HA) is capable of inducing nonenlarging fusion pores. Mol. Biol. Cell. *11*, 1143-1152.

Markosyan, R.M., Cohen, F.S., and Melikyan, G.B. (2003). HIV-1 envelope proteins complete their folding into six-helix bundles immediately after fusion pore formation. Mol. Biol. Cell. *14*, 926-938.

Marrink, S.J., and Mark, A.E. (2003). The mechanism of vesicle fusion as revealed by molecular dynamics simulations. J. Am. Chem. Soc. *125*, 11144-11145.

Martens, S., Kozlov, M.M., and McMahon, H.T. (2007). How synaptotagmin promotes membrane fusion. Science. *316*, 1205-1208.

Martens, S., and McMahon, H.T. (2008). Mechanisms of membrane fusion: Disparate players and common principles. Nat. Rev. Mol. Cell Biol. *9*, 543-556.

Martin-Serrano, J., and Neil, S.J. (2011). Host factors involved in retroviral budding and release. Nat. Rev. Microbiol. *9*, 519-531.

Matsuo, H., Chevallier, J., Mayran, N., Le Blanc, I., Ferguson, C., Faure, J., Blanc, N.S., Matile, S., Dubochet, J., Sadoul, R.*, et al.* (2004). Role of LBPA and alix in multivesicular liposome formation and endosome organization. Science. *303*, 531-534.

McDonald, B., and Martin-Serrano, J. (2009). No strings attached: The ESCRT machinery in viral budding and cytokinesis. J. Cell. Sci. *122*, 2167-2177.

McMahon, H.T., and Gallop, J.L. (2005). Membrane curvature and mechanisms of dynamic cell membrane remodelling. Nature. *438*, 590-596.

McMahon, H.T., Kozlov, M.M., and Martens, S. (2010). Membrane curvature in synaptic vesicle fusion and beyond. Cell. *140*, 601-605.

McNally, A.K., and Anderson, J.M. (1995). Interleukin-4 induces foreign body giant cells from human monocytes/macrophages. differential lymphokine regulation of macrophage fusion leads to morphological variants of multinucleated giant cells. Am. J. Pathol. *147*, 1487-1499.

Melikyan, G.B., Brener, S.A., Ok, D.C., and Cohen, F.S. (1997). Inner but not outer membrane leaflets control the transition from glycosylphosphatidylinositol-anchored influenza hemagglutinin-induced hemifusion to full fusion. J. Cell Biol. *136*, 995-1005.

Melikyan, G.B., Markosyan, R.M., Brener, S.A., Rozenberg, Y., and Cohen, F.S. (2000). Role of the cytoplasmic tail of ecotropic moloney murine leukemia virus env protein in fusion pore formation. J. Virol. *74*, 447-455.

Merten, C.A., Stitz, J., Braun, G., Medvedovska, J., Cichutek, K., and Buchholz, C.J. (2006). Fusoselect: Cell-cell fusion activity engineered by directed evolution of a retroviral glycoprotein. Nucleic Acids Res. *34*, e41.

Mi, S., Lee, X., Li, X., Veldman, G.M., Finnerty, H., Racie, L., LaVallie, E., Tang, X.Y., Edouard, P., Howes, S.*, et al.* (2000). Syncytin is a captive retroviral envelope protein involved in human placental morphogenesis. Nature. *403*, 785-789.

Mincheva-Nilsson, L., and Baranov, V. (2010). The role of placental exosomes in reproduction. Am. J. Reprod. Immunol. *63*, 520-533.

Miyado, K., Yoshida, K., Yamagata, K., Sakakibara, K., Okabe, M., Wang, X., Miyamoto, K., Akutsu, H., Kondo, T., Takahashi, Y*., et al.* (2008). The fusing ability of sperm is bestowed by CD9-containing vesicles released from eggs in mice. Proc. Natl. Acad. Sci. U. S. A. *105*, 12921-12926.

Mohler, W.A., Shemer, G., del Campo, J.J., Valansi, C., Opoku-Serebuoh, E., Scranton, V., Assaf, N., White, J.G., and Podbilewicz, B. (2002). The type I membrane protein EFF-1 is essential for developmental cell fusion. Dev. Cell. *2*, 355-362.

Mohler, W.A., Simske, J.S., Williams-Masson, E.M., Hardin, J.D., and White, J.G. (1998). Dynamics and ultrastructure of developmental cell fusions in the caenorhabditis elegans hypodermis. Curr. Biol. *8*, 1087-1090.

Moll, M., Klenk, H.D., and Maisner, A. (2002). Importance of the cytoplasmic tails of the measles virus glycoproteins for fusogenic activity and the generation of recombinant measles viruses. J. Virol. *76*, 7174-7186.

Montecalvo, A., Larregina, A.T., Shufesky, W.J., Stolz, D.B., Sullivan, M.L., Karlsson, J.M., Baty, C.J., Gibson, G.A., Erdos, G., Wang, Z*., et al.* (2012). Mechanism of transfer of functional microRNAs between mouse dendritic cells via exosomes. Blood. *119*, 756-766.

Moreno, J.L., Mikhailenko, I., Tondravi, M.M., and Keegan, A.D. (2007). IL-4 promotes the formation of multinucleated giant cells from macrophage precursors by a STAT6-dependent, homotypic mechanism: Contribution of E-cadherin. J. Leukoc. Biol. *82*, 1542-1553.

Moss, T.J., Andreazza, C., Verma, A., Daga, A., and McNew, J.A. (2011). Membrane fusion by the GTPase atlastin requires a conserved C-terminal cytoplasmic tail and dimerization through the middle domain. Proc. Natl. Acad. Sci. U. S. A. *108*, 11133-11138.

Muralidharan-Chari, V., Clancy, J., Plou, C., Romao, M., Chavrier, P., Raposo, G., and D'Souza-Schorey, C. (2009). ARF6-regulated shedding of tumor cell-derived plasma membrane microvesicles. Curr. Biol. *19*, 1875-1885.

Muralidharan-Chari, V., Clancy, J.W., Sedgwick, A., and D'Souza-Schorey, C. (2010). Microvesicles: Mediators of extracellular communication during cancer progression. J. Cell. Sci. *123*, 1603-1611.

Nabhan, J.F., Hu, R., Oh, R.S., Cohen, S.N., and Lu, Q. (2012). Formation and release of arrestin domain-containing protein 1-mediated microvesicles (ARMMs) at plasma membrane by recruitment of TSG101 protein. Proc. Natl. Acad. Sci. U. S. A. *109*, 4146-4151.

Nagashima, S., Takahashi, M., Jirintai, S., Tanaka, T., Nishizawa, T., Yasuda, J., and Okamoto, H. (2011). Tumour susceptibility gene 101 and the vacuolar protein sorting pathway are required for the release of hepatitis E virions. J. Gen. Virol. *92*, 2838-2848.

Nanbo, A., Kawanishi, E., Yoshida, R., and Yoshiyama, H. (2013). Exosomes derived from epstein-barr virus-infected cells are internalized via caveola-dependent endocytosis and promote phenotypic modulation in target cells. J. Virol. *87*, 10334-10347.

Nguyen, C.Q., Hall, D.H., Yang, Y., and Fitch, D.H. (1999). Morphogenesis of the caenorhabditis elegans male tail tip. Dev. Biol. *207*, 86-106.

Nieva, J.L., Agirre, A., Nir, S., and Carrasco, L. (2003). Mechanisms of membrane permeabilization by picornavirus 2B viroporin. FEBS Lett. *552*, 68-73.

Nieva, J.L., Madan, V., and Carrasco, L. (2012). Viroporins: Structure and biological functions. Nat. Rev. Microbiol. *10*, 563-574.

Nishizawa, M., and Nishizawa, K. (2010). Molecular dynamics simulation analyses of viral fusion peptides in membranes prone to phase transition: Effects on membrane curvature, phase behavior and lipid-water interface destabilization. Journal of Biophysical Chemistry. *1*, 19-32.

Noyce, R.S., Taylor, K., Ciechonska, M., Collins, S.E., Duncan, R., and Mossman, K.L. (2011). Membrane perturbation elicits an IRF3-dependent, interferon-independent antiviral response. J. Virol. *85*, 10926-10931.

Oda, H., and Takeichi, M. (2011). Evolution: Structural and functional diversity of cadherin at the adherens junction. J. Cell Biol. *193*, 1137-1146.

Odell, D., Wanas, E., Yan, J., and Ghosh, H.P. (1997). Influence of membrane anchoring and cytoplasmic domains on the fusogenic activity of vesicular stomatitis virus glycoprotein G. J. Virol. *71*, 7996-8000.

Old, W.M., Meyer-Arendt, K., Aveline-Wolf, L., Pierce, K.G., Mendoza, A., Sevinsky, J.R., Resing, K.A., and Ahn, N.G. (2005). Comparison of label-free methods for quantifying human proteins by shotgun proteomics. Mol. Cell. Proteomics. *4*, 1487-1502.

Olmo, V.N., and Grote, E. (2010). Prm1 targeting to contact sites enhances fusion during mating in saccharomyces cerevisiae. Eukaryot. Cell. *9*, 1538-1548.

Olver, C., and Vidal, M. (2007). Proteomic analysis of secreted exosomes. Subcell. Biochem. *43*, 99-131.

Ostrowski, M., Carmo, N.B., Krumeich, S., Fanget, I., Raposo, G., Savina, A., Moita, C.F., Schauer, K., Hume, A.N., Freitas, R.P.*, et al.* (2010). Rab27a and Rab27b control different steps of the exosome secretion pathway. Nat. Cell Biol. *12*, 19-30; sup pp 1-13.

OuYang, B., and Chou, J.J. (2014). The minimalist architectures of viroporins and their therapeutic implications. Biochim. Biophys. Acta. *1838*, 1058-1067.

Pace, C.N., and Scholtz, J.M. (1998). A helix propensity scale based on experimental studies of peptides and proteins. Biophys. J. *75*, 422-427.

Pajcini, K.V., Pomerantz, J.H., Alkan, O., Doyonnas, R., and Blau, H.M. (2008). Myoblasts and macrophages share molecular components that contribute to cell-cell fusion. J. Cell Biol. *180*, 1005-1019.

Park, H.E., Gruenke, J.A., and White, J.M. (2003). Leash in the groove mechanism of membrane fusion. Nat. Struct. Biol. *10*, 1048-1053.

Park, S.H., and Opella, S.J. (2007). Conformational changes induced by a single amino acid substitution in the trans-membrane domain of vpu: Implications for HIV-1 susceptibility to channel blocking drugs. Protein Sci. *16*, 2205-2215.

Parmar, H.B., Barry, C., Kai, F., and Duncan, R. (2014). Golgi complex-plasma membrane trafficking directed by an autonomous, tribasic golgi export signal. Mol. Biol. Cell. *25*, 866-878.

Pawliczek, T., and Crump, C.M. (2009). Herpes simplex virus type 1 production requires a functional ESCRT-III complex but is independent of TSG101 and ALIX expression. J. Virol. *83*, 11254-11264.

Peck, J.W., Bowden, E.T., and Burbelo, P.D. (2004). Structure and function of human Vps20 and Snf7 proteins. Biochem. J. *377*, 693-700.

Pellegrino, M.W., Farooqui, S., Frohli, E., Rehrauer, H., Kaeser-Pebernard, S., Muller, F., Gasser, R.B., and Hajnal, A. (2011). LIN-39 and the EGFR/RAS/MAPK pathway regulate C. elegans vulval morphogenesis via the VAB-23 zinc finger protein. Development. *138*, 4649-4660.

Perez-Hernandez, D., Gutierrez-Vazquez, C., Jorge, I., Lopez-Martin, S., Ursa, A., Sanchez-Madrid, F., Vazquez, J., and Yanez-Mo, M. (2013). The intracellular interactome of tetraspanin-enriched microdomains reveals their function as sorting machineries toward exosomes. J. Biol. Chem. *288*, 11649-11661.

Perez-Vurgas, J., Krey, T., Valanci, C., Avinoam, O., Haouz, A., Jamin, M., Raveh-Barak, H., Podbilewicz, B., and Rey, F. (2014). Structural basis of eukaryotic cell-cell fusion. Cell. *157*, 407-419.

Pierce, G.B.,Jr, and Midgley, A.R.,Jr. (1963). The origin and function of human syncytiotrophoblastic giant cells. Am. J. Pathol. *43*, 153-173.

Plemper, R.K. (2011). Cell entry of enveloped viruses. Curr. Opin. Virol. *1*, 92-100.

Plomann, M., Wittmann, J.G., and Rudolph, M.G. (2010). A hinge in the distal end of the PACSIN 2 F-BAR domain may contribute to membrane-curvature sensing. J. Mol. Biol. *400*, 129-136.

Plonsky, I., Kingsley, D.H., Rashtian, A., Blank, P.S., and Zimmerberg, J. (2008). Initial size and dynamics of viral fusion pores are a function of the fusion protein mediating membrane fusion. Biol. Cell. *100*, 377-386.

Podbilewicz, B., Leikina, E., Sapir, A., Valansi, C., Suissa, M., Shemer, G., and Chernomordik, L.V. (2006). The C. elegans developmental fusogen EFF-1 mediates homotypic fusion in heterologous cells and in vivo. Dev. Cell. *11*, 471-481.

Pornillos, O., Alam, S.L., Davis, D.R., and Sundquist, W.I. (2002). Structure of the Tsg101 UEV domain in complex with the PTAP motif of the HIV-1 p6 protein. Nat. Struct. Biol. *9*, 812-817.

Pornillos, O., Higginson, D.S., Stray, K.M., Fisher, R.D., Garrus, J.E., Payne, M., He, G.P., Wang, H.E., Morham, S.G., and Sundquist, W.I. (2003). HIV gag mimics the Tsg101-recruiting activity of the human hrs protein. J. Cell Biol. *162*, 425-434.

Puissegur, M.P., Lay, G., Gilleron, M., Botella, L., Nigou, J., Marrakchi, H., Mari, B., Duteyrat, J.L., Guerardel, Y., Kremer, L.*, et al.* (2007). Mycobacterial lipomannan induces granuloma macrophage fusion via a TLR2-dependent, ADAM9- and beta1 integrin-mediated pathway. J. Immunol. *178*, 3161-3169.

Qiang, W., Sun, Y., and Weliky, D. (2009). A strong correlation between fusogenicity and membrane insertion depth of the HIV fusion peptide. Proc. Natl. Acad. Sci. *106*, 15314-15319.

Racine, T., Hurst, T., Barry, C., Shou, J., Kibenge, F.S., and Duncan, R. (2009). Aquareovirus effects syncytiogenesis using a novel member of the FAST protein family translated from a non-cononical translation start site. J Virol. *83*, in press.

Raghava, S., Giorda, K.M., Romano, F.B., Heuck, A.P., and Hebert, D.N. (2011). The SV40 late protein VP4 is a viroporin that forms pores to disrupt membranes for viral release. PLoS Pathog. *7*, e1002116.

Raiborg, C., Bache, K.G., Gillooly, D.J., Madshus, I.H., Stang, E., and Stenmark, H. (2002). Hrs sorts ubiquitinated proteins into clathrin-coated microdomains of early endosomes. Nat. Cell Biol. *4*, 394-398.

Raiborg, C., Bremnes, B., Mehlum, A., Gillooly, D.J., D'Arrigo, A., Stang, E., and Stenmark, H. (2001). FYVE and coiled-coil domains determine the specific localisation of hrs to early endosomes. J. Cell. Sci. *114*, 2255-2263.

Ramamurthi, K.S., Lecuyer, S., Stone, H.A., and Losick, R. (2009). Geometric cue for protein localization in a bacterium. Science. *323*, 1354-1357.

Rana, S., Yue, S., Stadel, D., and Zoller, M. (2012). Toward tailored exosomes: The exosomal tetraspanin web contributes to target cell selection. Int. J. Biochem. Cell Biol. *44*, 1574-1584.

Rana, S., and Zoller, M. (2011). Exosome target cell selection and the importance of exosomal tetraspanins: A hypothesis. Biochem. Soc. Trans. *39*, 559-562.

Raposo, G., and Stoorvogel, W. (2013). Extracellular vesicles: Exosomes, microvesicles, and friends. J. Cell Biol. *200*, 373-383.

Read, J.A., and Duncan, R. (2011). Biophysical and functional assays for viral membrane fusion peptides. Methods. *55*, 122-126.

Record, M. (2014). Intercellular communication by exosomes in placenta: A possible role in cell fusion? Placenta.

Redman, C.W., and Sargent, I.L. (2008). Circulating microparticles in normal pregnancy and pre-eclampsia. Placenta. *29 Suppl A*, S73-7.

Ren, G., Vajjhala, P., Lee, J.S., Winsor, B., and Munn, A.L. (2006). The BAR domain proteins: Molding membranes in fission, fusion, and phagy. Microbiol. Mol. Biol. Rev. *70*, 37-120.

Reuven, E.M., Dadon, Y., Viard, M., Manukovsky, N., Blumenthal, R., and Shai, Y. (2012). HIV-1 gp41 transmembrane domain interacts with the fusion peptide: Implication in lipid mixing and inhibition of virus-cell fusion. Biochemistry. *51*, 2867-2878.

Richard, J.P., Leikina, E., and Chernomordik, L.V. (2009). Cytoskeleton reorganization in influenza hemagglutinin-initiated syncytium formation. Biochim. Biophys. Acta. *1788*, 450-457.

Richard, J.P., Leikina, E., Langen, R., Henne, W.M., Popova, M., Balla, T., McMahon, H.T., Kozlov, M.M., and Chernomordik, L.V. (2011). Intracellular curvature-generating proteins in cell-to-cell fusion. Biochem. J. *440*, 185-193.

Richardson, B.E., Beckett, K., Nowak, S.J., and Baylies, M.K. (2007). SCAR/WAVE and Arp2/3 are crucial for cytoskeletal remodeling at the site of myoblast fusion. Development. *134*, 4357-4367.

Roberts, K.L., Leser, G.P., Ma, C., and Lamb, R.A. (2013). The amphipathic helix of influenza A virus M2 protein is required for filamentous bud formation and scission of filamentous and spherical particles. J. Virol. *87*, 9973-9982.

Roche, S., Bressanelli, S., Rey, F.A., and Gaudin, Y. (2006). Crystal structure of the low-pH form of the vesicular stomatitis virus glycoprotein G. Science. *313*, 187-191.

Roche, S., Rey, F.A., Gaudin, Y., and Bressanelli, S. (2007). Structure of the prefusion form of the vesicular stomatitis virus glycoprotein G. Science. *315*, 843-848.

Romancino, D.P., Paterniti, G., Campos, Y., De Luca, A., Di Felice, V., d'Azzo, A., and Bongiovanni, A. (2013). Identification and characterization of the nano-sized vesicles released by muscle cells. FEBS Lett. *587*, 1379-1384.

Rossman, J.S., Jing, X., Leser, G.P., and Lamb, R.A. (2010). Influenza virus M2 protein mediates ESCRT-independent membrane scission. Cell. *142*, 902-913.

Rossman, J.S., and Lamb, R.A. (2011). Influenza virus assembly and budding. Virology. *411*, 229-236.

Ruch, T.R., and Machamer, C.E. (2012). The coronavirus E protein: Assembly and beyond. Viruses. *4*, 363-382.

Runge, K.E., Evans, J.E., He, Z.Y., Gupta, S., McDonald, K.L., Stahlberg, H., Primakoff, P., and Myles, D.G. (2007). Oocyte CD9 is enriched on the microvillar membrane and required for normal microvillar shape and distribution. Dev. Biol. *304*, 317-325.

Russell, M.R.G., Nickerson, D.P., and Odorizzi, G. (2006). Molecular mechanisms of late endosome morphology, identity and sorting. Curr. Opin. Cell Biol. *18*, 422-428.

Salsman, J., Top, D., Barry, C., and Duncan, R. (2008). A virus-encoded cell-cell fusion machine dependent on surrogate adhesins. PLoS Path. *4*, e1000016.

Salsman, J., Top, D., Boutilier, J., and Duncan, R. (2005). Extensive syncytium formation mediated by the reovirus FAST proteins triggers apoptosis-induced membrane instability. J. Virol. *79*, 8090-8100.

Sapir, A., Avinoam, O., Podibilewicz, B., and Chernomordik, L. (2008). Viral and developmental cell fusion mechanisms: Conservation and convergence. Dev Cell. *14*, 11-21.

Sapir, A., Choi, J., Leikina, E., Avinoam, O., Valansi, C., Chernomordik, L.V., Newman, A.P., and Podbilewicz, B. (2007). AFF-1, a FOS-1-regulated fusogen, mediates fusion of the anchor cell in C. elegans. Dev. Cell. *12*, 683-698.

Savina, A., Furlan, M., Vidal, M., and Colombo, M.I. (2003). Exosome release is regulated by a calcium-dependent mechanism in K562 cells. J. Biol. Chem. *278*, 20083-20090.

Schmidt, N.W., Mishra, A., Wang, J., DeGrado, W.F., and Wong, G.C. (2013). Influenza virus A M2 protein generates negative gaussian membrane curvature necessary for budding and scission. J. Am. Chem. Soc. *135*, 13710-13719.

Seiler, F., Malsam, J., Krause, J.M., and Sollner, T.H. (2009). A role of complexin-lipid interactions in membrane fusion. FEBS Lett. *583*, 2343-2348.

Sens, K.L., Zhang, S., Jin, P., Duan, R., Zhang, G., Luo, F., Parachini, L., and Chen, E.H. (2010). An invasive podosome-like structure promotes fusion pore formation during myoblast fusion. J. Cell Biol. *191*, 1013-1027.

Shemer, G., Suissa, M., Kolotuev, I., Nguyen, K.C., Hall, D.H., and Podbilewicz, B. (2004). EFF-1 is sufficient to initiate and execute tissue-specific cell fusion in C. elegans. Curr. Biol. *14*, 1587-1591.

Shen, B., Wu, N., Yang, J.M., and Gould, S.J. (2011). Protein targeting to exosomes/microvesicles by plasma membrane anchors. J. Biol. Chem. *286*, 14383-14395.

Shields, S.B., Oestreich, A.J., Winistorfer, S., Nguyen, D., Payne, J.A., Katzmann, D.J., and Piper, R. (2009). ESCRT ubiquitin-binding domains function cooperatively during MVB cargo sorting. J. Cell Biol. *185*, 213-224.

Shilagardi, K., Li, S., Luo, F., Marikar, F., Duan, R., Jin, P., Kim, J.H., Murnen, K., and Chen, E.H. (2013). Actin-propelled invasive membrane protrusions promote fusogenic protein engagement during cell-cell fusion. Science. *340*, 359-363.

Shmulevitz, M., Salsman, J., and Duncan, R. (2003). Palmitoylation, membrane-proximal basic residues, and transmembrane glycine residues in the reovirus p10 protein are essential for syncytium formation. J. Virol. *77*, 9769-9779.

Shmulevitz, M., and Duncan, R. (2000). A new class of fusion-associated small transmembrane (FAST) proteins encoded by the non-enveloped fusogenic reoviruses. EMBO J. *19*, 902-912.

Silvestri, L.S., Ruthel, G., Kallstrom, G., Warfield, K.L., Swenson, D.L., Nelle, T., Iversen, P.L., Bavari, S., and Aman, M.J. (2007). Involvement of vacuolar protein sorting pathway in ebola virus release independent of TSG101 interaction. J. Infect. Dis. *196 Suppl 2*, S264-70.

Simpson, R.J., Kalra, H., and Mathivanan, S. (2012). ExoCarta as a resource for exosomal research. J. Extracell Vesicles. *1*, 10.3402/jev.v1i0.18374. eCollection 2012.

Skehel, J.J., Bayley, P.M., Brown, E.B., Martin, S.R., Waterfield, M.D., White, J.M., Wilson, I.A., and Wiley, D.C. (1982). Changes in the conformation of influenza virus hemagglutinin at the pH optimum of virus-mediated membrane fusion. Proc. Natl. Acad. Sci. U. S. A. *79*, 968-972.

Skehel, J.J., and Wiley, D.C. (2000). Receptor binding and membrane fusion in virus entry: The influenza hemagglutinin. Annu. Rev. Biochem. *69*, 531-569.

Slagsvold, T., Aasland, R., Hirano, S., Bache, K.G., Raiborg, C., Trambaiolo, D., Wakatsuki, S., and Stenmark, H. (2005). Eap45 in mammalian ESCRT-II binds ubiquitin via a phosphoinositide-interacting GLUE domain. J. Biol. Chem. *280*, 19600-19606.

Smith, E.C., Popa, A., Chang, A., Masante, C., and Dutch, R.E. (2009). Viral entry mechanisms: The increasing diversity of paramyxovirus entry. FEBS J. *276*, 7217-7227.

Southcombe, J., Tannetta, D., Redman, C., and Sargent, I. (2011). The immunomodulatory role of syncytiotrophoblast microvesicles. PLoS One. *6*, e20245.

Stachowiak, J.C., Brodsky, F.M., and Miller, E.A. (2013). A cost-benefit analysis of the physical mechanisms of membrane curvature. Nat. Cell Biol. *15*, 1019-1027.

Stein, K.K., Primakoff, P., and Myles, D. (2004). Sperm-egg fusion: Events at the plasma membrane. J. Cell. Sci. *117*, 6269-6274.

Stenqvist, A.C., Nagaeva, O., Baranov, V., and Mincheva-Nilsson, L. (2013). Exosomes secreted by human placenta carry functional fas ligand and TRAIL molecules and convey

apoptosis in activated immune cells, suggesting exosome-mediated immune privilege of the fetus. J. Immunol. *191*, 5515-5523.

Stieneke-Grober, A., Vey, M., Angliker, H., Shaw, E., Thomas, G., Roberts, C., Klenk, H.D., and Garten, W. (1992). Influenza virus hemagglutinin with multibasic cleavage site is activated by furin, a subtilisin-like endoprotease. EMBO J. *11*, 2407-2414.

Stoltz, D., and Makkay, A. (2000). Co-replication of a reovirus and a polydnavirus in the ichneumonid parasitoid hyposoter exiguae. Virology. *278*, 266-275.

Suzuki, H., Konno, T., and Numazaki, Y. (1993). Electron microscopic evidence for budding process-independent assembly of double-shelled rotavirus particles during passage through endoplasmic reticulum membranes. J. Gen. Virol. *74 (Pt 9)*, 2015-2018.

Tamm, L.K. (2003). Hypothesis: Spring-loaded boomerang mechanism of influenza hemagglutinin-mediated membrane fusion. Biochim. Biophys. Acta. *1614*, 14-23.

Tamm, L.K., and Han, X. (2000). Viral fusion peptides: A tool set to disrupt and connect biological membranes. Biosci. Rep. *20*, 501-518.

Taylor, D.R., and Hooper, N.M. (2007). Role of lipid rafts in the processing of the pathogenic prion and alzheimer's amyloid-beta proteins. Semin. Cell Dev. Biol. *18*, 638-648.

Teis, D., Saksena, S., and Emr, S.D. (2008). Ordered assembly of the ESCRT-III complex on endosomes is required to sequester cargo during MVB formation. Dev. Cell. *15*, 578-589.

Tenchov, B.G., MacDonald, R.C., and Lentz, B.R. (2013). Fusion peptides promote formation of bilayer cubic phases in lipid dispersions. an x-ray diffraction study. Biophys. J. *104*, 1029-1037.

Teo, H., Gill, D.J., Sun, J., Perisic, O., Veprintsev, D.B., Vallis, Y., Emr, S.D., and Williams, R.L. (2006). ESCRT-I core and ESCRT-II GLUE domain structures reveal role for GLUE in linking to ESCRT-I and membranes. Cell. *125*, 99-111.

Teo, H., Veprintsev, D.B., and Williams, R.L. (2004). Structural insights into endosomal sorting complex required for transport (ESCRT-I) recognition of ubiquitinated proteins. J. Biol. Chem. *279*, 28689-28696.

Thalmann, C.M., Cummins, D.M., Yu, M., Lunt, R., Pritchard, L.I., Hansson, E., Crameri, S., Hyatt, A., and Wang, L.F. (2010). Broome virus, a new fusogenic orthoreovirus species isolated from an australian fruit bat. Virology. *402*, 26-40.

Thery, C., Ostrowski, M., and Segura, E. (2009). Membrane vesicles as conveyors of immune responses. Nat. Rev. Immunol. *9*, 581-593.

Tian, T., Wang, Y., Wang, H., Zhu, Z., and Xiao, Z. (2010). Visualizing of the cellular uptake and intracellular trafficking of exosomes by live-cell microscopy. J. Cell. Biochem. *111*, 488-496.

Tinevez, J.Y., Schulze, U., Salbreux, G., Roensch, J., Joanny, J.F., and Paluch, E. (2009). Role of cortical tension in bleb growth. Proc. Natl. Acad. Sci. U. S. A. *106*, 18581-18586.

Tolosa, J.M., Schjenken, J.E., Clifton, V.L., Vargas, A., Barbeau, B., Lowry, P., Maiti, K., and Smith, R. (2012). The endogenous retroviral envelope protein syncytin-1 inhibits LPS/PHA-stimulated cytokine responses in human blood and is sorted into placental exosomes. Placenta. *33*, 933-941.

Top, D., Barry, C., Racine, T., Ellis, C.L., and Duncan, R. (2009). Enhanced fusion pore expansion mediated by the *trans*-acting endodomain of the reovirus FAST proteins. PLoS Path. *5*, e10000331.

Top, D., de Antueno, R., Salsman, J., Corcoran, J., Mader, J., Hoskin, D., Touhami, A., Jericho, M.H., and Duncan, R. (2005). Liposome reconstitution of a minimal protein-mediated membrane fusion machine. EMBO J. *24*, 2980-2988.

Top, D., Read, J.A., Dawe, S.J., Syvitski, R.T., and Duncan, R. (2012). Cell-cell membrane fusion induced by p15 fusion-associated small transmembrane (FAST) protein requires a novel fusion peptide motif containing a myristoylated polyproline type II helix. J. Biol. Chem. *287*, 3403-3414.

Trajkovic, K., Hsu, C., Chiantia, S., Rajendran, L., Wenzel, D., Wieland, F., Schwille, P., Brugger, B., and Simons, M. (2008). Ceramide triggers budding of exosome vesicles into multivesicular endosomes. Science. *319*, 1244-1247.

Trouillon, R., and Ewing, A.G. (2013). Amperometric measurements at cells support a role for dynamin in the dilation of the fusion pore during exocytosis. Chemphyschem. *14*, 2295-2301.

Usaite, R., Wohlschlegel, J., Venable, J.D., Park, S.K., Nielsen, J., Olsson, L., and Yates Iii, J.R. (2008). Characterization of global yeast quantitative proteome data generated from the wild-type and glucose repression saccharomyces cerevisiae strains: The comparison of two quantitative methods. J. Proteome Res. *7*, 266-275.

Valadi, H., Ekstrom, K., Bossios, A., Sjostrand, M., Lee, J.J., and Lotvall, J.O. (2007). Exosome-mediated transfer of mRNAs and microRNAs is a novel mechanism of genetic exchange between cells. Nat. Cell Biol. *9*, 654-659.

Vamparys, L., Gautier, R., Vanni, S., Bennett, W.F., Tieleman, D.P., Antonny, B., Etchebest, C., and Fuchs, P.F. (2013). Conical lipids in flat bilayers induce packing defects similar to that induced by positive curvature. Biophys. J. *104*, 585-593.

van Niel, G., Charrin, S., Simoes, S., Romao, M., Rochin, L., Saftig, P., Marks, M.S., Rubinstein, E., and Raposo, G. (2011). The tetraspanin CD63 regulates ESCRT-independent and -dependent endosomal sorting during melanogenesis. Dev. Cell. *21*, 708-721.

Vanlandingham, P.A., and Ceresa, B.P. (2009). Rab7 regulates late endocytic trafficking downstream of multivesicular body biogenesis and cargo sequestration. J. Biol. Chem. *284*, 12110-12124.

Vanni, S., Vamparys, L., Gautier, R., Drin, G., Etchebest, C., Fuchs, P.F., and Antonny, B. (2013). Amphipathic lipid packing sensor motifs: Probing bilayer defects with hydrophobic residues. Biophys. J. *104*, 575-584.

Vidal, M., Mangeat, P., and Hoekstra, D. (1997). Aggregation reroutes molecules from a recycling to a vesicle-mediated secretion pathway during reticulocyte maturation. J. Cell. Sci. *110 (Pt 16)*, 1867-1877.

Vieyres, G., Brohm, C., Friesland, M., Gentzsch, J., Wolk, B., Roingeard, P., Steinmann, E., and Pietschmann, T. (2013). Subcellular localization and function of an epitope-tagged p7 viroporin in hepatitis C virus-producing cells. J. Virol. *87*, 1664-1678.

Vignery, A. (2000). Osteoclasts and giant cells: Macrophage-macrophage fusion mechanism. Int. J. Exp. Pathol. *81*, 291-304.

Vignery, A. (2005). Macrophage fusion: The making of osteoclasts and giant cells. J. Exp. Med. *202*, 337-340.

Vlassov, A.V., Magdaleno, S., Setterquist, R., and Conrad, R. (2012). Exosomes: Current knowledge of their composition, biological functions, and diagnostic and therapeutic potentials. Biochim. Biophys. Acta. *1820*, 940-948.

Wang, C., Takeuchi, K., Pinto, L.H., and Lamb, R.A. (1993). Ion channel activity of influenza A virus M2 protein: Characterization of the amantadine block. J. Virol. *67*, 5585-5594.

Wang, S., Thibault, G., and Ng, D.T. (2011). Routing misfolded proteins through the multivesicular body (MVB) pathway protects against proteotoxicity. J. Biol. Chem. *286*, 29376-29387.

Wengler, G., Wengler, G., and Rey, F.A. (1999). The isolation of the ectodomain of the alphavirus E1 protein as a soluble hemagglutinin and its crystallization. Virology. *257*, 472-482.

White JM, Delos SE, Brecher M, and Schornberg K. (2008). Structures and mechanisms of viral membrane fusion proteins: Multiple variations on a common theme. Crit Rev Biochem Mol Biol. *43*, 183-219.

Wilson, I.A., Skehel, J.J., and Wiley, D.C. (1981). Structure of the haemagglutinin membrane glycoprotein of influenza virus at 3 A resolution. Nature. *289*, 366-373.

Wirblich, C., Bhattacharya, B., and Roy, P. (2006). Nonstructural protein 3 of bluetongue virus assists virus release by recruiting ESCRT-I protein Tsg101. J. Virol. *80*, 460-473.

Witwer, K.W., Buzas, E.I., Bemis, L.T., Bora, A., Lasser, C., Lotvall, J., Nolte-'t Hoen, E.N., Piper, M.G., Sivaraman, S., Skog, J.*, et al.* (2013). Standardization of sample collection, isolation and analysis methods in extracellular vesicle research. J. Extracell Vesicles. *2*, 10.3402/jev.v2i0.20360. eCollection 2013.

Wollert, T., and Hurley, J.H. (2010). Molecular mechanism of multivesicular body biogenesis by ESCRT complexes. Nature. *464*, 864-869.

Wong, J.L., and Johnson, M.A. (2010). Is HAP2-GCS1 an ancestral gamete fusogen? Trends Cell Biol. *20*, 134-141.

Wong, J.L., Leydon, A.R., and Johnson, M.A. (2010). HAP2(GCS1)-dependent gamete fusion requires a positively charged carboxy-terminal domain. PLoS Genet. *6*, e1000882.

Wurdinger, T., Gatson, N.N., Balaj, L., Kaur, B., Breakefield, X.O., and Pegtel, D.M. (2012). Extracellular vesicles and their convergence with viral pathways. Adv. Virol. *2012*, 767694.

Xing, L., Xiu, Y., and Boyce, B.F. (2012). Osteoclast fusion and regulation by RANKL-dependent and independent factors. World J. Orthop. *3*, 212-222.

Xu, Y., Zhang, F., Su, Z., McNew, J.A., and Shin, Y.-K. (2005). Hemifusion in SNARE-mediated membrane fusion. Nat. Struct. Mol. Biol. *12*, 417-422.

Xu, H., Zick, M., Wickner, W.T., and Jun, Y. (2011). A lipid-anchored SNARE supports membrane fusion. Proc. Natl. Acad. Sci. U. S. A. *108*, 17325-17330.

Xu, Y., Zhang, F., Su, Z., McNew, J.A., and Shin, Y.K. (2005). Hemifusion in SNARE-mediated membrane fusion. Nat. Struct. Mol. Biol. *12*, 417-422.

Yagi, M., Miyamoto, T., Sawatani, Y., Iwamoto, K., Hosogane, N., Fujita, N., Morita, K., Ninomiya, K., Suzuki, T., Miyamoto, K.*, et al.* (2005). DC-STAMP is essential for cell-cell fusion in osteoclasts and foreign body giant cells. J. Exp. Med. *202*, 345-351.

Yang, P., Ai, L.S., Huang, S.C., Li, H.F., Chan, W.E., Chang, C.W., Ko, C.Y., and Chen, S.S. (2010). The cytoplasmic domain of human immunodeficiency virus type 1 transmembrane protein gp41 harbors lipid raft association determinants. J. Virol. *84*, 59-75.

Yao, H., and Hong, M. (2013). Membrane-dependent conformation, dynamics, and lipid interactions of the fusion peptide of the paramyxovirus PIV5 from solid-state NMR. J. Mol. Biol. *425*, 563-576.

Yao, H., and Hong, M. (2014). Conformation and lipid interaction of the fusion peptide of the paramyxovirus PIV5 in anionic and negative-curvature membranes from solid-state NMR. J. Am. Chem. Soc. *136*, 2611-2624.

Yao, Q., and Compans, R.W. (1995). Differences in the role of the cytoplasmic domain of human parainfluenza virus fusion proteins. J Virol. *69*, 7045-53.

Zhang, Z., and Jackson, M.B. (2010). Membrane bending energy and fusion pore kinetics in Ca(2+)-triggered exocytosis. Biophys. J. *98*, 2524-2534.

Zhao, Q., Topham, N., Anderson, J.M., Hiltner, A., Lodoen, G., and Payet, C.R. (1991). Foreign-body giant cells and polyurethane biostability: In vivo correlation of cell adhesion and surface cracking. J. Biomed. Mater. Res. *25*, 177-183.

Zhou, P., Bacaj, T., Yang, X., Pang, Z.P., and Sudhof, T.C. (2013). Lipid-anchored SNAREs lacking transmembrane regions fully support membrane fusion during neurotransmitter release. Neuron. *80*, 470-483.

Appendix A

Table A1. Proteins indentified in both biological replicates of control exosomes.

Uniprot ID	Description	Gene Name	% Coverage	#Unique Peptides	PSM Score
P05387	60S acidic ribosomal protein P2	RPLP2	84.35	4	11
Q9UBI6	Guanine nucleotide-binding protein G(I)/G(S)/G(	GNG12	79.17	6	10
P80723	Brain acid soluble protein 1	BASP1	75.77	10	28
P07437	Tubulin beta chain	TUBB	73.42	5	64
P07355	Annexin A2	ANXA2	71.68	27	94
P35908	Keratin, type II cytoskeletal 2 epidermal	KRT2	71.52	26	70
P60709	Actin, cytoplasmic 1	ACTB	70.13	10	97
P04406	Glyceraldehyde-3-phosphate dehydrogenase	GAPDH	68.66	14	32
P08758	Annexin A5	ANXA5	68.44	18	39
P04899	Guanine nucleotide-binding protein G(i) subunit alpha-2	GNAI2	67.89	9	44
P31949	Protein S100-A11	S100A11	67.62	5	11
P68371	Tubulin beta-4B chain	TUBB4B	64.49	1	56
P04083	Annexin A1	ANXA1	63.58	19	36
P08754	Guanine nucleotide-binding protein G(k) subunit alpha	GNAI3	63.28	10	36
P61224	Ras-related protein Rap-1b	RAP1B	63.04	3	20
P13645	Keratin, type I cytoskeletal 10	KRT10	63.01	29	83
P35527	Keratin, type I cytoskeletal 9	KRT9	62.76	27	67
P26038	Moesin	MSN	61.87	28	70
P62937	Peptidyl-prolyl cis-trans isomerase A	PPIA	59.39	10	16
P62873	Guanine nucleotide-binding protein G(I)/G(S)/G(T) subunit beta-1	GNB1	57.94	6	27
G3V1A4	Cofilin 1 (Non-muscle), isoform CRA_a	CFL1	57.72	6	10
P14618	Pyruvate kinase PKM	PKM	57.06	25	41
P04264	Keratin, type II cytoskeletal 1	KRT1	56.21	31	84
P02751-17	Isoform 17 of Fibronectin	FN1	55.84	89	251
P15144	Aminopeptidase N	ANPEP	55.22	53	155
P63104	14-3-3 protein zeta/delta	YWHAZ	54.29	9	28
O00299	Chloride intracellular channel protein 1	CLIC1	53.11	10	19
F8WF65	Elongation factor 1-beta	EEF1B2	51.72	1	1
P62805	Histone H4	HIST1H4A	51.46	6	10
P61204	ADP-ribosylation factor 3	ARF3	51.38	5	16
A8MUB1	Tubulin alpha-4A chain	TUBA4A	50.81	5	43
P07996	Thrombospondin-1	THBS1	50.60	51	174
P15153	Ras-related C3 botulinum toxin substrate 2	RAC2	49.48	5	14
P63000	Ras-related C3 botulinum toxin substrate 1	RAC1	49.48	4	15
P61981	14-3-3 protein gamma	YWHAG	48.18	6	18
P11142	Heat shock cognate 71 kDa protein	HSPA8	47.83	26	59
P31946-2	Isoform Short of 14-3-3 protein beta/alpha	YWHAB	47.13	5	23
P62258	14-3-3 protein epsilon	YWHAE	46.27	10	23
Q08629	Testican-1	SP	46.01	15	37
P60953	Cell division control protein 42 homolog	CDC42	45.55	4	10
P08133	Annexin A6	ANXA6	45.17	22	42
P07737	Profilin-1	PFN1	45.00	6	10
O00468-6	Isoform 6 of Agrin	AGRN	44.74	63	133
P05556	Integrin beta-1	ITGB1	44.36	29	144
P62424	60S ribosomal protein L7a	RPL7A	43.98	10	17
P51149	Ras-related protein Rab-7a	RAB7A	43.96	8	12
P09382	Galectin-1	LGALS1	43.70	5	11
P27348	14-3-3 protein theta	YWHAQ	43.67	7	20
P06733	Alpha-enolase	EN	43.55	14	34
P10599	Thioredoxin	TXN	42.86	4	6
O00622	Protein CYR61	CYR61	42.26	13	26

P05023-3	Isoform 3 of Sodium/potassium-transporting ATPase subunit alpha-1	ATP1A1	41.94	36	75
P78539-5	Isoform 5 of Sushi repeat-containing protein SRPX	SRPX	41.67	13	25
P06748	Nucleophosmin	NPM1	41.50	12	30
Q5JR95	40S ribosomal protein S8	RPS8	41.49	7	9
P17301	Integrin alpha-2	ITGA2	41.15	7	96
P35613-2	Isoform 2 of Basigin	BSG	40.89	7	17
Q9H223	EH domain-containing protein 4	EHD4	40.11	14	27
F5H157	Ras-related protein Rab-35 (Fragment)	RAB35	40.00	6	15
P30050	60S ribosomal protein L12	RPL12	40.00	4	6
P60174-1	Isoform 2 of Triosephosphate isomerase	TPI1	39.76	6	10
P08195-2	Isoform 2 of 4F2 cell-surface antigen heavy chain	SLC3A2	38.19	16	40
P68104	Elongation factor 1-alpha 1	EEF1A1	37.66	15	33
Q08380	Galectin-3-binding protein	LGALS3BP	36.92	17	36
P29317	Ephrin type-A receptor 2	EPHA2	36.78	25	52
P10124	Serglycin	SRGN	36.71	7	17
P13639	Elongation factor 2	EEF2	36.71	22	32
Q9H4M9	EH domain-containing protein 1	EHD1	36.14	12	18
Q96KK5	Histone H2A type 1-H	HIST1H2AH	35.94	4	9
Q9P2B2	Prostaglandin F2 receptor negative regulator	PTGFRN	35.72	27	43
P12111	Collagen alpha-3(VI) chain	COL6A3	35.69	82	141
P05388	60S acidic ribosomal protein P0	RPLP0	35.65	8	10
P81605	Dermcidin	DCD	35.45	4	8
P69905	Hemoglobin subunit alpha	HBA1	34.51	4	12
A2ARK8	HLA class I histocompatibility antigen, A-68 alpha chain	HLA-A	33.44	4	12
C9J9K3	40S ribosomal protein SA (Fragment)	RPSA	33.33	5	7
P11233	Ras-related protein Ral-A	RALA	33.01	5	9
E9PSH3	Tetraspanin-4 (Fragment)	TSPAN4	33.00	3	5
P32970	CD70 antigen	CD70	32.64	5	11
P08238	Heat shock protein HSP 90-beta	HSP90AB1	32.04	14	43
P49006	MARCKS-related protein	MARCKSL1	31.79	3	7
Q5T7C4	High mobility group protein B1	HMGB1	31.65	4	5
P62906	60S ribosomal protein L10a	RPL10A	31.34	5	8
O43854-2	Isoform 2 of EGF-like repeat and discoidin I-like domain-containing protein 3	EDIL3	31.28	11	19
P50395	Rab GDP dissociation inhibitor beta	GDI2	31.01	11	18
O60814	Histone H2B type 1-K	HIST1H2BK	30.95	5	6
E9PNW4	CD59 glycoprotein	CD59	30.56	5	15
P39023	60S ribosomal protein L3	RPL3	30.52	10	14
P02533	Keratin, type I cytoskeletal 14	KRT14	30.51	9	20
O00560-2	Isoform 2 of Syntenin-1	SDCBP	30.30	5	13
P18084	Integrin beta-5	ITGB5	30.04	14	24
B4DP21	Prostaglandin E synthase 3	PTGES3	30.00	4	5
B4E2J3	Serine protease 23	PRSS23	29.63	7	10
P63092-3	Isoform 3 of Guanine nucleotide-binding protein G(s) subunit alpha isoforms short	GNAS	29.55	6	15
Q9Y696	Chloride intracellular channel protein 4	CLIC4	29.25	5	10
P23229-4	Isoform Alpha-6X2A of Integrin alpha-6	ITGA6	29.21	23	36
P49207	60S ribosomal protein L34	RPL34	29.06	5	8
Q15758	Neutral amino acid transporter B(0)	SLC1A5	28.47	11	24
P26006	Integrin alpha-3	ITGA3	27.40	28	83
P19338	Nucleolin	NCL	27.18	16	29
C9J0K6	Sorcin	SRI	27.10	3	3
P61106	Ras-related protein Rab-14	RAB14	26.05	2	3
P61026	Ras-related protein Rab-10	RAB10	26.00	2	10
P43121	Cell surface glycoprotein MUC18	MCAM	24.92	11	15
B4E241	Serine/arginine-rich-splicing factor 3	SFRS3	24.19	2	3
P02786	Transferrin receptor protein 1	TFRC	24.08	14	22
A8MUD9	60S ribosomal protein L7	RPL7	24.04	4	9

O75131	Copine-3	CPNE3	24.02	8	15
P08582	Melanotransferrin	MFI2	23.98	11	15
F8VRJ2	Nucleosome assembly protein 1-like 1 (Fragment)	NAP1L1	23.68	2	2
Q06830	Peroxiredoxin-1	PRDX1	23.62	5	9
E9PEP6	Protein kinase C-binding protein NELL1	NRP1	23.18	13	25
P37802	Transgelin-2	TAGLN2	22.61	3	5
M0R3D6	60S ribosomal protein L18a (Fragment)	RPL18A	21.99	3	4
C9JD32	60S ribosomal protein L23 (Fragment)	RPL23	21.98	1	2
P12109	Collagen alpha-1(VI) chain	COL6A1	21.79	15	33
P08648	Integrin alpha-5	ITGA5	21.07	18	25
P06756-3	Isoform 3 of Integrin alpha-V	ITGAV	21.06	16	26
H0YEN5	40S ribosomal protein S2 (Fragment)	RPS2	21.03	4	5
Q9Y2J2-2	Isoform B of Band 4.1-like protein 3	EPB41L3	20.81	13	22
P08473	Neprilysin	MME	20.80	12	18
P12110	Collagen alpha-2(VI) chain	COL6A2	20.61	15	28
J3QSB5	60S ribosomal protein L36	RPL36	20.21	2	3
P00338	L-lactate dehydrogenase A chain	LDHA	19.58	4	8
P22413	Ectonucleotide pyrophosphatase/phosphodiesterase family member 1	ENPP1	19.57	9	12
E7EPB3	60S ribosomal protein L14	RPL14	19.35	2	3
P25398	40S ribosomal protein S12	RPS12	18.94	2	3
Q00839-2	Isoform Short of Heterogeneous nuclear ribonucleoprotein U	HNRNPU	18.61	9	10
J3QSU6	Tenascin	TNC	18.52	26	37
P18465	HLA class I histocompatibility antigen, B-57 alpha chain	HLA-B	18.51	2	5
Q9NQC3-2	Isoform 2 of Reticulon-4	RTN4	18.50	4	5
B4DIT7	Protein-glutamine gamma-glutamyltransferase 2	TGM2	17.82	8	12
P36578	60S ribosomal protein L4	RPL4	17.80	7	17
R4GN98	Protein S100-A6 (Fragment)	S100A6	17.65	2	3
P15151-3	Isoform Gamma of Poliovirus receptor	PVR	17.03	5	9
P13647	Keratin, type II cytoskeletal 5	KRT5	16.95	4	18
P20020-6	Isoform K of Plasma membrane calcium-transporting ATPase 1	ATP2B1	15.63	12	20
B7Z7A9	Phosphoglycerate kinase	PGK1	15.42	4	5
P11166	Solute carrier family 2, facilitated glucose transporter member 1	SLC2A1	15.24	6	16
P07942	Laminin subunit beta-1	LAMB1	15.01	16	21
P07900	Heat shock protein HSP 90-alpha	HSP90AA1	14.34	5	16
P54709	Sodium/potassium-transporting ATPase subunit beta-3	ATP1B3	14.34	3	4
P14209-3	Isoform 3 of CD99 antigen	CD99	14.20	2	6
Q6P452	Annexin	ANXA4	14.05	3	5
P35579	Myosin-9	MYH9	13.83	22	32
P07195	L-lactate dehydrogenase B chain	LDHB	13.77	3	6
P55072	Transitional endoplasmic reticulum ATPase	VCP	13.77	6	7
E9PFT6	Hemoglobin subunit delta	HBD	13.48	2	4
P11047	Laminin subunit gamma-1	LAMC1	12.74	13	19
Q99808	Equilibrative nucleoside transporter 1	SLC29A1	12.50	4	8
P53985	Monocarboxylate transporter 1	SLC16A1	12.00	4	8
Q8WUM4	Programmed cell death 6-interacting protein	PDCD6IP	11.75	6	9
Q15043-2	Isoform 2 of Zinc transporter ZIP14	SLC39A14	11.23	4	9
Q6YHK3	CD109 antigen	CD109	11.21	10	14
B7Z2F4	T-complex protein 1 subunit delta	CCT4	10.80	3	4
B7Z5C0	DnaJ homolog subfamily A member 1	DNAJA1	10.42	1	1
Q01105-3	Isoform 3 of Protein SET	SET	10.19	2	2
B4DVE7	Annexin	ANXA11	10.17	4	6
P47914	60S ribosomal protein L29	RPL29	9.43	1	1

Q8IZP0-10	Isoform 10 of Abl interactor 1	ABI1	9.28	3	4
P27701	CD82 antigen	CD82	8.99	2	3
Q04941	Proteolipid protein 2	PLP2	8.55	1	1
P14174	Macrophage migration inhibitory factor	MIF	7.83	1	2
B1AP58	Copine-1 (Fragment)	CPN1	7.35	1	1
P11279	Lysosome-associated membrane glycoprotein 1	LAMP1	7.19	3	4
Q08722-2	Isoform OA3-293 of Leukocyte surface antigen CD47	CD47	6.51	2	4
Q01650	Large neutral amino acids transporter small subunit 1	SLC7A5	6.31	2	7
P49327	Fatty acid synthase	FASN	5.54	7	10
P02765	Alpha-2-HS-glycoprotein	AHSG	5.45	3	9
Q5TCU6	Talin-1	TLN1	5.15	6	8
P01024	Complement C3	C3	4.93	6	10
Q5T985	Inter-alpha-trypsin inhibitor heavy chain H2	ITIH2	4.81	4	5
O15427	Monocarboxylate transporter 4	SLC16A3	4.52	2	5
P02462-2	Isoform 2 of Collagen alpha-1(IV) chain	COL4A1	3.95	4	6
Q14764	Major vault protein	MVP	3.81	2	4
Q8WWI5-3	Isoform 3 of Choline transporter-like protein 1	SLC44A1	3.68	2	2
P01023	Alpha-2-macroglobulin	A2M	3.46	3	21
Q09666	Neuroblast differentiation-associated protein AHNAK	AHNAK	3.36	2	5
B4DXI2	Bromodomain-containing protein 9	BRD9	3.27	1	2
P23526-2	Isoform 2 of Adenosylhomocysteinase	AHCY	3.22	1	1
P02788-2	Isoform DeltaLf of Lactotransferrin	LTF	3.15	2	3
Q86SJ2	Amphoterin-induced protein 2	AMIG	2.68	1	2
P20742	Pregnancy zone protein	PZP	2.29	1	20
P26641	Elongation factor 1-gamma	EEF1G	2.29	1	2
B4DLW8	Probable ATP-dependent RNA helicase DDX5	DDX5	2.24	1	2
P50281	Matrix metalloproteinase-14	MMP14	2.06	1	1
P12259	Coagulation factor V	F5	1.66	3	5

Table A2. Proteins identified in both biological replicates of p14-exosomes.

Uniprot ID	Description	Gene Name	% Coverage	#Unique Peptides	PSM Score
P80723	Brain acid soluble protein 1	BASP1	79.30	10	24
Q9UBI6	Guanine nucleotide-binding protein G(I)/G(S)/G(	GNG12	79.17	6	13
P07355	Annexin A2	ANXA2	71.98	27	69
P07437	Tubulin beta chain	TUBB	70.95	5	40
P04406	Glyceraldehyde-3-phosphate dehydrogenase	GAPDH	70.45	13	27
P49006	MARCKS-related protein	MARCKSL1	68.72	5	6
P60709	Actin, cytoplasmic 1	ACTB	68.53	11	68
P04899	Guanine nucleotide-binding protein G(i) subunit alpha-2	GNAI2	65.35	11	36
P35527	Keratin, type I cytoskeletal 9	KRT9	60.35	25	60
P35908	Keratin, type II cytoskeletal 2 epidermal	KRT2	59.78	21	56
P13645	Keratin, type I cytoskeletal 10	KRT10	59.59	28	91
P62937	Peptidyl-prolyl cis-trans isomerase A	PPIA	59.39	9	17
P31949	Protein S100-A11	S100A11	59.05	4	6
P09382	Galectin-1	LGALS1	58.52	7	15
P62873	Guanine nucleotide-binding protein G(I)/G(S)/G(T) subunit beta-1	GNB1	57.94	6	27
G3V1A4	Cofilin 1 (Non-muscle), isoform CRA_a	CFL1	57.72	6	13
P27348	14-3-3 protein theta	YWHAQ	57.14	9	22
P63104	14-3-3 protein zeta/delta	YWHAZ	57.14	11	22
P08754	Guanine nucleotide-binding protein G(k) subunit alpha	GNAI3	56.78	10	32
P02751-17	Isoform 17 of Fibronectin	FN1	56.57	91	262
P51149	Ras-related protein Rab-7a	RAB7A	56.52	9	20
O00299	Chloride intracellular channel protein 1	CLIC1	56.43	11	20
P04264	Keratin, type II cytoskeletal 1	KRT1	56.37	34	82
P26038	Moesin	MSN	54.07	23	55
P68371	Tubulin beta-4B chain	TUBB4B	53.93	1	29
P14618	Pyruvate kinase PKM	PKM	53.67	22	41
P29317	Ephrin type-A receptor 2	EPHA2	51.95	29	49
P15144	Aminopeptidase N	ANPEP	51.40	49	133
P61225	Ras-related protein Rap-2b	RAP2B	50.82	4	12
P35613-2	Isoform 2 of Basigin	BSG	49.81	10	21
P61224-3	Isoform 3 of Ras-related protein Rap-1b	RAP1B	49.70	3	15
P15153	Ras-related C3 botulinum toxin substrate 2	RAC2	49.48	4	10
P63000	Ras-related C3 botulinum toxin substrate 1	RAC1	49.48	4	13
P12111-2	Isoform 2 of Collagen alpha-3(VI) chain	COL6A3	49.31	108	209
O43854-2	Isoform 2 of EGF-like repeat and discoidin I-like domain-containing protein 3	EDIL3	49.15	21	43
P05556	Integrin beta-1	ITGB1	49.12	32	139
P60174-1	Isoform 2 of Triosephosphate isomerase	TPI1	48.19	7	12
P08758	Annexin A5	ANXA5	48.13	13	23
Q9H223	EH domain-containing protein 4	EHD4	47.50	15	34
P60953	Cell division control protein 42 homolog	CDC42	46.60	4	8
P04083	Annexin A1	ANXA1	45.95	12	25
P62258	14-3-3 protein epsilon	YWHAE	45.88	9	20
P13639	Elongation factor 2	EEF2	44.29	25	41
Q9P2B2	Prostaglandin F2 receptor negative regulator	PTGFRN	44.03	29	57
Q08629	Testican-1	SP	43.96	13	28
P07996	Thrombospondin-1	THBS1	43.93	40	104
P31946-2	Isoform Short of 14-3-3 protein beta/alpha	YWHAB	43.44	4	15
Q08380	Galectin-3-binding protein	LGALS3BP	43.42	22	62
F5H157	Ras-related protein Rab-35 (Fragment)	RAB35	43.24	6	16
P11142	Heat shock cognate 71 kDa protein	HSPA8	43.19	24	56
P05023-3	Isoform 3 of Sodium/potassium-transporting ATPase subunit alpha-1	ATP1A1	42.74	38	70
O00468-6	Isoform 6 of Agrin	AGRN	42.10	60	138
P17301	Integrin alpha-2	ITGA2	41.74	7	96

P08195-2	Isoform 2 of 4F2 cell-surface antigen heavy chain	SLC3A2	41.21	17	40
P05387	60S acidic ribosomal protein P2	RPLP2	40.87	3	6
P12109	Collagen alpha-1(VI) chain	COL6A1	39.20	29	54
P62805	Histone H4	HIST1H4A	38.83	4	7
Q9HAV0	Guanine nucleotide-binding protein subunit beta-4	GNB4	38.53	3	19
P61981	14-3-3 protein gamma	YWHAG	38.06	5	13
P10124	Serglycin	SRGN	36.71	4	6
P07737	Profilin-1	PFN1	36.43	5	9
P68104	Elongation factor 1-alpha 1	EEF1A1	36.36	14	32
P62158	Calmodulin	CALM1	34.90	3	7
Q06830	Peroxiredoxin-1	PRDX1	34.67	6	9
P69905	Hemoglobin subunit alpha	HBA1	34.51	4	16
P23229-4	Isoform Alpha-6X2A of Integrin alpha-6	ITGA6	33.71	25	44
P08582	Melanotransferrin	MFI2	33.60	14	21
E9PNW4	CD59 glycoprotein	CD59	33.33	6	13
P63092-3	Isoform 3 of Guanine nucleotide-binding protein G(s) subunit alpha isoforms short	GNAS	32.45	8	18
B7Z7A9	Phosphoglycerate kinase	PGK1	32.13	7	11
P50395	Rab GDP dissociation inhibitor beta	GDI2	32.13	10	15
P06733	Alpha-enolase	EN	32.03	12	20
P54709	Sodium/potassium-transporting ATPase subunit beta-3	ATP1B3	31.90	5	9
P26006	Integrin alpha-3	ITGA3	31.30	31	78
P18084	Integrin beta-5	ITGB5	31.04	14	24
E5RI99	60S ribosomal protein L30 (Fragment)	RPL30	30.70	2	2
P10599	Thioredoxin	TXN	30.48	3	5
B4E2J3	Serine protease 23	PRSS23	30.20	7	14
Q9H4M9	EH domain-containing protein 1	EHD1	29.59	8	16
P02787	Serotransferrin	TF	28.80	14	19
P62820	Ras-related protein Rab-1A	RAB1A	28.29	3	11
Q96KK5	Histone H2A type 1-H	HIST1H2AH	27.34	3	4
P12110	Collagen alpha-2(VI) chain	COL6A2	26.30	21	45
P08238	Heat shock protein HSP 90-beta	HSP90AB1	26.10	10	28
Q15758	Neutral amino acid transporter B(0)	SLC1A5	26.06	10	18
P02533	Keratin, type I cytoskeletal 14	KRT14	24.58	3	20
P06756-3	Isoform 3 of Integrin alpha-V	ITGAV	24.55	18	30
P00338	L-lactate dehydrogenase A chain	LDHA	24.40	4	8
P61353	60S ribosomal protein L27	RPL27	24.26	2	4
P06748-3	Isoform 3 of Nucleophosmin	NPM1	23.94	3	6
P08648	Integrin alpha-5	ITGA5	23.45	19	31
O00622	Protein CYR61	CYR61	23.10	7	16
P61026	Ras-related protein Rab-10	RAB10	22.50	2	11
C9JD32	60S ribosomal protein L23 (Fragment)	RPL23	21.98	1	2
B1AKC9	Ephrin type-B receptor 2	EPHB2	21.67	12	20
P43121	Cell surface glycoprotein MUC18	MCAM	20.74	10	16
P08473	Neprilysin	MME	20.67	11	14
P37802	Transgelin-2	TAGLN2	20.60	3	5
Q8WUM4	Programmed cell death 6-interacting protein	PDCD6IP	20.39	11	16
P81605	Dermcidin	DCD	20.00	2	2
O60814	Histone H2B type 1-K	HIST1H2BK	19.05	2	4
P02786	Transferrin receptor protein 1	TFRC	18.55	11	16
P18465	HLA class I histocompatibility antigen, B-57 alpha chain	HLA-B	18.51	2	10
Q5JR95	40S ribosomal protein S8	RPS8	18.09	3	4
R4GN98	Protein S100-A6 (Fragment)	S100A6	17.65	2	3
Q80FJ1	Membrane fusion protein p14		17.60	1	3
P11233	Ras-related protein Ral-A	RALA	17.48	2	7
P27701	CD82 antigen	CD82	16.48	3	7
Q92743	Serine protease HTRA1	HTRA1	16.04	5	8
P11047	Laminin subunit gamma-1	LAMC1	15.72	17	25

P07195	L-lactate dehydrogenase B chain	LDHB	15.27	3	7
C9J9K3	40S ribosomal protein SA (Fragment)	RPSA	15.15	2	3
P07942	Laminin subunit beta-1	LAMB1	15.01	14	23
F8VRJ2	Nucleosome assembly protein 1-like 1 (Fragment)	NAP1L1	14.91	1	1
Q99808	Equilibrative nucleoside transporter 1	SLC29A1	14.91	5	9
E9PFT6	Hemoglobin subunit delta	HBD	13.48	2	6
P11166	Solute carrier family 2, facilitated glucose transporter member 1	SLC2A1	13.41	5	17
P06702	Protein S100-A9	S100A9	13.16	1	1
P15151-3	Isoform Gamma of Poliovirus receptor	PVR	12.91	3	6
D6RF44	Heterogeneous nuclear ribonucleoprotein D0 (Fragment)	HNRNPD	12.50	1	1
P30050-2	Isoform 2 of 60S ribosomal protein L12	RPL12	12.12	1	1
P53985	Monocarboxylate transporter 1	SLC16A1	12.00	4	7
O43491	Band 4.1-like protein 2	EPB41L2	11.44	6	8
P25398	40S ribosomal protein S12	RPS12	11.36	1	1
P13647	Keratin, type II cytoskeletal 5	KRT5	11.19	3	14
P36578	60S ribosomal protein L4	RPL4	11.01	3	5
O75131	Copine-3	CPNE3	10.61	3	5
P07900	Heat shock protein HSP 90-alpha	HSP90AA1	9.97	3	11
Q15043-2	Isoform 2 of Zinc transporter ZIP14	SLC39A14	9.36	3	8
A8MUD9	60S ribosomal protein L7	RPL7	9.13	1	1
H7C0V9	Gamma-secretase C-terminal fragment 59 (Fragment)	APP	9.07	4	7
D6RBJ7	Vitamin D-binding protein	GC	8.62	2	2
Q04941	Proteolipid protein 2	PLP2	8.55	1	1
P49327	Fatty acid synthase	FASN	8.24	9	14
P14174	Macrophage migration inhibitory factor	MIF	7.83	1	2
A6NEP9	Tetraspanin-14 (Fragment)	TSPAN14	7.62	1	1
C9JNR5	Insulin B chain (Fragment)	INS	7.61	1	1
P62906	60S ribosomal protein L10a	RPL10A	7.37	1	2
P02462-2	Isoform 2 of Collagen alpha-1(IV) chain	COL4A1	7.36	5	7
B1AP58	Copine-1 (Fragment)	CPN1	7.35	1	1
O15427	Monocarboxylate transporter 4	SLC16A3	7.31	4	5
P62851	40S ribosomal protein S25	RPS25	7.20	1	1
P11279	Lysosome-associated membrane glycoprotein 1	LAMP1	7.19	2	3
P49207	60S ribosomal protein L34	RPL34	6.84	1	1
P01024	Complement C3	C3	6.49	11	26
Q5T985	Inter-alpha-trypsin inhibitor heavy chain H2	ITIH2	6.42	5	10
Q8WWI5	Choline transporter-like protein 1	SLC44A1	6.39	3	4
Q01650	Large neutral amino acids transporter small subunit 1	SLC7A5	6.31	2	3
F2Z388	60S ribosomal protein L35	RPL35	6.25	1	1
Q5TCU6	Talin-1	TLN1	6.01	8	11
P62269	40S ribosomal protein S18	RPS18	5.92	1	1
P02765	Alpha-2-HS-glycoprotein	AHSG	5.45	3	11
P46783	40S ribosomal protein S10	RPS10	5.45	1	1
P35579	Myosin-9	MYH9	4.85	5	6
Q9Y696	Chloride intracellular channel protein 4	CLIC4	4.74	1	3
J3QR09	Ribosomal protein L19	RPL19	4.66	1	2
P78539-4	Isoform 4 of Sushi repeat-containing protein SRPX	SRPX	4.49	1	2
P55072	Transitional endoplasmic reticulum ATPase	VCP	4.34	1	1
B4DVE7	Annexin	ANXA11	4.24	2	3
P01023	Alpha-2-macroglobulin	A2M	3.93	5	33
Q00610-2	Isoform 2 of Clathrin heavy chain 1	CLTC	3.66	3	3
P23526-2	Isoform 2 of Adenosylhomocysteinase	AHCY	3.22	1	1
P04004	Vitronectin	VTN	3.14	1	4
Q14764	Major vault protein	MVP	3.02	1	1
Q00839-2	Isoform Short of Heterogeneous nuclear ribonucleoprotein U	HNRNPU	2.73	1	3

Q86SJ2	Amphoterin-induced protein 2	AMIG	2.68	1	2
P20742	Pregnancy zone protein	PZP	2.29	1	29
P26641	Elongation factor 1-gamma	EEF1G	2.29	1	1
P12259	Coagulation factor V	F5	1.66	3	5
P02788-2	Isoform DeltaLf of Lactotransferrin	LTF	1.35	1	2
Q09666	Neuroblast differentiation-associated protein AHNAK	AHNAK	1.22	1	1
Q494V2	Coiled-coil domain-containing protein 37	CCDC37	1.15	1	2

Table A3. Comparison of control and p14-exosomes with ExoCarta Exosome Proteome Database.

ExoCarta Top Exosome Proteins	Present in control exosomes	Present in p14-exosomes
HSPA1_8; heat shock 70kDa protein 1/8	Y	Y
CD9, TSPAN29; CD9 antigen	Y	Y
GAPDH, gapA; glyceraldehyde 3-phosphate dehydrogenase	Y	Y
Actin beta	Y	Y
CD63, MLA1, TSPAN30; CD63 antigen	Y	Y
CD81, TAPA1, TSPAN28; CD81 antigen	Y	Y
ANXA2; annexin A2	Y	Y
ENO, eno; enolase	Y	Y
htpG, HSP90A; molecular chaperone HtpG	Y	Y
EEF1A; elongation factor 1-alpha	Y	Y
YWHAE	Y	Y
SYNDECAN BINDING PROTEIN	N	N
ALIX, RIM20; programmed cell death 6-interacting protein	Y	Y
ALBUMIN	Y	Y
YWHAZ	Y	Y
EEF2; elongation factor 2	Y	Y
ACTIN GAMMA 1	N	N
LDH, ldh; L-lactate dehydrogenase	Y	Y
ALDO; fructose-bisphosphate aldolase	N	N
MSN; moesin	Y	Y
ANXA5; annexin A5	Y	Y
PHOSPHOGLYCERATE KINASE	Y	Y
CFL; cofilin	Y	Y

Table A4. Comparision of control and p14-exosomes with KEGG Brite Exosome Portein Cluster.

KEGG Brite List of Exosomal Proteins	Present in control	Present in p14
MHC1; major histocompatibility complex, class I	N	N
CD9, TSPAN29; CD9 antigen	Y	Y
CD63, MLA1, TSPAN30; CD63 antigen	Y	Y
CD81, TAPA1, TSPAN28; CD81 antigen	Y	Y
ITGB1; integrin beta 1	Y	Y
MFGE8; lactadherin	N	N
ICAM1; intercellular adhesion molecule 1	N	N
ACTB_G1; actin beta/gamma 1	Y	Y
CFL; cofilin	Y	Y
DYNC1H; dynein heavy chain 1, cytosolic	N	N
VIL2; villin 2 (ezrin)	N	N
MSN; moesin	Y	Y
MYO1; myosin I	Y	Y
PFN; profilin	Y	Y
E1.11.1.15, PRDX, ahpC; peroxiredoxin	Y	Y
RDX; radixin	N	N
HSPA1_8; heat shock 70kDa protein 1/8	Y	Y
htpG, HSP90A; molecular chaperone HtpG	Y	Y
ALDO; fructose-bisphosphate aldolase	N	N
ENO, eno; enolase	Y	Y
GAPDH, gapA; glyceraldehyde 3-phosphate dehydrogenase	Y	Y
PGK, pgk; phosphoglycerate kinase	Y	Y
PK, pyk; pyruvate kinase	Y	Y
PPIA; peptidyl-prolyl cis-trans isomerase A	Y	Y
DPEP1; membrane dipeptidase	N	N
PRDX1; peroxiredoxin 1	Y	Y
ALIX, RIM20; programmed cell death 6-interacting protein	Y	Y
ESCRT-I complex subunit TSG101	N	N
CLIC1; chloride intracellular channel protein 1	Y	Y
SDCBP; syntenin-1	Y	Y
GNAI; guanine nucleotide-binding protein G(i) subunit alpha	Y	Y
GNB2; guanine nucleotide-binding protein G(I)/G(S)/G(T) subunit beta-2	Y	Y
YWHAB_Q_Z; 14-3-3 protein beta/theta/zeta	Y	Y
14-3-3 protein epsilon	Y	Y
YWHAG_H; 14-3-3 protein gamma/eta	Y	Y
EEF1A; elongation factor 1-alpha	Y	Y
EEF2; elongation factor 2	Y	Y
ANXA1; annexin A1	Y	Y
ANXA2; annexin A2	Y	Y
ANXA5; annexin A5	Y	Y
ANXA6; annexin A6	Y	Y
ARF1; ADP-ribosylation factor 1	N	N
CLTC; clathrin heavy chain	Y	Y
EHD1; EH domain-containing protein 1	Y	Y
EHD4; EH domain-containing protein 4	Y	Y
GDI1_2; Rab GDP dissociation inhibitor	Y	Y
FLOT; flotillin	N	N